SYNTHESIS AND ANALYSIS OF NOVEL PLATINUM GROUP METAL CHALCOGENIDE METAL QUANTUM DOT AND ELECTROCHEMICAL MARKERS

By

EZO NXUSANI

BSc Honours Chemistry (*Cum Laude*), MSc Chemistry (*Cum Laude*), University of Western Cape

A thesis submitted in fulfilment of the requirements for the degree of

PHILOSOPHIAE DOCTOR

In the

Department of Chemistry
Faculty of Science
University of the Western Cape, South Africa

Supervisor: Professor Emmanuel I. Iwuoha
Co-supervisor: Professor Priscilla Baker
June 2018

ABSTRACT

Although cadmium and lead chalcogenide quantum dot have excellent optical and photoluminescent properties that are highly favorable for biological applications, there still exists increasing concerns due to the toxicity of these metals. We, therefore, report the synthesis of new aqueous soluble IrSe quantum dot at room temperature utilizing a bottom-up wet chemistry approach. NaHSe and H_2IrCl_6 were utilized as the Se and Ir source, respectively. High-resolution transmission electron microscopy reveals that the synthesized 3MPA-IrSe Qd are 3 nm in diameter. The characteristics and properties of the IrSe Qd are investigated utilizing, Selected Area electron diffraction, ATR- Fourier Transform Infra-Red Spectroscopy, Energy Dispersive X-ray spectroscopy, Photoluminescence, Cyclic Voltammetry and chronocoulometry. A 3 fold increase in the optical band gap of IrSe quantum dot in comparison to reported bulk IrSe is observed consistent with the effective mass approximation theory for semiconductor materials of particles sizes < 10 nm. The PL emission of the IrSe quantum dot is at 519 nm. Their electro-activity is studied on gold electrodes and exhibit reduction and oxidation at -107 mV and +641 mV, with lowered reductive potentials. The synthesized quantum dot are suitable for low energy requiring electrochemical applications such as biological sensors and candidates for further investigation as photoluminescent biological labels. Simultaneous synthesis of rhodium selenide quantum dot and nanoshells has been accomplished utilizing a very simple and water-based approach. The nano-shells were then confirmed utilizing high-resolution transition electron microscope (HRTEM) whereby with sizes ranging from 15-20 nm. The HRTEM of the RhSe quantum dot revealed that very narrow sized particles of 3.5 nm have been simultaneously formed. The nanocrystals were then further characterized utilizing UV-vis spectroscopy, energy dispersive X-ray, SAED, solid-state carbon nuclear magnetic resonance (SS-CNMR). RhSe networks within carbon screen-printed electrodes were studied utilizing high resolution scanning electron microscope HRSEM equipped with backscattering (BSE). The SEM-BSE revealed that RhSe quantum dot, due to

2

their narrow size interwoven themselves into nanotubes of about 251 nm in diameter within the electrode instead of on top of the electrodes, into vein-like networks. The flow behavior of the nanocrystals in water has been investigated using Rheometer and a decrease in viscosity with increasing applied pressure (shear thinning) has been observed, an ideal behavior for biological applications or nano-fluids.

Furthermore, a novel electrochemical DNA sequencing technique (**EcSeq**) utilizing the "sequencing by synthesis" approach has been successfully demonstrated. The study commenced with the development of a facile synthetic approach towards labeling nucleotides at the 3'-OH utilizing ferrocene as a label and redox marker. The in-house synthesized 3'-O-ferrocene thymidine triphosphate was confirmed by LC/MS and phosphorus NMR with intermediates characterized also with proton and carbon NMR. Enzyme-assisted DNA extension on electrode bound DNA was then performed utilizing the 3'-O-ferrocene thymidine triphosphate and a distinct differential pulse voltammetry response at 435 mV arising from the oxidation of ferrocene was obtained. Palladium catalyzed the chemical cleavage of the 3'-O-ferrocene label, with 78% signal loss and 2nd base extension with signal regeneration were successfully performed. Thus we have demonstrated the feasibility of electrochemical-based DNA sequencing of short sequences, having possible applicability in point of care devices due to portability and miniaturization of electrochemical techniques.

3

KEYWORDS

Platinum group metal

Chalcogenide

Room temperature synthesis of nanocrystals

Quantum dots

Backscattering electron - high resolution single electron microscopy

Electrochemistry

Nucleoside synthesis

Mass spectrometry

DNA sequencing

Enzyme

DECLARATION

I declare that **Synthesis and analysis of novel platinum group metal chalcogenide metal quantum dot and electrochemical markers** is my own work, that it has not been submitted before for any degree or examination in any other university, and that all the sources I have used or quoted have been indicated and acknowledged as complete references.

Signature --------------------------------   18 May 2018

Ezo Nxusani   **Day Month Year**

DEDICATION

I dedicate this thesis

to my Mother

Sarah Sondishe -Nxusani

ACKNOWLEDGEMENT

I first and foremost thank the God of heaven who created me, gave me the strength and through His providence, this study was made.

To my supervisor, thank you for the advice and guidance throughout the course of the years. I've learnt more than chemistry throughout the duration of the thesis.

To SensorLab staff and members; chemistry department staff UWC and all others that I met throughout the course, thank you for your support and motivations.

To my family, your overwhelming support, love and constant belief has been a constant for motivation me throughout the period especially the hard parts.

To my friends that prayed and supported me especially throughout the end (you know who you are) much thanks.

"Whatever line of investigation we pursue, with a sincere purpose to arrive at truth, we are brought in touch with the unseen, Mighty Intelligence that is working in and through all."

–Education pg 14 Ellen G. White

7

LIST OF PUBLICATIONS

- E. Nxusani, E. Iwuoha Room temperature synthesis of photo-active and electro-active IrSe quantum dot. (Draft)
- E. Nxusani, E. Iwuoha, One pot synthesis of novel rhodium selenide quantum dot, nanoshells, and nanorods (Draft)

8

TABLE OF CONTENTS

9

10

LIST OF FIGURES

	quantum dot in LiOCl4 at 60 mV/s . The quantum dot were drop-coated on the electrodes. All experiments were performed on gold electrodes, referenced with Ag/AgCl and a platinum wire as a counter electrode	
Figure 7	Electrochemical properties of the IrSe quantum dot using a) multi-scan rate study of IrSe quantum dot using cyclic voltammetry, the scan rate of 10-300 mV/s and in PBS pH 7.4, b) Linear plot of cathodic peak current versus scan rate and c) Chronocoulometry of 3MPA-IrSe quantum dot	55
Figure 8	Synthesis of RhSe quantum dot and nanoshells whereby A) before injection of the Selenium precursor, B) after 60 min of reaction stirring, C) 1 hour 30 min of stirring, D) after 4 h30 min of stirring	65
Figure 9	HRTEM of RhSe quantum dot at 20 -2nm scale on a copper grid	67
Figure 10	HRTEM of RhSe nanoshells at 200-5 nm scale on a copper grid	68
Figure 11	SAED of the RhSe quantum dot and histogram	69
Figure 12	EDX of 3-MPA-RhSe nano-shells taken on copper grid (Cu)	70
Figure 13	Energy dispersive X-ray spectroscopy of RhSe quantum dot on a copper grid	71
Figure 14	(Above) UV-vis spectroscopy of RhSe quantum dot taken at time intervals, (Below) Taucs plot of the band gap of the RhSe quantum dot	75
Figure 15	Flow curve and behavior of RhSe Qd under shear stress	77
Figure 16	HRSEM (right) and BSE (left) of bare screen-printed carbon electrodes	81

14

16

17

	(t,1H), 3.30 (dt,1H), 3.17 (m,2H), 2.68 (m,2H), 2.52 (m,2H), 2.29 (ddd,1H), 2.24 (m,1H), 1.90(d,3H), 1.49(dt,4H), 1.35(m,4H), 0.93(s,7H), 0.13	
Figure 55	H'NMR of compound 2T (400MHz, CD3OD) δ 7.66 (d, 1H), 6.29 (m,1H), 5.75 (m,1H), 5.70 (m,1H), 5.50 (m,2H), 4.36 (dt,1H), 3.97(q,1H), 3.87(m,2H), 3.55 (t,1H), 3.30 (dt,1H), 3.17 (m,2H), 2.68 (m,2H), 2.52 (m,2H), 2.29 (ddd,1H), 2.24 (m,1H), 1.90(d,3H), 1.49(dt,4H), 1.35(m,4H), 0.93(s,7H), 0.13	145
Figure 56	13CNMR of compound 2T (500MHz, CD3OD) δ 164, 151,133,132,131,125,111, 88, 86, 77, 72, 63, 49,52, 43,42, 33,30,28,27, 26,17, 14,8, 7, 5	145
Figure 57	ESI-TOF-MS (FAB+) calculated for C26H49N4O5Si [M + H]+ is 526.7891 g/mol and was obtained 525.3547 g/mol	145
Figure 58	HNMR of compound 4T, 400MHz, (CD3OD) δ 7.66 (d, 1H), 6.29 (m, 1H), 5.70 (m, 2H), 4.94 (s, 4H), 4.90 (m, 2H), 4.65 (m,2H), 4.50 (m,2H), 4.37 (s, 5H), 4.36 (dt,1H), 3.97 (q,1H), 3.87 (m,2H), 3.55 (t,1H), 3.30 (dt,1H), 3.17 (m,2H), 2.68 (m,2H), 2.52 (m,2H), 2.29 (ddd,1H), 2.24 (m,1H), 1.90 (d,3H), 1.49 (dt,4H), 1.35 (m,4H), 0.93 (s,6H), 0.13 (s,9H)	147
Figure 59	13CNMR of compound 4T (500MHz, CD3OD) δ 173, 164, 151,134,132,123,109, 88,86, 75, 72,71,70,68, 63,52,49,48, 47, 46, 43,40,39,29,28, 27, 26,17, 14,8,4	148
Figure 60	ESI-TOF-MS of compound 4T (FAB+) calculated for C37H57FeN4O6Si [M + H]+ 738.8272 g/mol g/mol was obtained as 737.3404 g/mol g/mol	149
Figure 61	ESI-TOF-MS of compound 1C (FAB+) calculated for C26H36BrN3O5Si [M + H] 579.5843 g/ mol obtained as 600.1473 g/mol	150

	30 min at 62°C on a gold electrode versus Ag/AgCl at scan rate 20 mV/s in PBS. 78.2% signal loss has been achieved	
Figure 70	(Above) Differential pulse voltammetry (DPV) of 3'-O-ferrocene-thymidine triphosphate (a) in 0.01M phosphate buffered saline (PBS), (b) incorporated by 0.1 u/µL DNA Thermo sequenase after 10 min of incubation at 62 degrees Celsius; at a gold electrode versus Ag/AgCl at scan rate 20 mV/s, revealing the potential shift caused by incorporation. (Below) Scan rate study of anodic peak of incorporated 3'-O-ferrocene-thymidine triphosphate showing linear relationship between anodic peak current (I) and scan rate, a characteristic behaviour of electrode bound electro-active species.	160
Figure 71	Differential pulse voltammetry detection of the (b) 2nd or re-incorporation of 3'-O-ferrocene-thymidine triphosphate on model target DNA by 0.1 u/µL Thermo sequenase after 10 min of incubation at 62 degrees Celsius with gold electrode as the working electrode versus Ag/AgCl in 0.01M phosphate buffered saline (PBS) at scan rate 20 mV/s	161
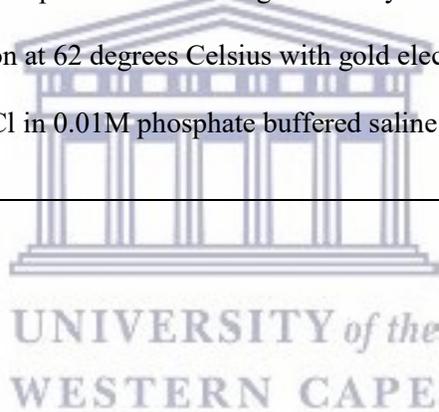
LIST OF TABLES

UNIVERSITY *of the*

WESTERN CAPE

CHAPTER 1
1.1 Research aims and objectives

The main focus of the study is the synthesis of platinum group metal iridium and novel rhodium selenide quantum dot and interrogation. And the objectives include:

a. Synthesis of iridium selenide quantum dot

b. Morphological characterization of the iridium quantum dot utilizing electron microscope

c. Spectroscopically interrogation of the iridium quantum dot

d. Electrochemical interrogation of the iridium quantum dot

e. Synthesis of rhodium selenide quantum dot

f. Morphological characterization of the rhodium quantum dot utilizing electron microscope

g. Spectroscopically interrogation of the rhodium quantum dot

h. Rheological interrogation of the rhodium quantum dot

i. Electrochemical characterization of the rhodium quantum dot

j.
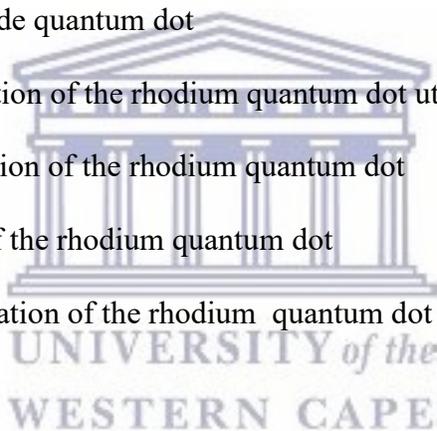
Furthermore, the aim of the study is the development of a synthetic approach towards the labeling of nucleotides at the 3'-hydroxyl for use in enzyme assisted electrochemical next-generation DNA sequencing technique, utilizing the sequencing by synthesis approach with electro-active labels at the 3'-OH position. This includes:

a. Design and synthesis of labeled thymidine at 3'-hydroxyl position with ferrocene

b. Purification of intermediates and characterization

c. Nuclear magnetic characterization of intermediates

d. Mass spectroscopic characterization of intermediates and the final product

e. Enzymatic assisted incorporation of in-house synthesized 3'-O-ferrocene thymidine on DNA immobilized on gold electrodes

f. Electrochemical characterization

g. Palladium-catalyzed chemical cleavage of labels and electrochemical interrogation

1.2 Research questions

1. What are the properties and characteristics of quantum dots synthesized utilizing iridium salt in aqueous media

2. Can a new quantum dot be synthesized utilising rhodium salts in aqueous media

3. What method can be used to label nucleosides at the 3'-hydroxyl labelling with electroactive labels

4. Is electrochemistry a feasible tool for the detection of enzymatically assisted DNA sequencing using a nucleotide with and electroactive label
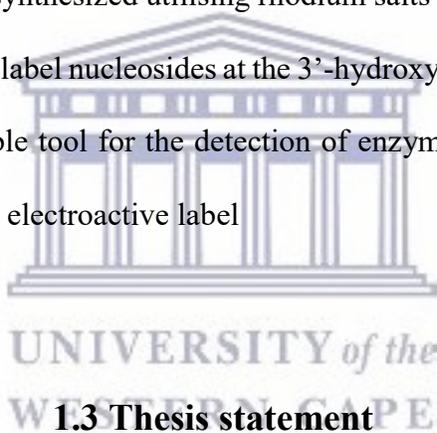
1.3 Thesis statement

Platinum group metal selenide quantum dot based on group 9 transition metals can be synthesized and characterized. Furthermore, an organic synthetic pathway for the labeling of nucleosides with electroactive labels at the 3'-hydroxyl can be designed and demonstrated in a 3 step electrochemical DNA sequencing approach.

CHAPTER 2
Review paper - Synthesis of platinum group chalcogenide quantum dot

23

Abstract

Chalcogenide quantum dot are the most widely synthesized quantum dot due to their interesting properties and application. This review covers the 3 main popular methods for the general synthesis of chalcogenide quantum dot namely hot injection method, cation exchange method and the room temperature method and the different main chalcogenide sources utilized. Chalcogenide quantum dot are generally used in a wide range of applications with platinum group metal chalcogenide quantum dot finding their main applicability in catalysis.

Keywords: chalcogenides quantum dot, quantum dot, synthesis

2.1 Introduction

Platinum group metals (PGMs) are generally known for their similarities in physical and chemical properties. They are attracting attention in nanotechnology due to their catalytic activity, thermodynamic stability; with platinum and palladium on the forefront. From these, PGM chalcogenide, platinum group metal compounds that contain Selenium, Tellurium, Sulphur, and sometimes Oxygen (though oft are called oxides); due to the applicability of palladium chalcogenides in the electronic industry in multilayer ceramic capacitors (MLCCs) and because of their semiconductor properties, they are being used and investigated as low resistance ohmic contacts. They also find applicability in recording films in optical discs and lithographic films and a light image receiving materials with silver halides.

Quantum dot are semiconductive materials from with sizes less than 10 nm and metal chalcogenides produced below/ around 10 nm diameter length scale. Generally, the synthetic method and the type of stabilizer and chalcogenide utilized during synthesis determines the quality and properties of the quantum dot produced. Herein we present the different main synthetic methods and stabilizing agents oft utilized in chalcogenide quantum dot synthesis and deferent applications of quantum dot.

24

2.2 Discussion

1. **Synthetic methods of quantum dot**

Various methods for the synthesis of chalcogenide quantum dot, in general, have been developed and improved over the years. They are based on hot injection method, cationic exchange method, and recently room temperature method.

a. **Hot injection method**

The hot-injection method generally involves the injection of reactants into a hot reaction mixture of all the precursors and stabilizers all at the same rate. Generally, nucleation of the quantum dot occurs spontaneously. The advantage of this method is that the size is engineered by a variation in concentration of precursors and reaction time of particle growth. Zeng *et al* 2015[1] reported the synthesis of CdSe quantum dot utilizing the hot injection method whereby a solution of selenium and trioctylphosphine in octadecene was rapidly injected under nitrogen into a hot mixture of precursor cadmium oxide and trioctylphosphine oxide in octadecene at a temperature of 275 degress Celsuis. This yielded water-insoluble quantum dot of sizes ranging from 2.8 nm - 4.6 nm.

In a similar method, Tyrakowski *et al* 2015 [2] synthesized Zinc Selenide quantum dot as a precursor to core shell Zinc Selenide-Cadmium Sulphide-Zinc Sulphide quantum dot. In their approach, a solution of selenium, trioctylphosphine and diethylzinc precursors were rapidly injected into hexadeclamine at 310 degrees Celsuis.

The disadvantage of this method is that it generally yields water-insoluble quantum dot limiting their use for aqueous based methods.

b. **Cationic exchange method**

The less popular cationic exchange method involves the use of quantum dot as the anion template or precursor for the synthesis of quantum dot. Kim *et al* 2015 [3] described the synthesis of air-stable lead selenide quantum dot utilizing the cation exchange method. In their method pre-prepared zinc selenide quantum dot, the selenium source in octadecene where injected under nitrogen to lead iodide solution heated at 150 degrees Celsius. This yielded colloids of about 3.3 nm. Lambert *et al* 2009 [4] reported the synthesis of cadmium telluride quantum dot from cation exchange method from lead telluride quantum dot, whereby cadmium oleate in octadecene was injected to lead telluride anion precursor in toluene at 100 degrees Celsius. Their method yielded core-shell quantum dot of 6.7 nm utilizing this method. This disadvantage of this method is the possibility of the growth of the intended quantum dot grow as a shell in the residual template (anion source) quantum dot.

c. Room temperature method

Recently, room temperature synthetic methods for the preparation of quantum dot have been developed as that eliminate high boiling point organic solvents. Mirzai *et al* 2014[5] reported the room temperature synthesis of mercury selenide quantum dot. In their approach, to a solution of mercury acetate in octadecene was injected with selenium solution and the reaction maintained at room temperature until completion. This yielded in comparison to elevated temperatures method performed for the same particles, narrowly sized colloids with UV absorption blue shifted signifying much wider band gap. Silver and copper selenide quantum dot were synthesized by Lu *et al* 2017 [6] utilizing the room temperature approach in tetrahydrofuran. Their approach yielded highly monodispersed quantum dot. Also, CdSe quantum dot have been synthesized utilizing the room temperature method.

26

2. Introduction of chalcogenides in quantum dot

The key step in chalcogenide quantum dot synthesis is the good selection of a chalcogenide source as this affects the quality and yields of the quantum dot. Typically selenides, sulfides and telluride are the most common chalcogenides used for quantum dot synthesis with few reports on oxides.

a) Selenides

In metal selenide quantum dot are the most commonly synthesized quantum dot to date due to the properties of selenium[7], with the material formed finding vast applications. There exist various sources and methods of introducing the selenium anion in the formation of metal selenide crystals. Subila *et al* 2013 [8] reported the introduction of selenium by injecting hot selenium solution in trioctylphosphine along with capping agents. This resulted in the successful formation of 3.5 - 3.8 nm sized cadmium selenide quantum dot.

Ndangili *et al* 2011[9] reported the synthesis of zinc selenide quantum dot utilizing pre-synthesized NaHSe via the reduction of selenium powder by sodium borohydride, as a selenium precursor in aqueous solution and yielded highly luminescent quantum dot.[10] Zinc selenide quantum dot were utilized as the selenium anion precursor in the cationic exchange synthesis of lead selenide quantum dot.[3] Sodium selenite has also been reported to be used as the selenium anion source in the synthesis of cadmium selenide quantum dot. The sodium selenite was pre-synthesized by heating sodium sulfite and selenium powder in water at 90 degrees Celsius.[11] Singh *et al* 2012 [12] reported the use of a palladium selenoether complex for the synthesis of palladium selenide nanocrystals at 300 degrees Celsius.

By far only methods utilizing NaHSe precursor as a selenium anion source where performed at room temperature, the rest require temperature ranging from 90 - 300 degrees Celsius.

b) Tellurides

Telluride chalcogenide quantum dot have been reported over the years. Keuleyan *et al 2014* [13] utilized tellurium in triocytylphosphine injected at 120 degrees Celsius to mercury chloride including capping agents to introduce the tellurium anion for the synthesis of mercury telluride quantum dot. This yielded non-spherical crystals with sizes ranging from 5.5 - 15 nm. Takahashi *et al 2011* [14] utilized tellurium chloride and citric acid in aqueous solution whereby the tellurium –citric acid complex formed was the main tellurium source for the room temperature synthesis of Palladium telluride nanocrystals. This method yielded highly crystalline spherical nanocrystals.

Samal *et al 2010* [15] reported the synthesis of platinum telluride nanocrystals utilizing template-assisted method. Pre-Synthesized tellurium nanowires were utilized as a tellurium anion source at room temperature for 24 hrs. Also, the reducing agent was formed as a by-product in the galvanic reaction between the tellurium nanowire and the platinum precursor. This method yielded PtTe spherical nanocrystals with a diameter of approximately 4 nm. El-Sadek *et al 2010* [16] utilized potassium telluride as the tellurium anion source in the synthesis of cadmium telluride quantum dot whereby potassium telluride was injected to a solution of cadmium precursor and a capping agent in water and particle growth performed in a microwave-assisted reaction. This method yielded highly clustered particles of about 7.7 nm. Masikini *et al 2015* [17] reported the synthesis of palladium telluride quantum dot utilizing hydrogen telluride gas as tellurium ion source.

c) **Sulfides**

Sulfide-based quantum dot are the most common chalcogenide quantum dot second to selenium.

Pan reported the synthesis of cadmium sulfide nanocrystals utilizing thiourea as the sulfur anion source. To a cadmium source precursor in chlorobenzene, thiourea solution in water was injected and the resulting reaction mixture was heated to 90 degrees Celsius for 150 min. This yielded narrow size distribution of

28

the cadmium sulfide crystals.[11] Ko *et al 2016* [18] reported the synthesis of lead sulfide quantum dot utilizing hexamethyldisilathaiane as the sulfur anion source. In this method a solution hexamethyldisilathiane in octadecene was quickly injected to a hot solution of lead acetate at 150 degrees Celsius. Cheng *et al 2015* [19] reported the synthesis of lead sulfide quantum dot utilizing sulfur powder as the sulfide anion source. In this method, a solution of sulfur in oleylamine is injected into the lead chloride precursor mixture at elevated temperatures. This yielded spherical monodispersed quantum dot with sizes ranging from 8 - 12 nm. Zhao *et al 2015* [20] reported the synthesis of copper-indium-sulfide quantum dot dodecanethiol as a sulfide anion source. In this method all precursors including the dodecanethiol in octadecene were pre-mixed and reaction performed at 230 degrees Celsius.

3. Stabilizers/ capping agents in chalcogenide quantum dot synthesis

The selection of a suitable capping agent or ligand is highly crucial in quantum dot synthesis. As it affects the particle size, agglomeration, stability and overall application of the nanocrystals.

a. Hydrophilic capping ligands

Water solubility of the quantum dot is achieved by utilizing molecules that are hydrophobic by nature as capping agents. And this is generally obtained by introducing a hydrophilic molecule for a capping agent during the synthesis or by a secondary ligand exchange reaction whereby a hydrophobic capping agent is exchanged for a hydrophilic molecule.

Functionalizing quantum dot with amphiphilic molecules such as 3-mercaptoacetic acid[21], mercapto-carboxylic acid (3MPA), cysteine[22][23] during the nucleation stage of the quantum dot offers a simplistic route for producing aqueous soluble colloids and is the most widely used method. Ndangili *et*

al 2011[9] utilized mercaptopropionic acid during the synthesis of zinc selenide quantum dot and yielded water-soluble quantum dot with strong photoluminescent properties in aqueous media.

Alternatively, biphase ligand exchange reaction is performed in a suitable solvent, such as described by Reinhart *et al 2015* [24] which involves the exchange of the hydrophobic stabilizer oleic acid (OA) with the hydrophilic mercaptopropionic acid (MPA) stabilizer.

b. Hydrophilic stabilizers

Generally, hot injection method often utilizes hydrophobic stabilizers such as an oleic acid (OA), triocytl phosphine oxide (TOPO) and triocytylphosphine (TOP). Zeng *et al 2015* [1] reported the synthesis of triocytlyphosphine (TOP) capped Cadmium selenide quantum dot prepared in octadecene. This resulted in water-insoluble quantum dot with sizes ranging from 2.8-3 nm. The TOP was involved in the overall photochemistry of the CdSe quantum dot.
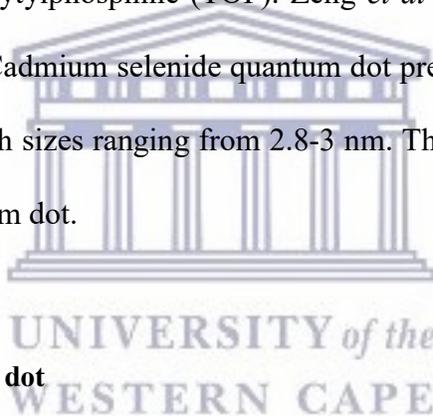
2.2.3 Applications of PGM quantum dot

Quantum dot are generally used in different various applications due to the electron confinement at 3 dimensions which generally give rise to diverse and interesting properties. These include Bioimaging[20], cellular labeling[25], fingerprint identification[26], for photoelectric ink[27], electrochemical supercapacitor[28], and electrochemical sensors[10]. Platinum group metal chalcogenide quantum dot due to the intrinsic catalytical properties of platinum group metals. Table 1 shows the main applications of platinum group metal chalcogenide quantum dot.

Table 1 Main application of platinum group metal chalcogenide quantum dot

Nanoparticle Composition	Size	Application/ potential application	Reference
$Pd_{20}Te_7$	12 - 15 nm	Catalysis	[29]
PdTe	5 nm	Catalysis	[12]
$RuSe_2$ nanotubes	6 nm wall thickness	Various	[30]
$Pd_{17}Se_{15}$ nanotubes	6 nm wall thickness	Various	[30]
Pt_3Te_4	4 nm	Catalysis	[15]
$Pd_{17}Se_{15}$	50 nm	Catalysis	[31]
$Ir_{50}Se_{50}/C$	Not reported due to agglomeration	Catalysis	[32]

2.3 Conclusion

Chalcogenide quantum dot are the most widely synthesized quantum dot due to their interesting properties and application. Quality and properties of the quantum dot are dependent on the synthetic method, chalcogenide source and the kind of stabilizer utilized. The 3 main methods for the general synthesis of chalcogenide quantum dot namely hot injection method, cation exchange method, and the room temperature method. Chalcogenide quantum dot are generally used in a wide range of applications with platinum group metal chalcogenide quantum dot finding main applicability in catalysis.

31

References

[1]   Y. Zeng and D. F. Kelley, "Two-Photon Photochemistry of CdSe Quantum Dots," *ACS Nano*, vol. 9, no. 10, pp. 10471–10481, 2015.

[2]   C. M. Tyrakowski, A. Shamirian, C. E. Rowland, H. Shen, A. Das, R. D. Schaller, and P. T. Snee, "Bright Type II Quantum Dots," *Chem. Mater.*, vol. 27, no. 21, pp. 7276–7281, 2015.

[3]   S. Kim, A. R. Marshall, D. M. Kroupa, E. M. Miller, J. M. Luther, S. Jeong, M. C. Beard, and K. I. M. E. T. Al, "Air-Stable and E ffi cient PbSe Quantum-Dot Solar Cells Based upon ZnSe and PbSe Cation-exchanged Quantum Dots," no. 8, pp. 8157–8164, 2015.

[4]   K. Lambert, B. De Geyter, I. Moreels, and Z. Hens, "PbTe| CdTe core| shell particles by cation exchange, a HR-TEM study," *Chem. Mater*, vol. 21, pp. 778–780, 2009.

[5]   H. Mirzai, M. N. Nordin, R. J. Curry, J.-S. Bouillard, a. V. Zayats, and M. Green, "The room temperature phosphine-free synthesis of near-infrared emitting HgSe quantum dots," *J. Mater. Chem. C*, vol. 2, no. 12, p. 2107, 2014.

[6]   H. Lu and R. L. Brutchey, "Tunable Room-Temperature Synthesis of Coinage Metal Chalcogenide Nanocrystals from *N* -Heterocyclic Carbene Synthons," *Chem. Mater.*, p. acs.chemmater.6b05293, 2017.

[7]   S. Nath, S. K. Ghosh, S. Panigahi, T. Thundat, and T. Pal, "Synthesis of selenium nanoparticle and its photocatalytic application for decolorization of methylene blue under UV irradiation," *Langmuir*, vol. 20, no. 18, pp. 7880–7883, 2004.

[8]   K. B. Subila, G. Kishore Kumar, S. M. Shivaprasad, and K. George Thomas, "Luminescence Properties of CdSe Quantum Dots: Role of Crystal Structure and Surface Composition," *J. Phys. Chem. Lett.*, vol. 4, pp. 2774–2779, 2013.

[9]   P. M. Ndangili, A. M. Jijana, P. G. L. Baker, and E. I. Iwuoha, "3-Mercaptopropionic acid capped ZnSe quantum dot-cytochrome P450 3A4 enzyme biotransducer for 17beta-estradiol," *J. Electroanal. Chem.*, vol. 653, no. 1–2, pp. 67–74, 2011.

[10]   P. M. Ndangili, O. a. Arotiba, P. G. L. Baker, and E. I. Iwuoha, "A potential masking approach in the detection of dopamine on 3-mercaptopropionic acid capped ZnSe quantum dots modified gold electrode in the presence of interferences," *J. Electroanal. Chem.*, vol. 643, no. 1–2, pp. 77–81, 2010.

[11]   D. Pan, Q. Wang, S. Jiang, X. Ji, and L. An, "Low-temperature synthesis of oil-soluble CdSe, CdS, and CdSe/CdS core-shell nanocrystals by using various water-soluble anion precursors," *J. Phys. Chem. C*, vol. 111, no. 15, pp. 5661–5666, 2007.

[12]   V. V. Singh, G. K. Rao, A. Kumar, and A. K. Singh, "Palladium(ii)–selenoether complexes as new single source precursors: First synthesis of Pd4Se and Pd7Se4 nanoparticles," *Dalt. Trans.*, vol. 41, no. 4, p. 1142, 2012.

[13]   S. E. Keuleyan, P. Guyot-sionnest, C. Delerue, and G. Allan, "Mercury Telluride Colloidal Quantum Dots : Electronic Structure , Photocurrent Detection up to 12 μ m," *ACS Nano*, vol. 8, no. 8, pp. 8676–8682, 2014.

[14]   H. Takahashi, N. Konishi, H. Ohno, K. Takahashi, Y. Koike, K. Asakura, and A. Muramatsu, "Preparation of well-crystallized Pd20Te7 alloy nanoparticulate catalysts with uniform structure and composition in liquid-phase," *Appl. Catal. A Gen.*, vol. 392, no. 1–2, pp. 80–85, 2011.

[15]   A. K. Samal and T. Pradeep, "Pt3Te4 nanoparticles from tellurium nanowires," *Langmuir*, vol. 26, no. 24,

pp. 19136–19141, 2010.

[16]   M. S. Abd El-sadek, J. Ram Kumar, and S. Moorthy Babu, "The role of potassium tellurite as tellurium source in mercaptoacetic acid-capped CdTe nanoparticles," *Curr. Appl. Phys.*, vol. 10, no. 1, pp. 317–322, 2010.

[17]   M. Masikini, S. N. Mailu, A. Tsegaye, N. Njomo, K. M. Molapo, C. O. Ikpo, C. E. Sunday, C. Rassie, L. Wilson, P. G. L. Baker, and E. I. Iwuoha, "A fumonisins immunosensor based on polyanilino-carbon nanotubes doped with palladium telluride quantum dots," *Sensors (Switzerland)*, vol. 15, no. 1, pp. 529–546, 2015.

[18]   D.-K. Ko, A. Maurano, S. K. Suh, D. Kim, G. W. Hwang, J. C. Grossman, V. Bulović, and M. G. Bawendi, "Photovoltaic Performance of PbS Quantum Dots Treated with Metal Salts," *ACS Nano*, p. acsnano.5b07186, 2016.

[19]   H. Cheng, Y. Wang, H. Dai, J.-B. Han, and X. Li, "Nonlinear Optical Properties of PbS Colloidal Quantum Dots Fabricated via Solvothermal Method," *J. Phys. Chem. C*, vol. 119, no. 6, pp. 3288–3292, 2015.

[20]   C. Zhao, Z. Bai, X. Liu, Y. Zhang, B. Zou, and H. Zhong, "Small GSH-Capped CuInS2 Quantum Dots: MPA-Assisted Aqueous Phase Transfer and Bioimaging Applications," *ACS Appl. Mater. Interfaces*, vol. 7, no. 32, pp. 17623–17629, 2015.

[21]   J. J. Andrade, a. G. Brasil, P. M. a Farias, a. Fontes, and B. S. Santos, "Synthesis and characterization of blue emitting ZnSe quantum dots," *Microelectronics J.*, vol. 40, no. 3, pp. 641–643, 2009.

[22]   B. P. Bloom, V. Kiran, V. Varade, R. Naaman, and D. H. Waldeck, "Spin selective charge transport through cysteine capped CdSe quantum dots," *Nano Lett.*, vol. 16, no. 7, pp. 4583–4589, 2016.

[23]   D. Deng, L. Qu, Y. Li, and Y. Gu, "Versatile self-assembly of water-soluble thiol-capped cdte quantum dots: External destabilization and internal stability of colloidal qds," *Langmuir*, vol. 29, no. 34, pp. 10907–10914, 2013.

[24]   C. C. Reinhart and E. Johansson, "Colloidally Prepared 3-Mercaptopropionic Acid Capped Lead Sulfide Quantum Dots," *Chem. Mater.*, vol. 27, no. 21, pp. 7313–7320, 2015.

[25]   C. E. Bradburne, J. B. Delehanty, K. Boeneman Gemmill, B. C. Mei, H. Mattoussi, K. Susumu, J. B. Blanco-Canosa, P. E. Dawson, and I. L. Medintz, "Cytotoxicity of quantum dots used for in vitro cellular labeling: Role of QD surface ligand, delivery modality, cell type, and direct comparison to organic fluorophores," *Bioconjug. Chem.*, vol. 24, no. 9, pp. 1570–1583, 2013.

[26]   E. Biology, "Room temperature synthesis of water-soluble starch-stabilized CdSe quantum dots for latent fingerprints detection," no. January 2014, 2016.

[27]   A. Tang, Y. Liu, Q. Wang, R. Chen, W. Liu, Z. Fang, and L. Wang, "A new photoelectric ink based on nanocellulose/CdS quantum dots for screen-printing," *Carbohydr. Polym.*, vol. 148, pp. 29–35, 2016.

[28]   V. Bonu, B. Gupta, S. Chandra, A. Das, S. Dhara, and a. K. Tyagi, "Electrochemical supercapacitor performance of SnO2 quantum dots," *Electrochim. Acta*, vol. 203, pp. 230–237, 2016.

[29]   H. Takahashi, N. Konishi, H. Ohno, K. Takahashi, Y. Koike, K. Asakura, and A. Muramatsu, "Preparation of well-crystallized Pd20Te7 alloy nanoparticulate catalysts with uniform structure and composition in liquid-phase," *Appl. Catal. A Gen.*, vol. 392, no. 1–2, pp. 80–85, 2011.

[30]   X. Jiang, B. Mayers, Y. Wang, B. Cattle, and Y. Xia, "Template-engaged synthesis of RuSe 2 and Pd 17 Se 15 nanotubes by reacting precursor salts with selenium nanowires," vol. 385, pp. 472–476, 2004.

[31] J. Akhtar, R. F. Mehmood, M. A. Malik, N. Iqbal, P. O'Brien, and J. Raftery, "A novel single source precursor: [bis(N,N-diethyl-N'-naphthoyl-selenoureato)palladium(II)] for palladium selenide thin films and nanoparticles.," *Chem. Commun. (Camb).*, vol. 47, no. 6, pp. 1899–901, 2011.

[32] G. Liu and H. Zhang, "Facile Synthesis of Carbon-Supported Ir x Se y Chalcogenide Nanoparticles and Their Electrocatalytic Activity for the Oxygen Reduction Reaction," pp. 2058–2065, 2008.

[33] M. Grydlik, F. Hackl, H. Groiss, M. Glaser, A. Halilovic, T. Fromherz, W. Jantsch, F. Schäffler, and M. Brehm, "Lasing from Glassy Ge Quantum Dots in Crystalline Si," *ACS Photonics*, vol. 3, no. 2, pp. 298–303, 2016.

[34] C. C. Shen and W. L. Tseng, "One-step synthesis of white-light-emitting quantum dots at low temperature," *Inorg. Chem.*, vol. 48, no. 18, pp. 8689–8694, 2009.

[35] M. M. Tavakoli, H. Aashuri, A. Simchi, S. Kalytchuk, and Z. Fan, "Quasi Core/Shell Lead Sulfide/Graphene Quantum Dots for Bulk Heterojunction Solar Cells," *J. Phys. Chem. C*, vol. 119, no. 33, pp. 18886–18895, 2015.

[36] D. Deng, J. Cao, L. Qu, S. Achilefu, and Y. Gu, "Highly luminescent water-soluble quaternary Zn-Ag-In-S quantum dots for tumor cell-targeted imaging.," *Phys. Chem. Chem. Phys.*, vol. 15, no. 14, pp. 5078–83, 2013.

[37] C. W. Kuo, D. Y. Chueh, N. Singh, F. C. Chien, and P. Chen, "Targeted nuclear delivery using peptide-coated quantum dots," *Bioconjug. Chem.*, vol. 22, no. 6, pp. 1073–1080, 2011.

[38] O. Lahad, N. Meir, I. Pinkas, and D. Oron, "Long-lived population inversion in isovalently doped quantum dots," *ACS Nano*, vol. 9, no. 1, pp. 817–824, 2015.

[39] I. A. Mir, K. Das, K. Rawat, and H. B. Bohidar, "Hot injection versus room temperature synthesis of CdSe quantum dots: A differential spectroscopic and bioanalyte sensing efficacy evaluation," *Colloids Surfaces A Physicochem. Eng. Asp.*, vol. 494, pp. 162–169, 2016.

[40] O. M. Primera-Pedrozo, Z. Arslan, B. Rasulev, and J. Leszczynski, "Room temperature synthesis of PbSe quantum dots in aqueous solution: stabilization by interactions with ligands.," *Nanoscale*, vol. 4, no. 4, pp. 1312–20, 2012.

[41] S. Rong, P. Zhang, Y. Yang, and F. Liu, "Room temperature synthesis of manganese oxide quantum dots and their application as a fluorescent probe for the detection of metal ions in aqueous media," *RSC Adv.*, vol. 6, no. 115, pp. 114632–114638, 2016.

[42] E. Oh, R. Liu, A. Nel, K. B. Gemill, M. Bilal, Y. Cohen, and I. L. Medintz, "Meta-analysis of cellular toxicity for cadmium-containing quantum dots," *Nat Nano*, vol. 11, no. 5, p. doi:10.1038/nnano.2015.338, 2016.

[43] W. E. Smith, J. Brownell, C. C. White, Z. Afsharinejad, J. Tsai, X. Hu, S. J. Polyak, X. Gao, T. J. Kavanagh, D. L. Eaton, and S. E. T. Al, "In Vitro Toxicity Assessment of Human Liver Cell Models," no. 11, pp. 9475–9484, 2012.

[44] I. a. Minigalieva, B. a. Katsnelson, V. G. Panov, L. I. Privalova, A. N. Varaksin, V. B. Gurvich, M. P. Sutunkova, V. Y. Shur, E. V. Shishkina, I. E. Valamina, I. V. Zubarev, O. H. Makeyev, E. Y. Meshtcheryakova, and S. V. Klinova, "In vivo toxicity of copper oxide, lead oxide and zinc oxide nanoparticles acting in different combinations and its attenuation with a complex of innocuous bio-protectors," *Toxicology*, vol. 380, pp. 72–93, 2017.

[45] S. Skalickova, V. Milosavljevic, K. Cihalova, P. Horky, L. Richtera, and V. Adam, "Selenium nanoparticles as a nutritional supplement," *Nutrition*, vol. 33, pp. 83–90, 2016.

[46]   T. H. D. Nguyen, B. Vardhanabhuti, M. Lin, and A. Mustapha, "Antibacterial properties of selenium nanoparticles and their toxicity to Caco-2 cells," *Food Control*, vol. 77, pp. 17–24, 2017.

[47]   X. Fang, X. Wu, C. Li, B. Zhou, X. Chen, T. Chen, and F. Yang, "Targeting selenium nanoparticles combined with baicalin to treat HBV-infected liver cancer," *RSC Adv.*, vol. 7, no. 14, pp. 8178–8185, 2017.

[48]   H. Su, D. D. Liu, M. Zhao, W. L. Hu, S. S. Xue, Q. Cao, X. Y. Le, L. N. Ji, and Z. W. Mao, "Dual-enzyme characteristics of polyvinylpyrrolidone-capped iridium nanoparticles and their cellular protective effect against H2O2-induced oxidative damage," *ACS Appl. Mater. Interfaces*, vol. 7, no. 15, pp. 8233–8242, 2015.

[49]   A. a. Gambardella, N. S. Bjorge, V. K. Alspaugh, and R. W. Murray, "Voltammetry of diffusing 2 nm iridium oxide nanoparticles," *J. Phys. Chem. C*, vol. 115, no. 44, pp. 21659–21665, 2011.

[50]   G. Liu and H. Zhang, "Facile Synthesis of Carbon-Supported Ir x Se y Chalcogenide Nanoparticles and Their Electrocatalytic Activity for the Oxygen Reduction Reaction," *J. Phys. Chem. C*, vol. 112, pp. 2058–2065, 2008.

[51]   S. Kurbanoglu, L. Rivas, S. a. Ozkan, and A. Merko??i, "Electrochemically reduced graphene and iridium oxide nanoparticles for inhibition-based angiotensin-converting enzyme inhibitor detection," *Biosens. Bioelectron.*, vol. 88, pp. 122–129, 2017.

[52]   D. Xu, P. Diao, T. Jin, Q. Wu, X. Liu, X. Guo, H. Gong, F. Li, M. Xiang, and Y. Ronghai, "Iridium Oxide Nanoparticles and Iridium/Iridium Oxide Nanocomposites: Photochemical Fabrication and Application in Catalytic Reduction of 4-Nitrophenol," *ACS Appl. Mater. Interfaces*, vol. 7, no. 30, pp. 16738–16749, 2015.

[53]   D. L. Klayman and T. S. Griffin, "Reaction of Selenium with Sodium Borohydride in Protic Solvents. A Facile Method for the Introduction of Selenium into Organic Molecules," *J. Am. Chem. Soc.*, vol. 2, no. 1, pp. 197–199, 1973.

[54]   W. Chen and S. Chen, "Iridium-platinum alloy nanoparticles: Composition-dependent electrocatalytic activity for formic acid oxidation," *J. Mater. Chem.*, vol. 21, no. 25, p. 9169, 2011.

[55]   L. Jimenez-Hernandez, O. Estavez-Hernandez, M. Hernandez-Sanchez, J. a. Diaz, M. Farias- Sanchez, and E. Reguera, "3-mercaptopropionic acid surface modification of Cu-doped ZnO nanoparticles: Their properties and peroxidase conjugation," *Colloids Surfaces A Physicochem. Eng. Asp.*, vol. 489, no. November, pp. 351–359, 2016.

[56]   Y. Li and N. Chopra, "Fabrication of nanoscale heterostructures comprised of graphene-encapsulated gold nanoparticles and semiconducting quantum dots for photocatalysis," *Phys. Chem. Chem. Phys.*, vol. 17, no. 19, pp. 12881–12893, 2015.

[57]   R. Enhanced, T. Alloys, R. P. P. Compound, H. T. Superconductors, P. Electrodes, A. Sensor, P. Group, M. Conference, N. Palladium, P. Catalyst, N. A. Plants, and N. Patents, "Platinum Metals Review," *Platin. Met. Rev.*, vol. 52, no. 1, pp. 54–62, 2008.

[58]   L. Brus, "Electronic wave functions in semiconductor clusters: experiment and theory," *J. Phys. Chem.*, vol. 90, no. 12, pp. 2555–2560, 1986.

[59]   J. Hambrock, A. Birkner, and R. a Fischer, "Synthesis of CdSe nanoparticles using various organometallic cadmium precursors," *J. Mater. Chem.*, vol. 11, no. 12, pp. 3197–3201, 2001.

[60]   B. Pejova and I. Grozdanov, "Three-dimensional confinement effects in semiconducting zinc selenide quantum dots deposited in thin-film form," *Mater. Chem. Phys.*, vol. 90, no. 1, pp. 35–46, 2005.

[61]   N. Gaponik, S. K. Poznyak, N. P. Osipovich, A. Shavel, and A. Eychmüller, "Electrochemical probing of thiol-capped nanocrystals," *Microchim. Acta*, vol. 160, no. 3, pp. 327–334, 2008.

[62]   M. J. N. Pourbaix, J. Van Muylder, N. de Zoubov, and C. Protection, "Electrochemical properties of the platinum metals," *Platin. Met. Rev.*, vol. 3, no. 2, pp. 47–53, 1959.

CHAPTER 3
Synthesis of Iridium and Rhodium Selenide Quantum dot

3.1 Introduction

Quantum dot, semiconductor materials smaller than 10 nm in diameter, have received great attention due to their use in a wide range of application. Current applications include microelectronic devices[33], light emitting diodes (LEDs)[34], solar cells[35], cell imaging[36] and drug delivery[37].

The hot-injection method reported by Subila *et al 2013* [8] in the synthesis of CdSe is the most commonly used approach for producing quantum dot in wet chemistry. It generally involves the injection of reactants into a hot reaction mixture of all the precursors and stabilizers all at the same rate with the temperatures ranging from 250 to 300 degrees Celsius. Hence the solvents of choice in this particular method are organic solvents in-order to maintain these high temperatures with typical stabilizers utilized including, TOP[1], oleic acid (OA)[38], which are generally insoluble in aqueous solution thus resulting to water insoluble quantum dot. Though quantum dot produced utilizing the hot injection method generally exhibit higher PL quantum yields they are generally limited to sensing applications.[39]

For cell imaging, drug deliverer and bio-sensing applications quantum dot that are water soluble are highly necessary as such studies are performed in aqueous solution. Water solubility is generally achieved through biphase ligand exchange, such as described by Reinhart *et al 2015* [24] which involves the exchange of the hydrophobic stabilizer oleic acid (OA) with the hydrophilic mercaptopropionic acid (MPA) stabilizer. Alternatively,functionalizing quantum dot with amphiphilic molecules such as a 3-mercapto-carboxylic acid (3MPA) during the nucleation stage of the quantum dot offers a simplistic route for producing aqueous soluble colloids while avoiding an additional ligand exchange step. The carboxylic group of 3MPA favorably undergoes an EDC/NHS assisted amine coupling, offering ease of labeling bio-molecules such as enzymes, antibodies, amine functionalized DNA and aptamers.

Recently, in an attempt to make the synthesis of quantum dot relatively "green", room temperature synthetic methods for the preparation of quantum dot have been developed as that eliminate high boiling point organic solvents. Primera-Pedrozo *et al 2012* [40] reported the room temperature approach of PbSe quantum dot in water while employing different thiol stabilizing agents. Pre-generated hydrogen selenide gas is constantly transferred under nitrogen flow into a reaction mixture containing lead thiolate complex at room temperature. This method yields water-soluble quantum dot of 5 - 10 nm particle sizes after 2 hours. Also, Shaopeng Rong *et al 2016* [41] demonstrated the room temperature synthesis of manganese oxide quantum dot at room temperature in aqueous solution in a two-step procedure involving first the synthesis of manganese oxide nanosheets for 12 h and a secondary ultra-filtration step to yield the quantum dot. This approach yielded photo-stable and water-soluble quantum dot of 3 - 9 nm particle sizes. Reports of the room temperature preparation of CdSe quantum dot in aqueous solution have been made.[39]

Extensive research has been performed on Cadmium (Cd) and leads (Pb) chalcogenide quantum dot (chalcogenide = S,Se,Te,O) due to their excellent optical properties, photostability and achieving high quantum yields thus are studied for sensing and bioimaging applications. Though these Cd and Pb based quantum dot show very interesting properties and applicability, there has been an increasing concern due to their associated toxicity.[42],[43],[44] Therefore quantum dot based on non-toxic/ less toxic metal chalcogenides for biomedical applications is needed.

Alternatively, selenium nanoparticles have been greatly investigated for pharmaceutical and biomedical applications. They have been studied as nutritional supplements due to their delayed release after ingestion in comparison with bulk selenium.[45] Selenium nanoparticles have been demonstrated to exhibit antibacterial properties against E-coli and Salmonella cells which are food born pathogens.[46] Also, Fang *et al 2017* [47] described the potential use of functionalized selenium nanoparticles towards treating HBV infected cancer cells.

38

Also, iridium, being the most stable of the platinum group metals in acid, consequently Su *et al 2015* [48] demonstrated that Iridium nanoparticles exhibit protection against oxidative cellular damage through its reaction with hydrogen peroxide thus lowering the levels of intracellular reactive oxygen species in lung cancer cells. Iridium-based nanocrystal have been demonstrated to have good electrocatalytic properties. Iridium oxide (IrO) nanoparticles of 2 nm sizes have been reported to poses very clear redox activity in aqueous solution.[49] Liu *et al 2008* [50] reported the preparation and electro-catalytical properties of carbon supported IrSe nanoparticles catalyst synthesized by microwave-assisted polyol process. The higher catalytic behavior for the oxidation-reduction reaction in comparison with conventional carbon supported platinum catalyst was demonstrated. Kurbanoglu *et al 2017* [51] demonstrated that the incorporation of IrO nanoparticles in their reduced-graphene-tyrosinase based electrochemical biosensor, increased the sensitivity of the sensor towards the detection of catechol Photo-catalytical activity of IrO nanoparticles have been demonstrated[52]
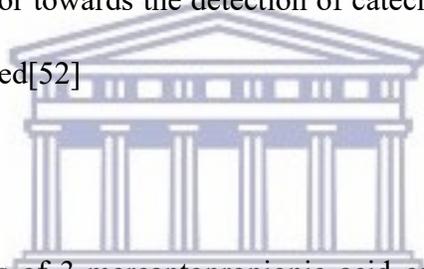
Herewith we describe the synthesis of 3-mercaptopropionic acid capped IrSe and RhSe quantum dot utilizing water as a solvent at room temperature. We have demonstrated that there are both optically and electrochemically active in aqueous solution thus being favorable candidates as labels for photoluminescence and electrochemical bio-sensing applications. This is the first report of narrow sized RhSe quantum dot synthesized at room temperature in aqueous solution.

CHAPTER 3A

Room temperature synthesis of photo-active and electro-active IrSe quantum dot

Abstract

Although cadmium and lead chalcogenide quantum dot have excellent optical and photoluminescent properties that are highly favorable for biological applications, there still exists increasing concerns due to the toxicity of these metals. We, therefore, report the synthesis of new aqueous soluble IrSe quantum dot at room temperature utilizing a bottom-up wet chemistry approach. NaHSe and H_2IrCl_6 were utilized as the Se and Ir source, respectively. High-resolution transmission electron microscopy reveals that the synthesized 3MPA-IrSe Qd are 3 nm in diameter. The characteristics and properties of the IrSe Qd are investigated utilizing, Selected Area electron diffraction, ATR- Fourier Transform Infra-Red Spectroscopy, Energy Dispersive X-ray spectroscopy, Photoluminescence, Cyclic Voltammetry and Chronocoulometry. A 3 fold increase in the optical band gap of IrSe quantum dot in comparison to reported bulk IrSe is observed consistent with the effective mass approximation theory for semiconductor materials of particles sizes < 10 nm. The PL emission of the IrSe quantum dot is at 519 nm. Their electro-activity is studied on gold electrodes and exhibit reduction and oxidation at -107 mV and +641 mV, with lowered reductive potentials. The synthesized quantum dot are suitable for low energy requiring electrochemical applications such as biological sensors and candidates for further investigation as photoluminescent biological labels.

40

Graphical abstract

Keywords: Room temperature synthesis, Iridium selenide quantum dot, electrochemistry, the optical band gap

3A.1 Experimental Section

Reagents

Analytical grade 3-mercaptopropionic acid ($HSCH_2CH_2CO_2H$, 3-MPA), sodium hydroxide, selenium powder, sodium borohydrate, hydrogen hexachloro-iridate (IV) hydrate, disodium hydrogen phosphate, sodium dihydrogen phosphate, potassium chloride, DMSO, absolute ethanol, were all purchased from Sigma-Aldrich (Cape Town, South Africa). All chemicals were utilized without further purification.

41

Room temperature synthesis of 3 mercaptopropionic acids capped iridium selenide Qd

NaHSe precursor was prepared by mixing 0.16 g of Se powder with 0.15 g of $NaBH_4$ in a round bottom flask and adding de-ionized water to make a 100 mL solution containing 0.02 M Se and 0.04 M $NaBH_4$ room temperature. The mixture was then stirred vigorously at room temperature under nitrogen for 30 min until an orange colored solution was obtained. In a separate flask, 0.04 M Ir^{IV} precursor solution was prepared by dissolving $H_2IrCl_6.xH_20$ to which 69.60 μL of 3MPA was added. The pH of the mixture was adjusted to pH12 using NaOH and saturated with N_2 for 30 min. Then the freshly prepared NaHSe was injected into the Ir-3MPA complex solution and the reaction was continued to stirring under nitrogen for 60 min and after which the dark brown solution was formed. The Qd were precipitated five times with absolute ethanol and stored at -18℃.

Instruments

High-resolution transmission electron microscopy (HR-TEM), selected area electron diffraction (SAED) and energy dispersive x-ray spectroscopy were performed utilizing a Field emission transmission electron microscope Tacnai G2 F20X-Twin MAT 200 kV from FEI (Eindhoven, NL), Electron Microscopy Unit, Physics, at UWC. The experiments were performed on a copper grid.

Ultraviolet-visible (UV-vis) absorption measurements were performed on a Nicolet Evolution 100 UV visible spectrometer (Thermo Electron, UK), utilizing quartz cuvette. All UV-Vis experiments were performed in solution. Photoluminescence spectroscopy was performed utilizing a Horiba NanoLogTM 3-22-TRIAX (USA), with double grating excitation and emission monochromators at a slit width of 5 nm. All PL measurements were performed in dimethyl sulfoxide. Raman spectroscopy was performed

utilizing Horiba scientific, Xplora, Olympus TH4-200 with Horiba Diode-pumped solid-state (DPSS) at a wavelength of 534 nm with samples prepared on glass slides

All voltammetry and chronocoulometry experiments were carried out using a BAS 100W integrated and automated electrochemical workstation obtained from BioAnalytical Systems (BAS), Lafayette, USA. A 10 mL cell comprising a 0.0201 cm^2 gold working electrode from BAS, Pt wire auxiliary electrode from Sigma Aldrich and Ag/AgCl (3 M KCl type) from BAS was used in all electrochemical studies. The Au working electrode was polished with alumina micro polish from Buehler, IL, USA,

3A.2 Results and discussion
3A.2.1 Synthesis of the IrSe quantum dot

Room temperature synthesis of the IrSe quantum dot is achieved utilizing a bottom-up wet chemistry approach described by Ndangili et al 2011 [9] for the synthesis of ZnSe quantum dot with modifications. Beginning with the preparation of NaHSe, black elemental selenium is reduced with 2 equivalents of NaBH$_4$ in water to obtain the orange selenium source which forms very rapidly at room temperature, following reaction (i) in Figure 1.[53] The reaction is then kept in an oxygen-free environment to avoid the oxidation of the oxygen-sensitive Se ion. Thereafter, to initiate the nucleation and growth of the quantum dot, the freshly prepared NaHSe is injected into the Ir-MPA complex at a Basic pH (12), with H$_2$IrCl$_6$ utilized as the iridium ion precursor as shown in reaction (ii) of Figure 1. After the 60th minute, the intensity of the color changes from orange to dark brown and this signals the formation of the IrSe colloidal crystals.

The rapid formation of narrow sized metal selenide quantum dot is achievable by utilizing NaHSe[11] as selenium source due to its high reactivity over organo-selenium. This is consistent with the observations made by Mir *et al 2016* [39] in the room temperature preparation of CdSe quantum dot utilizing NaHSe as the selenium ion source. Also, Liu *et al 2008* [50] prepared carbon supported IrSe nanoparticle catalyst utilizing H_2IrCl_6 as iridium ion source and sodium selenite (Na_2SeO_3) in water. As Na_2SeO_3 is less reactive, the nanoparticles formation is facilitated by microwave-assisted polyol process, at 190 degrees Celsius. Tert-butyldimethylsilyl selenide $(TBDMS)_2Se$ has also been utilized for the rapid formation of quantum dot at room temperature but it requires strict moisture and oxygen conditions due to its high volatility and formation of toxic side products[6].

We have successfully prepared water-soluble IrSe quantum dot that are synthesized at room temperature isothermally, in aqueous media (water). Below is the chemical reaction for the formation of the 3 MPA-IrSe Qd were (i) and (ii) describe the formation of the NaHSe precursor and Ir^{iV} source, respectively.

(i) $2Se + 4NaBH_4 + 7H_2O \longrightarrow 2NaHSe + Na_2B_4O_7 + 14 H_2 \uparrow$

(ii) $H_2IrCl_6 .xH_2O + H_2O + HSCH_2CH_2CO_2H \longrightarrow HCO_2CH_2CH_2S\text{-}Ir + HCl + H_2O$

(iii) $NaHSe + HCO_2CH_2CH_2S\text{-}Ir \longrightarrow$
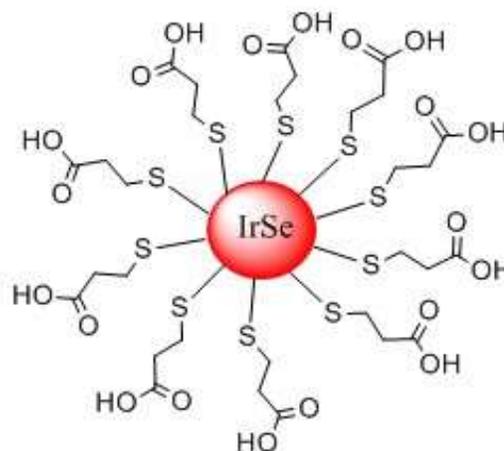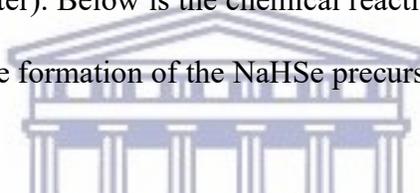
3MPA-IrSe quantum dots

Figure 1 Reaction scheme for the preparation of mercaptopropionic acid capped IrSe quantum dot in the water

44

3A.2.2 Structural properties of IrSe quantum dot

The morphology and crystallinity of the IrSe quantum dot were investigated utilizing high-resolution transmission electron microscopy (HRTEM) and selected area electron diffraction. The micrograph shown in Figure 2 (A-B), reveals that narrow-sized quantum dot of 3 nm are formed. The colloids are quasi-dispersed and have a spherical morphology. A close inspection of the HRTEM images as shown in Figure 2E reveals the (111) crystalline plane of facets of face-centered cubic (fcc) iridium[52] with a d-spacing of 0.210 nm [54], which confirms that formation of crystalline colloids. The elastic scattering of electrons from crystalline material is observable utilizing selected area electron diffraction (SAED). The SAED of IrSe quantum dot, shown in Figure 2D reveals the combination of rings and bright spots which is typical diffraction of polycrystalline material such as semiconductors. The bright spots arise from the Bragg reflection from individual crystallites consistent with the observations made from HRTEM analysis.
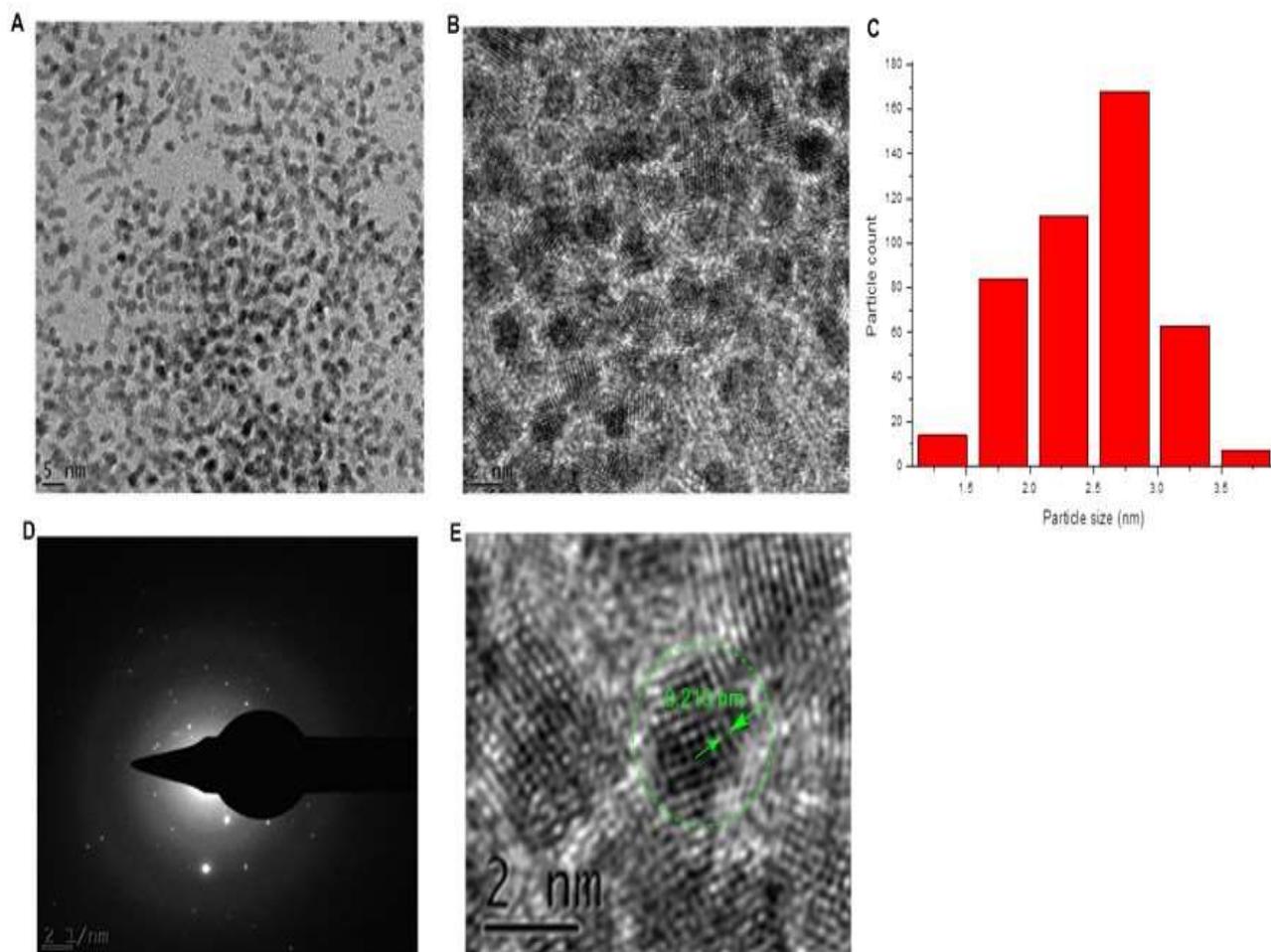
Figure 2 HRTEM at A) 5 nm, B) 2 nm magnifications with an average diameter of 2.7 nm shown in the histograph C) and selected area electron diffraction (SAED) shown in D.

Furthermore, Energy Dispersive X-ray spectroscopy (EDX) was used to study the elemental composition of the IrSe quantum dot. The EDX shown in Figure 3, reveal the pre-dominant peaks of iridium and selenium from the IrSe Qd core. The carbon, sulfur, and oxygen arise from the mercaptopropionic acid capping agent where the. The predominant peak of copper arises from the grid on which the spectrum is recorded.

46
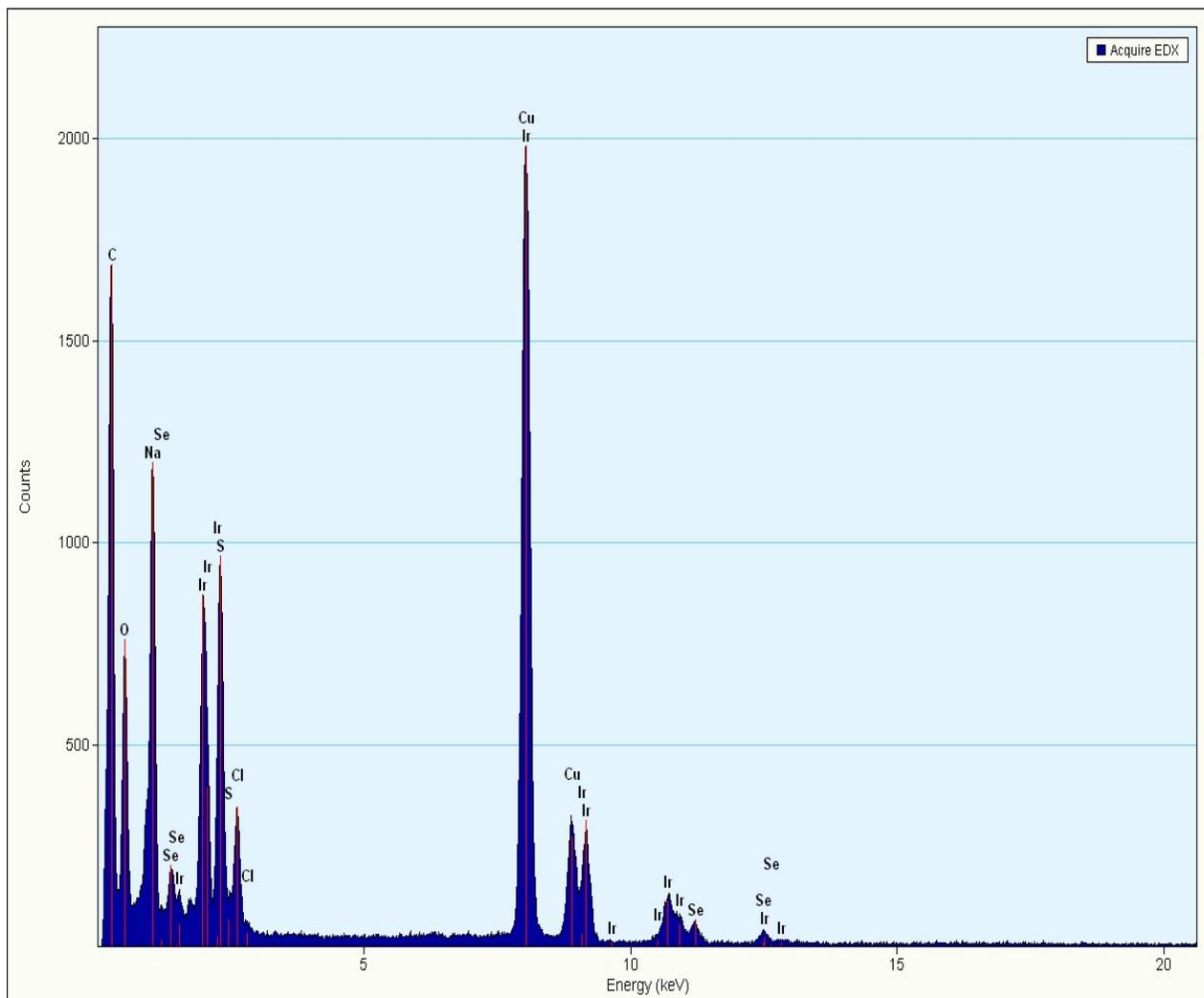
Figure 3 Energy Dispersive X-ray spectroscopy of 3MPA-IrSe quantum dot prepared on copper grids

The 3MPA-IrSe quantum dot were characterized by FTIR and Raman spectroscopy (Figure 4). The FTIR spectrum of the 3-MPA- capped quantum dots shown in Figure 4A, revealed bands corresponding to the asymmetric and symmetric stretching vibration of carboxylate group at 1555 and 1387 cm^{-1}, indicates the presence of 3-MPA on the particles. The bands appeared in a lower frequency then that of free 3-MPA which is a result of the deprotonation of –COOH- group in basic media during synthesis and its interaction with the quantum dot core.[55]Also there appeared the bands at 3296 and 1640 cm^{-1} corresponding to υ(-OH) and δ (H_2O) vibrations indicate the presence of water adsorbed on the Qd. The Raman spectrum of 3MPA-IrSe revealed also peaks characteristic to 3MPA in agreement the adsorption of an organic layer

47

(3MPA) on the Qd surface (Figure 4B). By comparison with the 3MPA spectrum, the most prominent bands at 2967 and 2911 cm^{-1}, corresponding to υ(C−H), of the mercaptopropionic acid are observed in both spectra.
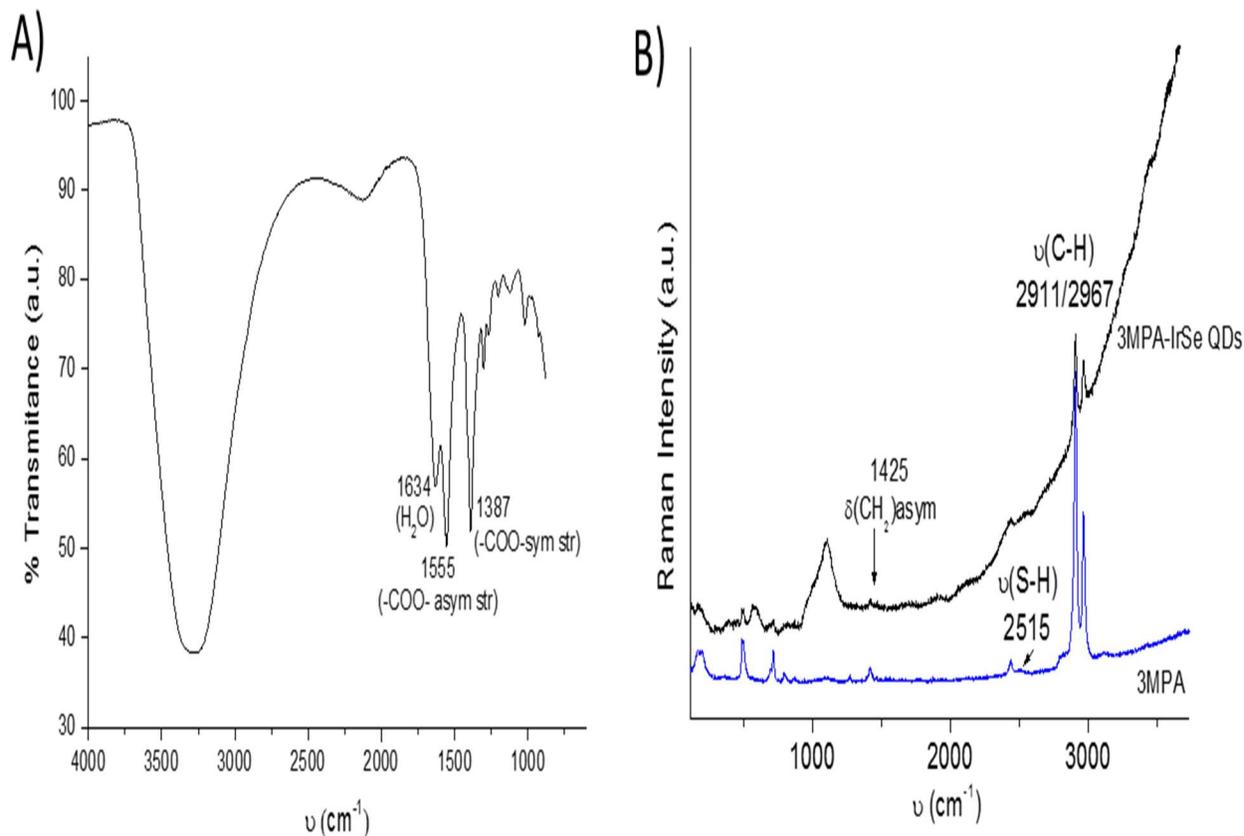
Figure 4 FTIR (A) and Raman (B) spectra of 3MPA-IrSe quantum dot. (In B, the spectrum of 3MPA (blue colour) for comparison)

3A.2.3 Optical properties of the synthesized IrSe quantum dot

The optical properties of the Qd were studied utilizing UV-vis and photoluminescence spectroscopy. Figure 4 shows the absorbance of the IrSe quantum dot, NaHSe and H_2IrCl_6 precursors in water revealing the sharp absorption peak of IrSe quantum dot at 210 nm, broad absorption peak of NaHSe at 261 nm;

48

and the 4 absorption wavelengths of H_2IrCl_6 at 233, 309, 427 and 490 nm. Also, it is noted that the absorption maximum of the IrSe quantum dot is blue-shifted with respect to its parent material attributes of small particle size formation in agreement with the results obtained in HRTEM.[5] The absorption bandwidth of the IrSe quantum dot is 29 nm at full width at half maxima (FWHM) indicating that the colloids formed are highly uniform in size without any significant spectral line broadening due to inhomogeneity. The optical band gap of the IrSe quantum dot is 3.2 eV which is calculated by extrapolation of the linear region to $\alpha hv=0$ of the taucs plot $(\alpha hv)^2$ versus (hv) as shown in Figure 5c and expressed in the following equation:

$$\alpha hv = C(hv-Eg)^n$$

Where "α" is the absorption coefficient, hv the photon energy and gap energy, A is a constant, Eg is the band gap energy and n=1/2 for allowed direct transitions observable in quantum dot. [56]

The nature of the interaction between the valence and conduction band and the size of the band gap, determine the optical properties of Qd, as the electrons move from the lowest occupied molecular orbital (LOMO) to the highest unoccupied molecular orbital (HUMO). The optical band gap of the IrSe quantum dot is 3 fold that of bulk iridium selenide reported to be approximately 1.0 eV [57]. This is an attribute of the formation of very small sized particles confirmed by HRTEM and also consistent with the effective mass approximation (EMA) first described by Louis Brus *et al 1986* [58]. The EMA predicts the widening of the band gap with decreasing particle size due to quantum size effect (QSE) arising from the 3-dimensional confinement of electrons in quantum dot [59].[60].

The emission properties of the IrSe where investigated utilizing Photoluminescence spectroscopy (PL) of the colloids in dimethyl sulfoxide (DMSO) at an excitation wavelength of 419 nm. The PL shown in Figure 5b reveals that the IrSe quantum dot emit at 519 nm comparable with that of CdSe quantum dot in chloroform excited at 400 nm. The emission bandwidth of the colloids is 98 nm at FWHM and 3 times in

comparison to absorption bandwidth and a large Stokes shift relative to the exciton absorption is observed. This is primarily due to the agglomeration of the particles during the sample preparation of drying the quantum dot at 80° C under vacuum for 24 hfor to complete the surface passivation of the quantum dot, hence an inhomogeneous size distribution is observed in the PL emission.
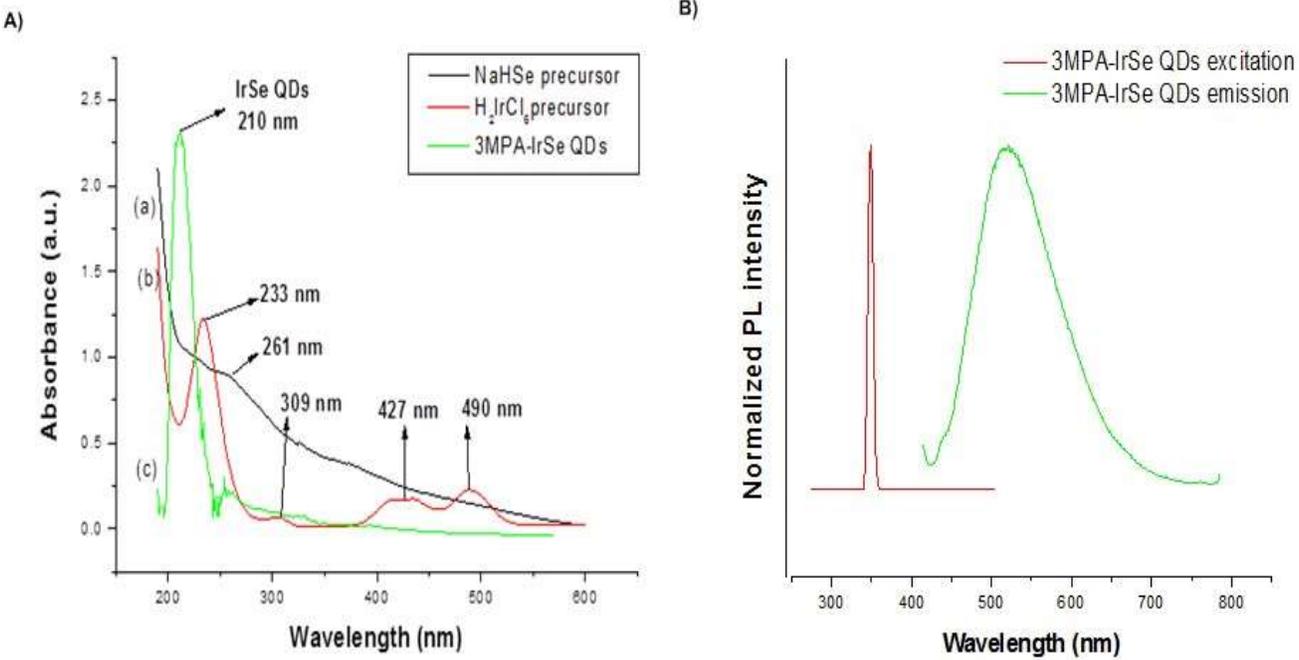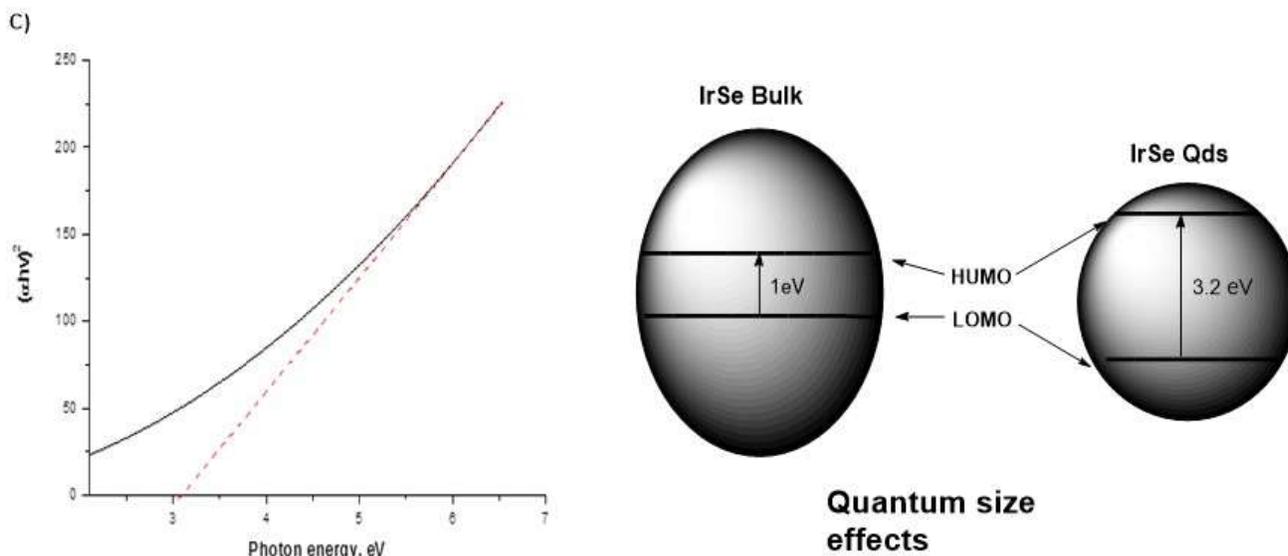
Figure 5 a) UV-vis spectroscopy of IrSe quantum dot, H₂IrCl₆ and NaHSe precursors in water, b) PL excitation and emission spectra of 3-MPA IrSe quantum dot in DMSO utilizing excitation wavelength of 415 nm, and c) Taucs plot

3A.2.4 The electrochemistry of the IrSe quantum dot

The electrochemical properties of 3MPA-IrSe Qd where evaluated utilizing cyclic voltammetry (CV). The CV of 3MPA-IrSe Qd in 0.01 M PBS, pH 7.4 shown in Figure 6, revealed the presence of a single reduction and a separate oxidation peak. A significant shift was observed of the reduction potential of the iridium core of the Qd from -182 mV to -107 mV as shown in Figure 6.1 and a shift in the selenium oxidation from +820 mV to +641 mV in comparison with the starting metal precursor as seen in Figure 6.3. This is due to electron-confinement in three dimensions, which intern enhances the electrochemical reaction. The quantum size lowers the activation energy for the reaction, this in turn caused a shift of the reduction potential towards lower reductive potentials, which indicates that a faster reduction reaction than that of the parent material has occurred.

51
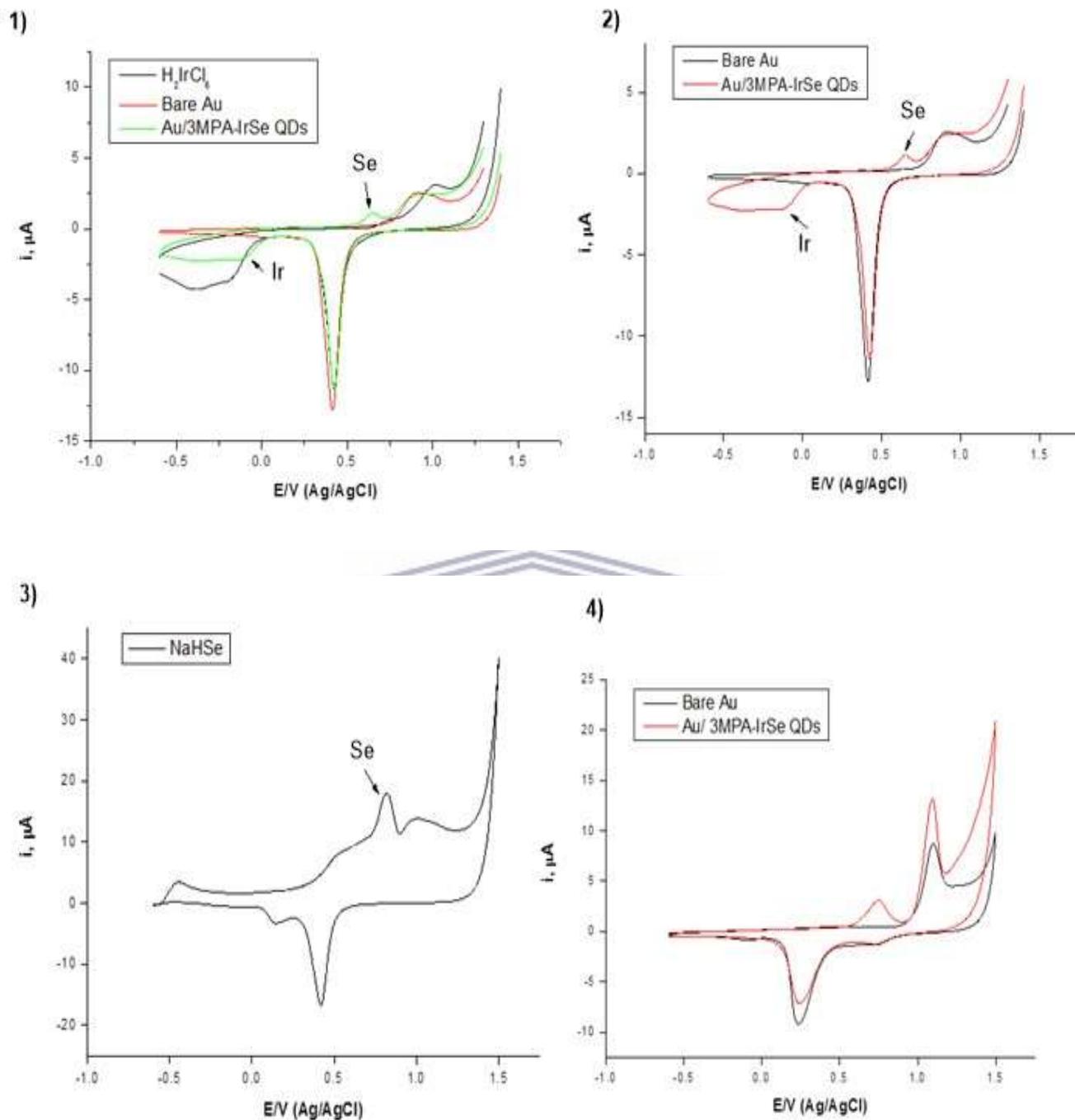
Figure 6 **Cyclic voltammograms of 1)&2) 3MPA-IrSe quantum dot and Iridium ion source in 0.01M Phosphate buffer saline pH 7.4 at 50 mV/s, 3) Selenium ion source in 0.01M Phosphate buffer saline pH 7.4 at 50 mV/s at 30 mV/s 4) 3MPA-IrSe quantum dot in LiOCl4 at 60 mV/s . The quantum dot were drop-coated on the electrodes. All experiments were performed on gold electrodes, referenced with Ag/AgCl and a platinum wire as a counter electrode.**

To further understand the electrochemistry of the Qd, a multi-scan rate study of the 3MPA-IrSe Qd on a gold electrode was performed as indicated in Figure.7 (A-B). The peaks A, B and C were observed. The reduction potential of Ir ions denoted in peak A is independent of the scan rate, and the oxidation potential of Se denoted by peak C exhibits a nonlinear change with scan rate. The nonlinearity of C is due to the anodic stripping of Se, arising from the electro-oxidation of Se related surface states [61].

To estimate the no of electrons involved in the reduction of Ir (Peak A), the two equations:

$$I_p = \omega n^2 F^2 A \Gamma v / 4RT \qquad \text{(I) Laviron's equation}$$

$$Q = nFA\Gamma \qquad \text{(III)}$$

were re-expressed to the following equation:

$$i_p = nFQv / 4RT \qquad \text{(III)}$$

Where ω is the angular frequency, n the no of electrons, F is Faraday's constant (96 584 C/ mol), A is the electrode area, Γ is the surface concentration (mol/ cm^2), v is the scan rate, R is the gas constant (8.314 J/ mol. K), T is the temperature (298 K), Q is the quantity of charge calculated from the reduction peak area of the voltammograms. From the slope of plot i_p versus v Figure 7, with the use of equation (III) the reduction process of the Ir of the quantum dot is estimated to involve four electrons. This indicates the reduction of Ir^{IV} to Ir, which is a four-electron process [62]. Thus, the oxidation state of the iridium metal of the quantum dot is Ir^{IV}.

Furthermore, the reduction of Qd was studied using Chronocoulometry at the potential for the reduction of iridium, as shown in Figure 7C. In Anson's plot estimation the surface concentration of the adsorbed species is given by:

$$Qads = nFA\Gamma$$

53

Where Q_{ads} is the charge due to the electrolysis of the adsorbed species, and Γ is the surface concentration of the adsorbed species. The charge due to the electrolysis of the 3MPA-IrSe$_2$ Qd is 4.0 nC and the surface concentration is 5.15×10^{-13} mol/cm^2.

Also in the anson's plot (using BAS 100), at a pulse width of 20 millis, the plots showed a wider peak separation. Using Anson's equation:

$$Q = 2nFCD^{1/2}t^{1/2} / \pi^{1/2}$$

Where n is the no of electrons, F is the Faraday's constant, D is the diffusion coeffiecient, t is the time, C concentration (0.1 mol/dm^3 of PBS), and π; from the slope of the Anson's plot (forward) scan, the diffusion coefficient is calculated to be 6.215×10^{-26} m^2/s.

Figure 7 Electrochemical properties of the IrSe quantum dot using a) multi-scan rate study of IrSe quantum dot using cyclic voltammetry, the scan rate of 10-300 mV/s and in PBS pH 7.4, b) Linear plot of cathodic peak current versus scan rate and c) Chronocoulometry of 3MPA-IrSe quantum dot.

3A.3 Conclusion

Water-soluble IrSe quantum dot have been successfully synthesized at room temperature utilizing H_2ICl_6 and NaHSe as a source of iridium and selenium ion respectively. The spherical 3 nm colloids were studied utilizing HRTEM, EDX, and SAED. Their PL emission was observed at 519 nm while exhibiting a very narrow absorption width thus further indicative of the formation of narrow sized particles. Characteristic reduction potential at 107 mV and oxidation at 641 mV in phosphate buffer, pH 7.41 ideal for biological samples, was observed utilizing cyclic voltammetry. Thus the 3-mercaptopropionic acid functionalized

55

IrSe quantum dot exhibited optical and electrochemical properties worthy of further investigation as biological labels and mediators in bio-sensing devices.

References

[1]   Y. Zeng and D. F. Kelley, "Two-Photon Photochemistry of CdSe Quantum Dots," *ACS Nano*, vol. 9, no. 10, pp. 10471–10481, 2015.

[2]   C. M. Tyrakowski, A. Shamirian, C. E. Rowland, H. Shen, A. Das, R. D. Schaller, and P. T. Snee, "Bright Type II Quantum Dots," *Chem. Mater.*, vol. 27, no. 21, pp. 7276–7281, 2015.

[3]   Z. P. Cation-exchanged, S. Kim, A. R. Marshall, D. M. Kroupa, E. M. Miller, J. M. Luther, S. Jeong, M. C. Beard, and K. I. M. E. T. Al, "Air-Stable and E ffi cient PbSe Quantum-Dot Solar Cells Based upon Quantum Dots," no. 8, pp. 8157–8164, 2015.

[4]   K. Lambert, B. De Geyter, I. Moreels, and Z. Hens, "PbTe| CdTe core| shell particles by cation exchange, a HR-TEM study," *Chem. Mater*, vol. 21, pp. 778–780, 2009.

[5]   H. Mirzai, M. N. Nordin, R. J. Curry, J.-S. Bouillard, a. V. Zayats, and M. Green, "The room temperature phosphine-free synthesis of near-infrared emitting HgSe quantum dots," *J. Mater. Chem. C*, vol. 2, no. 12, p. 2107, 2014.

[6]   H. Lu and R. L. Brutchey, "Tunable Room-Temperature Synthesis of Coinage Metal Chalcogenide Nanocrystals from *N* -Heterocyclic Carbene Synthons," *Chem. Mater.*, p. acs.chemmater.6b05293, 2017.

[7]   S. Nath, S. K. Ghosh, S. Panigahi, T. Thundat, and T. Pal, "Synthesis of selenium nanoparticle and its photocatalytic application for decolorization of methylene blue under UV irradiation," *Langmuir*, vol. 20, no. 18, pp. 7880–7883, 2004.

[8]   K. B. Subila, G. Kishore Kumar, S. M. Shivaprasad, and K. George Thomas, "Luminescence Properties of CdSe Quantum Dots: Role of Crystal Structure and Surface Composition," *J. Phys. Chem. Lett.*, vol. 4, pp. 2774–2779, 2013.

[9]   P. M. Ndangili, A. M. Jijana, P. G. L. Baker, and E. I. Iwuoha, "3-Mercaptopropionic acid capped ZnSe quantum dot-cytochrome P450 3A4 enzyme biotransducer for 17beta-estradiol," *J. Electroanal. Chem.*, vol. 653, no. 1–2, pp. 67–74, 2011.

[10]   P. M. Ndangili, O. Arotiba, P. G. L. Baker, and E. I. Iwuoha, "A potential masking approach in the detection of dopamine on 3-mercaptopropionic acid capped ZnSe quantum dots modified gold electrode in the presence of interferences," *J. Electroanal. Chem.*, vol. 643, no. 1–2, pp. 77–81, 2010.

[11]   D. Pan, Q. Wang, S. Jiang, X. Ji, and L. An, "Low-temperature synthesis of oil-soluble CdSe, CdS, and CdSe/CdS core-shell nanocrystals by using various water-soluble anion precursors," *J. Phys. Chem. C*, vol. 111, no. 15, pp. 5661–5666, 2007.

[12]   V. V. Singh, G. K. Rao, A. Kumar, and A. K. Singh, "Palladium(ii)–selenoether complexes as new single source precursors: First synthesis of Pd4Se and Pd7Se4 nanoparticles," *Dalt. Trans.*, vol. 41, no. 4, p. 1142, 2012.

[13]   S. E. Keuleyan, P. Guyot-sionnest, C. Delerue, and G. Allan, "Mercury Telluride Colloidal Quantum Dots : Electronic Structure , Photocurrent Detection up to 12 μ m," *ACS Nano*, vol. 8, no. 8, pp. 8676–8682, 2014.

[14]   H. Takahashi, N. Konishi, H. Ohno, K. Takahashi, Y. Koike, K. Asakura, and A. Muramatsu, "Preparation of well-crystallized Pd20Te7 alloy nanoparticulate catalysts with uniform structure and composition in

liquid-phase," *Appl. Catal. A Gen.*, vol. 392, no. 1–2, pp. 80–85, 2011.

[15]   A. K. Samal and T. Pradeep, "Pt3Te4 nanoparticles from tellurium nanowires," *Langmuir*, vol. 26, no. 24, pp. 19136–19141, 2010.

[16]   M. S. Abd El-sadek, J. Ram Kumar, and S. Moorthy Babu, "The role of potassium tellurite as tellurium source in mercaptoacetic acid-capped CdTe nanoparticles," *Curr. Appl. Phys.*, vol. 10, no. 1, pp. 317–322, 2010.

[17]   M. Masikini, S. N. Mailu, A. Tsegaye, N. Njomo, K. M. Molapo, C. O. Ikpo, C. E. Sunday, C. Rassie, L. Wilson, P. G. L. Baker, and E. I. Iwuoha, "A fumonisins immunosensor based on polyanilino-carbon nanotubes doped with palladium telluride quantum dots," *Sensors (Switzerland)*, vol. 15, no. 1, pp. 529–546, 2015.

[18]   D.-K. Ko, A. Maurano, S. K. Suh, D. Kim, G. W. Hwang, J. C. Grossman, V. Bulović, and M. G. Bawendi, "Photovoltaic Performance of PbS Quantum Dots Treated with Metal Salts," *ACS Nano*, p. acsnano.5b07186, 2016.

[19]   H. Cheng, Y. Wang, H. Dai, J.-B. Han, and X. Li, "Nonlinear Optical Properties of PbS Colloidal Quantum Dots Fabricated via Solvothermal Method," *J. Phys. Chem. C*, vol. 119, no. 6, pp. 3288–3292, 2015.

[20]   C. Zhao, Z. Bai, X. Liu, Y. Zhang, B. Zou, and H. Zhong, "Small GSH-Capped CuInS$_2$ Quantum Dots: MPA-Assisted Aqueous Phase Transfer and Bioimaging Applications," *ACS Appl. Mater. Interfaces*, vol. 7, no. 32, pp. 17623–17629, 2015.

[21]   J. J. Andrade, a. G. Brasil, P. M. a Farias, a. Fontes, and B. S. Santos, "Synthesis and characterization of blue emitting ZnSe quantum dots," *Microelectronics J.*, vol. 40, no. 3, pp. 641–643, 2009.

[22]   B. P. Bloom, V. Kiran, V. Varade, R. Naaman, and D. H. Waldeck, "Spin selective charge transport through cysteine capped CdSe quantum dots," *Nano Lett.*, vol. 16, no. 7, pp. 4583–4589, 2016.

[23]   D. Deng, L. Qu, Y. Li, and Y. Gu, "Versatile self-assembly of water-soluble thiol-capped cdte quantum dots: External destabilization and internal stability of colloidal qds," *Langmuir*, vol. 29, no. 34, pp. 10907–10914, 2013.

[24]   C. C. Reinhart and E. Johansson, "Colloidally Prepared 3-Mercaptopropionic Acid Capped Lead Sulfide Quantum Dots," *Chem. Mater.*, vol. 27, no. 21, pp. 7313–7320, 2015.

[25]   C. E. Bradburne, J. B. Delehanty, K. Boeneman Gemmill, B. C. Mei, H. Mattoussi, K. Susumu, J. B. Blanco-Canosa, P. E. Dawson, and I. L. Medintz, "Cytotoxicity of quantum dots used for in vitro cellular labeling: Role of QD surface ligand, delivery modality, cell type, and direct comparison to organic fluorophores," *Bioconjug. Chem.*, vol. 24, no. 9, pp. 1570–1583, 2013.

[26]   E. Biology, "Room temperature synthesis of water-soluble starch-stabilized CdSe quantum dots for latent fingerprints detection," no. January 2014, 2016.

[27]   A. Tang, Y. Liu, Q. Wang, R. Chen, W. Liu, Z. Fang, and L. Wang, "A new photoelectric ink based on nanocellulose/CdS quantum dots for screen-printing," *Carbohydr. Polym.*, vol. 148, pp. 29–35, 2016.

[28]   V. Bonu, B. Gupta, S. Chandra, A. Das, S. Dhara, and a. K. Tyagi, "Electrochemical supercapacitor performance of SnO2 quantum dots," *Electrochim. Acta*, vol. 203, pp. 230–237, 2016.

[29]   H. Takahashi, N. Konishi, H. Ohno, K. Takahashi, Y. Koike, K. Asakura, and A. Muramatsu, "Preparation of well-crystallized Pd20Te7 alloy nanoparticulate catalysts with uniform structure and composition in liquid-phase," *Appl. Catal. A Gen.*, vol. 392, no. 1–2, pp. 80–85, 2011.

[30]   X. Jiang, B. Mayers, Y. Wang, B. Cattle, and Y. Xia, "Template-engaged synthesis of RuSe 2 and Pd 17 Se 15 nanotubes by reacting precursor salts with selenium nanowires," vol. 385, pp. 472–476, 2004.

[31]   J. Akhtar, R. F. Mehmood, M. A. Malik, N. Iqbal, P. O'Brien, and J. Raftery, "A novel single source precursor: [bis(N,N-diethyl-N'-naphthoyl-selenoureato)palladium(II)] for palladium selenide thin films and nanoparticles.," *Chem. Commun. (Camb).*, vol. 47, no. 6, pp. 1899–901, 2011.

[32]   G. Liu and H. Zhang, "Facile Synthesis of Carbon-Supported Ir x Se y Chalcogenide Nanoparticles and Their Electrocatalytic Activity for the Oxygen Reduction Reaction," pp. 2058–2065, 2008.

[33]   M. Grydlik, F. Hackl, H. Groiss, M. Glaser, A. Halilovic, T. Fromherz, W. Jantsch, F. Schäffler, and M. Brehm, "Lasing from Glassy Ge Quantum Dots in Crystalline Si," *ACS Photonics*, vol. 3, no. 2, pp. 298–303, 2016.

[34]   C. C. Shen and W. L. Tseng, "One-step synthesis of white-light-emitting quantum dots at low temperature," *Inorg. Chem.*, vol. 48, no. 18, pp. 8689–8694, 2009.

[35]   M. M. Tavakoli, H. Aashuri, A. Simchi, S. Kalytchuk, and Z. Fan, "Quasi Core/Shell Lead Sulfide/Graphene Quantum Dots for Bulk Heterojunction Solar Cells," *J. Phys. Chem. C*, vol. 119, no. 33, pp. 18886–18895, 2015.

[36]   D. Deng, J. Cao, L. Qu, S. Achilefu, and Y. Gu, "Highly luminescent water-soluble quaternary Zn-Ag-In-S quantum dots for tumor cell-targeted imaging.," *Phys. Chem. Chem. Phys.*, vol. 15, no. 14, pp. 5078–83, 2013.

[37]   C. W. Kuo, D. Y. Chueh, N. Singh, F. C. Chien, and P. Chen, "Targeted nuclear delivery using peptide-coated quantum dots," *Bioconjug. Chem.*, vol. 22, no. 6, pp. 1073–1080, 2011.

[38]   O. Lahad, N. Meir, I. Pinkas, and D. Oron, "Long-lived population inversion in isovalently doped quantum dots," *ACS Nano*, vol. 9, no. 1, pp. 817–824, 2015.

[39]   I. A. Mir, K. Das, K. Rawat, and H. B. Bohidar, "Hot injection versus room temperature synthesis of CdSe quantum dots: A differential spectroscopic and bioanalyte sensing efficacy evaluation," *Colloids Surfaces A Physicochem. Eng. Asp.*, vol. 494, pp. 162–169, 2016.

[40]   O. M. Primera-Pedrozo, Z. Arslan, B. Rasulev, and J. Leszczynski, "Room temperature synthesis of PbSe quantum dots in aqueous solution: stabilization by interactions with ligands.," *Nanoscale*, vol. 4, no. 4, pp. 1312–20, 2012.

[41]   S. Rong, P. Zhang, Y. Yang, and F. Liu, "Room temperature synthesis of manganese oxide quantum dots and their application as a fluorescent probe for the detection of metal ions in aqueous media," *RSC Adv.*, vol. 6, no. 115, pp. 114632–114638, 2016.

[42]   E. Oh, R. Liu, A. Nel, K. B. Gemill, M. Bilal, Y. Cohen, and I. L. Medintz, "Meta-analysis of cellular toxicity for cadmium-containing quantum dots," *Nat Nano*, vol. 11, no. 5, p. doi:10.1038/nnano.2015.338, 2016.

[43]   W. E. Smith, J. Brownell, C. C. White, Z. Afsharinejad, J. Tsai, X. Hu, S. J. Polyak, X. Gao, T. J. Kavanagh, D. L. Eaton, and S. E. T. Al, "In Vitro Toxicity Assessment of Human Liver Cell Models," no. 11, pp. 9475–9484, 2012.

[44]   I. a. Minigalieva, B. a. Katsnelson, V. G. Panov, L. I. Privalova, A. N. Varaksin, V. B. Gurvich, M. P. Sutunkova, V. Y. Shur, E. V. Shishkina, I. E. Valamina, I. V. Zubarev, O. H. Makeyev, E. Y. Meshtcheryakova, and S. V. Klinova, "In vivo toxicity of copper oxide, lead oxide and zinc oxide nanoparticles acting in different combinations and its attenuation with a complex of innocuous bio-protectors," *Toxicology*, vol. 380, pp. 72–93, 2017.

[45]   S. Skalickova, V. Milosavljevic, K. Cihalova, P. Horky, L. Richtera, and V. Adam, "Selenium nanoparticles as a nutritional supplement," *Nutrition*, vol. 33, pp. 83–90, 2016.

[46]   T. H. D. Nguyen, B. Vardhanabhuti, M. Lin, and A. Mustapha, "Antibacterial properties of selenium nanoparticles and their toxicity to Caco-2 cells," *Food Control*, vol. 77, pp. 17–24, 2017.

[47]   X. Fang, X. Wu, C. Li, B. Zhou, X. Chen, T. Chen, and F. Yang, "Targeting selenium nanoparticles combined with baicalin to treat HBV-infected liver cancer," *RSC Adv.*, vol. 7, no. 14, pp. 8178–8185, 2017.

[48]   H. Su, D. D. Liu, M. Zhao, W. L. Hu, S. S. Xue, Q. Cao, X. Y. Le, L. N. Ji, and Z. W. Mao, "Dual-enzyme characteristics of polyvinylpyrrolidone-capped iridium nanoparticles and their cellular protective effect against H2O2-induced oxidative damage," *ACS Appl. Mater. Interfaces*, vol. 7, no. 15, pp. 8233–

8242, 2015.

[49]   A. a. Gambardella, N. S. Bjorge, V. K. Alspaugh, and R. W. Murray, "Voltammetry of diffusing 2 nm iridium oxide nanoparticles," *J. Phys. Chem. C*, vol. 115, no. 44, pp. 21659–21665, 2011.

[50]   G. Liu and H. Zhang, "Facile Synthesis of Carbon-Supported Ir x Se y Chalcogenide Nanoparticles and Their Electrocatalytic Activity for the Oxygen Reduction Reaction," *J. Phys. Chem. C*, vol. 112, pp. 2058–2065, 2008.

[51]   S. Kurbanoglu, L. Rivas, S. a. Ozkan, and A. Merkoci, "Electrochemically reduced graphene and iridium oxide nanoparticles for inhibition-based angiotensin-converting enzyme inhibitor detection," *Biosens. Bioelectron.*, vol. 88, pp. 122–129, 2017.

[52]   D. Xu, P. Diao, T. Jin, Q. Wu, X. Liu, X. Guo, H. Gong, F. Li, M. Xiang, and Y. Ronghai, "Iridium Oxide Nanoparticles and Iridium/Iridium Oxide Nanocomposites: Photochemical Fabrication and Application in Catalytic Reduction of 4-Nitrophenol," *ACS Appl. Mater. Interfaces*, vol. 7, no. 30, pp. 16738–16749, 2015.

[53]   D. L. Klayman and T. S. Griffin, "Reaction of Selenium with Sodium Borohydride in Protic Solvents. A Facile Method for the Introduction of Selenium into Organic Molecules," *J. Am. Chem. Soc.*, vol. 2, no. 1, pp. 197–199, 1973.

[54]   W. Chen and S. Chen, "Iridium-platinum alloy nanoparticles: Composition-dependent electrocatalytic activity for formic acid oxidation," *J. Mater. Chem.*, vol. 21, no. 25, p. 9169, 2011.

[55]   L. Jimanez-Hernendez, O. Estavez-Hernandez, M. Hernandez-Sanchez, J. a. Diaz, M. Farias- Sanchez, and E. Reguera, "3-mercaptopropionic acid surface modification of Cu-doped ZnO nanoparticles: Their properties and peroxidase conjugation," *Colloids Surfaces A Physicochem. Eng. Asp.*, vol. 489, no. November, pp. 351–359, 2016.

[56]   Y. Li and N. Chopra, "Fabrication of nanoscale heterostructures comprised of graphene-encapsulated gold nanoparticles and semiconducting quantum dots for photocatalysis," *Phys. Chem. Chem. Phys.*, vol. 17, no. 19, pp. 12881–12893, 2015.

[57]   R. Enhanced, T. Alloys, R. P. P. Compound, H. T. Superconductors, P. Electrodes, A. Sensor, P. Group, M. Conference, N. Palladium, P. Catalyst, N. A. Plants, and N. Patents, "Platinum Metals Review," *Platin. Met. Rev.*, vol. 52, no. 1, pp. 54–62, 2008.

[58]   L. Brus, "Electronic wave functions in semiconductor clusters: experiment and theory," *J. Phys. Chem.*, vol. 90, no. 12, pp. 2555–2560, 1986.

[59]   J. Hambrock, A. Birkner, and R. a Fischer, "Synthesis of CdSe nanoparticles using various organometallic cadmium precursors," *J. Mater. Chem.*, vol. 11, no. 12, pp. 3197–3201, 2001.

[60]   B. Pejova and I. Grozdanov, "Three-dimensional confinement effects in semiconducting zinc selenide quantum dots deposited in thin-film form," *Mater. Chem. Phys.*, vol. 90, no. 1, pp. 35–46, 2005.

[61]   N. Gaponik, S. K. Poznyak, N. P. Osipovich, A. Shavel, and A. Eychmüller, "Electrochemical probing of thiol-capped nanocrystals," *Microchim. Acta*, vol. 160, no. 3, pp. 327–334, 2008.

[62]   M. J. N. Pourbaix, J. Van Muylder, N. de Zoubov, and C. Protection, "Electrochemical properties of the platinum metals," *Platin. Met. Rev.*, vol. 3, no. 2, pp. 47–53, 1959.

59

CHAPTER 3B

One pot synthesis of novel rhodium selenide quantum dot, nanoshells, and nanorods

Abstract

Simultaneous synthesis of rhodium selenide quantum dot and nanoshells has been accomplished utilizing a very simple and water-based approach. The nanoshells were then confirmed utilizing high-resolution transition electron microscope (HRTEM) whereby with sizes ranging from 15 - 20 nm. The HRTEM of the RhSe quantum dot revealed that very narrow sized particles of 3.5 nm have been simultaneously formed. The nanocrystals were then further characterized utilizing UV-vis spectroscopy, energy dispersive X-ray, SAED, solid-state carbon nuclear magnetic resonance (SS-CNMR). RhSe networks within carbon screen-printed electrodes were studied utilizing high resolution scanning electron microscope HRSEM equipped with backscattering (BSE). The SEM-BSE revealed that RhSe quantum dot, due to their narrow size interwoven themselves into nanotubes of about 251 nm in diameter within the electrode instead of on top of the electrodes, into vein-like networks. The flow behavior of the nanocrystals in water has been investigated using Rheometer and a decrease in viscosity with increasing applied pressure (shear thinning) has been observed, an ideal behavior for biological applications or nanofluids.

Keywords: Rhodium Selenide, Quantum dot, nanoshells, nanotubes, high-resolution transmission electron microscope, high resolution scanning electron microscope

3B.1 Experimental section

Reagents

Analytical grade 3-mercaptopropionic acid ($HSCH_2CH_2CO_2H$, 3-MPA), sodium hydroxide, selenium powder, sodium borohydrate, sodium hexachloro-rhodate (III), disodium hydrogen phosphate, sodium dihydrogen phosphate, potassium chloride, lithium perchlorate, DMSO, absolute ethanol, were all purchased from Sigma-Aldrich (Cape Town, South Africa). All chemicals were utilized without further purification.

Simultaneous synthesis of 3 mercaptopropionic acid capped Rhodium Selenide Qd and shells

NaHSe precursor was prepared by mixing 0.16 g of Se powder with 0.15 g of $NaBH_4$ in a round bottom flask and adding de-ionized water to make a 100 mL solution containing 0.02 M Se and 0.04 M $NaBH_4$ room temperature. The mixture was then stirred vigorously at room temperature under nitrogen for 30 min until an orange colored solution was obtained. In a separate flask 0.04 M Rh^{III} precursor solution was prepared by dissolving Na_3RhCl_6 to which 69.60 μL of 3MPA was added. The pH of the mixture was adjusted to pH12 using NaOH and saturated with N_2 for 30 min. Then the freshly prepared NaHSe was injected into the red Rh-3MPA complex solution and the reaction was continued to stirring under nitrogen for 1 hour and 30 min and after which the cream brown solution was formed. The Qd and shells were precipitated five times with absolute ethanol and stored at -18℃.

Preparation of quantum dot nano-rods in screen-printed electrodes

On new (Drop-sense) carbon screen-printed electrodes 1 ml of quantum dot was drop coated and incubated for 24 hrs at varied temperatures i.e room temperature and 40 degrees in the oven.

61

Instruments

High-resolution transmission electron microscopy (HR-TEM), selected area electron diffraction (SAED) and energy dispersive x-ray spectroscopy were performed utilizing a Field emission transmission electron microscope Tacnai G2 F20X-Twin MAT 200 kV from FEI (Eindhoven, NL), Electron Microscopy Unit, Physics, at UWC. The experiments were performed on a copper grid. High resolution scanning electron microscopy and backscattering electron signal (BSE) were performed on AURIGA microscope, also in Electron Microscopy Unit, Physics, at UWC.

Ultraviolet-visible (UV-vis) absorption measurements were performed on a Nicolet Evolution 100 UV visible spectrometer (Thermo Electron, UK), utilizing quartz cuvette. All UV-Vis experiments were performed in solution. Photoluminescence spectroscopy was performed utilizing a Horiba NanoLogTM 3-22-TRIAX (USA), with double grating excitation and emission monochromators at a slit width of 5 nm. All PL measurements were performed in dimethyl sulfoxide. Raman spectroscopy was performed utilizing Horiba scientific, Xplora, Olympus TH4-200 with Horiba Diode-pumped solid-state (DPSS) at a wavelength of 534 nm with samples prepared on glass slides

All voltammetry experiments were carried using a BAS 100W integrated and automated electrochemical workstation obtained from BioAnalytical Systems (BAS), Lafayette, USA. A 10 mL cell comprising a 0.0201 cm^2 gold working electrode from BAS, Pt wire auxiliary electrode from Sigma Aldrich and Ag/AgCl (3 M KCl type) from BAS was used in all electrochemical studies. The Au working electrode was polished with alumina micro polish from Buehler, IL, USA.

Rheological experiments were performed utilizing Anton Paar TwinDrive Rheometer MCR 702, Geometries: Lower Plate - L PP50 (lower parallel plate 50 mm diameter), Upper Plate - CP25 (parallel plate 50 mm diameter)

3B.2 Results and discussion

3B.2.1 Simultaneous synthesis of RhSe quantum dot and nanoshells

Simultaneous synthesis of RhSe quantum and nanoshells has been accomplished utilizing a very simple and water-based approach. Room temperature synthesis of the RhSe quantum dot is achieved utilizing a bottom-up wet chemistry approach, similar to that used in the synthesis of IrSe. The synthesis began with the preparation of NaHSe, black elemental selenium is reduced with 2 equivalents of $NaBH_4$ in water to obtain the orange selenium source which forms very rapidly at room temperature.[53] The reaction is then kept in an oxygen-free environment to avoid the oxidation of the oxygen-sensitive Se ion. Thereafter, to initiate the nucleation and growth of the quantum dot, the freshly prepared NaHSe is injected into the Rh-MPA complex at a basic pH (12), with Na_3RhCl_6 utilized as the rhodium ion precursor. The reaction was continued to stir for a period of 4.5 hours. As shown in figure 9, after the injection of NaHSe, the reaction mixture changed from bright red color to powdery pink at the 60th minute, turned yellow after a 1 hour 30 min and after 4.5 hof stirring the reaction remained brown to light brown. The quantum dot formed within the first 60 min whilst the shells formed after the 1.5 hof stirring.
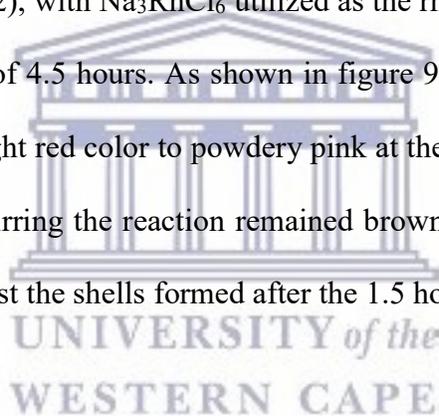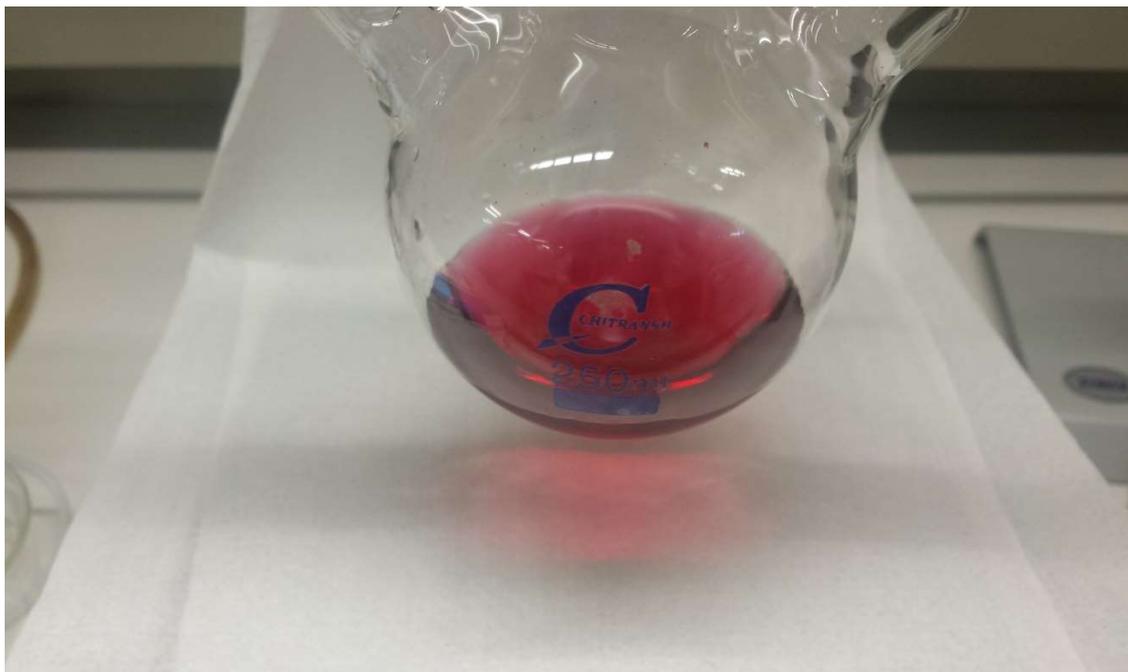
A)40 min NaRhCl$_6$ precursor

B) 1.30 h

C) 2.5 hNa$_3$RhCl$_6$

D)

Figure 8 Synthesis of RhSe quantum dot and nanoshells whereby A) before injection of the Selenium precursor, B) after 60 min of reaction stirring, C) 1 hour 30 min of stirring, D) after 4 h30 min of stirring.

3B.2.2 Structural and morphological properties RhSe quantum dot and nanoshells

The morphology and crystallinity of the RhSe quantum dot were investigated utilizing high-resolution transmission electron microscopy (HRTEM) and selected area electron diffraction. The HRTEM of the RhSe quantum dot shown in figure 9 revealed that very narrow sized spherical particles of 3.5 nm have been simultaneously formed. Similar to IrSe quantum dot, the RhSe colloids are quasi-dispersed and display a quasi-spherical morphological structure. High-resolution transition electron microscope (HRTEM) investigation of the nano-shells shown in figure 10 revealed well-dispersed hollow spheres ranging from 15-20 nm, with the outer-shell containing lattice fringes which discontinue within the spheres.

66
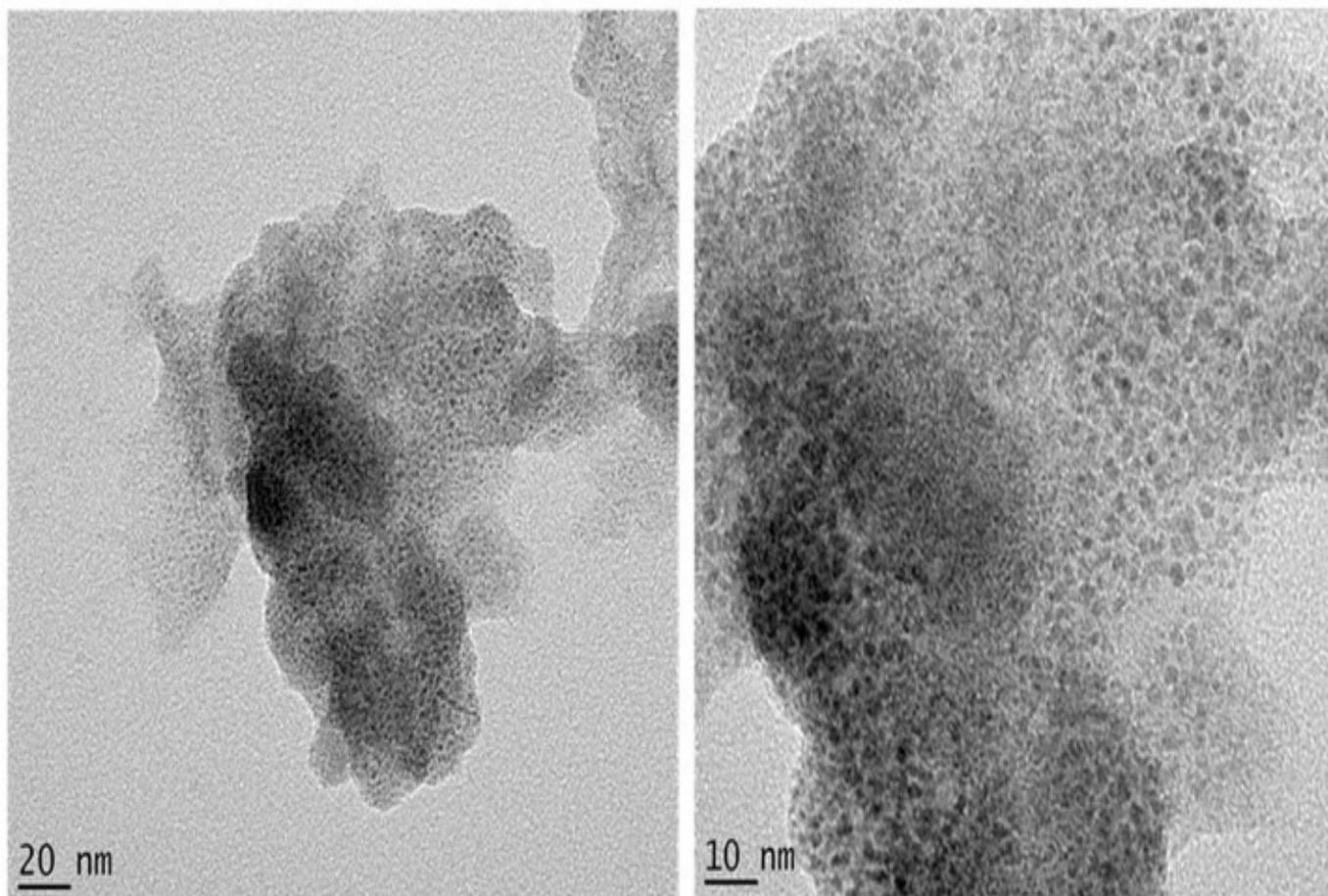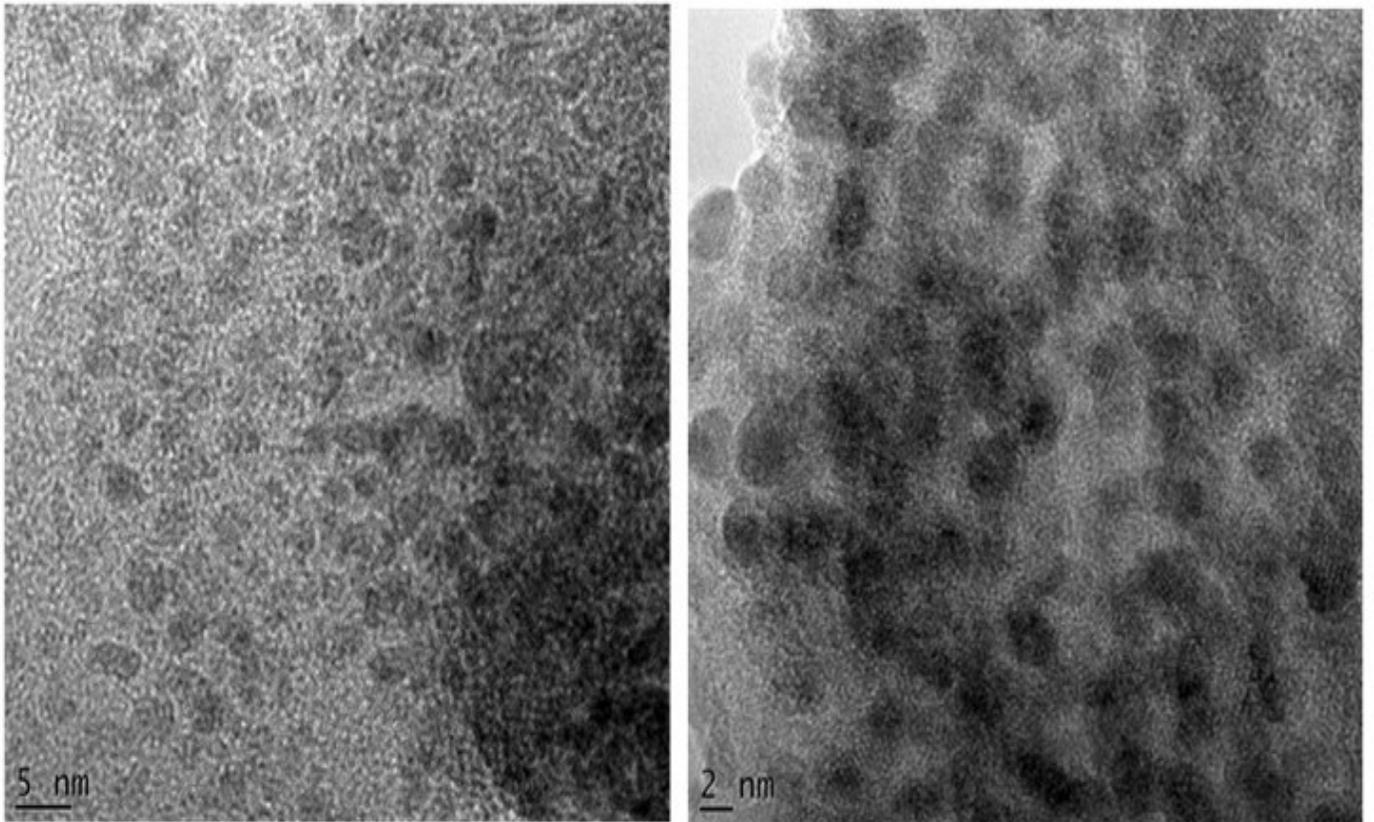
Figure 9 HRTEM of RhSe quantum dot at 20 -2nm scale on a copper grid
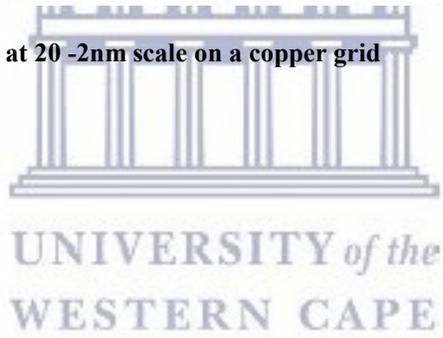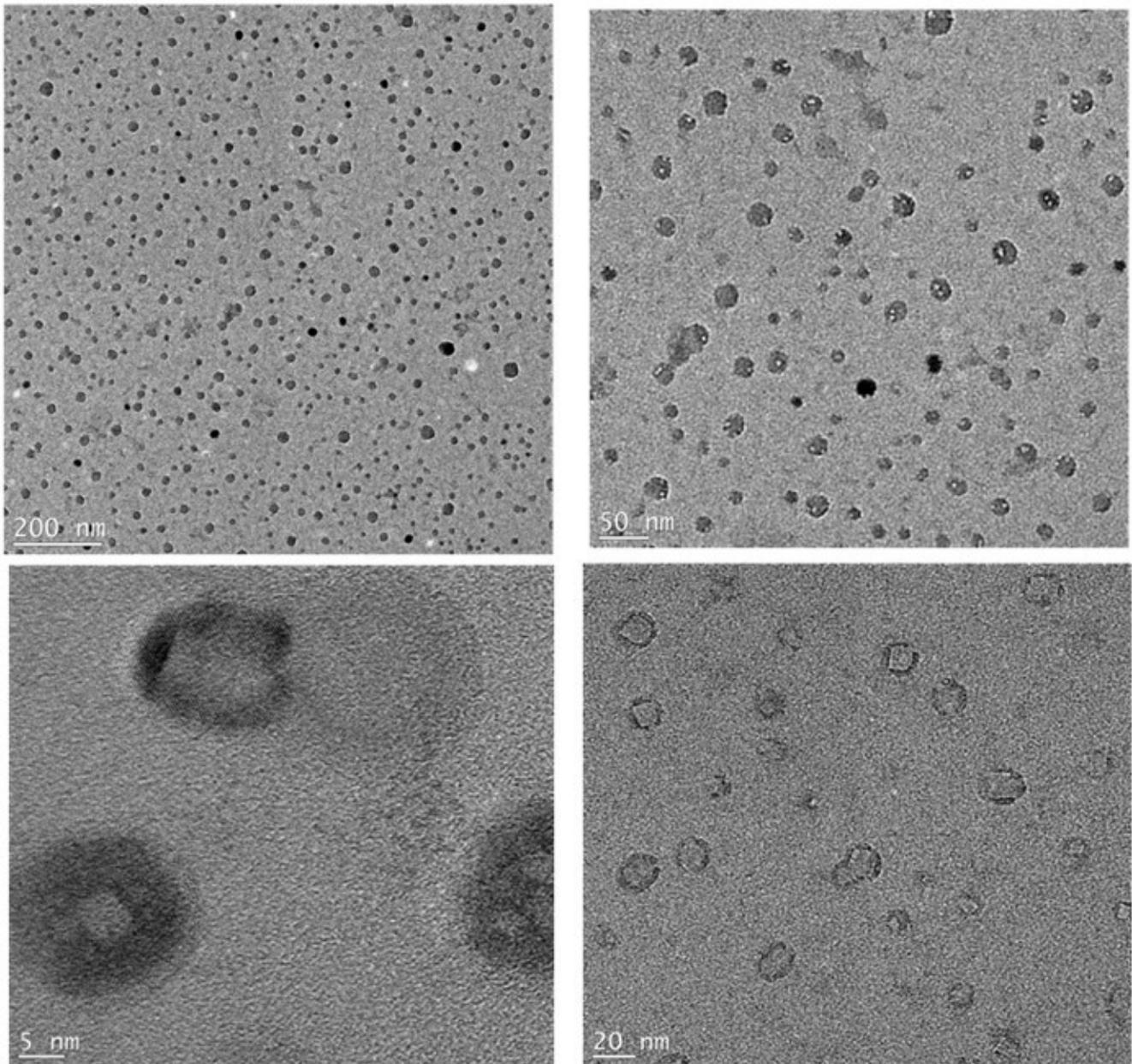
Figure 10 HRTEM of RhSe nanoshells at 200-5 nm scale on a copper grid

The elastic scattering of electrons from crystalline material is observable utilizing selected area electron diffraction (SAED). The SAED pattern of the RhSe quantum dot shown in figure 10 revealed clear rings and spots, a typical diffraction behavior of polycrystalline material such as semiconductors indicating that they are poly-nanocrystalline. The bright spots arise from the Bragg reflection from individual crystallites consistent with the observations made from HRTEM analysis.

68
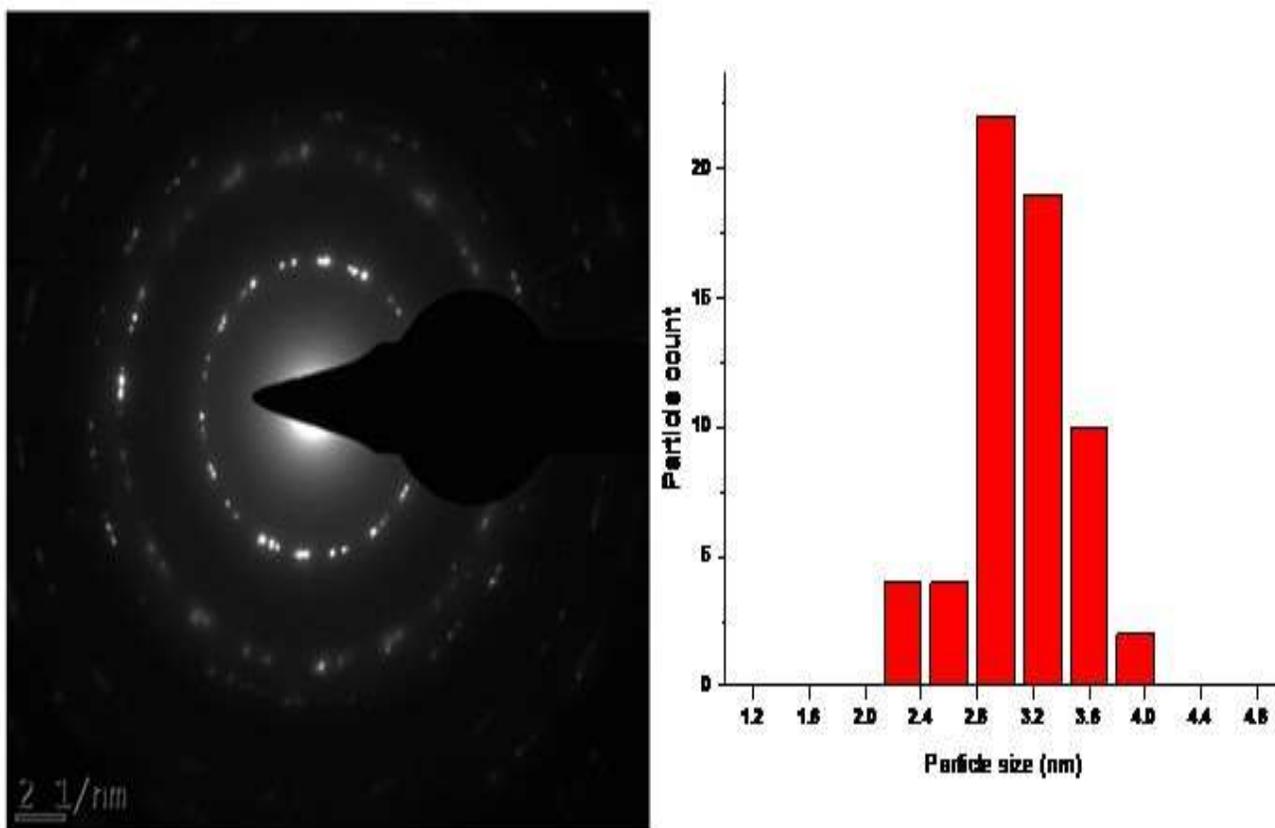
Figure 11 SAED of the RhSe quantum dot and histogram

Furthermore, Energy Dispersive X-ray spectroscopy (EDX) was used to study the elemental composition of the RhSe nanoshells and the quantum dot. The EDX of the nanoshell shown in Figure 12, reveals that the dominant is peak rhodium arising from the nanoshells with the selenium also appearing in the spectrum selenium. The carbon, sulfur, and oxygen arise from the mercaptopropionic acid capping agent and the copper peak arises from the grid on which the spectrum is recorded.

In figure 3, the EDX of the RhSe quantum dot is shown, revealing the peaks of rhodium and selenium arising from the RhSe Qd core. Similar to the nanoshells the carbon, sulfur, and oxygen arise from the mercaptopropionic acid capping agent peak of copper arises from the grid on which the spectrum is recorded. A close investigation of the rhodium to selenium ratio composition of the nanoshells verses the

quantum dot reveal that the nanoshells have a composition of 100:1 (Rh:Se) and quantum dot, whilst the quantum dot have a composition of about 50:50. This indicates that the nanoshells are mainly composed of rhodium as the first formed within 60 min of the reaction, whilst the quantum dot formed later starting at the 1 hour and 30th minute.
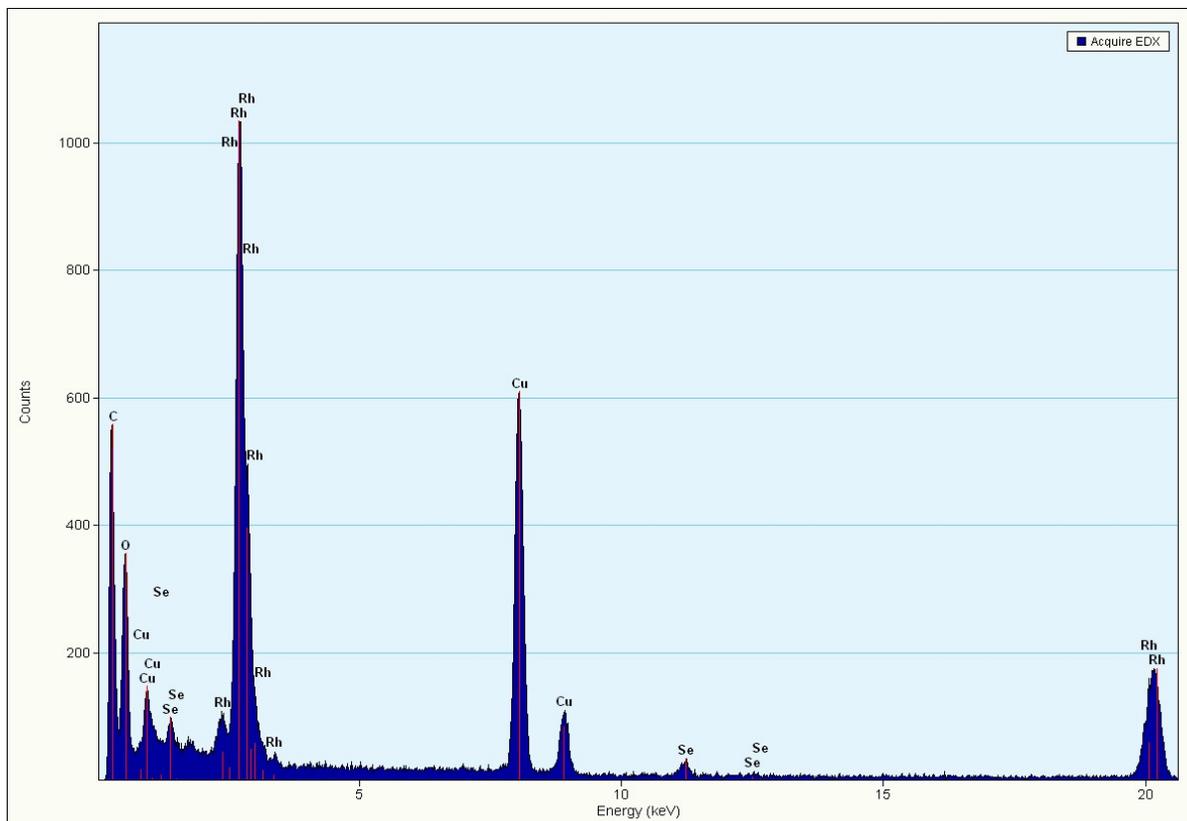
Figure 12 EDX of 3-MPA-RhSe nano-shells taken on copper grid (Cu)
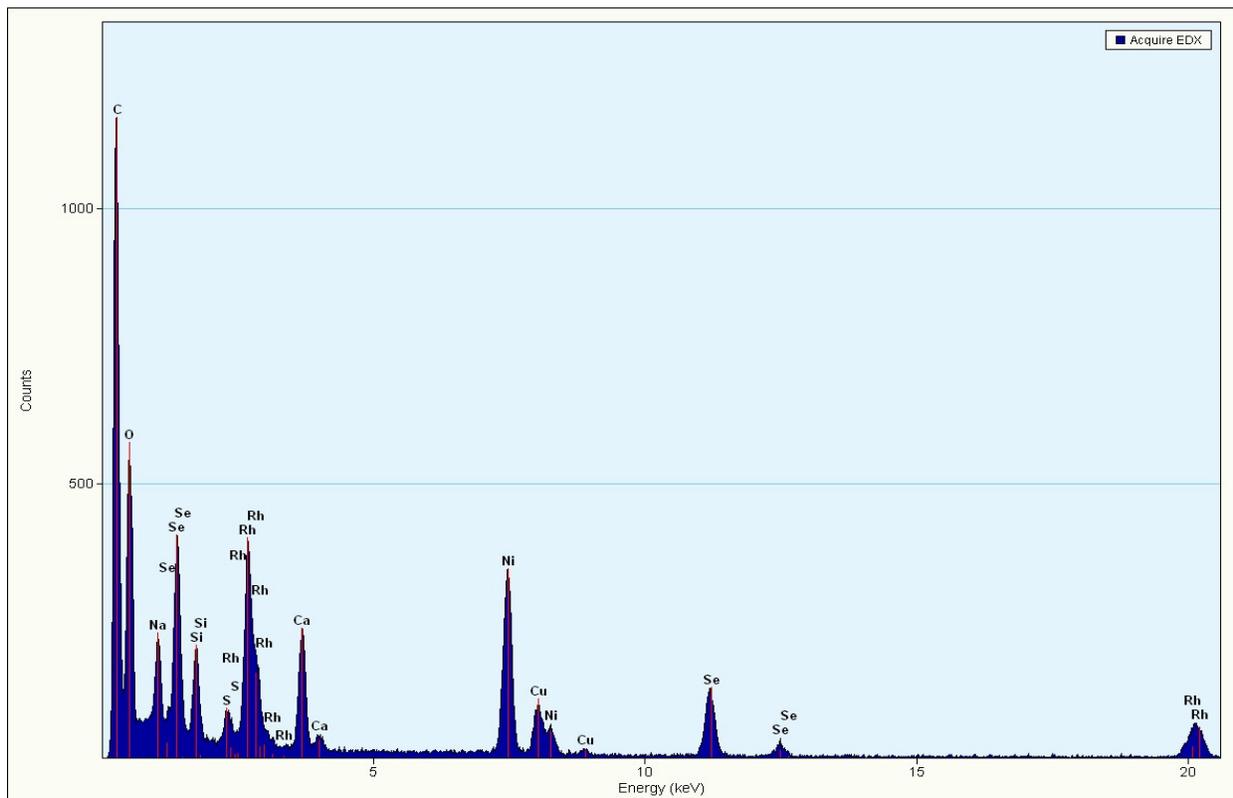
Figure 13 Energy dispersive X-ray spectroscopy of RhSe quantum dot on a copper grid
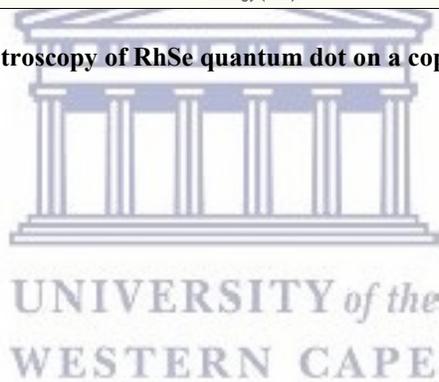
3B.2.3 Solid state CNMR of solid 3 MPA –RhSe quantum dot
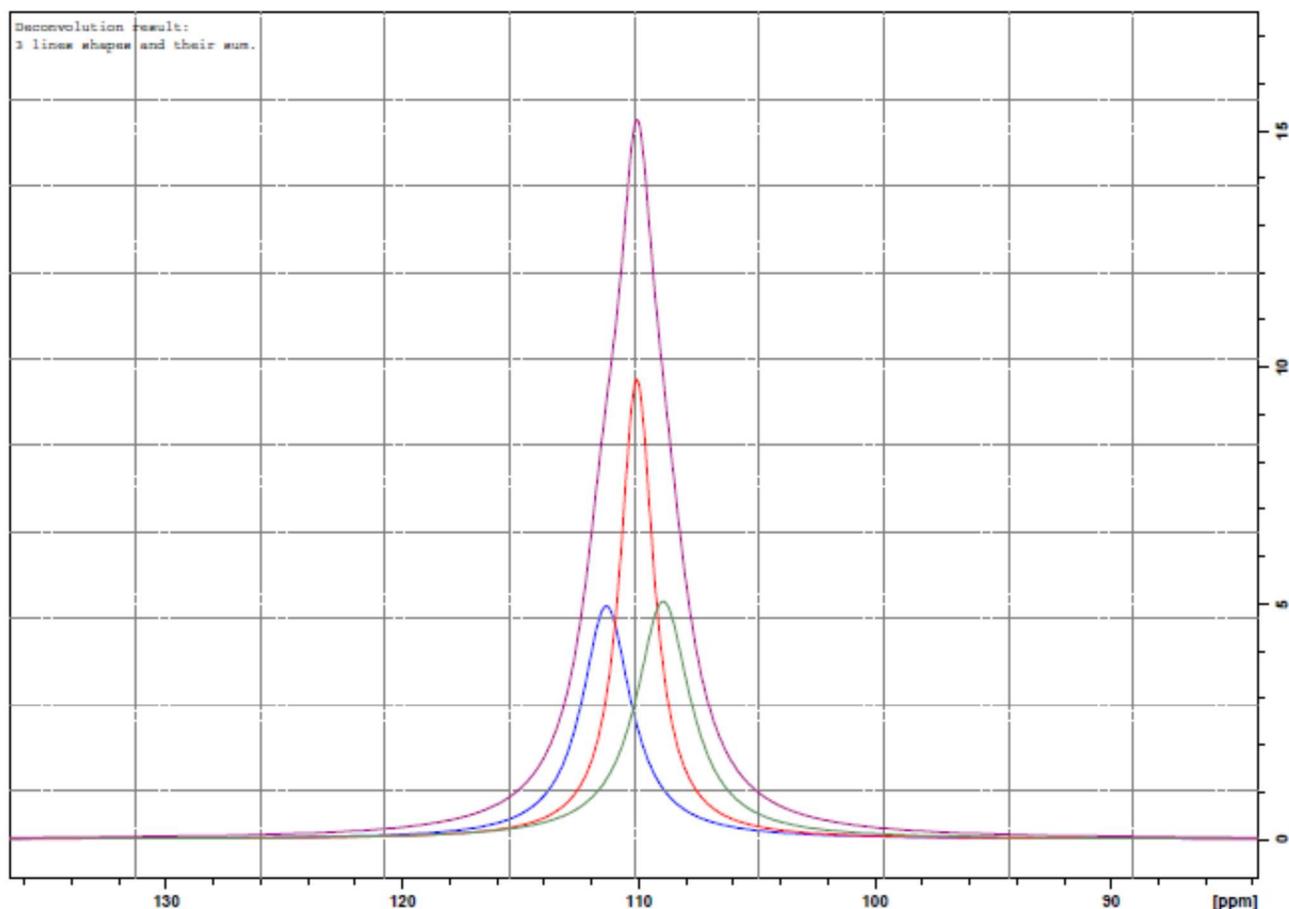
Solid state carbon nuclear magnetic resonance was utilized to further characterize the solid 3-MPA-RhSe quantum dot. After precipitation and drying the quantum dot in vacuum overnight the powder was analyzed utilized solid-state carbon nuclear magnetic resonance as shown in the figure. The spectra reveal the presence of the 3 carbons arising from the mercaptopropionic acid at 110 ppm after deconvolution of the broad peak. The peaks appeared shifted from the expected region and localized at 110 ppm, a region topical for alkene. This might be due to the electron delocalization throughout the whole propanoic acid backbone and due to the highly charged environment around the Rhodium selenide core. This further

confirmed the successful capping of the quantum dot with 3-mercaptopropionic acid, as was indicated by the EDX elemental analysis.

3B.2.4 Optical studies of the formation of RhSe quantum dot

The optical study of the formation of RhSe Qd was studied utilizing UV-vis. Figure 14 shows the absorbance of the RhSe quantum dot at different time intervals within the duration of the reaction. The spectra reveal that the RhSe quantum dot formation started after the 40 minute of stirring with the appearance of the absorption peak at 240 nm with a full width at half maxima (FWHM) of 31 nm. After 1 hour 30 min of stirring the absorption peak intensity increased whilst remaining at 240 nm with a full width at half maxima (FWHM) of 25. At 4 h30 min of stirring the absorption peak intensity at 240 nm increased with a full width at half maxima (FWHM) of 15 nm. Comparison of the absorption peak intensity and decrease in FWHM indicates that the uniformity of the particles and homogeneity improved with increasing reaction time, suggesting that the optimum reaction time for the synthesis of the Rhse quantum dot is 4 h30 min.

The optical band gap of the IrSe quantum dot is 6.2 eV which is calculated by extrapolation of the linear region to $\alpha hv=0$ of the taucs plot $(\alpha hv)^2$ versus (hv) as shown in Figure 14 and expressed in the following equation:

$$\alpha hv = C(hv-Eg)^n$$

Where "α" is the absorption coefficient, hv the photon energy and gap energy, A is a constant, Eg is the band gap energy and n=1/2 for allowed direct transitions observable in quantum dot. The optical band gap of the Rhodium Selenide quantum dot is two times larger than the optical band gap of Iridium Selenide quantum dot
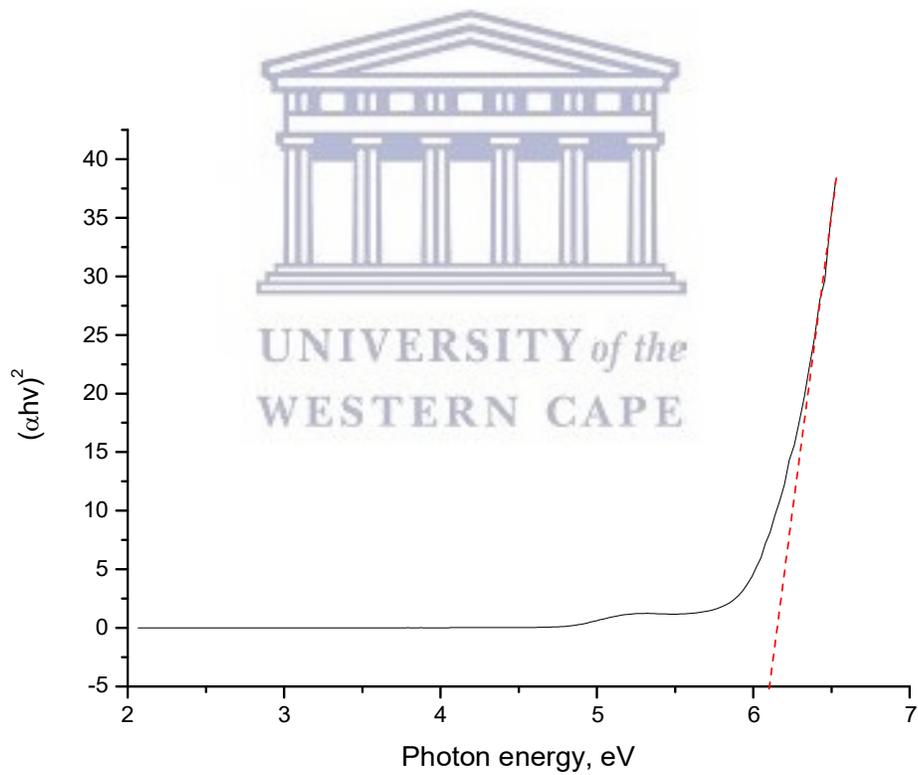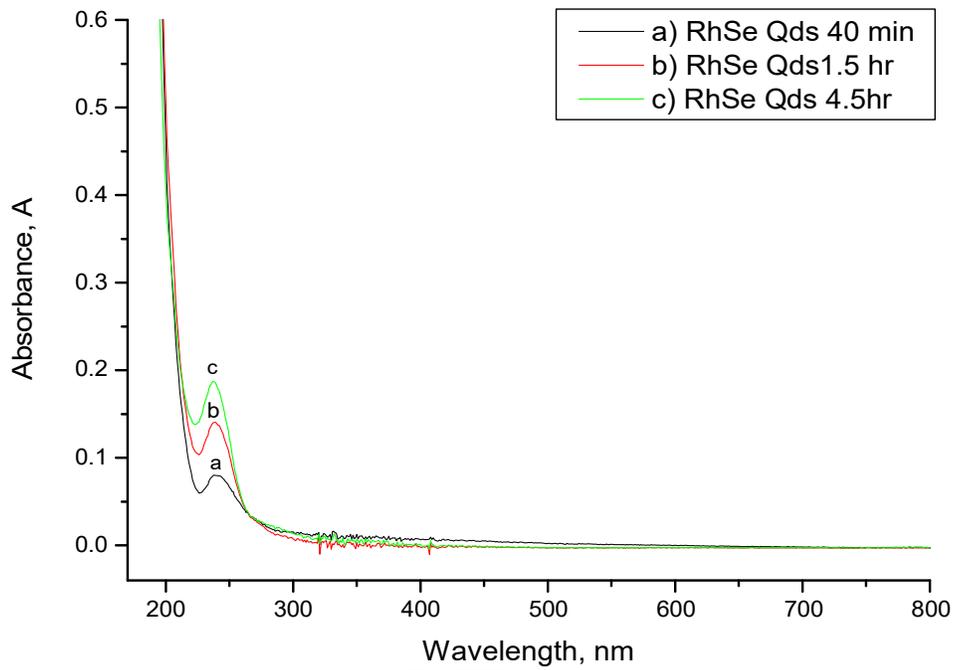
73

Figure 14 (Above) UV-vis spectroscopy of RhSe quantum dot taken at time intervals, **(Below)** Taucs plot of the band gap of the RhSe quantum dot

3B.2.5 Rheological study of RhSe quantum dot in solution (Flow curve)

The rheological behavior of the RhSe quantum dot nanocrystals in water ("nanofluid") has been investigated. The flow curve of the RhSe quantum dot exhibited a decrease in viscosity with increasing pressure shear thinning i.e non-Newtonian behavior as shown in figure 16. The rheological flow pattern of any fluid is explained in terms of the relationship between shear rate (γ) and shear stress (τ). The tangential force applied per unit area is defined as the shear stress and the change of shear strain per unit time is the shear rate. The viscosity (η) is the ratio of shear stress to a shear rate which is a measure of the resistance produced by the measuring plates to one another for the period of the flow of liquid suspension. The flow behavior exhibited by the RhSe quantum dot solution is an ideal behavior for fluids that have potential use as biomarkers as it requires sample injection thus a thining of the sample with applied pressure is ideal, and also as nano-fluids.
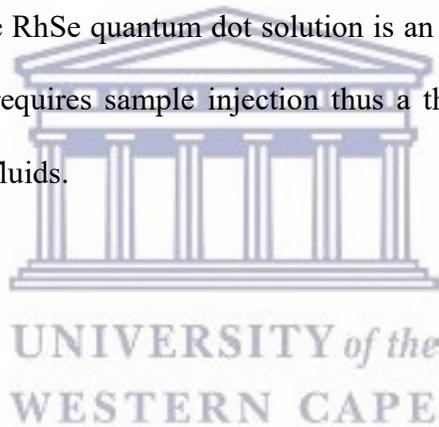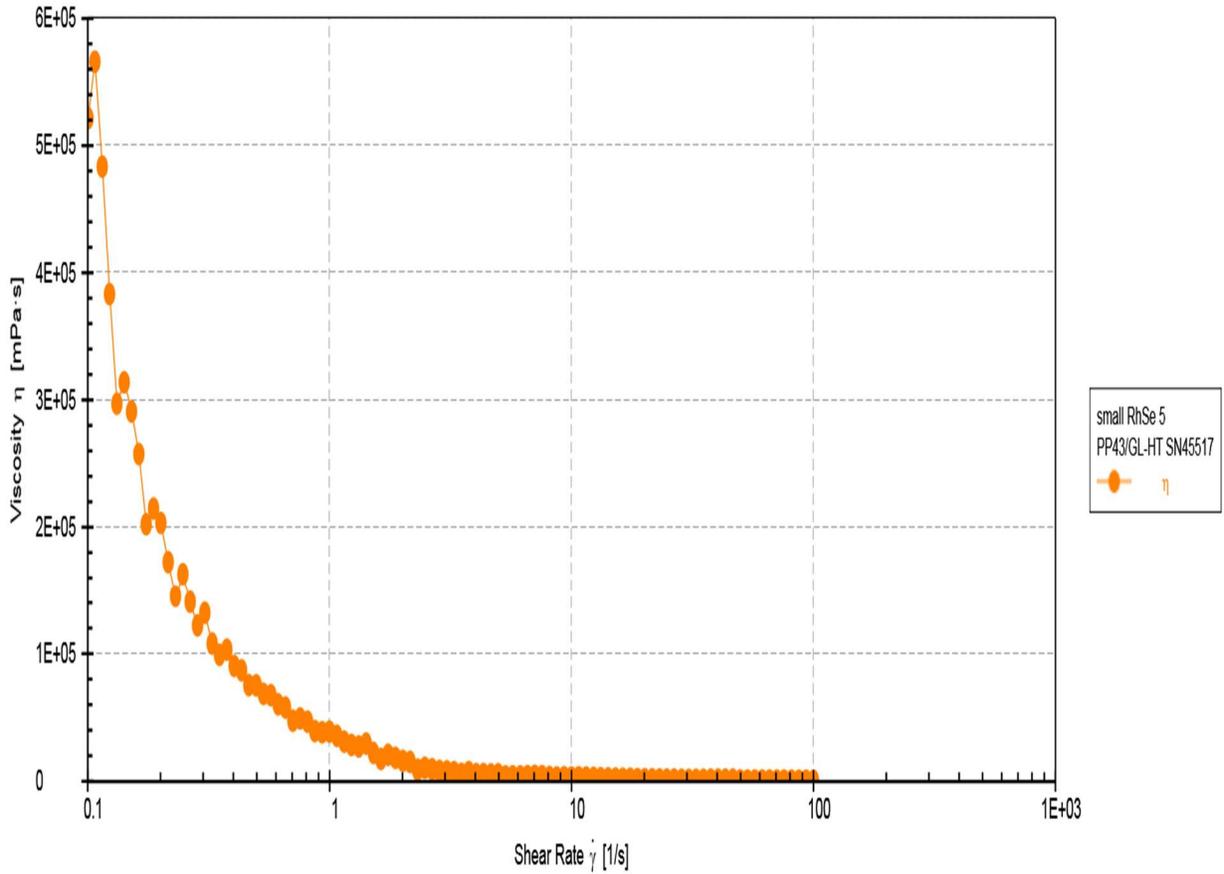
Figure 15 Flow curve and behavior of RhSe Qd under shear stress
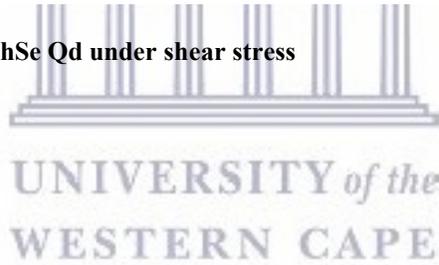
Point No.	Shear Rate	Shear Stress	Viscosity	Torque
	[1/s]	[Pa]	[Pa·s]	[mN·m]
1	0.1	52.377	521.3	1.2251
2	0.107	60.667	565.83	1.419
3	0.115	55.589	483.33	1.3002
4	0.123	47.228	383	1.1047
5	0.132	39.236	296.76	0.91773
6	0.142	44.464	313.62	1.04
7	0.152	44.172	290.62	1.0332
8	0.163	41.923	257.23	0.9806
9	0.175	35.301	201.98	0.8257
10	0.187	40.171	214.34	0.93961
11	0.201	40.788	203.02	0.95404
12	0.215	37.096	172.18	0.86769

13	0.231	33.5	145.01	0.78358
14	0.248	40.296	162.68	0.94253
15	0.266	37.28	140.37	0.87198
16	0.285	34.715	121.86	0.81199
17	0.305	40.236	131.76	0.94112
18	0.327	35.234	107.61	0.82413
19	0.351	34.679	98.762	0.81114
20	0.376	38.715	102.83	0.90555
21	0.404	36.366	90.075	0.85062
22	0.433	37.509	86.654	0.87734
23	0.464	34.803	74.983	0.81404
24	0.498	37.262	74.859	0.87158
25	0.534	36.333	68.09	0.84985
26	0.572	38.385	67.071	0.89783
27	0.613	36.8	59.984	0.86076
28	0.658	37.799	57.452	0.88414
29	0.706	33.28	47.167	0.77843
30	0.756	36.95	48.858	0.86426
31	0.811	37.616	46.37	0.87984
32	0.87	33.955	39.041	0.79421
33	0.933	35.541	38.112	0.83132
34	1	38.605	38.608	0.90297
35	1.07	37.878	35.322	0.88599
36	1.15	35.347	30.739	0.82677
37	1.23	34.666	28.121	0.81084
38	1.32	35.684	26.996	0.83467
39	1.42	41.403	29.223	0.96843
40	1.52	33.312	21.918	0.77917
41	1.63	28.026	17.188	0.65553
42	1.75	35.704	20.438	0.83513
43	1.87	33.809	18.047	0.7908
44	2.01	31.397	15.623	0.73439
45	2.15	31.998	14.863	0.74844
46	2.31	20.28	8.7699	0.47435
47	2.48	25.305	10.216	0.5919
48	2.65	24.083	9.0714	0.5633
49	2.85	22.125	7.7657	0.51752
50	3.05	22.783	7.4607	0.53289
51	3.27	22.215	6.7857	0.51963
52	3.51	19.409	5.526	0.45399
53	3.76	25.898	6.8831	0.60577
54	4.04	21.277	5.2679	0.49768
55	4.33	23.068	5.332	0.53957
56	4.64	23.414	5.0427	0.54765
57	4.98	25.744	5.1738	0.60216
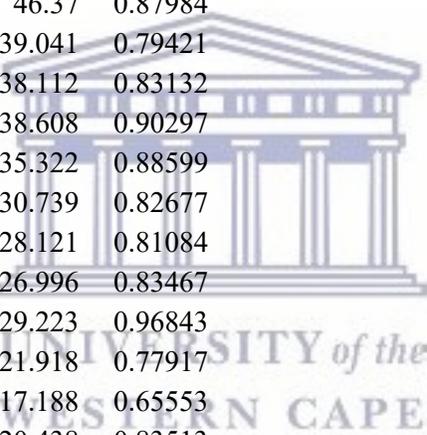
58	5.34	18.337	3.435	0.4289
59	5.72	20.267	3.5431	0.47404
60	6.14	21.333	3.4749	0.49898
61	6.58	24.287	3.6916	0.56807
62	7.05	27.325	3.8762	0.63915
63	7.56	27.561	3.6436	0.64467
64	8.11	24.346	3.0012	0.56945
65	8.69	23.062	2.654	0.53944
66	9.32	27.029	2.9004	0.63221
67	10	26.632	2.6629	0.62293
68	10.7	30.019	2.802	0.70216
69	11.5	29.576	2.572	0.6918
70	12.3	28.14	2.2813	0.65819
71	13.2	27.683	2.0947	0.6475
72	14.2	27.246	1.9214	0.63729
73	15.2	26.788	1.7625	0.62659
74	16.3	26.799	1.644	0.62683
75	17.5	28.718	1.6426	0.67171
76	18.7	25.77	1.3749	0.60278
77	20.1	25.437	1.2656	0.59498
78	21.5	25.956	1.2048	0.60711
79	23.1	24.928	1.079	0.58308
80	24.8	24.021	0.96966	0.56185
81	26.6	26.156	0.98483	0.6118
82	28.5	23.952	0.84102	0.56024
83	30.5	23.131	0.75749	0.54103
84	32.7	27.036	0.82623	0.63237
85	35.1	28.975	0.82538	0.67774
86	37.6	36.515	0.97064	0.8541
87	40.4	38.701	0.95882	0.90524
88	43.3	41.878	0.96822	0.97955
89	46.5	46.973	1.0111	1.0987
90	49.8	18.649	0.37459	0.4362
91	53.4	15.32	0.28693	0.35833
92	57.2	16.504	0.28841	0.38604
93	61.4	17.89	0.29149	0.41845
94	65.8	18.52	0.28151	0.4332
95	70.6	19.146	0.27133	0.44782
96	75.7	17.168	0.22692	0.40157
97	81.2	14.294	0.1761	0.33433
98	87.1	11.218	0.12883	0.2624
99	93.3	10.063	0.10783	0.23538
100	100	8.8754	0.088662	0.2076
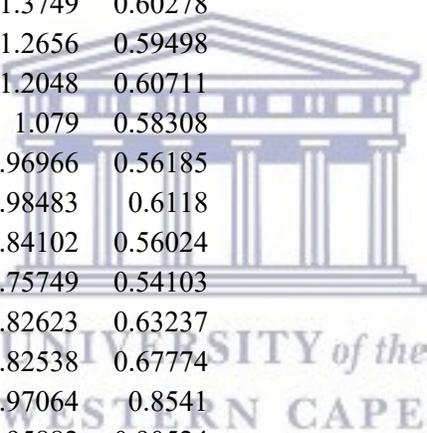
3B.2.6 SEM coupled with electron back scattering of RhSe quantum dot drop-coated on screen-printed carbon electrodes

The RhSe quantum dot were then utilized to grow semiconductor nanotubes and networks within carbon screen-printed at very mild temperatures Figure 9-17. The RhSe networks within the carbon screen-printed electrodes were the studied utilizing high resolution scanning electron microscope HRSEM equipped with backscattering electron (BSE). Under backscattering the metal components of the electrode showed contrast and appeared brighter than the carbon fiber thus allowing clear visibility and identification of the RhSe nanotubes. The SEM-BSE of a new bare carbon electrode without any quantum dot modification is shown in figure 17 whereby no metal is visible as was expected. After modification of the carbon electrode at room temperature, the quantum dot are visible seen under HRSEM-BSE dispersed across the surface of the electrode as shown in figure 18. At 40 degrees as shown in figure 19-25, the HRSEM-BSE revealed the RhSe quantum dot assembled themselves into vein-like ordered networks of nanotubes which are 251 nm in diameter formed within the screen-printed carbon. This is a typical behavior of rhodium-based nano-crystals as they have been reported to assemble themselves into structures such as spheres.
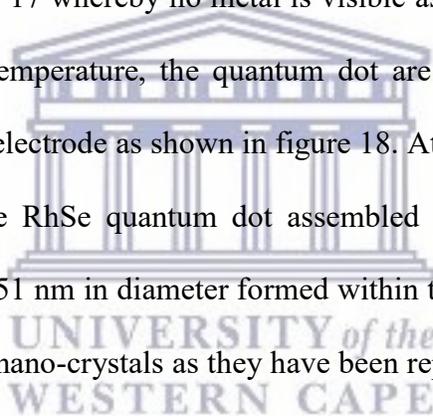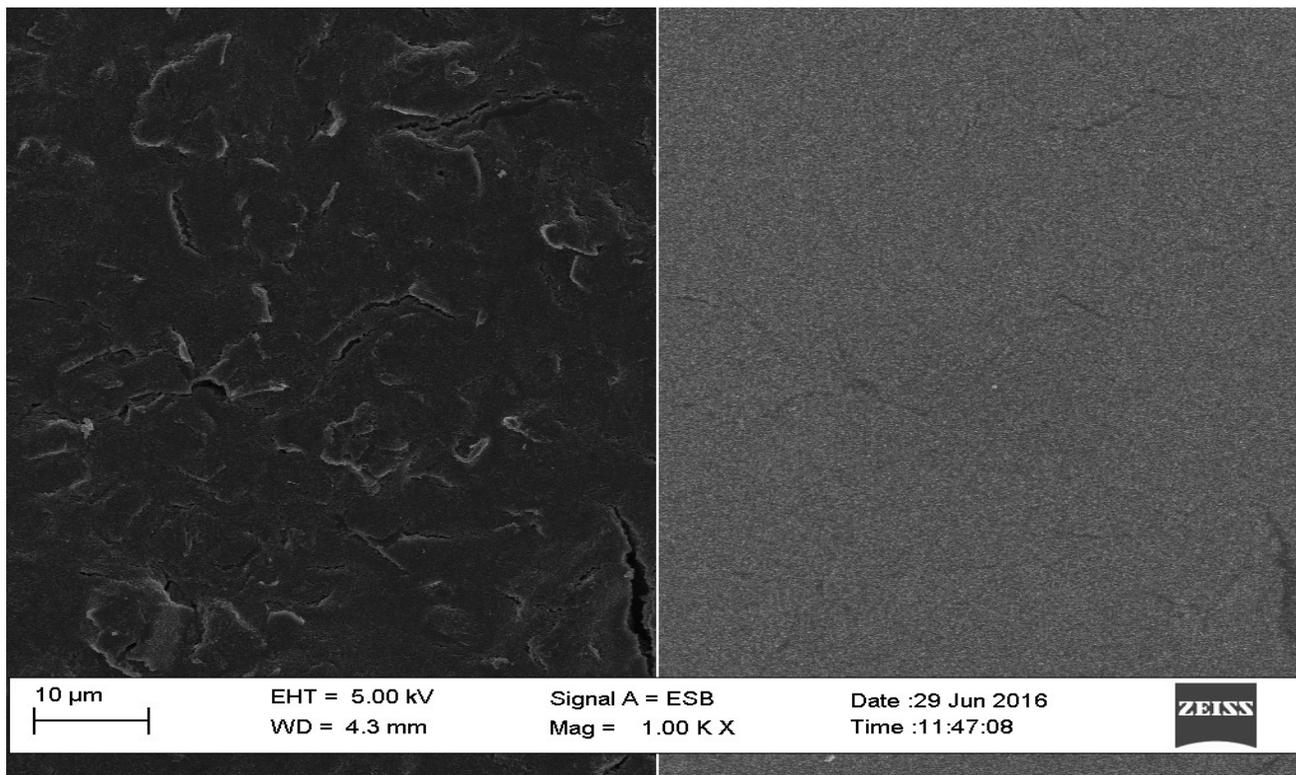
Figure 16 HRSEM (right) and BSE (left) of bare screen-printed carbon electrodes
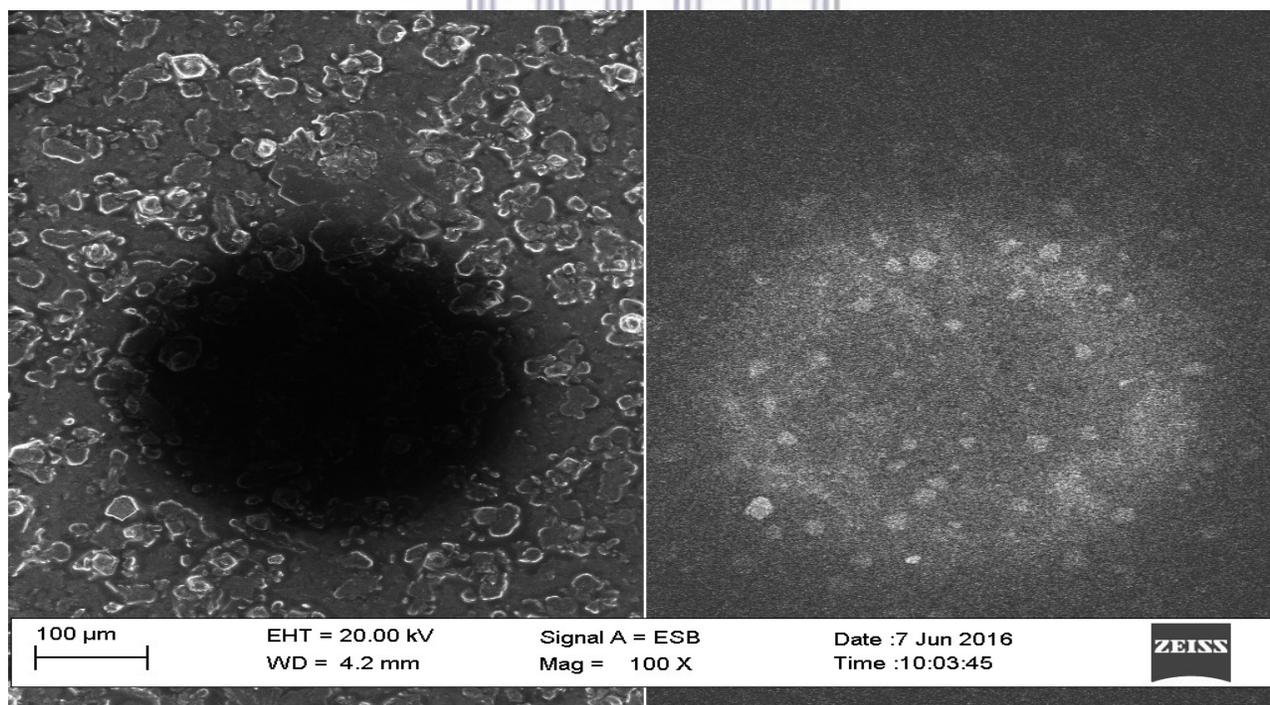
Figure 17 HRSEM (right) and BSE (left) RhSe-Qd modified screen-printed carbon electrodes prepared at room temperature.

| 100 µm | EHT = 20.00 kV | Signal A = ESB | Date :7 Jun 2016 | ZEISS |
| | WD = 4.4 mm | Mag = 100 X | Time :9:37:39 | |
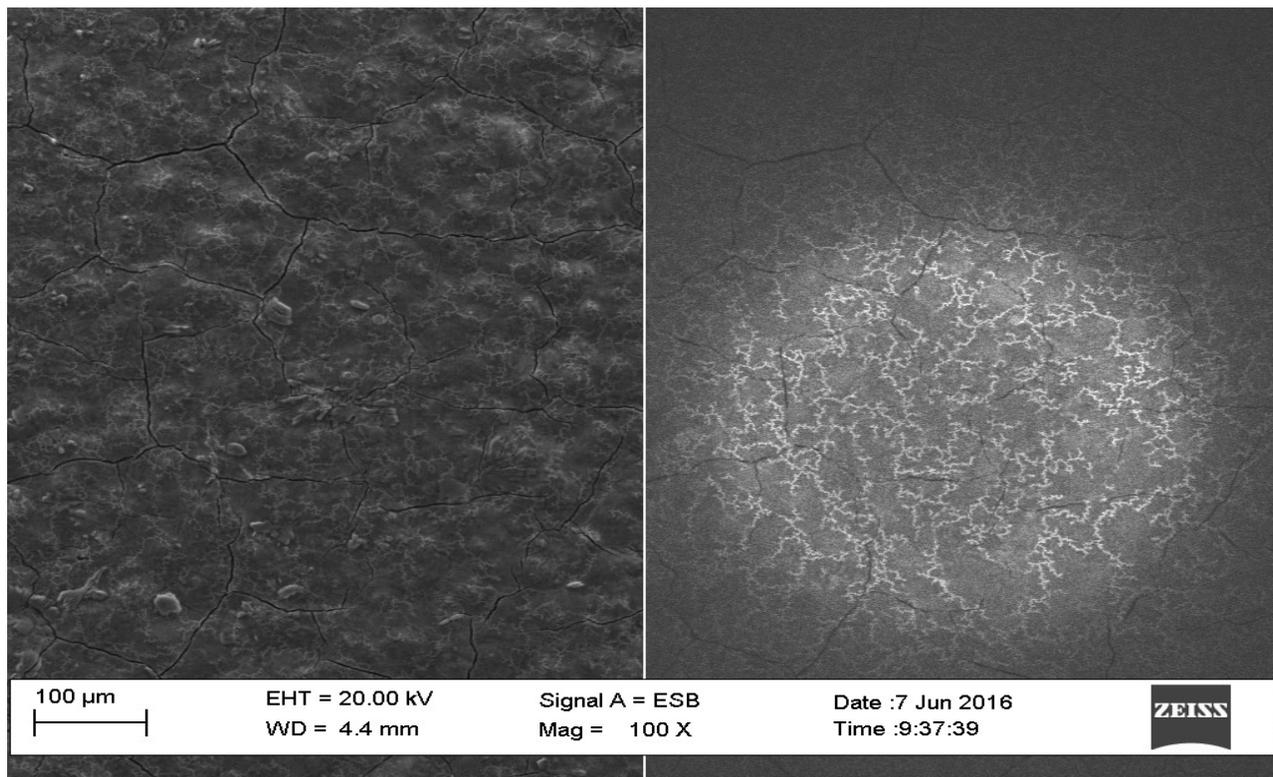
Figure 18 HRSEM (right) and BSE (left) RhSe-Qd modified screen printed carbon electrodes prepared at 40ºC (100µm scale).

| 10 µm | EHT = 20.00 kV | Signal A = ESB | Date :7 Jun 2016 | ZEISS |
| | WD = 4.2 mm | Mag = 500 X | Time :9:38:49 | |
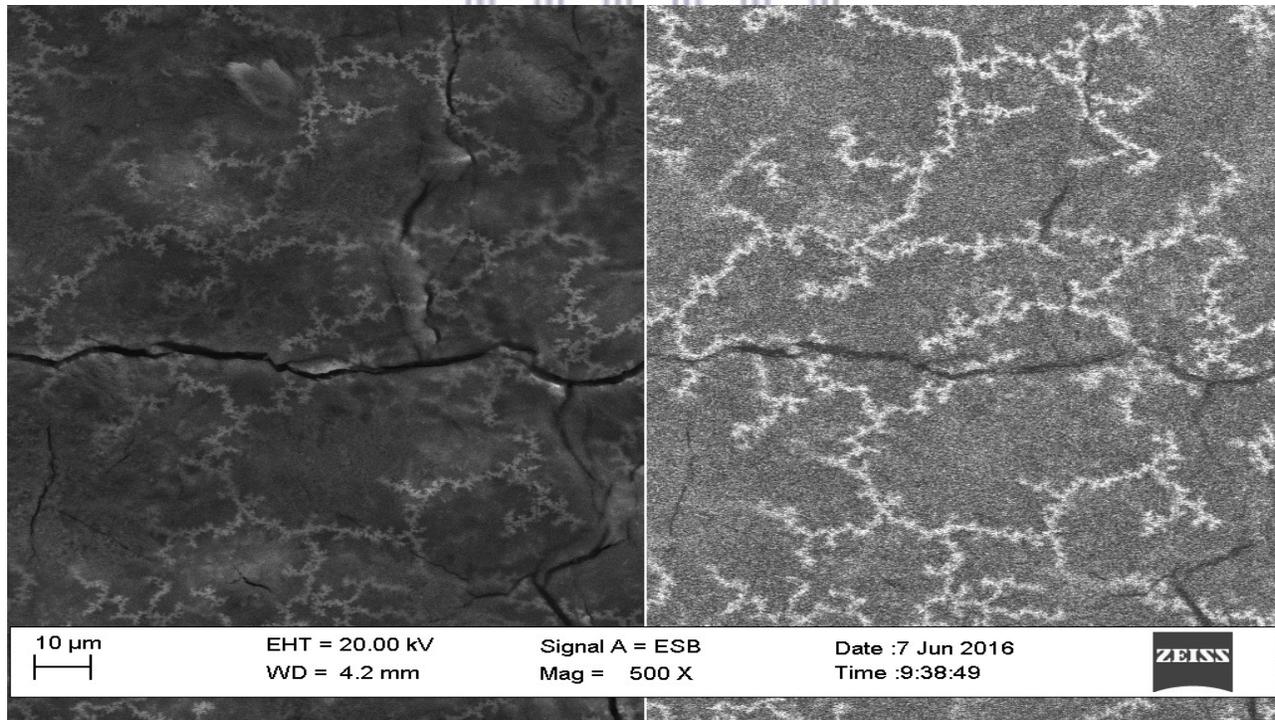
Figure 19 HRSEM (right) and BSE (left) RhSe-Qd modified screen-printed carbon electrodes prepared at 40ºC at (10µm scale).

82
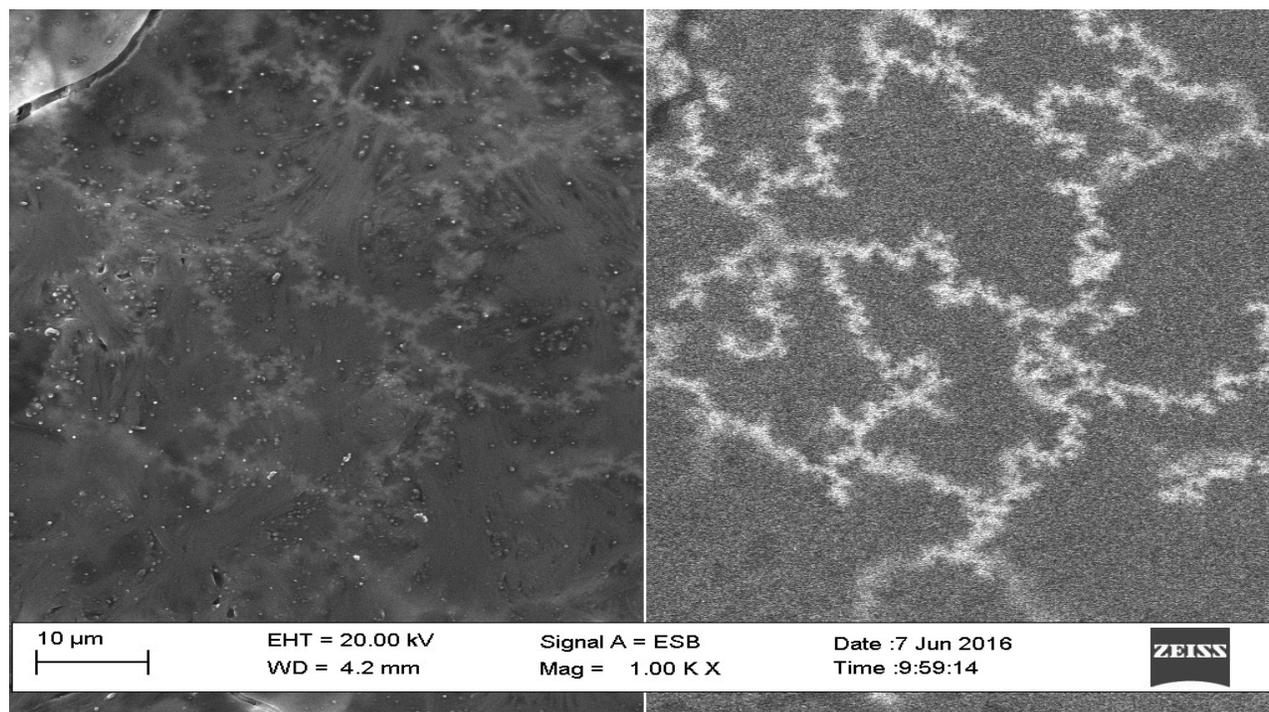
Figure 20 HRSEM (right) and BSE (left) RhSe-Qd modified screen-printed carbon electrodes prepared at 40ºC at (10µm scale).
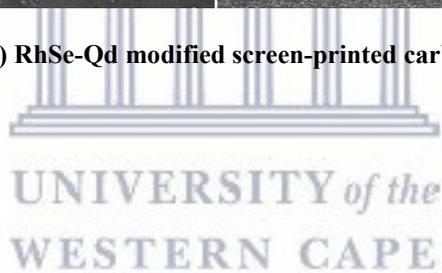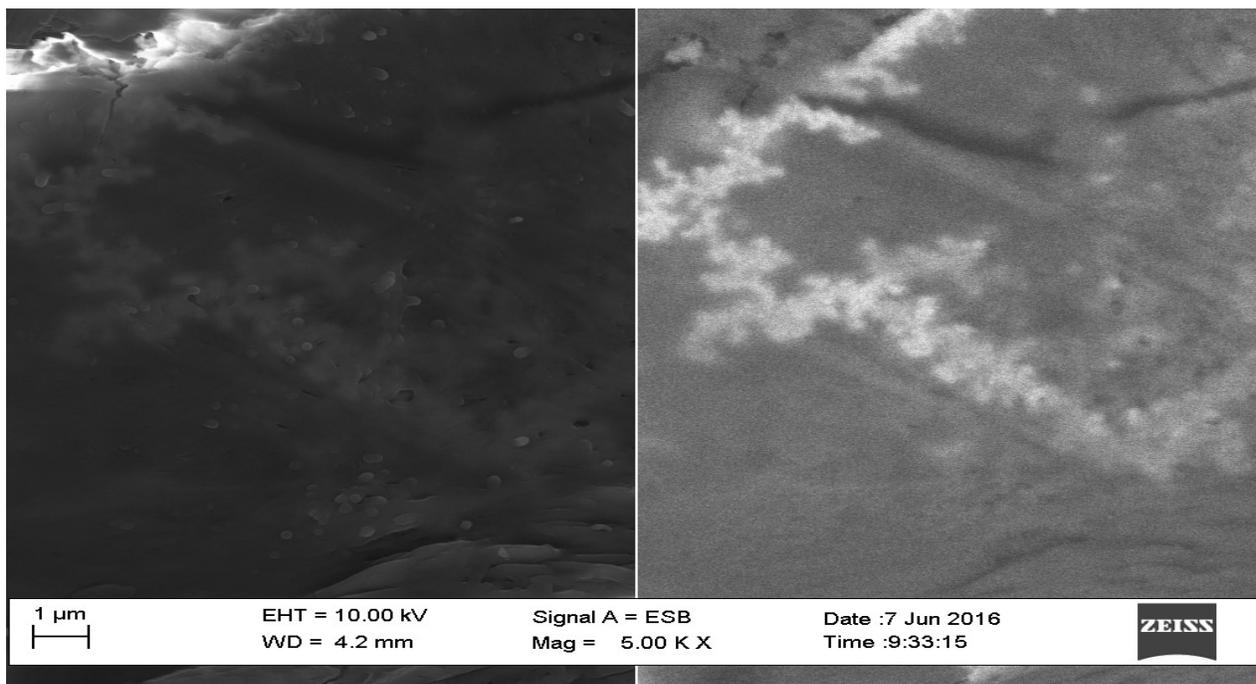
Figure 21 HRSEM (right) and BSE (left) RhSe-Qd modified screen printed carbon electrodes prepared at 40ºC at (1µm scale).
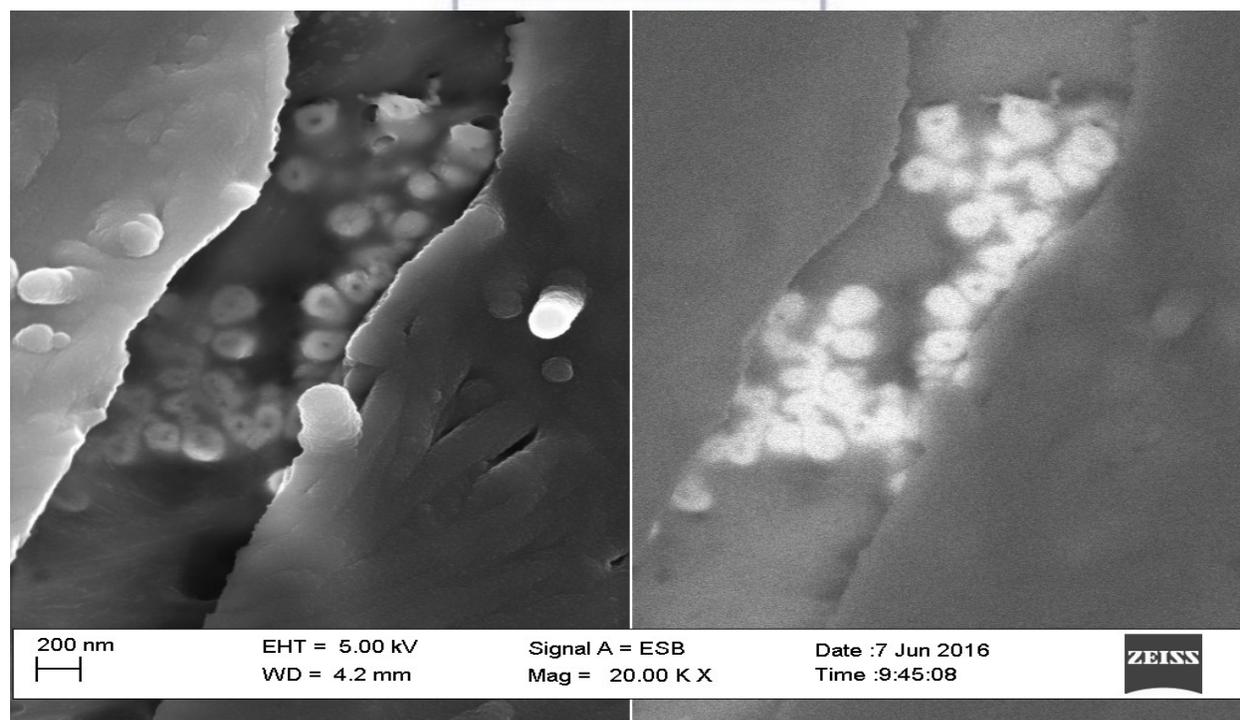
Figure 22 HRSEM (right) and BSE (left) RhSe-Qd modified screen-printed carbon electrodes prepared at 40ºC at (200 nm scale).
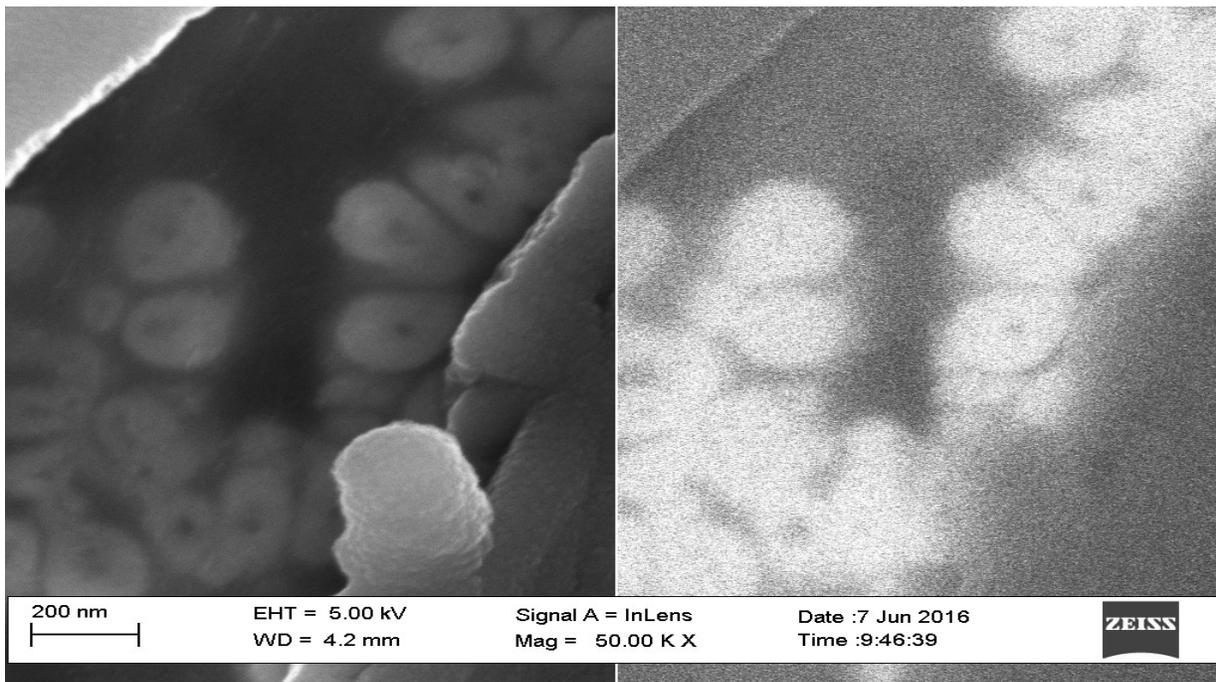
Figure 23 HRSEM (right) and BSE (left) RhSe-Qd modified screen printed carbon electrodes prepared at 40ºC at (200 nm scale).
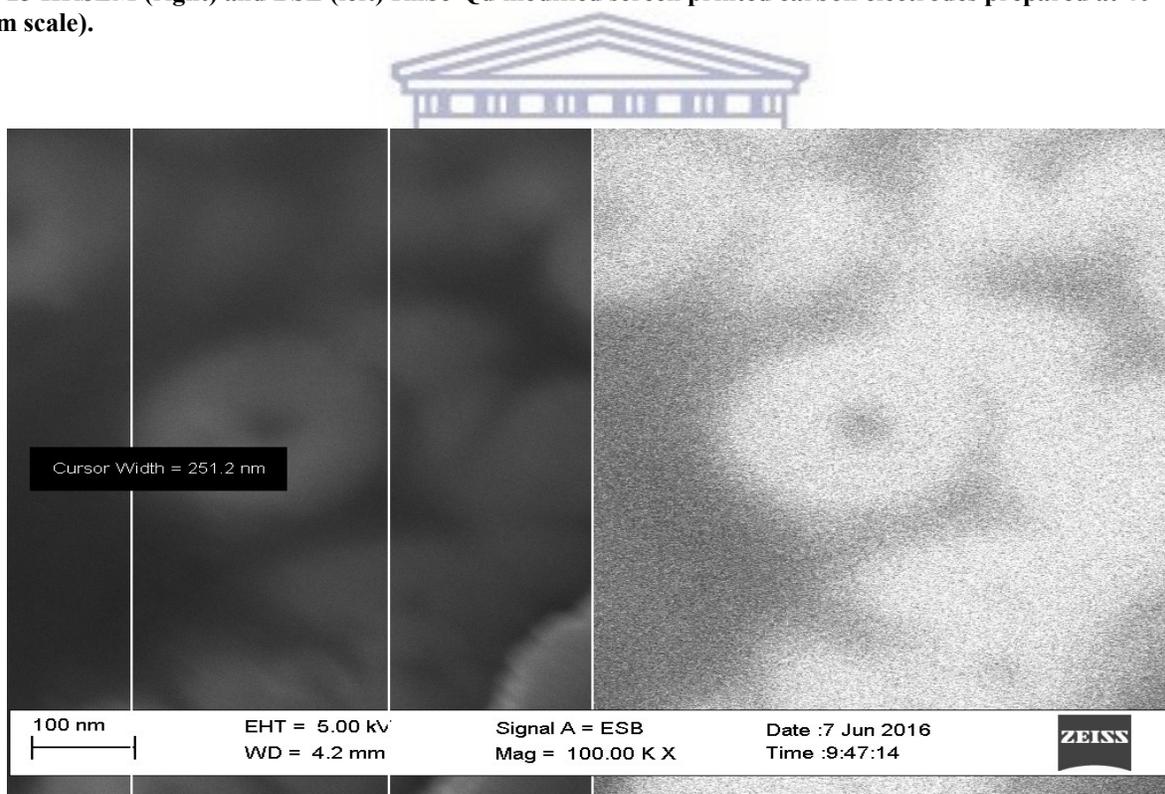
Figure 24 HRSEM (right) and BSE (left) RhSe-Qd modified screen-printed carbon electrodes prepared at 40ºC at (100 nm scale).

85

3B.2.7 Electrochemical characterisation of RhSe quantum dot on Indium tin oxide electrodes

The electrochemical properties of RhSe Qd where evaluated utilizing cyclic voltammetry (CV) on indium tin oxide electrodes. The CV of Na_3RhCl_6 in 0.01 M Lithium perchlorate solution is shown in Figure 25, whereby 5 redox peaks were obtained with redox couple A and E at -614 mV and -650 mV respectively, B and D at 64 mV and 30 mV respectively and the irreversible oxidation peak C at 510 mV. The CV of RhSe quantum dot in 0.01 M Lithium perchlorate solution also shown in Figure 25, reveal a significant irreversible oxidation peak (i) at 450 mV was observed. This peak was also present in the rhodium precursor as peak C, signifying that the peak arises from the irreversible oxidation of rhodium from the quantum dot core. Also, a significant shift of the oxidation potential of rhodium in precursor Na_3RhCl_6 and the rhodium in quantum dot, from 510 mV to 450 mV with a potential difference of 60 mV towards lower oxidative potential was observed. Similarly, to iridium selenide quantum dot, this is due to electron-confinement in three dimensions, which intern enhances the electrochemical reaction. The quantum size lowers the activation energy for the reaction, causing a shift towards lower reductive potential, denoting a lower energy requiring and faster reduction reaction in comparison to the parent material.
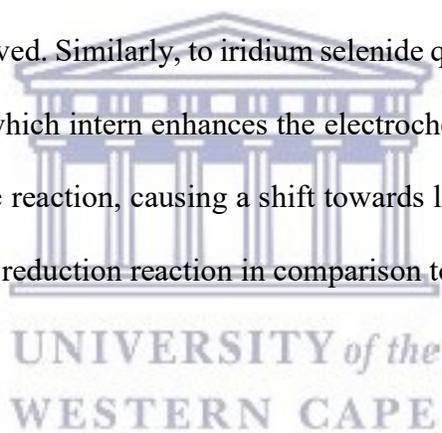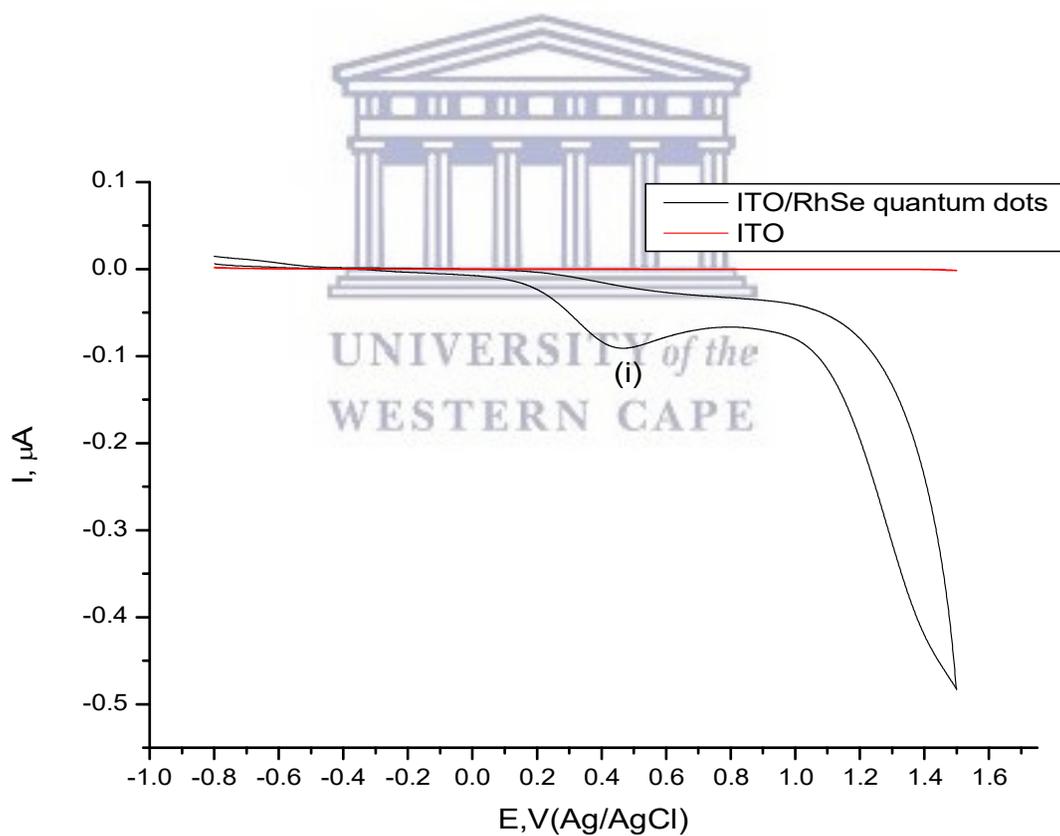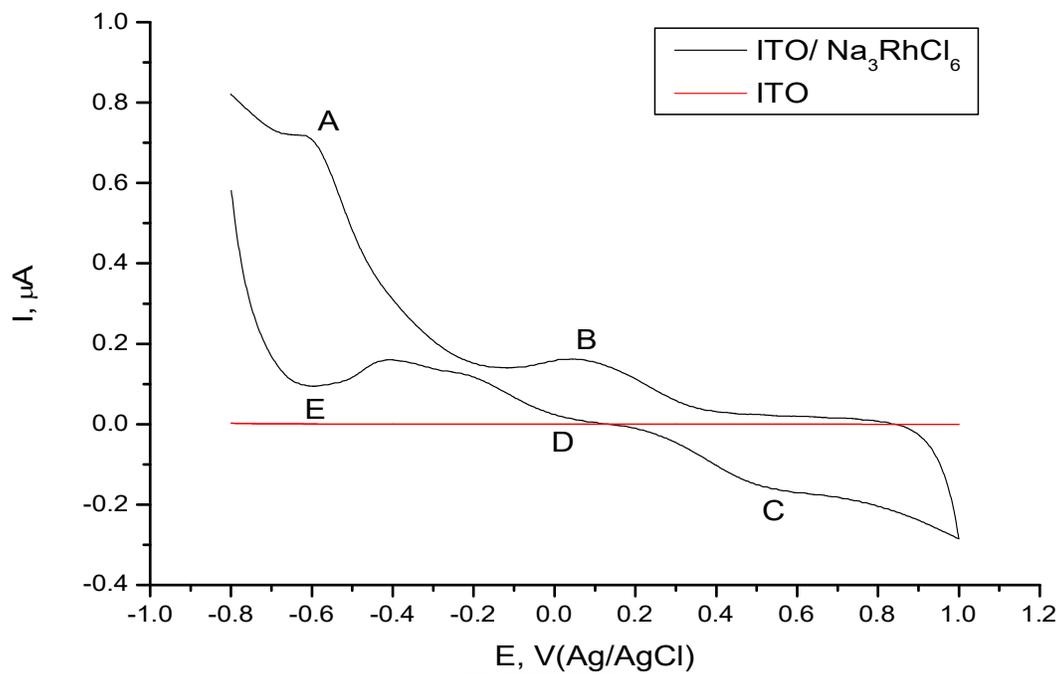
**Figure 25 Cyclic voltammograms of 1)&2) 3MPA-RhSe quantum dot and rhodium ion source Na₃RhCl₆ in 0.01M Lithium perchlorate at 50 mV/s. All experiments were performed on ITO electrodes, referenced with Ag/AgCl and a platinum wire as a counter electrode**

3B.3 Conclusion

Water-soluble RhSe quantum dot have been successfully synthesized at room temperature The nanoshells were then confirmed utilizing high-resolution transition electron microscope (HRTEM) whereby with sizes ranging from 15-20 nm. The HRTEM of the RhSe quantum dot revealed that very narrow sized particles of 3.5 nm have been simultaneously formed The SEM-BSE revealed that RhSe quantum dot, due to their narrow size interwoven themselves into nanotubes of about 251 nm in diameter within the electrode instead of on top of the electrodes, into vein-like networks. The flow behavior of the nanocrystals in water has been investigated using Rheometry and a decrease in viscosity with increasing applied pressure (shear thinning) has been observed, an ideal behavior for biological applications or nano-fluids. Lastly, the electro-activity of the RhSe quantum dot was performed on indium tin oxide electrodes and a characteristic oxidation peak at 450 mV was obtain.

References

[1]   Y. Zeng and D. F. Kelley, "Two-Photon Photochemistry of CdSe Quantum Dots," *ACS Nano*, vol. 9, no. 10, pp. 10471–10481, 2015.

[2]   C. M. Tyrakowski, A. Shamirian, C. E. Rowland, H. Shen, A. Das, R. D. Schaller, and P. T. Snee, "Bright Type II Quantum Dots," *Chem. Mater.*, vol. 27, no. 21, pp. 7276–7281, 2015.

[3]   Z. P. Cation-exchanged, S. Kim, A. R. Marshall, D. M. Kroupa, E. M. Miller, J. M. Luther, S. Jeong, M. C. Beard, and K. I. M. E. T. Al, "Air-Stable and E ffi cient PbSe Quantum-Dot Solar Cells Based upon Quantum Dots," no. 8, pp. 8157–8164, 2015.

[4]   K. Lambert, B. De Geyter, I. Moreels, and Z. Hens, "PbTe| CdTe core| shell particles by cation exchange, a HR-TEM study," *Chem. Mater*, vol. 21, pp. 778–780, 2009.

[5]   H. Mirzai, M. N. Nordin, R. J. Curry, J.-S. Bouillard, a. V. Zayats, and M. Green, "The room temperature phosphine-free synthesis of near-infrared emitting HgSe quantum dots," *J. Mater. Chem. C*, vol. 2, no. 12, p. 2107, 2014.

[6]   H. Lu and R. L. Brutchey, "Tunable Room-Temperature Synthesis of Coinage Metal Chalcogenide Nanocrystals from *N* -Heterocyclic Carbene Synthons," *Chem. Mater.*, p. acs.chemmater.6b05293, 2017.

[7]   S. Nath, S. K. Ghosh, S. Panigahi, T. Thundat, and T. Pal, "Synthesis of selenium nanoparticle and its photocatalytic application for decolorization of methylene blue under UV irradiation," *Langmuir*, vol. 20, no. 18, pp. 7880–7883, 2004.

[8]   K. B. Subila, G. Kishore Kumar, S. M. Shivaprasad, and K. George Thomas, "Luminescence Properties of

CdSe Quantum Dots: Role of Crystal Structure and Surface Composition," *J. Phys. Chem. Lett.*, vol. 4, pp. 2774–2779, 2013.

[9] P. M. Ndangili, A. M. Jijana, P. G. L. Baker, and E. I. Iwuoha, "3-Mercaptopropionic acid capped ZnSe quantum dot-cytochrome P450 3A4 enzyme biotransducer for 17beta-estradiol," *J. Electroanal. Chem.*, vol. 653, no. 1–2, pp. 67–74, 2011.

[10] P. M. Ndangili, O. Arotiba, P. G. L. Baker, and E. I. Iwuoha, "A potential masking approach in the detection of dopamine on 3-mercaptopropionic acid capped ZnSe quantum dots modified gold electrode in the presence of interferences," *J. Electroanal. Chem.*, vol. 643, no. 1–2, pp. 77–81, 2010.

[11] D. Pan, Q. Wang, S. Jiang, X. Ji, and L. An, "Low-temperature synthesis of oil-soluble CdSe, CdS, and CdSe/CdS core-shell nanocrystals by using various water-soluble anion precursors," *J. Phys. Chem. C*, vol. 111, no. 15, pp. 5661–5666, 2007.

[12] V. V. Singh, G. K. Rao, A. Kumar, and A. K. Singh, "Palladium(ii)–selenoether complexes as new single source precursors: First synthesis of Pd4Se and Pd7Se4 nanoparticles," *Dalt. Trans.*, vol. 41, no. 4, p. 1142, 2012.

[13] S. E. Keuleyan, P. Guyot-sionnest, C. Delerue, and G. Allan, "Mercury Telluride Colloidal Quantum Dots : Electronic Structure , Photocurrent Detection up to 12 μ m," *ACS Nano*, vol. 8, no. 8, pp. 8676–8682, 2014.

[14] H. Takahashi, N. Konishi, H. Ohno, K. Takahashi, Y. Koike, K. Asakura, and A. Muramatsu, "Preparation of well-crystallized Pd20Te7 alloy nanoparticulate catalysts with uniform structure and composition in liquid-phase," *Appl. Catal. A Gen.*, vol. 392, no. 1–2, pp. 80–85, 2011.

[15] A. K. Samal and T. Pradeep, "Pt3Te4 nanoparticles from tellurium nanowires," *Langmuir*, vol. 26, no. 24, pp. 19136–19141, 2010.

[16] M. S. Abd El-sadek, J. Ram Kumar, and S. Moorthy Babu, "The role of potassium tellurite as tellurium source in mercaptoacetic acid-capped CdTe nanoparticles," *Curr. Appl. Phys.*, vol. 10, no. 1, pp. 317–322, 2010.

[17] M. Masikini, S. N. Mailu, A. Tsegaye, N. Njomo, K. M. Molapo, C. O. Ikpo, C. E. Sunday, C. Rassie, L. Wilson, P. G. L. Baker, and E. I. Iwuoha, "A fumonisins immunosensor based on polyanilino-carbon nanotubes doped with palladium telluride quantum dots," *Sensors (Switzerland)*, vol. 15, no. 1, pp. 529–546, 2015.

[18] D.-K. Ko, A. Maurano, S. K. Suh, D. Kim, G. W. Hwang, J. C. Grossman, V. Bulović, and M. G. Bawendi, "Photovoltaic Performance of PbS Quantum Dots Treated with Metal Salts," *ACS Nano*, p. acsnano.5b07186, 2016.

[19] H. Cheng, Y. Wang, H. Dai, J.-B. Han, and X. Li, "Nonlinear Optical Properties of PbS Colloidal Quantum Dots Fabricated via Solvothermal Method," *J. Phys. Chem. C*, vol. 119, no. 6, pp. 3288–3292, 2015.

[20] C. Zhao, Z. Bai, X. Liu, Y. Zhang, B. Zou, and H. Zhong, "Small GSH-Capped CuInS<inf>2</inf> Quantum Dots: MPA-Assisted Aqueous Phase Transfer and Bioimaging Applications," *ACS Appl. Mater. Interfaces*, vol. 7, no. 32, pp. 17623–17629, 2015.

[21] J. J. Andrade, a. G. Brasil, P. M. a Farias, a. Fontes, and B. S. Santos, "Synthesis and characterization of blue emitting ZnSe quantum dots," *Microelectronics J.*, vol. 40, no. 3, pp. 641–643, 2009.

[22] B. P. Bloom, V. Kiran, V. Varade, R. Naaman, and D. H. Waldeck, "Spin selective charge transport through cysteine capped CdSe quantum dots," *Nano Lett.*, vol. 16, no. 7, pp. 4583–4589, 2016.

[23] D. Deng, L. Qu, Y. Li, and Y. Gu, "Versatile self-assembly of water-soluble thiol-capped cdte quantum dots: External destabilization and internal stability of colloidal qds," *Langmuir*, vol. 29, no. 34, pp. 10907–10914, 2013.

[24] C. C. Reinhart and E. Johansson, "Colloidally Prepared 3-Mercaptopropionic Acid Capped Lead Sulfide Quantum Dots," *Chem. Mater.*, vol. 27, no. 21, pp. 7313–7320, 2015.

89

[25] C. E. Bradburne, J. B. Delehanty, K. Boeneman Gemmill, B. C. Mei, H. Mattoussi, K. Susumu, J. B. Blanco-Canosa, P. E. Dawson, and I. L. Medintz, "Cytotoxicity of quantum dots used for in vitro cellular labeling: Role of QD surface ligand, delivery modality, cell type, and direct comparison to organic fluorophores," *Bioconjug. Chem.*, vol. 24, no. 9, pp. 1570–1583, 2013.

[26] E. Biology, "Room temperature synthesis of water-soluble starch-stabilized CdSe quantum dots for latent fingerprints detection," no. January 2014, 2016.

[27] A. Tang, Y. Liu, Q. Wang, R. Chen, W. Liu, Z. Fang, and L. Wang, "A new photoelectric ink based on nanocellulose/CdS quantum dots for screen-printing," *Carbohydr. Polym.*, vol. 148, pp. 29–35, 2016.

[28] V. Bonu, B. Gupta, S. Chandra, A. Das, S. Dhara, and a. K. Tyagi, "Electrochemical supercapacitor performance of SnO2 quantum dots," *Electrochim. Acta*, vol. 203, pp. 230–237, 2016.

[29] H. Takahashi, N. Konishi, H. Ohno, K. Takahashi, Y. Koike, K. Asakura, and A. Muramatsu, "Preparation of well-crystallized Pd20Te7 alloy nanoparticulate catalysts with uniform structure and composition in liquid-phase," *Appl. Catal. A Gen.*, vol. 392, no. 1–2, pp. 80–85, 2011.

[30] X. Jiang, B. Mayers, Y. Wang, B. Cattle, and Y. Xia, "Template-engaged synthesis of RuSe 2 and Pd 17 Se 15 nanotubes by reacting precursor salts with selenium nanowires," vol. 385, pp. 472–476, 2004.

[31] J. Akhtar, R. F. Mehmood, M. A. Malik, N. Iqbal, P. O'Brien, and J. Raftery, "A novel single source precursor: [bis(N,N-diethyl-N'-naphthoyl-selenoureato)palladium(II)] for palladium selenide thin films and nanoparticles.," *Chem. Commun. (Camb).*, vol. 47, no. 6, pp. 1899–901, 2011.

[32] G. Liu and H. Zhang, "Facile Synthesis of Carbon-Supported Ir x Se y Chalcogenide Nanoparticles and Their Electrocatalytic Activity for the Oxygen Reduction Reaction," pp. 2058–2065, 2008.

[33] M. Grydlik, F. Hackl, H. Groiss, M. Glaser, A. Halilovic, T. Fromherz, W. Jantsch, F. Schäffler, and M. Brehm, "Lasing from Glassy Ge Quantum Dots in Crystalline Si," *ACS Photonics*, vol. 3, no. 2, pp. 298–303, 2016.

[34] C. C. Shen and W. L. Tseng, "One-step synthesis of white-light-emitting quantum dots at low temperature," *Inorg. Chem.*, vol. 48, no. 18, pp. 8689–8694, 2009.

[35] M. M. Tavakoli, H. Aashuri, A. Simchi, S. Kalytchuk, and Z. Fan, "Quasi Core/Shell Lead Sulfide/Graphene Quantum Dots for Bulk Heterojunction Solar Cells," *J. Phys. Chem. C*, vol. 119, no. 33, pp. 18886–18895, 2015.

[36] D. Deng, J. Cao, L. Qu, S. Achilefu, and Y. Gu, "Highly luminescent water-soluble quaternary Zn-Ag-In-S quantum dots for tumor cell-targeted imaging.," *Phys. Chem. Chem. Phys.*, vol. 15, no. 14, pp. 5078–83, 2013.

[37] C. W. Kuo, D. Y. Chueh, N. Singh, F. C. Chien, and P. Chen, "Targeted nuclear delivery using peptide-coated quantum dots," *Bioconjug. Chem.*, vol. 22, no. 6, pp. 1073–1080, 2011.

[38] O. Lahad, N. Meir, I. Pinkas, and D. Oron, "Long-lived population inversion in isovalently doped quantum dots," *ACS Nano*, vol. 9, no. 1, pp. 817–824, 2015.

[39] I. A. Mir, K. Das, K. Rawat, and H. B. Bohidar, "Hot injection versus room temperature synthesis of CdSe quantum dots: A differential spectroscopic and bioanalyte sensing efficacy evaluation," *Colloids Surfaces A Physicochem. Eng. Asp.*, vol. 494, pp. 162–169, 2016.

[40] O. M. Primera-Pedrozo, Z. Arslan, B. Rasulev, and J. Leszczynski, "Room temperature synthesis of PbSe quantum dots in aqueous solution: stabilization by interactions with ligands.," *Nanoscale*, vol. 4, no. 4, pp. 1312–20, 2012.

[41] S. Rong, P. Zhang, Y. Yang, and F. Liu, "Room temperature synthesis of manganese oxide quantum dots and their application as a fluorescent probe for the detection of metal ions in aqueous media," *RSC Adv.*, vol. 6, no. 115, pp. 114632–114638, 2016.

[42] E. Oh, R. Liu, A. Nel, K. B. Gemill, M. Bilal, Y. Cohen, and I. L. Medintz, "Meta-analysis of cellular toxicity for cadmium-containing quantum dots," *Nat Nano*, vol. 11, no. 5, p. doi:10.1038/nnano.2015.338, 2016.

90

[43]   W. E. Smith, J. Brownell, C. C. White, Z. Afsharinejad, J. Tsai, X. Hu, S. J. Polyak, X. Gao, T. J. Kavanagh, D. L. Eaton, and S. E. T. Al, "In Vitro Toxicity Assessment of Human Liver Cell Models," no. 11, pp. 9475–9484, 2012.

[44]   I. a. Minigalieva, B. a. Katsnelson, V. G. Panov, L. I. Privalova, A. N. Varaksin, V. B. Gurvich, M. P. Sutunkova, V. Y. Shur, E. V. Shishkina, I. E. Valamina, I. V. Zubarev, O. H. Makeyev, E. Y. Meshtcheryakova, and S. V. Klinova, "In vivo toxicity of copper oxide, lead oxide and zinc oxide nanoparticles acting in different combinations and its attenuation with a complex of innocuous bio-protectors," *Toxicology*, vol. 380, pp. 72–93, 2017.

[45]   S. Skalickova, V. Milosavljevic, K. Cihalova, P. Horky, L. Richtera, and V. Adam, "Selenium nanoparticles as a nutritional supplement," *Nutrition*, vol. 33, pp. 83–90, 2016.

[46]   T. H. D. Nguyen, B. Vardhanabhuti, M. Lin, and A. Mustapha, "Antibacterial properties of selenium nanoparticles and their toxicity to Caco-2 cells," *Food Control*, vol. 77, pp. 17–24, 2017.

[47]   X. Fang, X. Wu, C. Li, B. Zhou, X. Chen, T. Chen, and F. Yang, "Targeting selenium nanoparticles combined with baicalin to treat HBV-infected liver cancer," *RSC Adv.*, vol. 7, no. 14, pp. 8178–8185, 2017.

[48]   H. Su, D. D. Liu, M. Zhao, W. L. Hu, S. S. Xue, Q. Cao, X. Y. Le, L. N. Ji, and Z. W. Mao, "Dual-enzyme characteristics of polyvinylpyrrolidone-capped iridium nanoparticles and their cellular protective effect against H2O2-induced oxidative damage," *ACS Appl. Mater. Interfaces*, vol. 7, no. 15, pp. 8233–8242, 2015.

[49]   A. a. Gambardella, N. S. Bjorge, V. K. Alspaugh, and R. W. Murray, "Voltammetry of diffusing 2 nm iridium oxide nanoparticles," *J. Phys. Chem. C*, vol. 115, no. 44, pp. 21659–21665, 2011.

[50]   G. Liu and H. Zhang, "Facile Synthesis of Carbon-Supported Ir x Se y Chalcogenide Nanoparticles and Their Electrocatalytic Activity for the Oxygen Reduction Reaction," *J. Phys. Chem. C*, vol. 112, pp. 2058–2065, 2008.

[51]   S. Kurbanoglu, L. Rivas, S. a. Ozkan, and A. Merkoci, "Electrochemically reduced graphene and iridium oxide nanoparticles for inhibition-based angiotensin-converting enzyme inhibitor detection," *Biosens. Bioelectron.*, vol. 88, pp. 122–129, 2017.

[52]   D. Xu, P. Diao, T. Jin, Q. Wu, X. Liu, X. Guo, H. Gong, F. Li, M. Xiang, and Y. Ronghai, "Iridium Oxide Nanoparticles and Iridium/Iridium Oxide Nanocomposites: Photochemical Fabrication and Application in Catalytic Reduction of 4-Nitrophenol," *ACS Appl. Mater. Interfaces*, vol. 7, no. 30, pp. 16738–16749, 2015.

[53]   D. L. Klayman and T. S. Griffin, "Reaction of Selenium with Sodium Borohydride in Protic Solvents. A Facile Method for the Introduction of Selenium into Organic Molecules," *J. Am. Chem. Soc.*, vol. 2, no. 1, pp. 197–199, 1973.

[54]   W. Chen and S. Chen, "Iridium-platinum alloy nanoparticles: Composition-dependent electrocatalytic activity for formic acid oxidation," *J. Mater. Chem.*, vol. 21, no. 25, p. 9169, 2011.

[55]   L. Jimanez-Hernendez, O. Estavez-Hernandez, M. Hernandez-Sanchez, J. a. Diaz, M. Farias- Sanchez, and E. Reguera, "3-mercaptopropionic acid surface modification of Cu-doped ZnO nanoparticles: Their properties and peroxidase conjugation," *Colloids Surfaces A Physicochem. Eng. Asp.*, vol. 489, no. November, pp. 351–359, 2016.

[56]   Y. Li and N. Chopra, "Fabrication of nanoscale heterostructures comprised of graphene-encapsulated gold nanoparticles and semiconducting quantum dots for photocatalysis," *Phys. Chem. Chem. Phys.*, vol. 17, no. 19, pp. 12881–12893, 2015.

[57]   R. Enhanced, T. Alloys, R. P. P. Compound, H. T. Superconductors, P. Electrodes, A. Sensor, P. Group, M. Conference, N. Palladium, P. Catalyst, N. A. Plants, and N. Patents, "Platinum Metals Review," *Platin. Met. Rev.*, vol. 52, no. 1, pp. 54–62, 2008.

[58]   L. Brus, "Electronic wave functions in semiconductor clusters: experiment and theory," *J. Phys. Chem.*,

vol. 90, no. 12, pp. 2555–2560, 1986.

[59]   J. Hambrock, A. Birkner, and R. a Fischer, "Synthesis of CdSe nanoparticles using various organometallic cadmium precursors," *J. Mater. Chem.*, vol. 11, no. 12, pp. 3197–3201, 2001.

[60]   B. Pejova and I. Grozdanov, "Three-dimensional confinement effects in semiconducting zinc selenide quantum dots deposited in thin-film form," *Mater. Chem. Phys.*, vol. 90, no. 1, pp. 35–46, 2005.

[61]   N. Gaponik, S. K. Poznyak, N. P. Osipovich, A. Shavel, and A. Eychmüller, "Electrochemical probing of thiol-capped nanocrystals," *Microchim. Acta*, vol. 160, no. 3, pp. 327–334, 2008.

[62]   M. J. N. Pourbaix, J. Van Muylder, N. de Zoubov, and C. Protection, "Electrochemical properties of the platinum metals," *Platin. Met. Rev.*, vol. 3, no. 2, pp. 47–53, 1959.

CHAPTER 4

Preparation of chemical cleavable linker for reversible termination of nucleotides in 3-OH for DNA sequencing

Abstract

In this report, we described a 7 step synthetic approach towards the development of a linker for reversible terminating and labeling nucleotides at 3'-OH position for application in Sequencing by Synthesis (SBS) DNA has been proposed and demonstrated. 6 new compounds not stipulated anywhere else in literature have been synthesized. All metal hydride steps have been replaced thus allowing all reaction steps to be performed in standard conditions. The developed tosylate precursor is a stable precursor with a the tosyl group a good leaving group ideal for the azide reaction required for 3'-OH labeling of nucleotides. The precursors were characterized utilizing techniques including Thin Layer Chromatography (TLC), Fourier transforms infrared spectroscopy (FTIR), Nuclear Magnetic Resonance Spectroscopy (^{1}H-NMR), Carbon Nuclear Magnetic Resonance Spectroscopy (^{13}C-NMR) and ESI-Tof mass spectrometry. The method offers a simplified alternative approach to the synthesis of universal linkers for labeling all four nucleotides at the 3'OH position for DNA sequencing applications.

Keywords: Sequencing by synthesis, universal linker, organic synthesis, reversible terminator, nucleotides

Graphical Abstract

dATP

Universal 3'OH linker

dGTP

dTTP

dCTP

dATP = Adenosine triphosphate
dGTP = Guanisne triphospate
dCTP = Cytodine triphosphate
dTTP = Thymidine triphophate
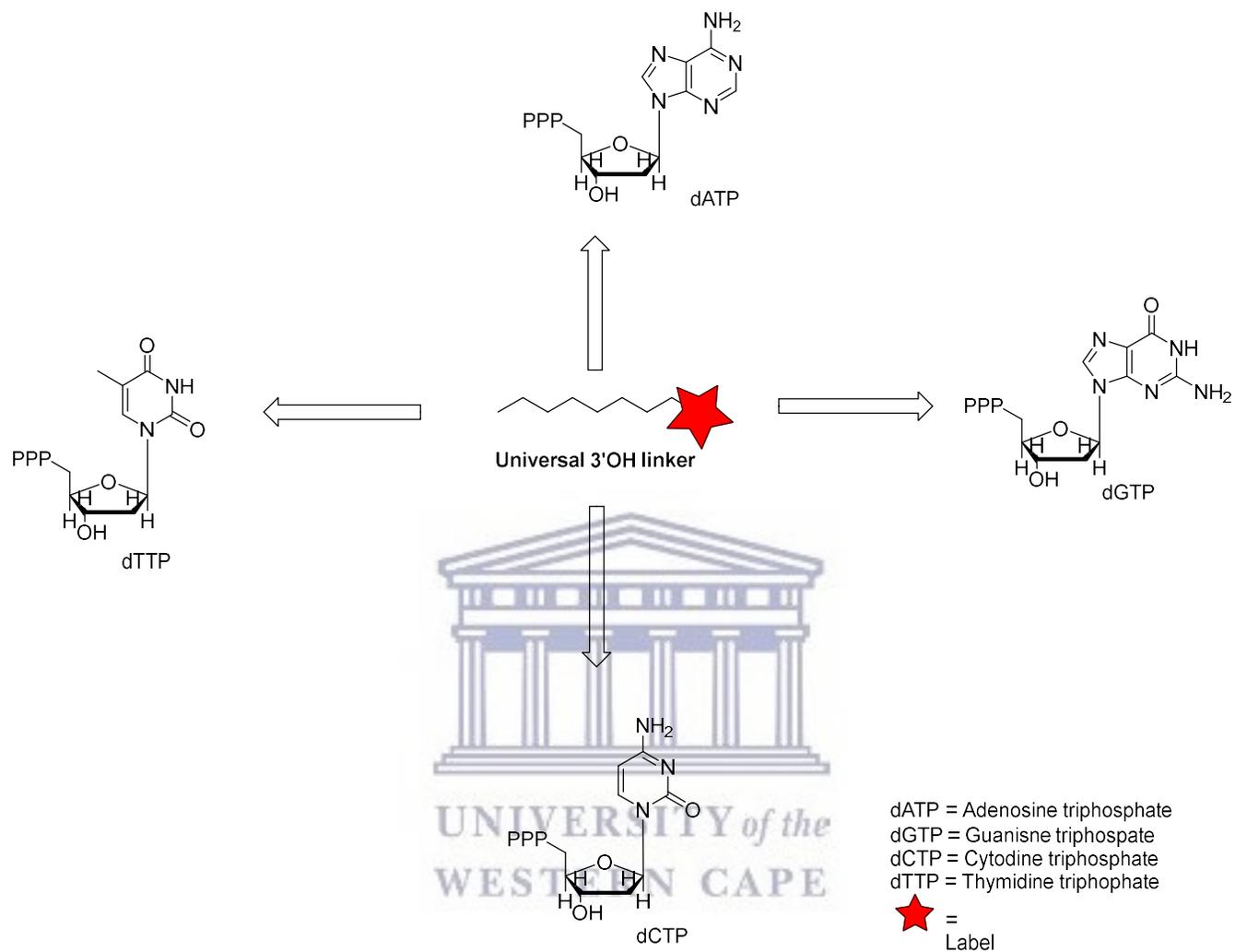
= Label

Universal linker for labeling nucleotides

4.1 Introduction

The advent of fluorescent labeling and reversible termination in the DNA sequencing arena has revolutionized the technology such that what took 13 years to complete, i.e. sequencing of the entire human genome, can be fully achieved in less than 4 weeks.[63][64] Leading in this technology is sequencing by synthesis (SBS) utilizing reversible terminators and labeled nucleotides. The process involves 1) fragmentation and library construction from target DNA, 2) amplification, 3) enzymatic incorporation of fluorescently labelled and reversibly terminated nucleotides, 4) detection and removal of label and terminator groups (where applicable).[65] Platforms utilizing this method are already commercialized by companies such as the Illumina, Pacific biosciences[66], Helicos.

Though these have been successful in replacing the use of electrophoresis with more sensitive, faster and cheaper approaches in comparison to the Sanger method, key issues still exist. High setup and running costs make them inadequate in low resource settings and many laboratories. They require skilled personnel, time-consuming bioinformatics and data analysis, possess errors due to massive parallelization and in homo-polymer DNA regions.[67] Portability, miniaturization and applicability in point-of-care testing (POCT) are some of the issues still existing in these technologies.

Also, though DNA sequencing has found various applications, in the field of diagnostics its highly focused on whole-genome sequencing as the search still continues for individual variations and/ mutations (e.g. single nucleotide polymorphism, SNPs) in the human genome to understand its contribution to disease and drug response consequently, sequencing has been focused on whole genome sequencing.[68], [69] As the discovery of specific DNA sequences as disease biomarkers/ gene markers increases this then has given rise to a need to develop disease-specific DNA sequencing platforms mainly adapted to point-of-care and personalized testing applications.

95

Electrochemical sensors/ biosensors are currently studied for disease-specific diagnosis and POCT applications, show promising results due to the increased sensitivity, low production cost, fast result output, portability and miniaturization that can be reached utilizing electrochemical detection methods. Most these approaches are centered on label-free DNA hybridization[70][71], labeled capture strand either immobilized on the electrode or introduced in solution in sandwich assay format.[72][73] Alternatively electro-active species are utilized for DNA intercalation and redox indicators.[74][75][76] SBS utilizing reversible termination has not yet been used in electrochemical DNA sensing.

The design of reversible terminating and labeled nucleotides is key in SBS approaches with the performance of the platform, in most cases, largely depending on it. Typically the label is attached at the base[65] or at the 5'-OH position. Labeling at the 5-position offers a great advantage as the label and linker are completely removed by virtue of the enzymatic incorporation of the modified nucleotide.[66] Though robust, the method suffers from high error rates in homo-polymeric regions of the DNA. Labeling at the base position suffers from the incomplete detachment of the labeling linker leaving a molecular scar at each point of incorporation in the DNA strand, thus limiting read length of the platform and also requires a modification at the 3'OH[77] for reversible termination.
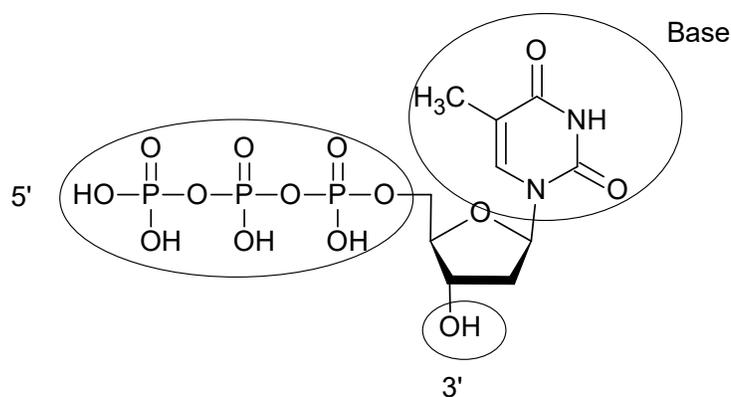


Figure 26 Nucleotide labeling positions

Recent advances have been achieved by labeling the nucleotides at the 3'-OH position with a cleavable linker/spacer as described by Kim *et al 2010* [78] and Da-Rae Kim *et al 2014* [79]. They demonstrated the successful enzymatic recognition of the 3'-OH labelled nucleotides by introducing a stable spacer molecule, selectively cleavable under mild conditions similar to allyl reversible terminators first described by Ju *et al 2006* [65]. The method offers the major advantage of a fully reversible terminating labelling method promising for use in homo-polymeric regions (depending on the mode of detection employed), dual cleaving process and complete regeneration of the 3'-OH leaving no molecular scar to the molecule. Though promising, the synthetic approach involves 17 steps for the synthesis and several purification steps of the spacer molecule utilizing hazardous materials such as metal hydrides, additional 5-6 steps for 3'-OH linkage, triphosphorylation, and labelling step, thus making the method expensive and time-consuming.

We, therefore, described the development of a 7 step synthetic approach for the development of a universal linker precursor for reversible terminating and labeling nucleotides at 3'-OH position and application in electrochemical SBS DNA sequencing approach while eliminating the use of metal hydrides, a modification of the 17 step Da-Rae Kim *et al 2014* [79] method. The precursors were synthesized and characterized utilizing Thin Layer Chromatography (TLC), Fourier transforms infrared spectroscopy (FTIR), Nuclear Magnetic Resonance Spectroscopy (^{1}H-NMR), Carbon Nuclear Magnetic Resonance Spectroscopy (^{13}C-NMR) and ESI-Tof mass spectrometry.

4.2 Experimental Section

**Synthesis of 5-(*tert*-Butyl-dimethyl-silanyloxy)-pentane-1-ol**
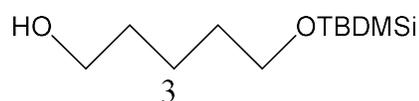
1,5-pentanediol (3.00 g, 28.8 mmol) and *tert*-butyldimethylsilyl chloride (4.34 g) were dissolved in CH$_2$Cl$_2$ (50 mL) followed by dropwise addition of triethylamine (6.0 mL) with stirring. The reaction mixture was continued stir for 3 h at room temperature. The reaction was quenched by the dilution of the mixture with CH$_2$Cl$_2$, washed with saturated aqueous NH$_4$Cl, and the organic phase was dried over anhydrous MgSO$_4$, and concentrated in vacuum. The crude reaction product was purified using column chromatography (silica gel, hexane:ethyl acetate = 5:1) to afford **2** (5 g, 80% yield) as a colourless oil.

Synthesis of 5-(*tert*-Butyl-dimethyl-silanyloxy)-pentanal (A)

A

To a solution of tetrabutylammonium bromide (TBAB) 2g, 2,2,6,6-Tetramethylpiperidin-1-yl)oxyl (TEMPO) (3 g) was added compound **3** (5.0 g, 59.6 mmol) in CH$_2$Cl$_2$ (50 mL) with vigorous stirring at zero degrees. The reaction mixture was then continued to stir for 2 hours. To quench the reaction the mixture was diluted with CH$_2$Cl$_2$, washed with saturated aqueous NH$_4$Cl, the organic part was dried over MgSO$_4$, and thereafter concentrated in a vacuum. The crude reaction product was the purified utilizing column chromatography (silica gel, hexane: EtOAc = 50:1) to afford **A** (4.16g, 71% yield) as a yellow-orange oil.

Synthesis of 7-(*tert*-Butyl-dimethyl-silanyloxy)-hept-2-enoic methyl ester

4

98
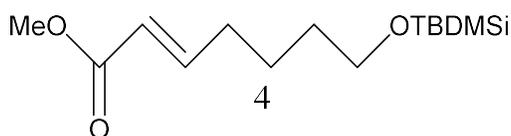
To a solution of Lithium Chloride was added methyl diethylphosphonoacetate dropwise (3.76 mL). To this reaction mixture was added **A** (2.99 g, 13.8 mmol) in THF (50 mL). Thereafter triethylamine (3 ml) was slowly added with stirring. The reaction was allowed to continued to stir at 25 degrees Celsius for 4 h. To stop the reaction, the saturated aqueous NH_4Cl solution was added. The solution was thereafter concentrated in a vacuum and crude material then diluted with ethyl acetate, washed with brine, and dried over $MgSO_4$, and then re-concentrated in a rotovap. The residue was thereafter purified by column chromatography the organic part was dried over $MgSO_4$, and thereafter concentrated *in vacuo*. The crude reaction product was then purified utilizing column chromatography (silica gel, hexane:ethyl acetate= 50:1) to afford **4** (2.90 g, 70% yield) as a colorless oil.

**Synthesis of (E)-7-(*tert*-Butyl-dimethyl-silanyloxy)-hept-2-en-1-ol (B).**

B
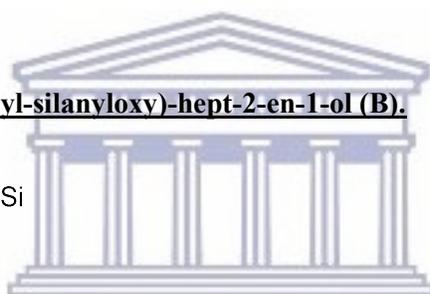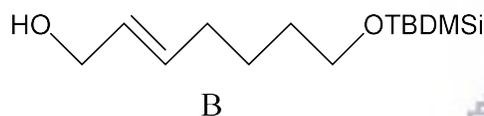
0.1 M solution of lithium borohydride ($LiBH_4$) was prepared by the vigorous stirring of lithium bromide and sodium borohydride in equimolar amounts in THF overnight at room temperature. After the formation of the NaBr precipitate as a white solid in the bottom of the flask, **4** (2.9g) was then introduced with vigorous stirring for 15h at room temperature. The crude material was filtered by celite pad and concentrated *in vacuo*. The crude product was then purified utilizing column chromatography (silica gel, hexane:ethyl acetate = 10:1) to afford **B** (2.0 g, 80% yield) as a colourrless oil.

Synthesis of 7-(tert-Butyl-dimethyl-silanyloxy)-hept-2-ene acetate

AcO〜〜〜OTBDMSi

5
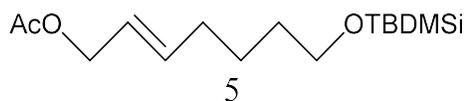
To a solution of acetic anhydride (12 mL) and **B (2.0 g)** in CH$_2$Cl$_2$ (50 mL) was added pyridine (12 mL) slowly with stirring**.** The reaction was continued to stir for 2 hat room temperature. The solvent was evaporated, and the crude material was diluted with CH$_2$Cl$_2$, washed with brine and dried over MgSO$_4$, and thereafter concentrated in a vacuum. The crude product was then purified utilizing column chromatography (silica gel, hexane:ethyl acetate = 5:1) to afford **5** (1.5 g) as a colorless oil.

Synthesis of compound C-OAc

AcO〜〜〜OH

C
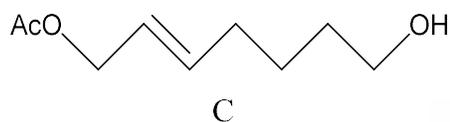
Compound **5** (1.5 g,) was dissolved in THF (20 mL) and tetrabutylammonium fluoride (1.0 M in THF 5.9 mL) was injected at room temperature and the reaction was continued to stir for 15 h. To quench the reaction the solvent was removed by evaporation, and the crude material was thereafter diluted with CH$_2$Cl$_2$, washed with brine, dried over MgSO$_4$, and thereafter concentrated in a vacuum. The crude product was then purified utilizing column chromatography (silica gel, petroleum ether: ethyl acetate 5:1, 2:1,1:1) to yield **C** (1.3 g) as a colorless oil.

Synthesis of 6

Compound C (1.3 g), toluene sulfonate chloride and DMAP (4-dimethylaminopyridine) were dissolved in CH$_2$Cl$_2$. Then triethylamine was added drop-wise with stirring. The reaction mixture was continued to stir for 3 hat room temperature. To quench the reaction the solvent was removed by evaporation, and the

100

crude material was thereafter diluted with CH$_2$Cl$_2$, washed with brine, was dried over MgSO$_4$, and thereafter concentrated in vacuum. The crude product was then purified utilizing column chromatography (silica gel, hexane: ethyl acetate 5:1) to yield **6** (1.3 g) as a colorless oil.

4.3 Results and discussion

### 4.3.1 Synthesis of chemically cleavable linker
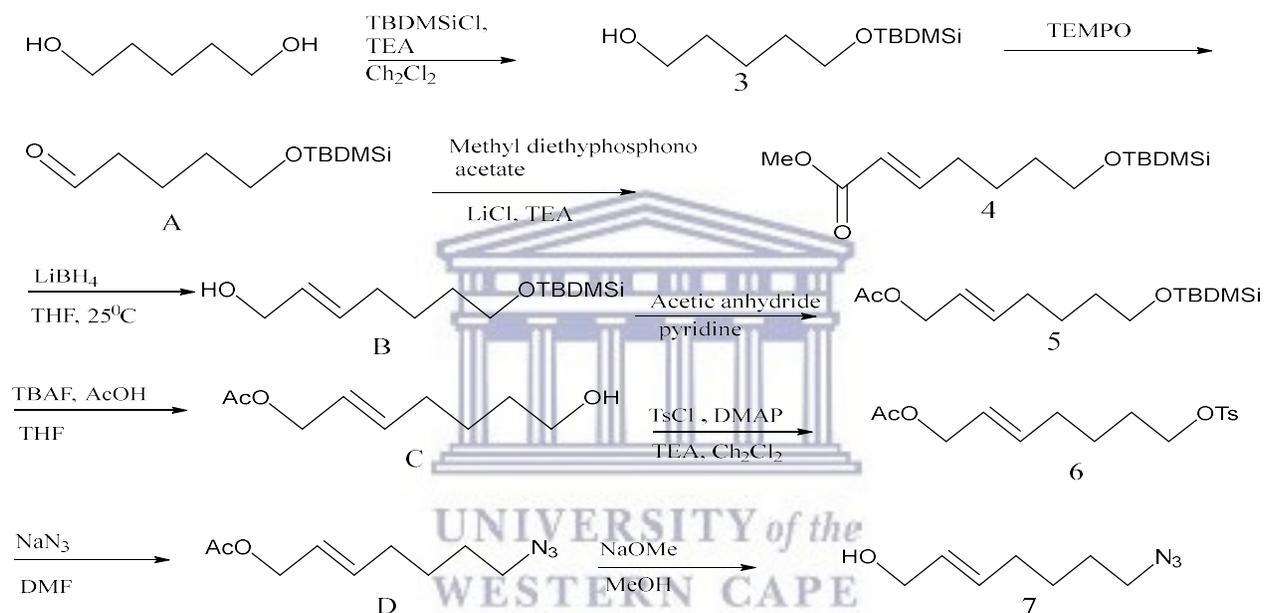
Figure 27 Reaction scheme for the preparation of the7- azido-bromo-hept-2-ene

4.3.1 Synthesis and characterisation of 5-(tert-Butyl-dimethyl-silanyloxy)-pentan-1-ol

Development of a synthetic approach for the synthesis of the chemically cleavable linker for the reversible labeling of thymidine at the 3'-OH with ferrocene commenced by following the approach described by Da-Rae Kim *et al 2014* [79] for the reversible labeling of thymidine at 3'-OH, with alterations. The 7-azido-bromo-hept-2-ene shown in figure 26, a chemically cleavable linker, was initially made in 9 step synthetic approach as shown in figure 2. Mono-sylation of the commercial diol is performed in the presences of a mild base triethylamine in dichloromethane, with the formation of the mono-sylation product as a competitive product in 70% yields. The compound was purified using Liquid Chromotography column (gravitation) packed with silica gel and utilizing hexane and ethyl acetate (5:1) as the mobile phase.

Fourier Transform Infrared Red spectroscopy was utilized to identify the purified product. The comparison of the spectra of the 1,5-pentanediol and the product shown in figure 27, revealed a significant reduction of the O-H broad absorption band (3400-3300 cm^{-1}) and the C-O band (1300 -1000 cm^{-1}). Also, the bands characteristic for aliphatic structures are still retained in the spectrum of compound 3. Comparing the commercial tert-butyldimethyl silyl chloride and the product also revealed the successful mono-substitution of the tert-butyldimethylsilyl protecting group by the presence of the Si-CH3 absorption bands (1275 -1245 cm^{-1}, 865 -755 cm^{-1}) with reduced intensities. From the absorption bands observed in the FTIR spectra confirmed the presence of compound 3.
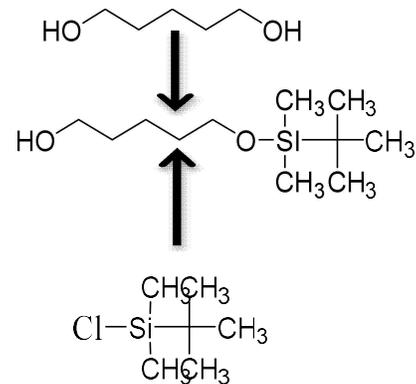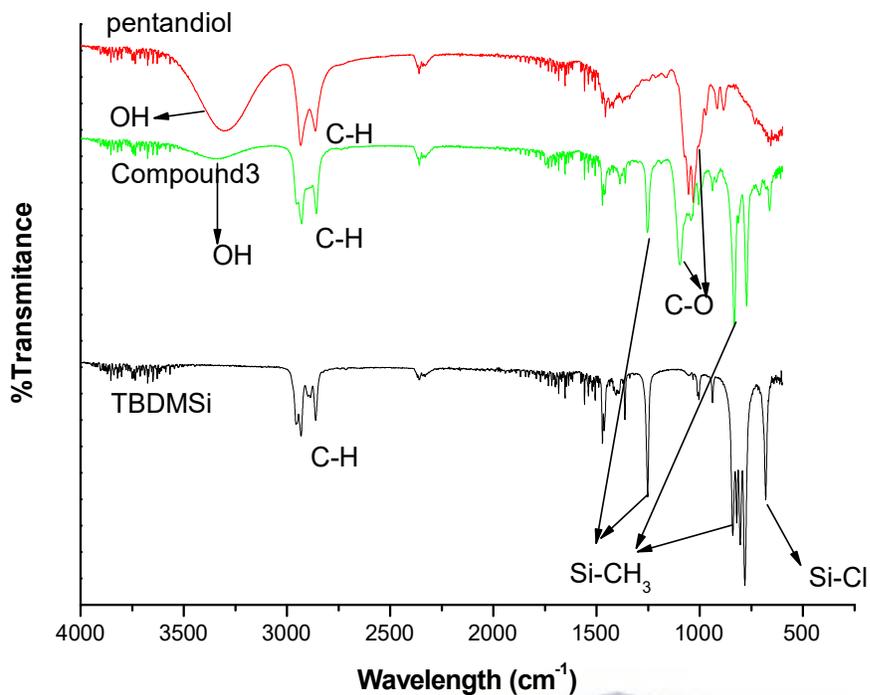
Figure 28 FTIR overlapped spectra of 1,5-pentanediol (starting material) , compound 3 (5-tert-Butyl-dimethyl-silanyloxy)-pentan-1-ol) and tert-butyldimethylsilyl chloride
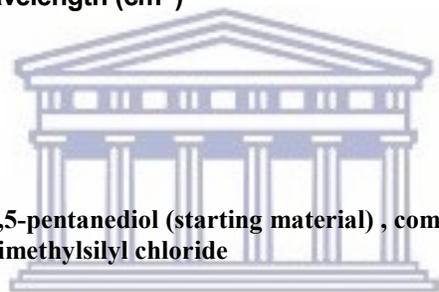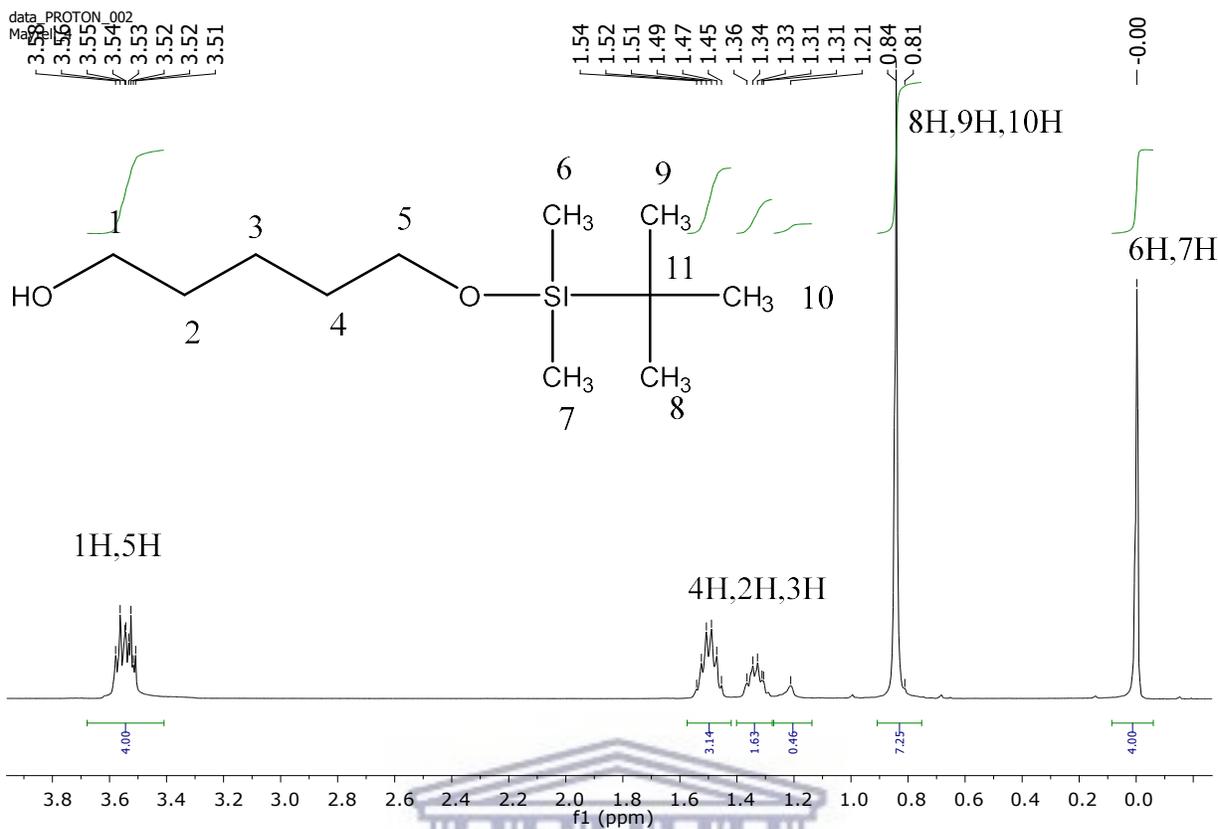
Figure 29 H'NMR of 5-(tert-Butyl-dimethyl-silanyloxy)-pentan-1-ol (compound 3), (400MHz, CDCl₃) *δ 7.54 (s,1H), 3.54 (m,2H), 3.53 (m,2H) 1.5 (m,2H), 1.35 (m, 2H), 0.84 (s, 9H), 0.0 (m,6H).*

104
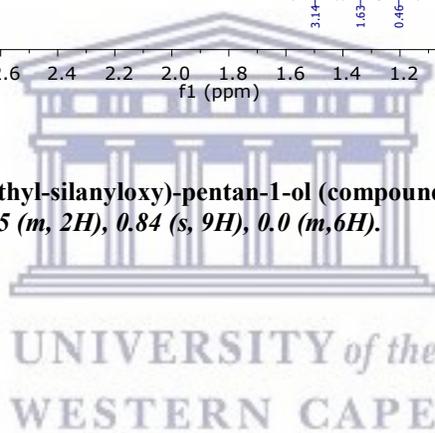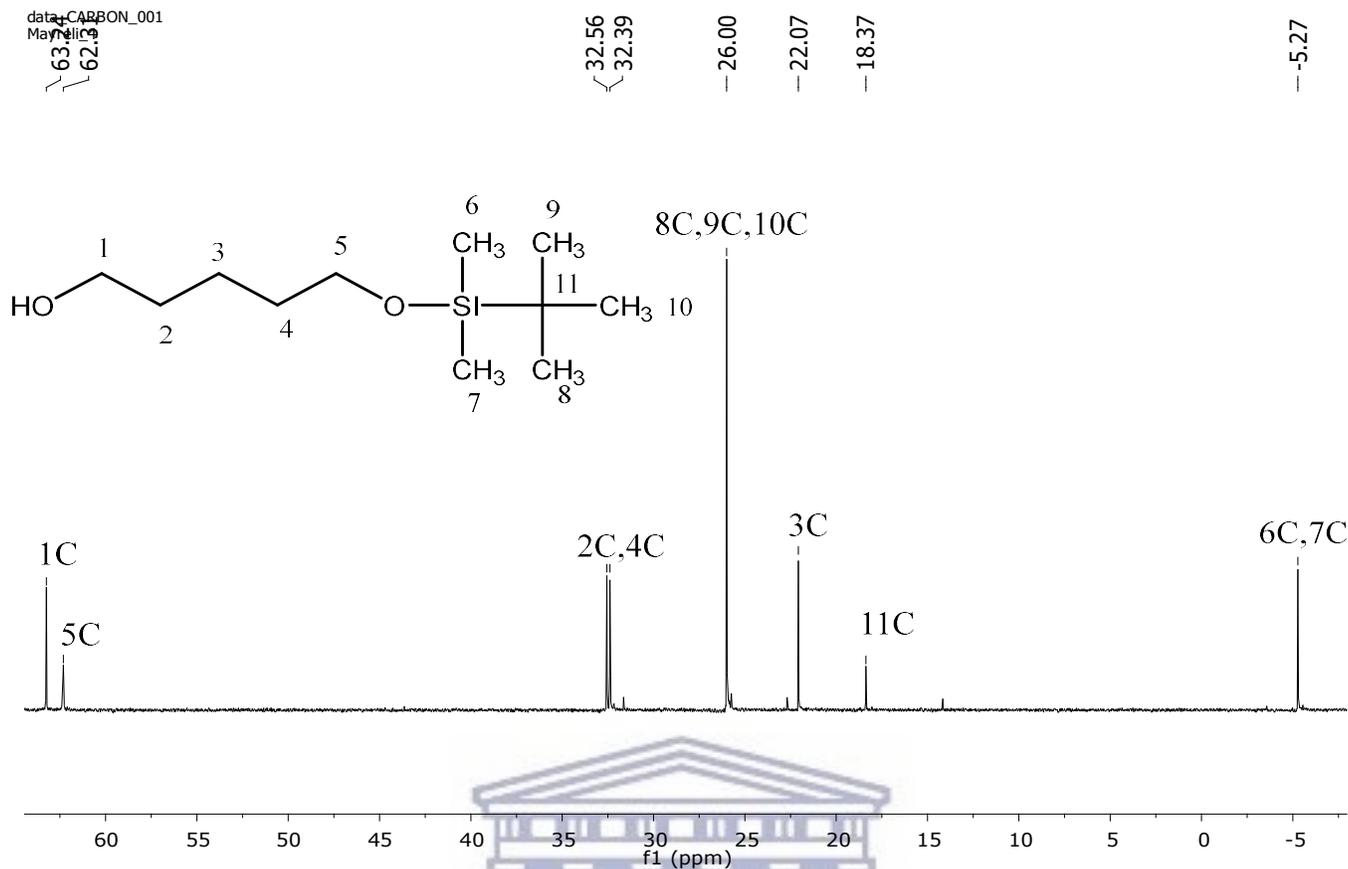
Figure 30 C'NMR of 5-(tert-Butyl-dimethyl-silanyloxy)-pentan-1-ol (compound 3) in chloroform-d , δ 63.24, 62.31, 32.56, 32.39, 26.00, 22.07, 18.37, 5.27

Furthermore, the proton and carbon nuclear magnetic resonance (NMR) was used to validate the product as shown in figure 28 and figure 29. Proton NMR reveals the presence of the singlets at 0.0 ppm and 0.8 ppm arising from the protons methyl groups due to the shielding effect of the tertial butyldimethyl group of the mono-sylation product. Also, the CH2 multiplet at 3.56 ppm is observed that arise from the deshielded protons on the carbons directly attached to the two oxygens 1, 5 as shown in figure 28. Consistent with the proton NMR, the carbon NMR also reveal the carbons from 1, 5 at 6.37 ppm. The presence of these peaks in the NMR spectra is crucial in identifying the monosylation thus in agreement with the FTIR spectra confirming the successful synthesis of compound 3.

105

4.3.2 Synthesis of 5-tert-Butyl-dimethyl-silanyloxy)-pentan-1-al
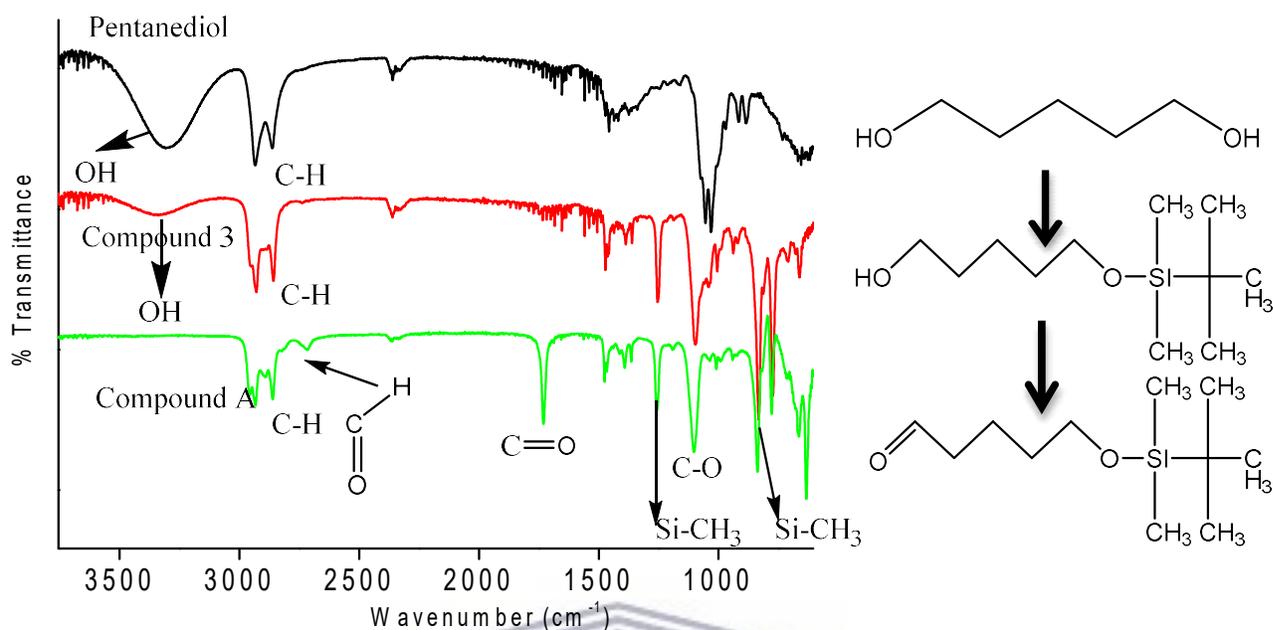
Figure 31 FTIR overlapped spectra of 1,5-pentanediol, compound 3 and compound A(5-tert-Butyl-dimethyl-silanyloxy)-pentan-1-al)

The monosylation reaction was then followed by the oxidation of the alcohol to the corresponding aldehyde, compound A. The oxidation of alcohols to aldehydes reaction is typically achieved through swern oxidation, whereby the alcohol is treated with equimolar amounts oxalyl chloride compound in the absence of oxygen (glove box) at -78 degrees. But in attempt to simplify the method, oxidation of the alcohol was achieved by treating the alcohol with equimolar amounts of TEMPO at room temperature. Column purification of synthesis compound A was performed utilizing mobile phase of hexane:ethylacetate in gradient ratios of (50:1), hexane: ethylacetate (25:1), hexane:ethyl acetate (1:1). This initially characterized using thin layer chromatography, shown in figure 31 developed with 2,4-

106

dinitrophenylhydrazine   HCl   which   is   specific   for   aldehydes.
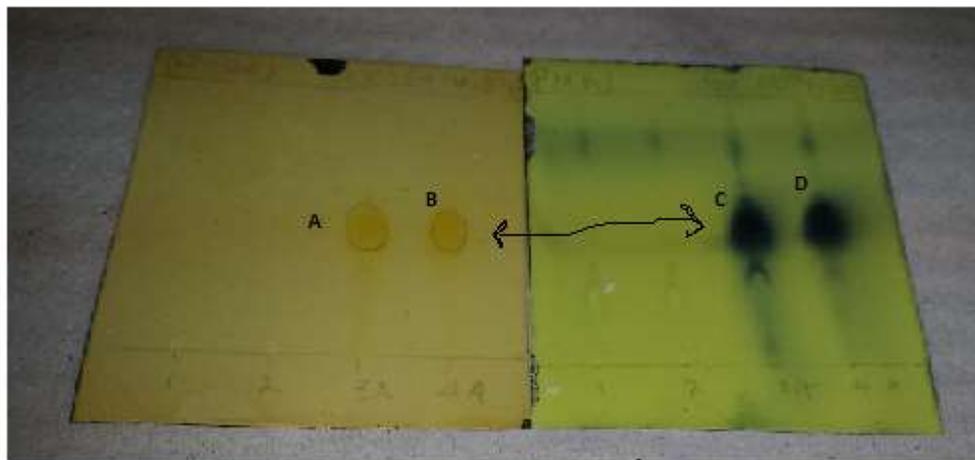
Figure 32 TLC plate of compound A developed with compound specific for aldehydes, 2,4-dinitrophenylhydrizine HCl(left) and universal developer, phosphomolybdic acid (PMA)(right)

The FTIR spectra of compound A revealed the presence of the C=O band corresponding to aliphatic aldehydes around 1740-1720 cm^{-1} and the Fermi doublet O=Csp−H around 2800-2700 cm^{-1}.Also it showed the total disappearance of the OH band (alcohol) around 3300 cm-1 which is present in the spectra of the alcohols further confirming the successful synthesis of compound A. The sylil protecting group was unaffected by the oxidation reaction due to the presence of the Si-CH3 absorption bands.

107
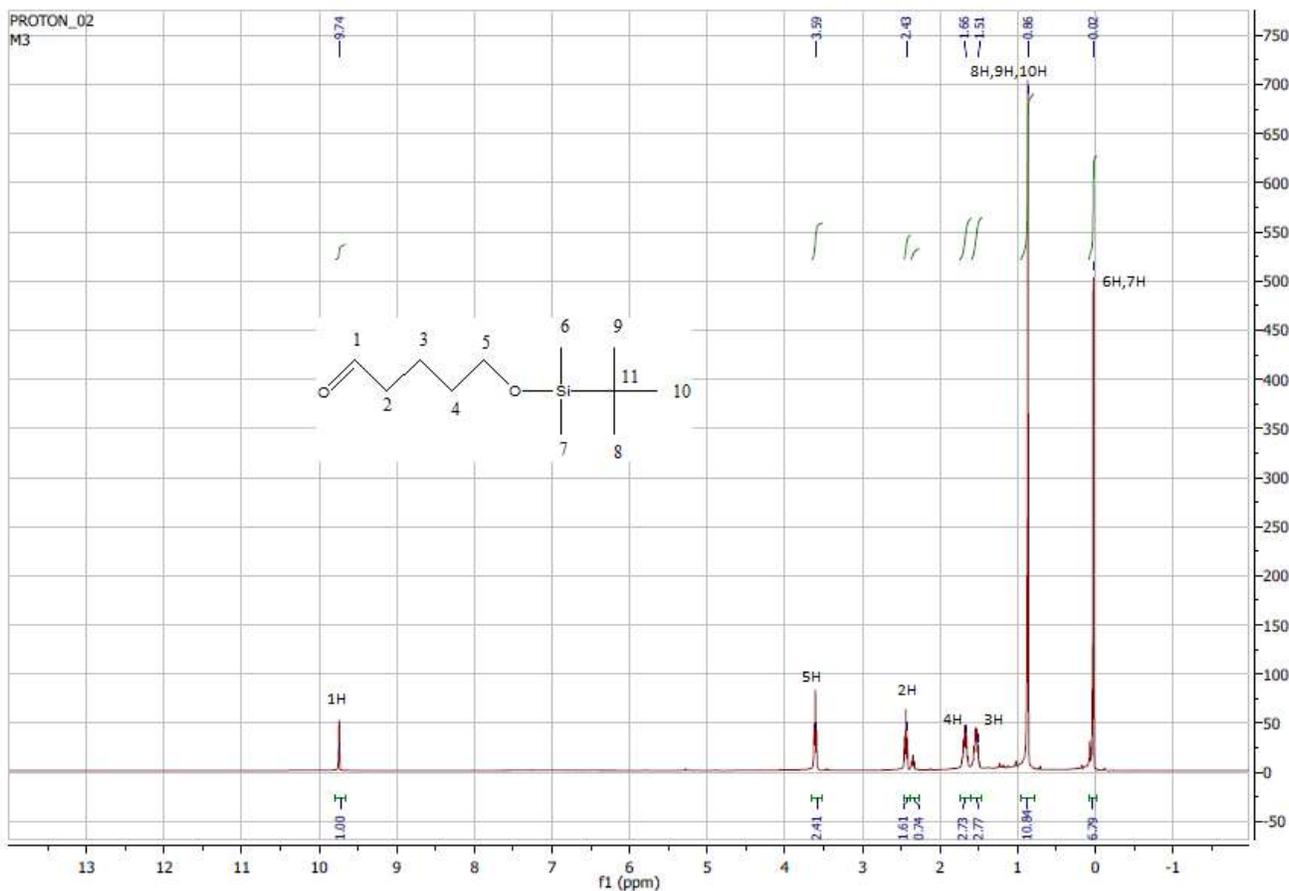
Figure 33 H'NMR of 5-(tert-Butyl-dimethyl-silanyloxy)-pentan-1-al (compound A) , (300 MHz, CDCl3); (δ, ppm = 9.74 (S, 1H) 3.99 (d, 2H) 2.43 (t, 2H) 1.66 (m, 2H) 1.51 (m, 2H) 0.85 (s, 9H) 0.02 (s, 6H)

The proton and carbon nuclear magnetic resonance (NMR) was used to validate the product as shown in figure 32 and figure 33. The singlet at 9.74 in the Proton NMR arising from the hydrogen directly attached to the carbonyl group which is highly deshielded, in agreement with the FTIR further confirms the successful oxidation of the alcohol. Also the presence of the singlets at 0.02 ppm and 0.85 ppm arising from the protons of the tertial butyldimethylsylil group confirms that the protecting group was retained during the oxidation reaction, similarly to what was observed in the FTIR. Also the CH2 doublet at 3.99 ppm is observed that arises from the deshielded protons on carbon 5, which is directly attached to the oxygen as shown in figure 32. Also consistent with the proton nmr, the carbon nmr also reveal the carbonyl carbon at 202.95 ppm characteristic of aldehydes.

108
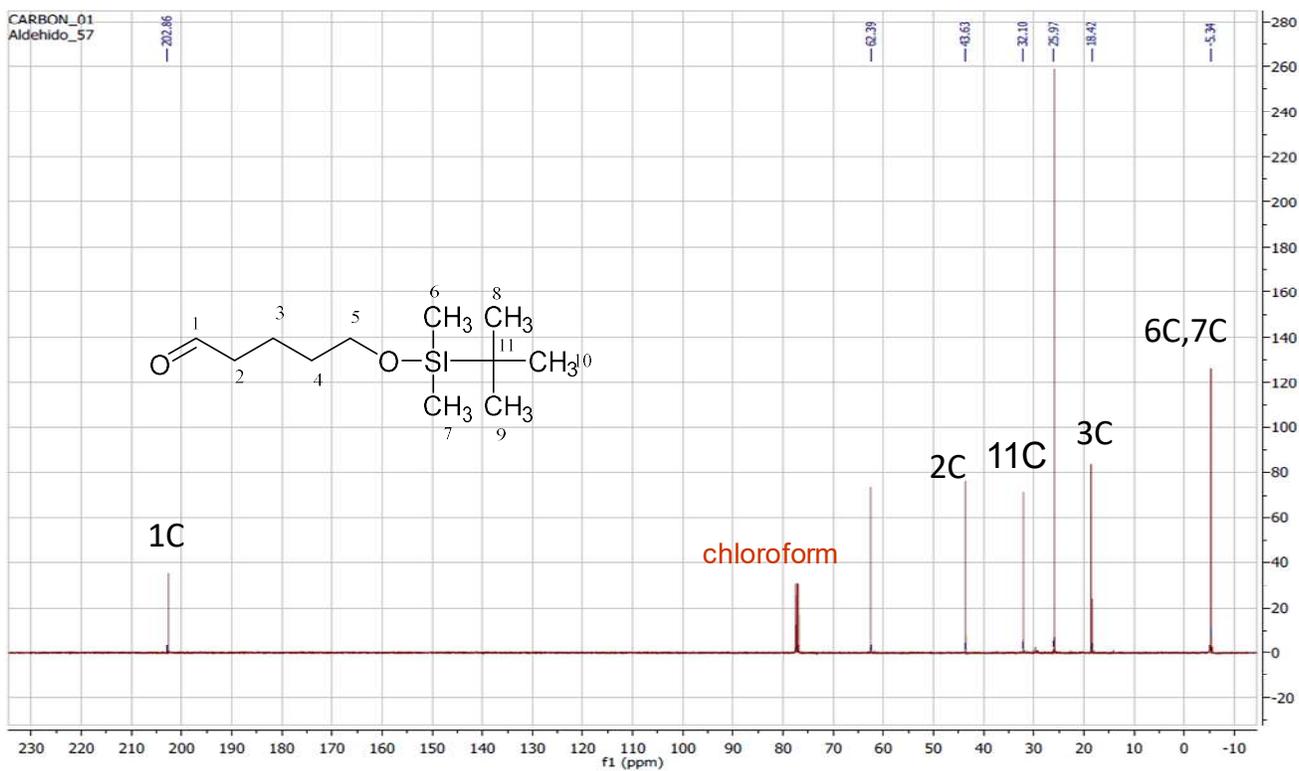
Figure 34 C'NMR of 5-(tert-Butyl-dimethyl-silanyloxy)-pentan-1-al (compound A), *δ 202.96, 62.39,43.63, 32.10, 25.97, 19.42, -5.34 ppm*

109

4.3.3 Synthesis and characterization of 7-(*tert*-Butyl-dimethyl-silanyloxy)-hept-2-enoic methyl ester
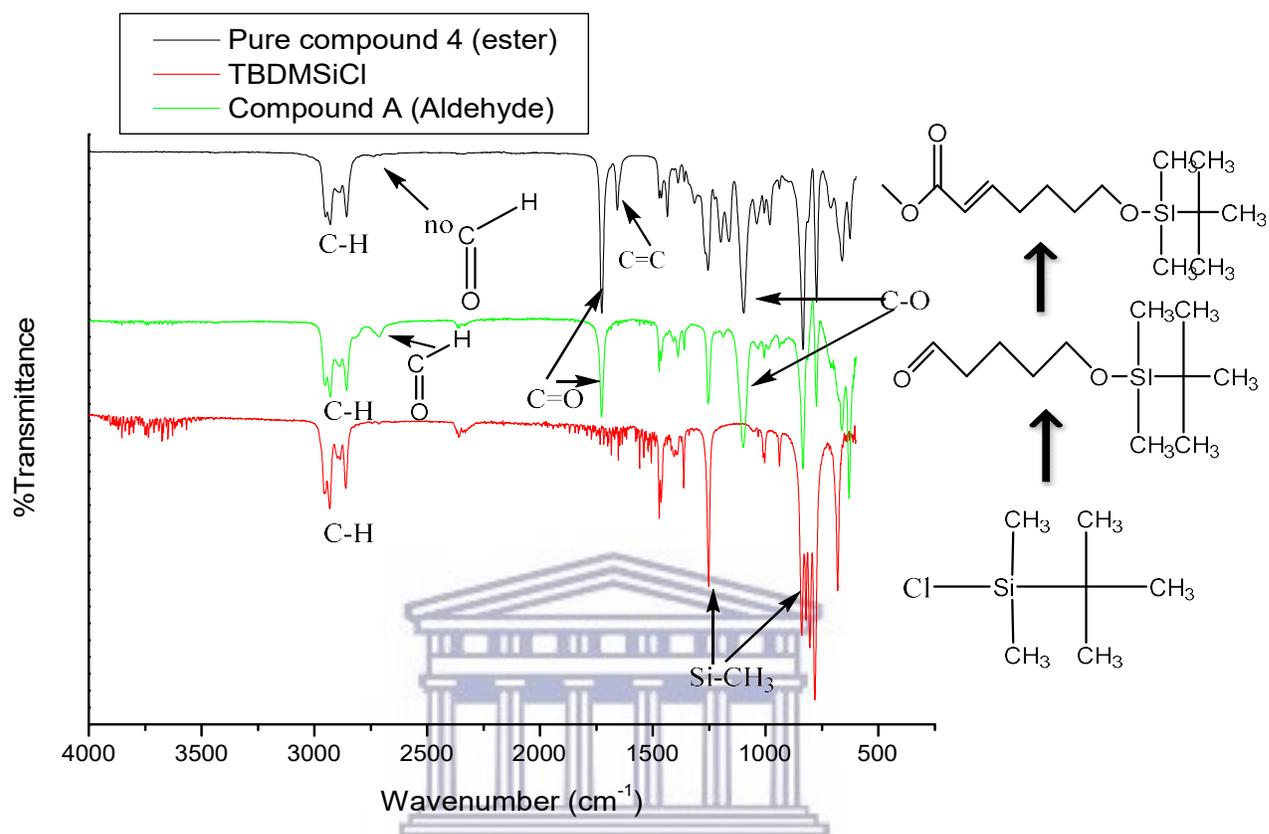

Figure 35 FTIR spectra of compound A (aldehyde), compound 4(7-(*tert*-Butyl-dimethyl-silanyloxy)-hept-2-enoic methyl ester) and tert-butyldimethylsilyl chloride

Thereafter the synthesis of compound 4, 7-(*tert*-Butyl-dimethyl-silanyloxy)-hept-2-enoic methyl ester (α-β unsaturated ester) was performed utilizing the Horner-Wadsworth-Emmons modification of the Wittig reaction[80]. Typically insertion of the olefin is performed utilizing sodium hydride (NaH) as a base, which requires a strictly oxygen free and moisture free environment at zero degrees[79]. In the alternative method, the olefination of the aldehyde was performed utilizing a milder base, triethylamine and lithium chloride (LiCl) at room temperature using a normal nitrogen line.
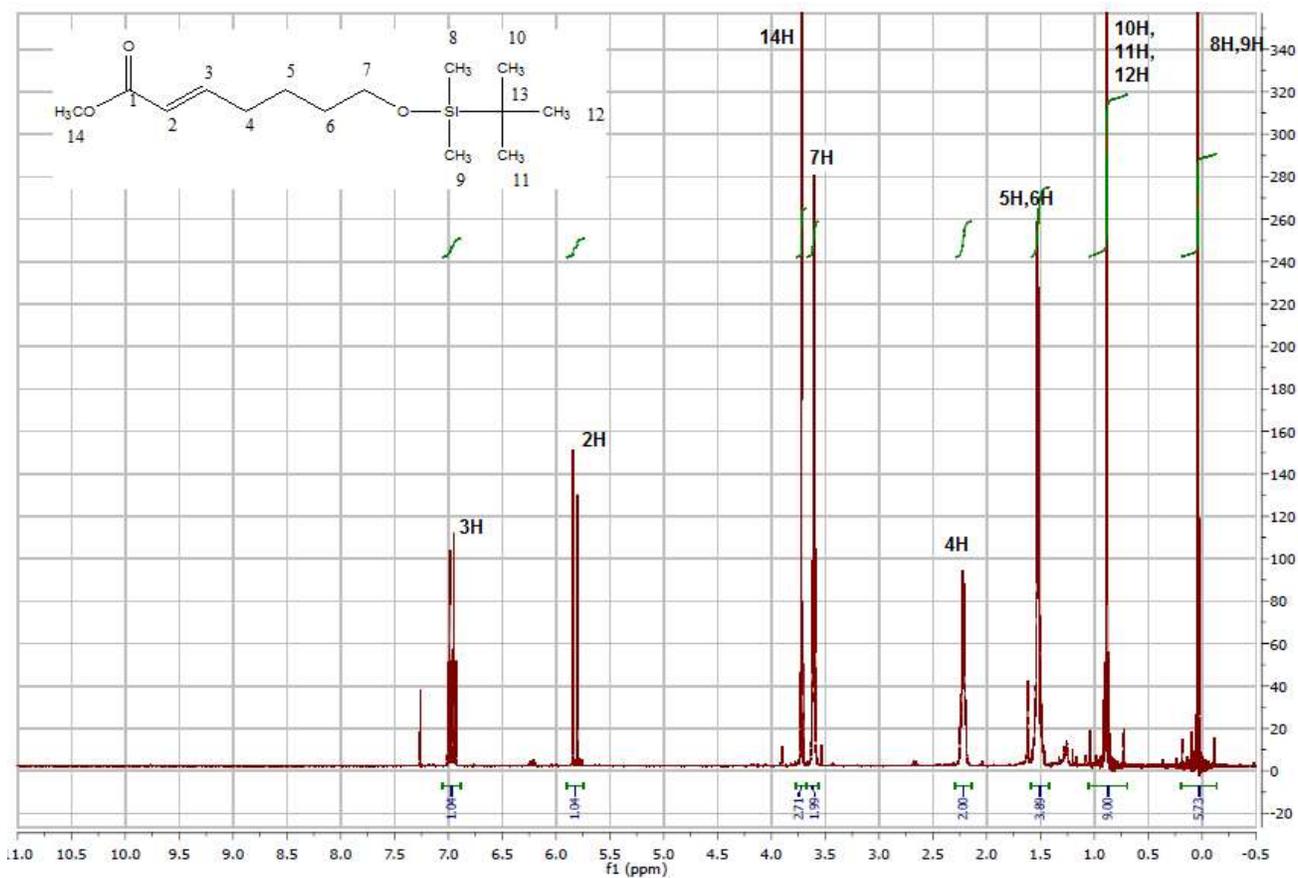
Figure 36 H'NMR of tert-Butyl-dimethyl-silanyloxy)-hept-2-enoic methyl ester (compound 4), (300 MHz, CDCl₃); δ, ppm = 6.99 (t, 1H) 5.75 (d, 1H) 3.75 (s, 3H) 3.66 (m, 2H) 2.25 (t, 2H) 1.5 (m, 4H) 0.98 (s, 9H) 0.0 (s, 6H)
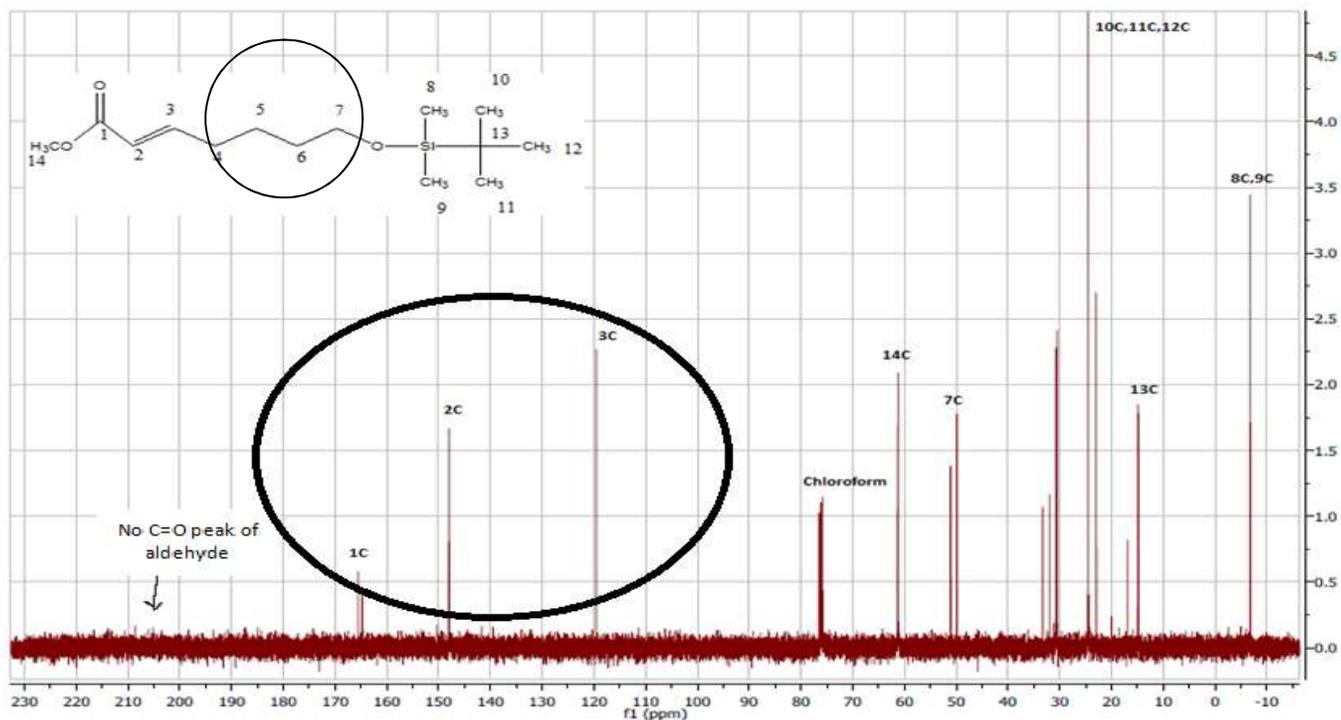
Figure 37 C'NMR of compound 4 -(*tert*-Butyl-dimethyl-silanyloxy)-hept-2-enoic methyl ester (α-β unsaturated ester), before purification , *δ ppm 165, 149, 120, 61, 25, 15, -5*

NMR characterisation of compound 4 (*tert*-Butyl-dimethyl-silanyloxy)-hept-2-enoic methyl ester (α-β unsaturated ester) is shown in figure 35 and figure 36 revealed the presence of the peaks. The integration of peaks labelled 3H (6.99 ppm, triplet) and 2H (5.75 ppm, doublet), reveal that they represent a single proton (1 hydrogen) each, in their respective environments characteristic of double bond protons. The carbon spectrum gives additional information on the ester, whereby the presence of peak 1C (~165 ppm) characteristic for esters and the absence of a significant peak for the aldehyde carbon which was around 210~200 ppm, further confirms that the aldehyde has been used up and converted to the α-β unsaturated ester.

4.3.4 Synthesis and characterization of 7-tert-butyl-dimethyl-silanyloxy-hept-2-en-1-ol

The reduction of the α-β unsaturated ester to a primary alcohol is typically performed utilizing Aluminium Hydrides such as $LiAlH_4$ and DIBAL-H, intern requiring temperatures of -78 degrees and strict moisture and oxygen free conditions as described by Kim *et al 2014* [79]. In this method the reduction was performed utilizing $LiBH_4$ by first preparing ~0.1 M solution of lithium borohydride by the vigorous stirring of lithium bromide and sodium borohydride in THF over night.[81] After the precipitation of NaBr (see equation 1), the ester compound 4 was introduced while stirring. The reaction was left over night to ensure complete conversion.

$$LiBr + NaBH_4 \xrightarrow[25^oC]{THF} LiBH_4 + NaBr \downarrow$$

equation 1
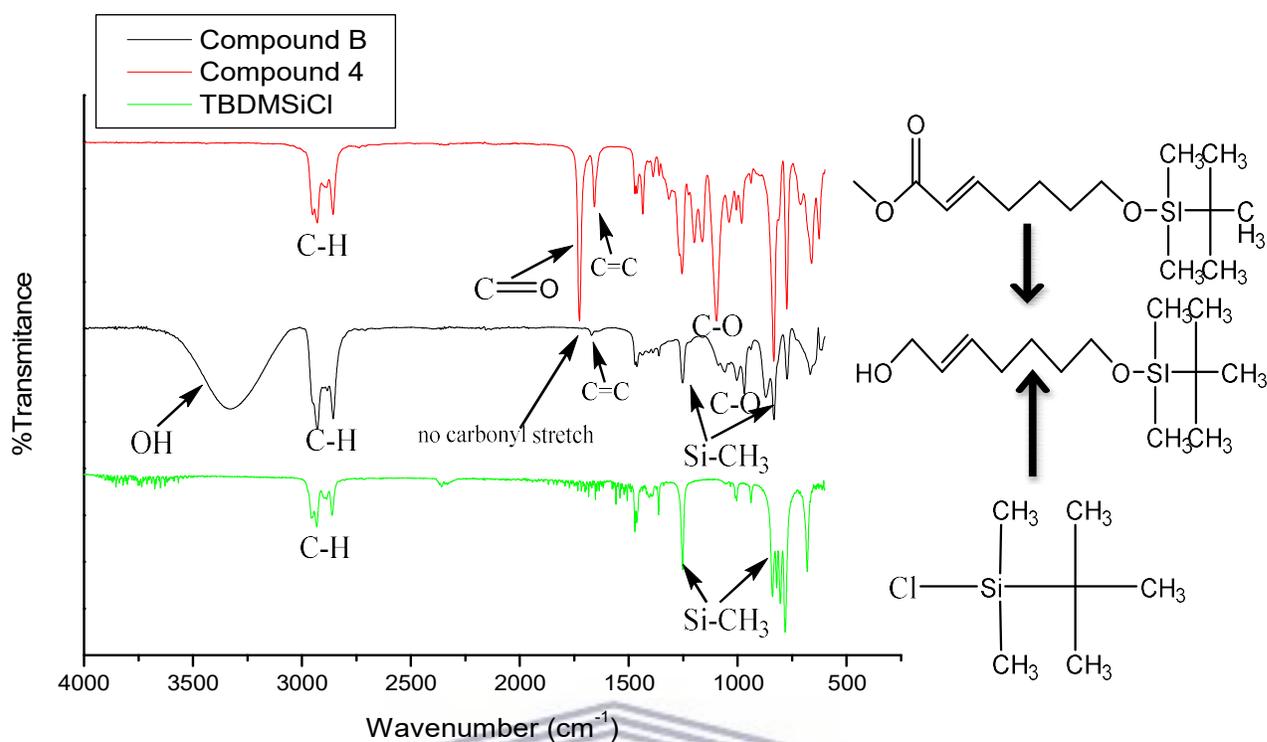
Figure 38 FTIR spectra of compound 4, compound B (7-tert-butyl-dimethyl-silanyloxy-hept-2-en-1-ol)

FTIR characterisation was performed to identify compound B. The spectra shown in figure 38, reveals the absence of the carbonyl band C=O (~1725 cm^{-1}, strong) characteristic of the ester group and the appearance of the OH band (~3330 cm^{-1}, broad) characteristic of alcohols, while retaining the C=C band (1680-1640 cm^{-1}, weak) arising from the conjugation. Also the retention of the Si-CH$_3$ bands from the sylil protecting group; further confirmed the successful reduction of the α-β unsaturated ester to the corresponding allylic primary alcohol without the loss of the tert butyl dimethylsylil protecting group under the utilized reaction conditions.

114
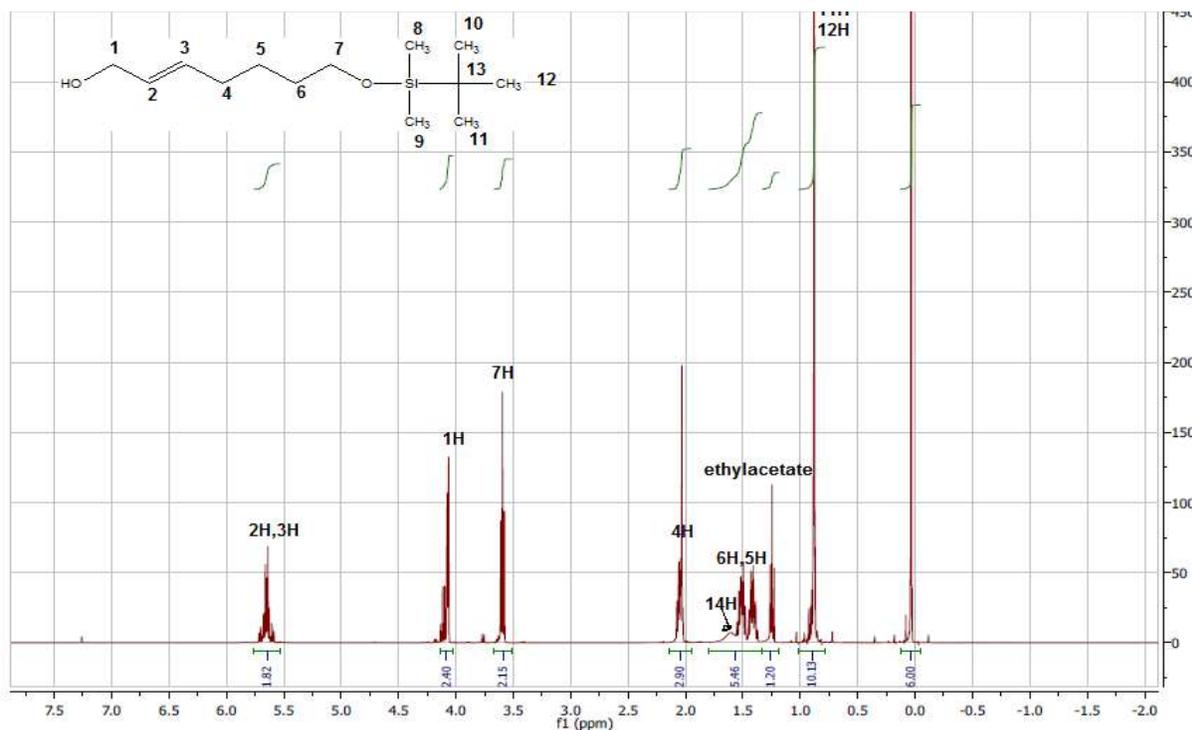
Figure 39 H'NMR of 7-(tert-Butyl-dimethyl-silanyloxy)-hept-2-en-1-ol (compound B), (300 MHz, CDCl₃); δ, ppm = **5.75 (m, 1H) 5.75 (m, 1H) 4.05 (d, 2H) 3.66 (d, 2H) 2.05 (t, 2H) 1.5 (m, 2H) 1.45 (m, 2H) 0.98 (s, 9H) 0.0 (s, 6H)**

Furthermore, NMR characterisation of compound B 7-(tert-Butyl-dimethyl-silanyloxy)-hept-2-en-1-ol is shown in figure 39 and figure 40. The spectrum reveals the appearance of the proton 1H at 4.05 ppm (doublet) on the carbon adjacent to the alcohol group and the further splitting of the proton 2H peak to a multiplet instead of a triplet, as it was in the case of the ester due to the absence of neighbouring protons on the carbon 1C. The carbon spectrum further compliments the observation seen in the proton nmr, whereby the absence of the peak at 165 ppm, which is characteristic of esters, and the appearance of 1C at 135 ppm, from the primary alcohol confirmed the successful reduction of the ester to the corresponding primary alcohol.
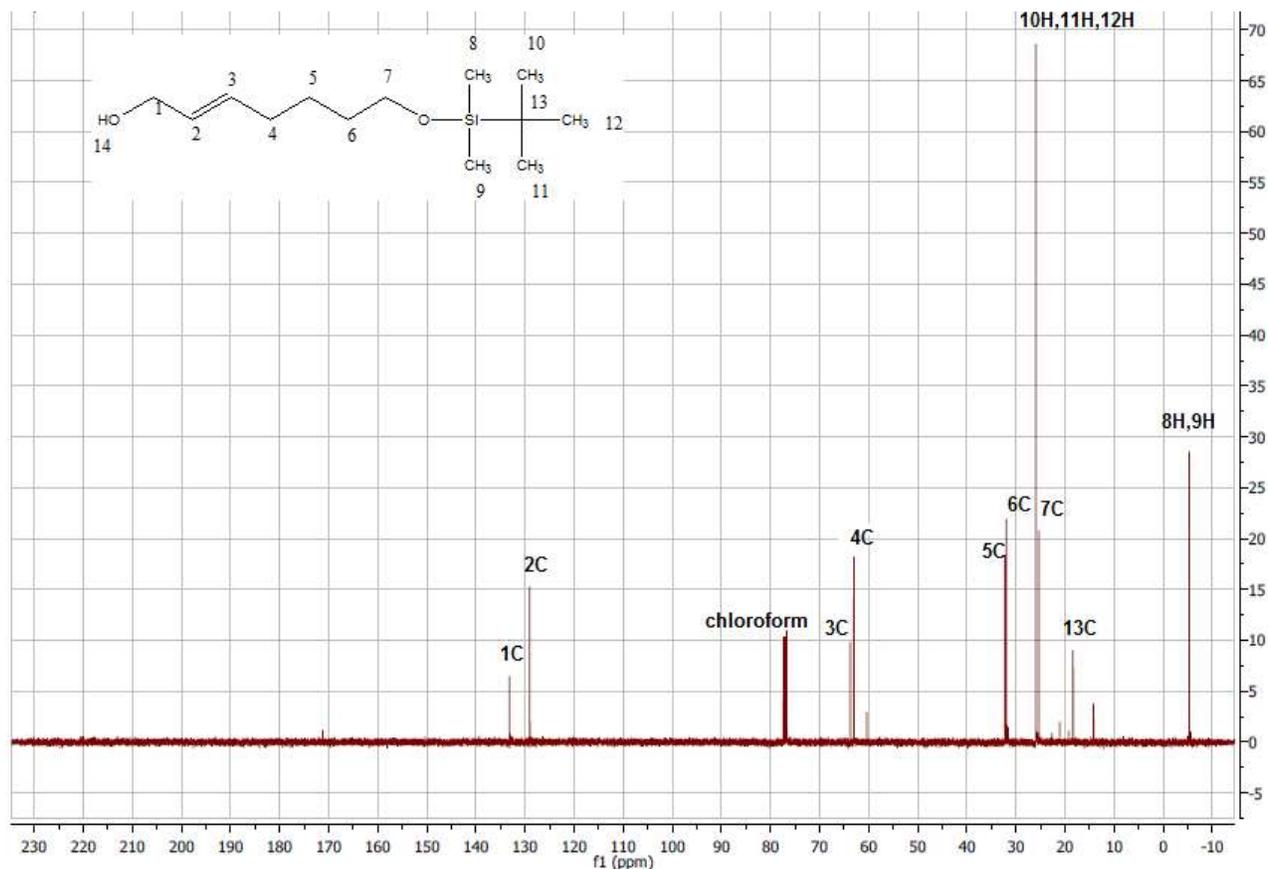
115

Figure 40 C'NMR of 7-(tert-Butyl-dimethyl-silanyloxy)-hept-2-en-1-ol (compound B), *δ ppm 135, 129, 65, 64, 32,31,25,18, -5*
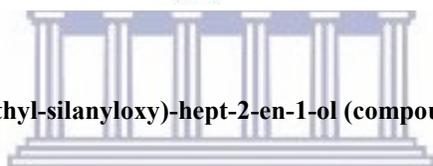
4.3.5 Synthesis and characterization of 7-(tert-Butyl-dimethyl-silanyloxy)-hept-2-ene acetate

The acylation of compound B was performed utilizing two approaches whereby firstly compound B with 2 equivalents of acetic anhydride and 2.5 equivalents of diisopropylethylamine (DIPEA) in CH_2Cl_2. Thin layer chromatography (TLC) of the reaction revealed that the starting material is slowly consumed (fig 4), as the intensity of the spot for the starting material (lower spot) is not significantly reduced over a period of 5 hours; signifying a slow formation of desired product. Hence the reaction was continued to stir for 24 hours, yielding a dark brown solution.

116

The more widely used second approach involved the treating of compound B with an excess of pyridine and acetic anhydride. The reaction was also followed utilizing thin layer chromatography (TLC) as shown in fig 5, revealed that the starting material was consumed after 2 hours. Therefore this method was then utilized to synthesize 7-(tert-Butyl-dimethyl-silanyloxy)-hept-2-ene acetate.
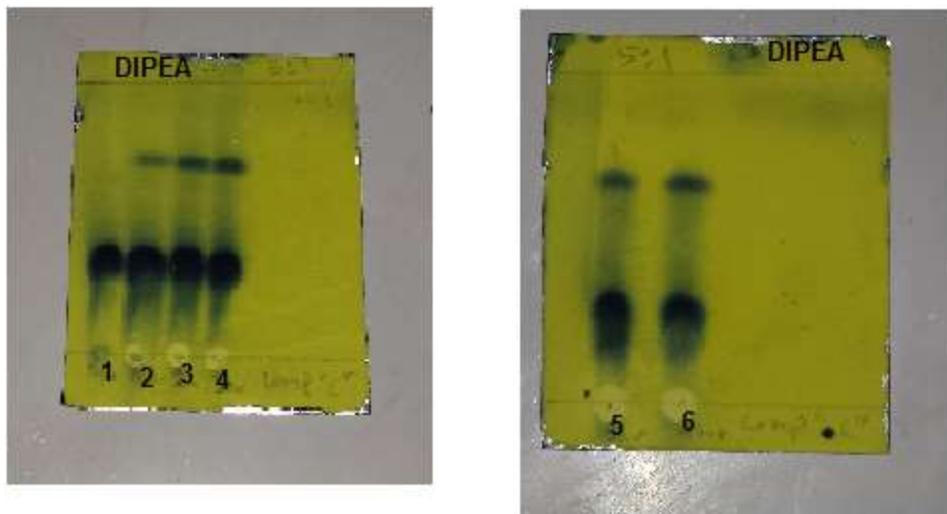

Figure 41TLC plate for protection of compound B with acetate via DIPEA method; whereby 1) Start of the reaction,2) after 1 hour,3) after 2 hours, 4) after 3 hours, 5)4 hand 6) after 5 hours
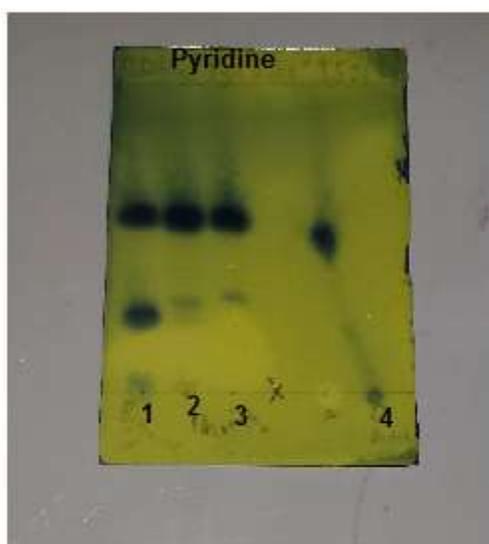
**Figure 42TLC plate for the protection of compound B with acetate via excess pyridine method whereby 1) reaction after 15 min,2) after 1 hour, 3) after 2 hour, 4) DIPEA product.**

117
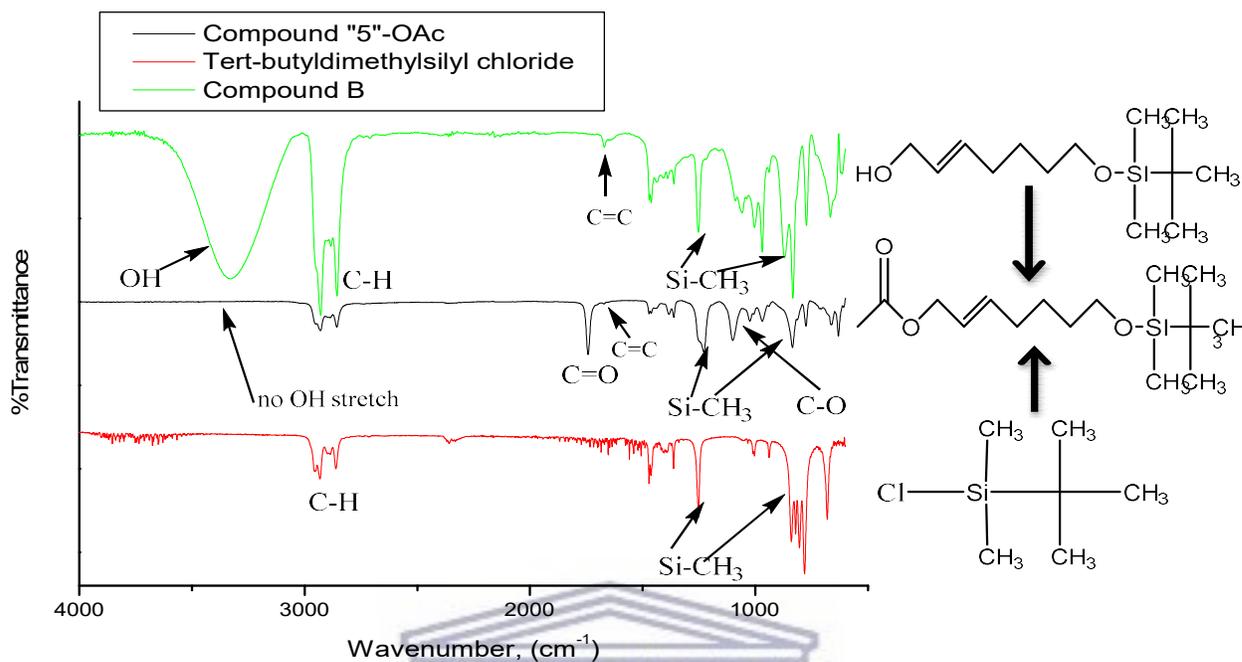
Figure 43 FTIR spectra of compound B, compound "5"-OAc and tert-butyldimethylsilyl chloride

Fourier Transform Infrared Red spectroscopy was utilized for the characterization of 7-(tert-Butyl-dimethyl-silanyloxy)-hept-2-ene acetate. The comparison of the spectrum of compound B, commercial tert-butyldimethyl silyl chloride precursor and the product is shown in figure 44. It revealed the absence of the alcohol ,OH (~3330 cm^{-1} , broad) band and the presence of the carbonyl (1740 cm^{-1} , sharp) band arising from the acetate while retaining the double bond c=c and Si-CH bands and this confirmed the successful acetylation of compound B without deprotecting the tert-butyldimethylsilyl group.
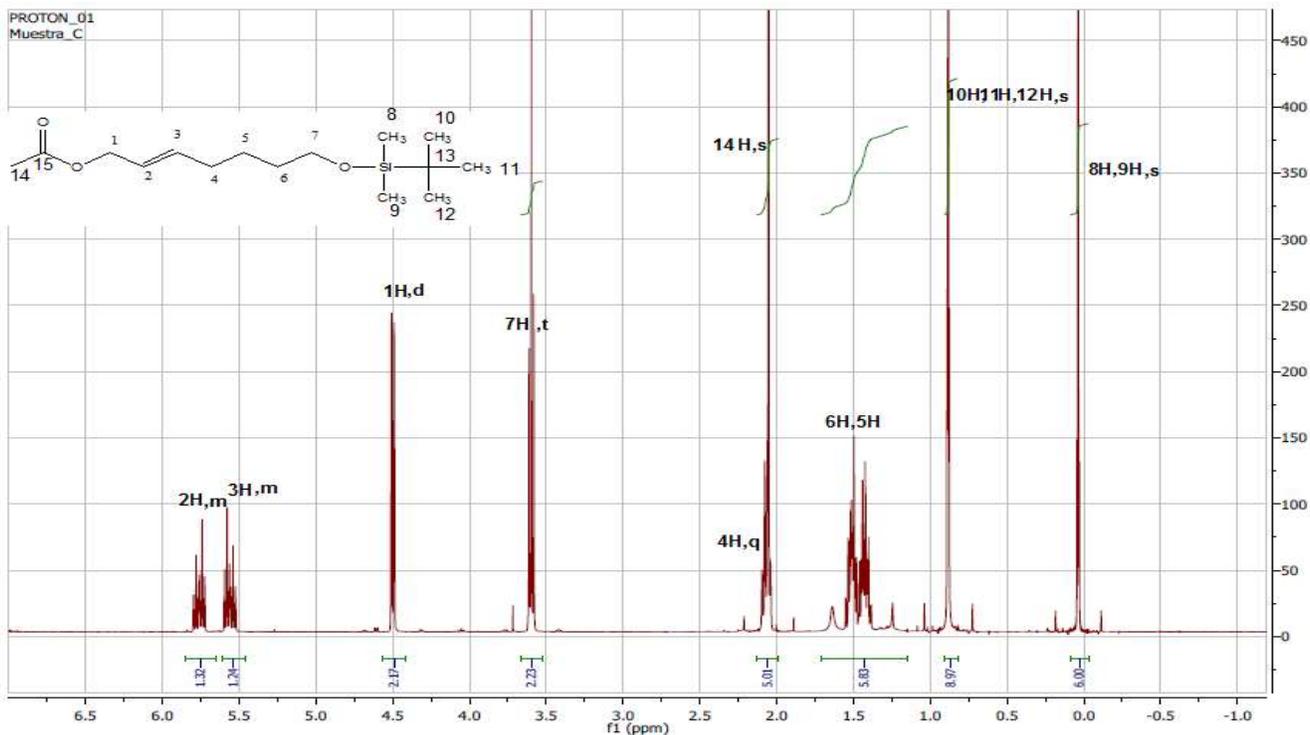
Figure 44 H'NMR of 7-(tert-Butyl-dimethyl-silanyloxy)-hept-2-ene acetate, compound 5, (300 MHz, CDCl₃) : δ, ppm = 5.75 (m, 1H) 5.55 (m, 1H) 4.50 (d, 2H) 3.66 (t, 2H) 2.05 (q, 2H) 1.5 (m, 2H) 1.45 (m, 2H) 0.98 (s, 9H) 0.01 (s, 6H)

Furthermore NMR characterisation of 7-(tert-Butyl-dimethyl-silanyloxy)-hept-2-ene acetate is shown in figure 45. The spectrum reveals the appearance of the proton 1H at 4.50 ppm (doublet) on the carbon adjacent to the acetate group at a higher chemical shift than the carbon adjacent to the alcohol in (figure 39) as the acetate group is more electronegative further confirmed successful acetalytion of compound **B** (alcohol). Also the olefin protons show two distinct chemical shifts in comparison to the alcohol signifying a drastic change in the chemical environment with the deshielding effect of the acetate group.

119

4.3.6 Synthesis and characterization of compound C

Deprotection of tert-butyldimethylsilyl group of compound "5"-OAc, to the corresponding primary alcohol compound "C"-OAc ; was performed using tetrabutylammonium fluoride (TBAF), overnight. The reaction product was then purified utilizing column chromatography with silica gel as a stationary phase and a gradient of petroleum ether: ethyl acetate in ratios of 5:1,2:1,1:1 as a stationary phase. The TLC (figure 46) revealed the complete conversion of the starting material, compound"5" (1), to form a new product travelling at slower rate (spot 2) indicative of a more polar compound formation, an expected behaviour from the intended product as the alcohol group is more polar than the silyl group.


Figure 45 TLC plate of the starting material 1) compound 5-OAc and 2) the reaction product.

120
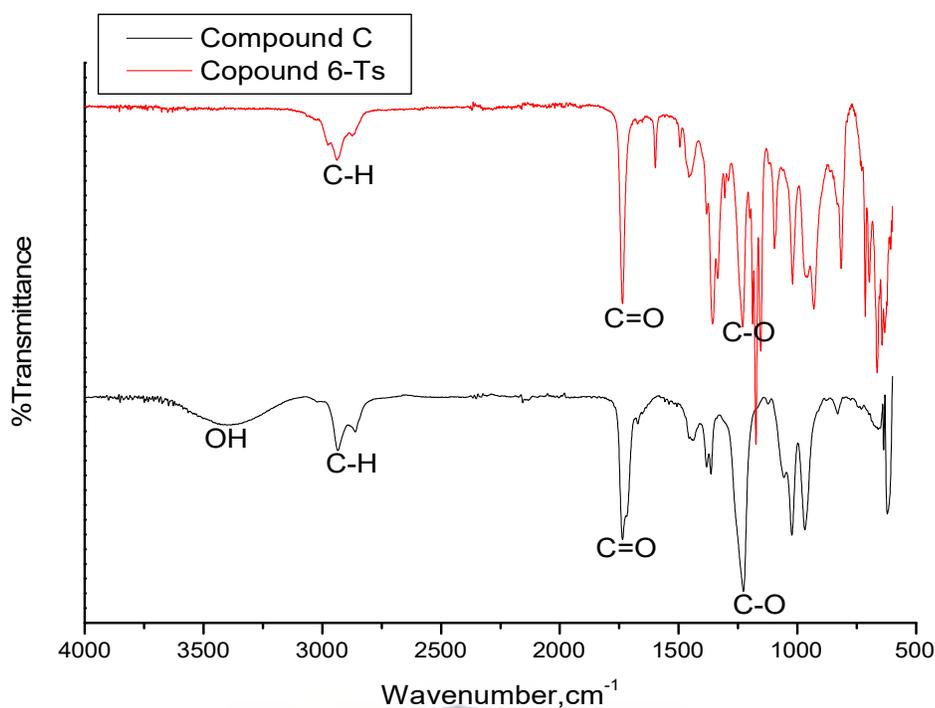
Figure 46 FTIR spectra of compound C and compound 6

Fourier Transform Infrared Red spectroscopy was utilized to characterize compound C. The spectrum shown in figure 49 revealed the appearance of the O-H broad absorption band (3400-3300 cm^{-1}) and the C-O band (1300 -1000 cm^{-1}) arising from the hydroxyl group. Also the absence of Si-CH$_3$ absorption bands Si-CH$_3$ absorption bands (1275 -1245 cm-^{1}, 865 -755 cm-^{1}) arising from the tert-butyl dimethyl silyl protecting group confirmed that the protecting group was successfully deprotected while retaining the acetate functional groups.

121
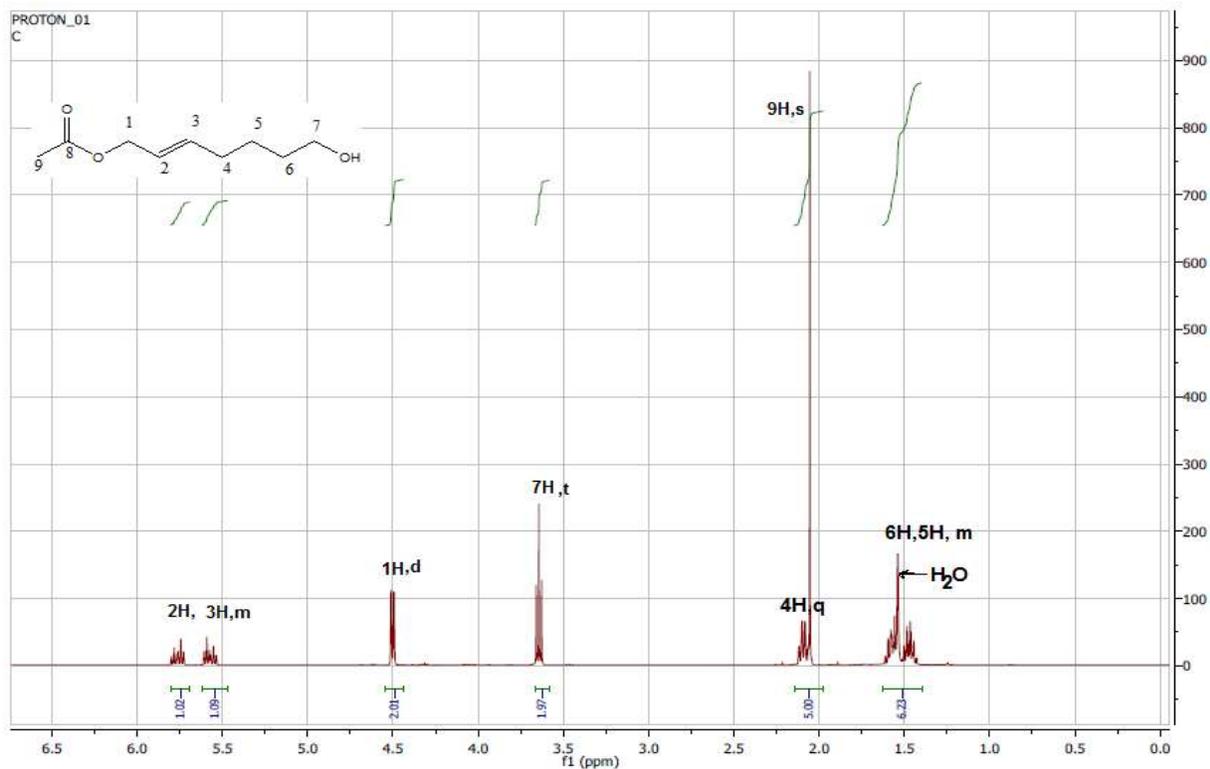
Figure 47 H'NMR of compound C, ¹HNMR (300 MHz, CDCl₃); δ, ppm = 5.75 (m, 1H) 5.60 (m, 1H) 4.50 (d, 2H) 3.70 (t, 2H) 2.05 (q, 2H) 1.5 (m, 2H) 1.45

Nuclear Magnetic Resonance (NMR) characterisation of 7-(tert-Butyl-dimethyl-silanyloxy)-hept-2-ene acetate is shown in figure 45. The total absence of the tert-butyldimethylsilyl protons at ~1 ppm to 0.0 ppm spectrum revealed the successful deprotection of the alcohol. Also the slight shift of the proton on carbon 7 towards from 3.66 ppm to 3.70 ppm is indicative of the presence of a more electronegative group further confirming the presence in the alcohol.

4.3.7 Synthesis and characterization of compound 6

The tosylation of the alcohol was performed as a precursor for the azide synthesis as toluene sulfonate is a strong leaving group as it is resonance stabilized. The reaction was then performed utilizing toluene sulfonate chloride and DMAP (4-dimethylaminopyridine) in the presence of triethylamine in dichloromethane. The reaction product was then characterized by thin layer chromatography as shown in figure 48 hereby after 3 h the starting material A, was almost completely consumed to form the intended product. The compound was then characterized utilizing mass spectrometry and the mass spectrum of compound 6 (figure 50) confirmed the success of the synthesis by the presence of the peak $[C_{16}H_{22}O_5S]^+$ at 344.1582, which is identical with the calculated molecular weight, 326 g/mol without the NH_4 (equipment).
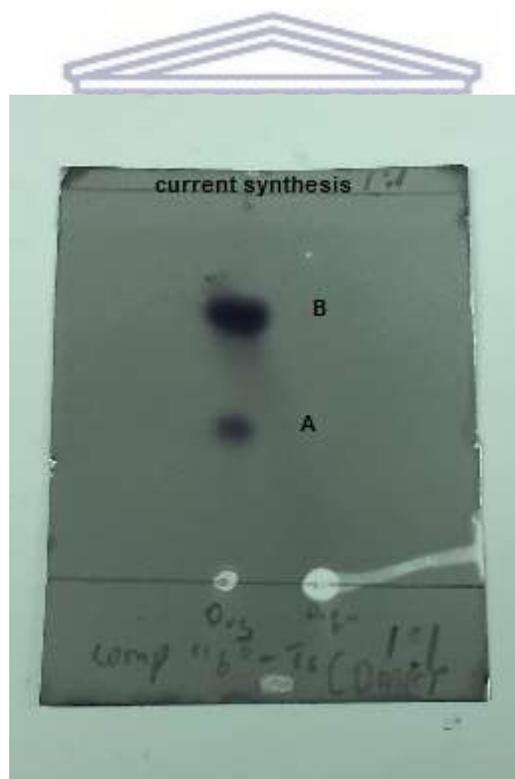

Figure 48 TLC plates for the synthesis of compound 6, whereby the pattern obtained are identical to the previously synthesized and characterized compound. A) Compound C and B) compound 6.
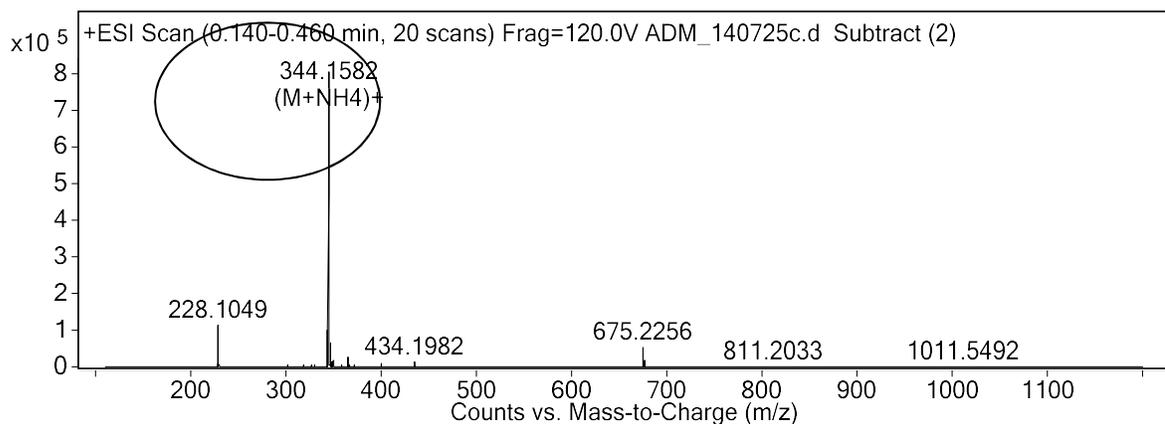
Figure 49 ESI-MS spectra of compound 6

4.4 Conclusion

A 7 step synthetic approach towards the development of a linker for reversible terminating and labelling nucleotides at 3'-OH position and application in electrochemical SBS DNA has been proposed and demonstrated. Only one of the reaction step has been retained from the Da-Rae Kim method and yielding 6 new compounds not stipulated anywhere else in literature, search performed utilizing Scifinder. All metal hydride steps have been replaced thus allowing all reaction steps to be performed in standard conditions. The tosylate last precursor is a good leaving group, an excellent stable precursor for the azide reaction required for labelling purposes. The precursors were synthesized and characterized utilizing Thin Layer Chromatography (TLC), Fourier transform infrared spectroscopy (FTIR), Nuclear Magnetic Resonance Spectroscopy (^{1}H-NMR), Carbon Nuclear Magnetic Resonance Spectroscopy (^{13}C-NMR) and ESI-Tof mass spectrometry. The method offers a simplified approach to the synthesis of an universal linker which can be utilized for labelling all four nucleotides at 3'OH position.

References

[63] E. R. Mardis, "Next-generation sequencing platforms.," *Annu. Rev. Anal. Chem. (Palo Alto. Calif).*, vol. 6, pp. 287–303, 2013.

[64] M. L. Metzker, "Sequencing technologies - the next generation.," *Nat. Rev. Genet.*, vol. 11, no. 1, pp. 31–46, 2010.

[65] J. Ju, D. H. Kim, L. Bi, Q. Meng, X. Bai, Z. Li, X. Li, M. S. Marma, S. Shi, J. Wu, J. R. Edwards, A. Romu, and N. J. Turro, "Four-color DNA sequencing by synthesis using cleavable fluorescent nucleotide reversible terminators.," *Proc. Natl. Acad. Sci. U. S. A.*, vol. 103, no. 52, pp. 19635–19640, 2006.

[66] J. Korlach, A. Bibillo, J. Wegener, P. Peluso, T. T. Pham, I. Park, S. Clark, G. a Otto, and S. W. Turner, "Long, processive enzymatic DNA synthesis using 100% dye-labeled terminal phosphate-linked nucleotides.," *Nucleosides. Nucleotides Nucleic Acids*, vol. 27, no. 9, pp. 1072–1083, 2008.

[67] E. L. van Dijk, H. Auger, Y. Jaszczyszyn, and C. Thermes, "Ten years of next-generation sequencing technology," *Trends Genet.*, vol. 30, no. 9, pp. 418–426, Aug. 2014.

[68] J. C. P. Esperança, W. R. R. Miranda, J. B. Netto, F. S. Lima, L. Baumworcel, L. Chimelli, R. Silva, T. P. Ürményi, P. H. Cabello, E. Rondinelli, and D. S. Faffe, "Polymorphisms in IL-10 and INF-γ genes are associated with early atherosclerosis in coronary but not in carotid arteries: A study of 122 autopsy cases of young adults," *BBA Clin.*, vol. 3, pp. 214–220, 2015.

[69] K. M. Hayden, J. M. McEvoy, C. Linnertz, D. Attix, M. Kuchibhatla, A. M. Saunders, M. W. Lutz, K. a. Welsh-Bohmer, A. D. Roses, and O. Chiba-Falek, "A homopolymer polymorphism in the TOMM40 gene contributes to cognitive performance in aging," *Alzheimer's Dement.*, vol. 8, no. 5, pp. 381–388, 2012.

[70] B. Li, G. Pan, N. D. Avent, R. B. Lowry, T. E. Madgett, and P. L. Waines, "Graphene electrode modified with electrochemically reduced graphene oxide for label-free DNA detection," *Biosens. Bioelectron.*, vol. 72, pp. 313–319, 2015.

[71] B. Xu, D. Zheng, W. Qiu, F. Gao, S. Jiang, and Q. Wang, "An ultrasensitive DNA biosensor based on covalent immobilization of probe DNA on fern leaf-like α-Fe2O3 and chitosan Hybrid film using terephthalaldehyde as arm-linker," *Biosens. Bioelectron.*, vol. 72, pp. 175–181, 2015.

[72] M. Li, Y. Wang, Y. Zhang, J. Yu, S. Ge, and M. Yan, "Graphene functionalized porous Au-paper based electrochemiluminescence device for detection of DNA using luminescent silver nanoparticles coated calcium carbonate/carboxymethyl chitosan hybrid microspheres as labels," *Biosens. Bioelectron.*, vol. 59, pp. 307–313, 2014.

[73] J. Zheng, C. Chen, X. Wang, F. Zhang, and P. He, "A sequence-specific DNA sensor for Hepatitis B virus diagnostics based on the host-guest recognition," *Sensors Actuators, B Chem.*, vol. 199, pp. 168–174, 2014.

[74] Y. Sun, X. He, J. Ji, M. Jia, Z. Wang, and X. Sun, "A highly selective and sensitive electrochemical CS–MWCNTs/Au-NPs composite DNA biosensor for Staphylococcus aureus gene sequence detection," *Talanta*, vol. 141, pp. 300–306, 2015.

[75] E. M. Regan, A. J. Hallett, L. C. C. Wong, I. Q. Saeed, E. E. Langdon-Jones, N. J. Buurma, S. J. a Pope, and P. Estrela, "A novel cobalt complex for enhancing amperometric and impedimetric DNA detection," *Electrochim. Acta*, vol. 128, pp. 10–15, 2014.

[76] P. Ling, J. Lei, L. Zhang, and H. Ju, "Porphyrin-Encapsulated Metal-Organic Frameworks as Mimetic Catalysts for Electrochemical DNA Sensing via Allosteric Switch of Hairpin DNA," *Anal. Chem.*, p. 150305143816005, 2015.

[77] D. C. Knapp, S. Serva, J. D'Onofrio, A. Keller, A. Lubys, A. Kurg, M. Remm, and J. W. Engels, "Fluoride-cleavable, fluorescently labelled reversible terminators: Synthesis and use in primer extension,"

125

Chem. - A Eur. J., vol. 17, no. 10, pp. 2903–2915, 2011.

[78]   T. S. Kim, D. R. Kim, H. C. Ahn, D. Shin, and D. R. Ahn, "Novel 3-O-fluorescently modified nucleotides for reversible termination of DNA synthesis," *ChemBioChem*, vol. 11, no. 1, pp. 75–78, 2010.

[79]   D. R. Kim, T. S. Kim, E. Kim, S. J. Min, D. Shin, and D. R. Ahn, "Synthesis of 3′-O-fluorescently mono-modified reversible terminators and their uses in sequencing-by-synthesis," *Bioorganic Med. Chem. Lett.*, vol. 24, no. 1, pp. 209–213, 2014.

[80]   M. W. Rathke and M. Nowak, "The Horner-Wadsworth-Emmons Modification of the Wittig Reaction Using Triethylamine and Lithium or Magnesium Salts," *J. Org. Chem.*, vol. 50, no. 15, pp. 2624–2626, 1985.

[81]   R. G. Giles, N. J. Lewis, J. K. Quick, M. J. Sasse, and M. W. J. Urquhart, "Regiospecific Reduction of 5-Benzylidene-2 , 4-Thiazolidinediones and 4-Oxo-2-thiazolidinethiones using Lithium Borohydride in Pyridine and Tetrahydrofuran," vol. 56, pp. 4531–4537, 2000.

[82]   C. W. Fuller, L. R. Middendorf, S. a Benner, G. M. Church, T. Harris, X. Huang, S. B. Jovanovich, J. R. Nelson, J. a Schloss, D. C. Schwartz, and D. V Vezenov, "The challenges of sequencing by synthesis.," *Nat. Biotechnol.*, vol. 27, no. 11, pp. 1013–1023, 2009.

[83]   R. N. Salvatore, A. S. Nagle, and W. J. Kyung, "Cesium effect: High chemoselectivity in direct N-alkylation of amines," *J. Org. Chem.*, vol. 67, no. 3, pp. 674–683, 2002.

[84]   I. Gillerman and B. Fischer, "An improved one-pot synthesis of nucleoside 5'-triphosphate analogues.," *Nucleosides. Nucleotides Nucleic Acids*, vol. 29, no. 3, pp. 245–56, 2010.

UNIVERSITY *of the*

WESTERN CAPE

126

Chapter 5

Novel electrochemical DNA sequencing (EcSeq) utilizing 3'-OH dually labelled nucleotides.

Abstract

A novel electrochemical DNA sequencing technique (**EcSeq**) utilizing the "sequencing by synthesis" approach has been successfully demonstrated. The study commenced with the development of a facile synthetic approach towards labelling nucleotides at the 3'-OH utilizing ferrocene as a label and redox marker. The in-house synthesized 3'-O-ferrocene thymidine triphosphate was confirmed by LC/MS and phosphorus NMR with intermediates characterized also with proton and carbon NMR. Enzyme assisted DNA extension on electrode bound DNA was then performed utilizing the 3'-O-ferrocene thymidine triphosphate and a distinct differential pulse voltammetry response at 435 mV arising from the oxidation of ferrocene was obtained. Palladium catalyzed chemical cleavage of the 3'-O-ferrocene label, with 78% signal loss and 2nd base extension with signal regeneration were successfully performed. Thus we have demonstrated the feasibility of electrochemical based DNA sequencing of short sequences, having possible applicability in point of care devices due to portability and miniaturization of electrochemical techniques.

Keywords: DNA sequencing, sequencing by synthesis, nucleotides, ferrocene, electrochemistry

127
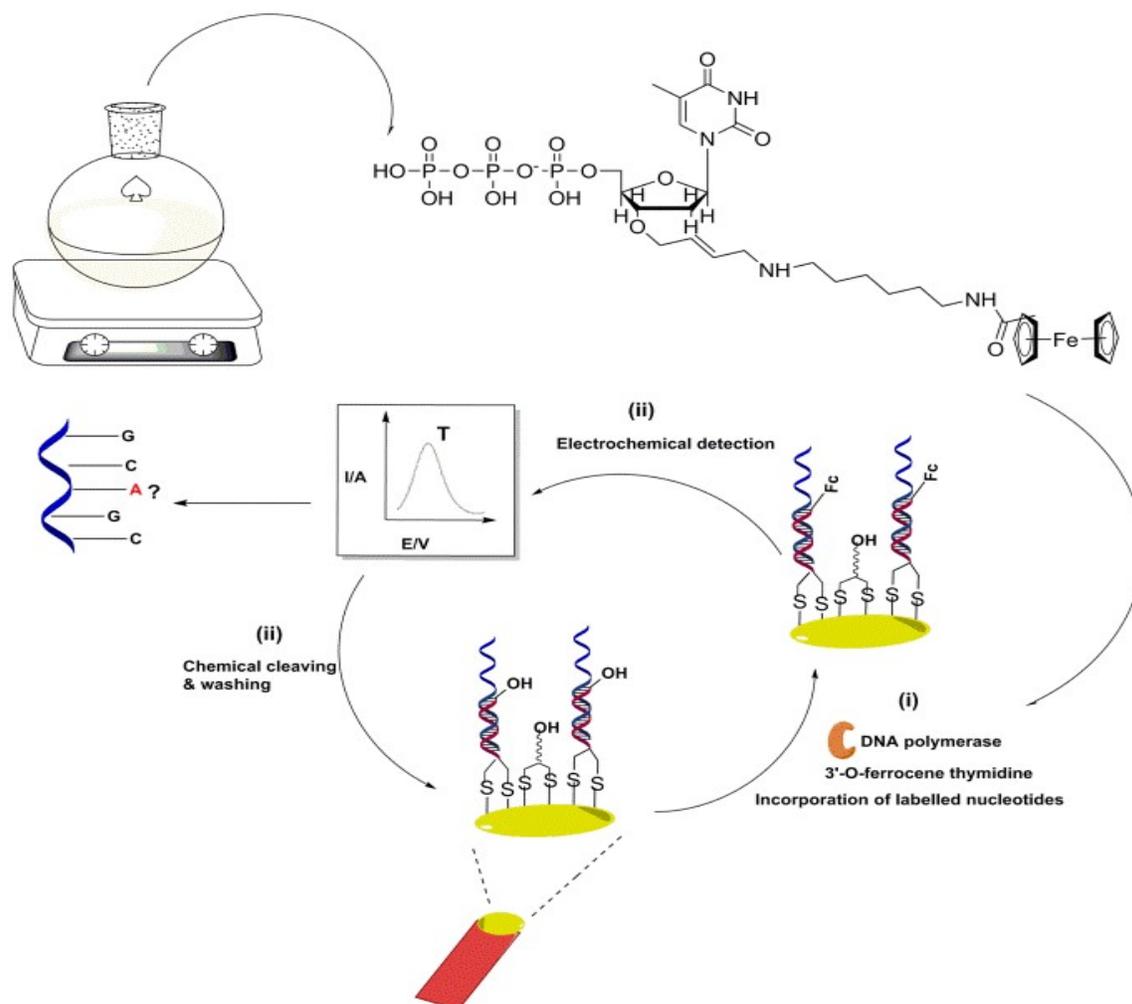
Schematic representation of the electrochemical DNA sequencer (EcSeq). Upon target hybridization (blue) with pre-immobilized primers (red), enzymatic incorporated 3'-O-ferrocene thymidine triphosphate is detected via the oxidation of ferrocene utilizing differential pulse voltammetry.

5.1 Introduction

Although DNA sequencing has found various applications, it remains highly focused on whole genome sequencing.[63] In the field of diagnostics, the search continues for individual variations and/ mutations (single nucleotide polymorphism, SNPs) in the human genome, in order to understand their contribution to disease and individual drug response.[68], [69]As the discovery of specific DNA sequences as disease biomarkers/ gene markers increases this then has given led to the need to develop disease-specific DNA sequencing platforms highly adapted to point-of-care and personalized testing. Electrochemical sensors/ biosensors are currently studied for diagnostic and point-of-care testing (POCT) applications, showing promising results due to the increased sensitivity, low cost, fast result output, portability and miniaturization that can be achieved utilizing electrochemical detection methods. Most of these approaches are centered on label-free DNA hybridization[70].[71], labeled capture strand either immobilized on the electrode or introduced in solution in sandwich assay format.[72].[73] Alternatively, electro-active species are utilized for DNA intercalation and as redox indicators.[74].[75].[76] "Sequencing by synthesis" (SBS) using reversible termination which has the advantage of versatility and robustness[82], has not yet been used in electrochemical DNA sensing, thus mainstream electrochemical DNA sensing heavily relies on the detection of known DNA sequences.

The design of reversibly terminated and labeled nucleotides is critical in SBS approaches with the performance of the platform, in most cases, largely depending on it. In this report, we described a simple, time and cost effective 6 step synthetic approach for reversible termination and labeling nucleotides at 3'-OH position and we successfully display the feasibility of electrochemical SBS DNA sequencing EcSeq utilizing redox labeled nucleotide. As a proof-of-concept, the EcSeq utilizes a primer modified gold electrode, 26 mer target model DNA sequences, ferrocene as a redox label and differential pulse voltammetry for label recognition/ detection. We then, successfully demonstrated the 4 main DNA

129

sequencing steps namely a) enzymatic incorporation of dual nucleotides (terminating and electro-active labeled) b) electrochemical detection of the label c) dual removal of the label and unblocking of 3'OH to continue the incorporation process and d) 2nd base extension and signal re-generation.

5.2 Experimental Section

### Synthesis of 3'-O-ferrocene-thymidine triphosphate

1. **Synthesis of Compound 1T**
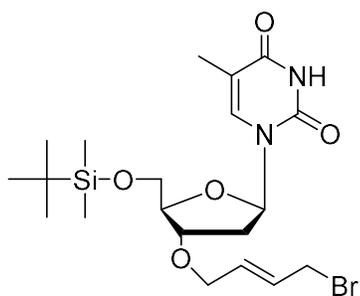
To a solution of 1,4-trans-dibromobut-2-ene (1.40 mmol) in a mixture of 2ml tetrahydrofuran and DMF (1:1 ratio), a vigorously stirred solution of 5'-O-(tert-butyldimethylsilyl) thymidine (0.28 mmol) and caesium carbonate (0.42 mmol) in 2 ml tetrahydrofuran and DMF(1:1 ratio) was dropwisely added over 20 min. The reaction mixture was then stirred for 4 hat room temperature. After completion, 20 ml diethyl ether was added to the reaction and extracted with 20 ml water 3-4 times. The organic layer was thereafter dried with anhydrous magnesium sulphate, filtered and concentrated in a rotovap. The residue was thereafter purified utilizing column chromatography (silica gel, dichloromethane: methyl alcohol=50:1) to afford 110 mg **1T** (80% yield) as clear oil.

2. **Synthesis of Compound 2T**
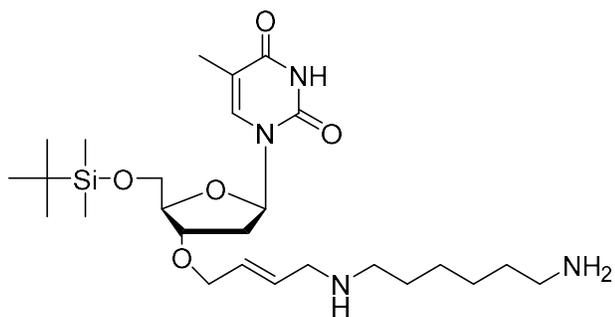
1,6-Hexanediamine (1 mmol) and caesium carbonate (0.4 mmol) were dissolved in 3 ml anhydrous tetrahydrofuran and stirred at 50 degrees Celsius. After 30 min, 1 ml solution of **1T** (0.2 mmol) in anhydrous tetrahydrofuran was added dropwise and reaction was continued to stir for 2 hat 50 degrees Celsius. Reaction solution was concentrated in vacuo. The pale yellow residue was purified utilizing column chromatography (silica gel, dichloromethane: methanol =3:1) to afford 77 mg 2b (70% yield) as pale yellow oil.

3. **Synthesis of NHS-ferrocene**
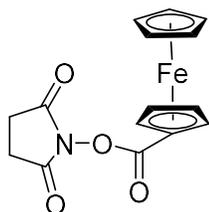
Ferrocenecarboxylic acid (0.23 mmol) was dissolved to a solution of N-hydroxysuccinimide (0.68 mmol) and N-(3-Dimethylaminopropyl)-N'-ethylcarbomidiimide hydrochloride (0.68 mmol) in 4 ml tetrahydrofuran. 80 µl of triethylamine was added and the reaction was stirred at room temperature for 4 hours. After completion, the reaction mixture was concentrated in rotovap. The residue was thereafter purified utilizing column chromatography (silica gel, dichloromethane: methanol=20:1) to afford 60 mg **NHS-ferrocene** (80% yield) as an orange solid.

Synthesis of Compound 4T
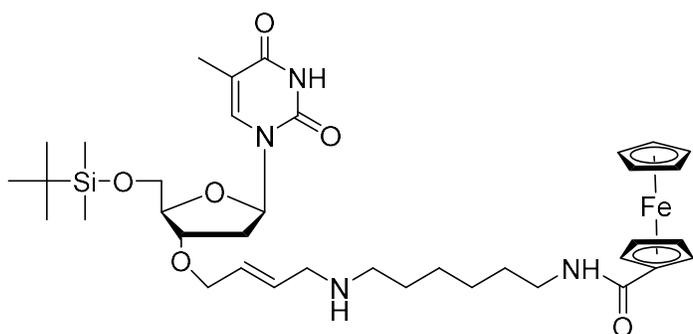
N-Hydroxysuccinimide ester of ferrocene (0.16 mmol) was dissolved to a solution of **2T** (0.12 mmol) in 4ml anhydrous acetonitrile. To the reaction mixture 20µl triethylamine was added dropwise and continued to stir at 25 degrees Celsius for 4hrs. The solution was thereafter concentrated in a vacuum and purified utilizing column chromatography (silica gel, dichloromethane= 10:1) to afford **4T** as orange oil (68%). **ESI-TOF-MS** (FAB[+]) calculated for $C_{37}H_{57}FeN_4O_6Si$ [M + H][+]: 737.3397 g/mol obtained 737.3397 g/mol.

4. **Synthesis of Compound 5T**
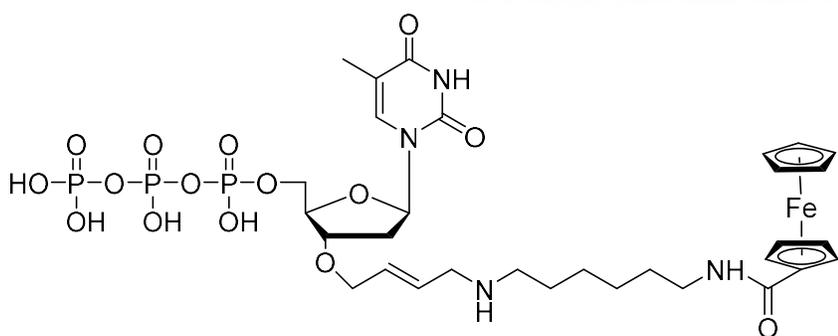
To a solution of **4T** (0.08 mmol) in 2ml anhydrous tetrahydrofuran an excess of 1M TBAF in THF (1mL) was added and stirred for 18 hrs at room temperature. After completion reaction mixtue was thereafter concentrated in vacuum and purified by column chromotagraphy (silica gel, dichloromethane:methanol =

132

10:1 and 5:1). **Compound 5** and 53 mg proton sponge were dissolved in 1 ml trimethylphosphate at room temperature, followed by a dropwise addition of 5 equivalents $POCl_3$ (20µL) at 0 degrees Celsius and stirred for 5h. There after a solution of tributylammonium pyrophosphate 10 equivalents (112 mg, 0.0205 mmol) and tributylamine (58 µL) in anhydrous DMF (2.6 mL) was well vortexed, injected at room temperature and stirred further for 3hrs. To stop the reaction the dropwise addition triethylammonium bicarbonate solution (0.1 M, TEAB 16 mL) was performed and stirred for 1 h while allowing the temperature of the reaction to slowly increase to room temperature. The sample was lyophilized.

Synthesis of 3'-OH cytidine phenothiazine

1. **Synthesis of Compound 1C**
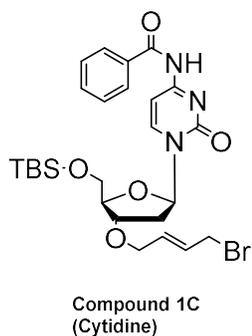
Compound 1C
(Cytidine)

To a solution of 1,4-trans-dibromobut-2-ene (1.40 mmol) in a mixture of 2ml tetrahydrofuran and DMF (1:1 ratio), a vigorously stirred solution of 5'-O-(tert-butyldimethylsilyl) cytidine (0.28 mmol) and caesium carbonate (0.42 mmol) in 2 ml tetrahydrofuran and DMF(1:1 ratio) was dropwisely added over 20 min. The reaction mixture was then stirred for 4 hat room temperature. After completion, 20 ml diethyl ether was added to the reaction and extracted with 20 ml water 3-4 times. The organic layer was thereafter dried with anhydrous magnesium sulphate, filtered and concentrated in rotovap. The residue was thereafter purified utilizing column chromatography (silica gel, dichloromethane: methyl alcohol=50:1) to afford 110 mg **1C** (80% yield) as clear oil.

## 2. Synthesis of Compound 2C
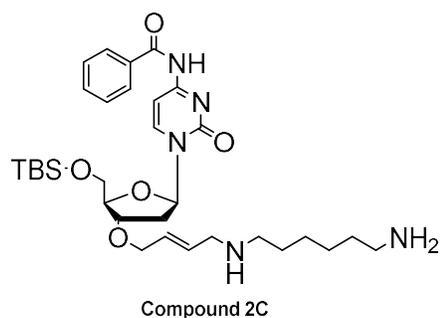
Compound 2C

1,6-Hexanediamine (1 mmol) and caesium carbonate (0.4 mmol) were dissolved in 3 ml anhydrous tetrahydrofuran and stirred at 50 degrees Celsius. After 30 min, 1 ml solution of **1C** (0.2 mmol) in anhydrous tetrahydrofuran was added dropwise and reaction was continued to stir for 2 hat 50 degrees Celsius. Reaction solution was concentrated in vacuo. The pale yellow residue was purified utilizing column chromatography (silica gel, dichloromethane: methanol =3:1) to afford 77 mg 2b (70% yield) as pale yellow oil
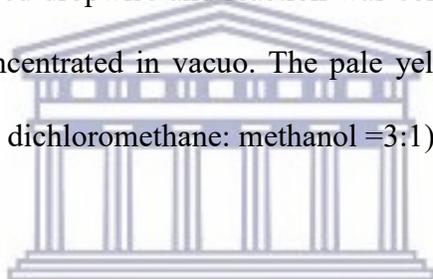
3. Synthesis of compound 3C

Compound 3C
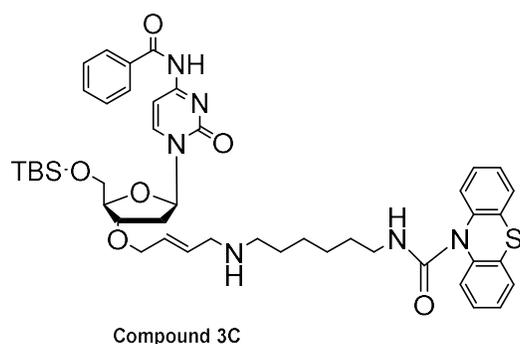
Phenothiazine carbonyl chloride (0.16 mmol) was dissolved to a solution of **2C** (0.12 mmol) in 4ml anhydrous acetonitrile. To the reaction mixture 20µl triethylamine was added dropwise and continued to

134

stir at 25 degrees Celsius for 4hrs. The solution was then concentrated in vacuum and purified utilizing column chromatography (silica gel, dichloromethane= 10:1) to afford **3C** as yellow solid (68%).

General procedure for DNA probe immobilization on gold electrodes

A solution of the thioctic acid DNA primer and DT1 spacer (20µL, 5µM and 50µM respectively) were drop-coated on bare gold electrode and incubated at 4 degrees Celsius for 24 h. Electrodes were washed with 0.01 M PBS buffer solution (pH7.4, containing 0.5 M NaCl) and dried under nitrogen. Specific synthetic oligonucleotide targets were hybridized with the immobilized DNA primers for 1 h at room temperature, washed and dried with nitrogen gas. For the enzymatic DNA incorporation of 3'-O-ferrocene-thymidine-tryphosphate (Fc-dTTP), 40µL of the enzyme-Fc-dTTP solution (Fc-dTTP, 0.1 µ/µL Thermosequenase DNA polymerase in Thermosequenase reaction buffer) was dropcoated on DNA modified gold electrode, incubated for 10 min at 62 degrees Celsius and washed with PBS buffer solution. After DPV detection, the electrodes were immersed in 200 µL cleavage solution containing 17 nM sodium tetrachloropalladate(II) and 131.5 nM triphenylphosphine-3,3',3''-trisulfonic acid trisodium salt (TPPS) in de-ionized MilliQ water and incubated at 62 degrees Celsius for 30 min. The electrodes were immediately washed with 1 M Tris-HCl buffer (pH8.5), acetonitrile and water (1:1 vol/vol) solution and PBS buffer solution. Re-incorporation was performed under the same conditions as the initial enzymatic incorporation.

5.3 Results and Discussion

5.3.1 Synthesis of 3-O'-ferrocene- thymidine

The labelling of ferrocene thymidine commenced with commercially available 5-O'-tert-butyldimethylsilyl (TBS) thymidine and trans- 1,4-dibromobutene, the 3'-hydroxyl of the TBS-thymidine was selectively allylated in the presence of cesium carbonate in anhydrous DMF:THF(1:1) for 4 hours, affording 1a in 80% yields. This was followed by the introduction of commercial 1,6-hexanediamine by performing an amine alkylation reaction utilizing cesium carbonate as a base in THF at 50 degrees Celsius, yielding 70% of 2b. Cesium carbonate was selected as a base due to its mild basic characteristics and cesium's good selectivity towards obtaining mono-amine alkylation over di-alkylation side reactions.[83] Conjugation of the freshly prepared ferrocene-N-hydroxysuccinimide ester at the linker terminal amine of 2b resulted to 68% yields of the redox active 4T.

136
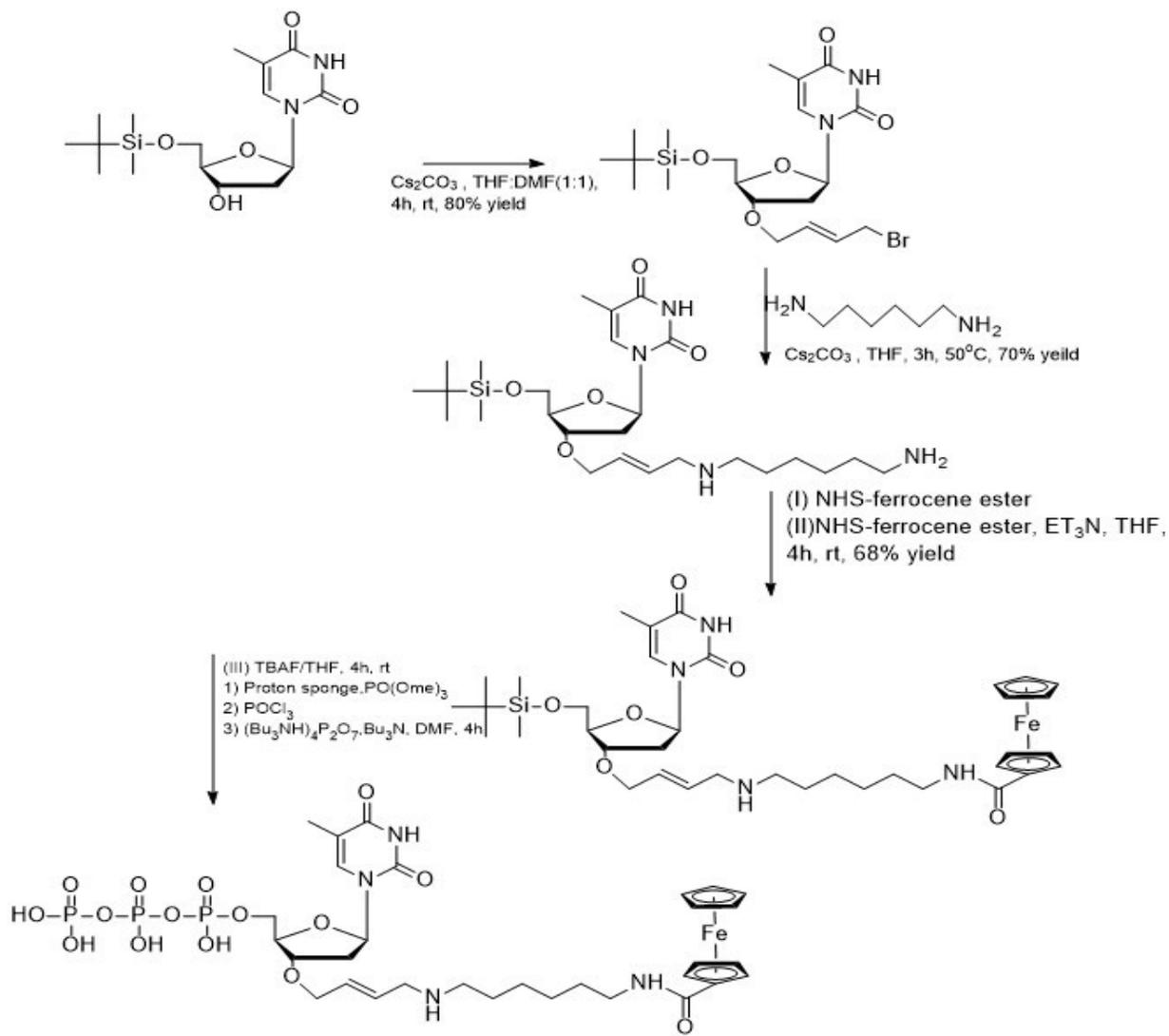
Figure 50 Reaction scheme for the 6 step synthesis of 3'-O-ferrocene thymidine triphosphate.

5.3.2 Synthesis of 3'-OH cytidine phenothiazine

To demonstrate the feasibility and the applicability of the developed synthetic approach towards labelling nucleosides at the 3'-hydroxyl, 3'-O-Cytidine phenothiazine was synthesized utilizing the same approach as with 3'-O-thymidine-ferrocene. Beginning with commercially available 5-O'-tert-butyldimethylsilyl (TBS) cytosine and trans- 1,4-dibromobutene, the 3'-hydroxyl of the TBS-cytosine was selectively allylated in the presence of cesium carbonate in anhydrous DMF:THF(1:1) for 4 hours, affording 1C in 70% yields. Similarly to thymidine this was followed by the introduction of commercial 1,6-

137

hexanediamine by performing an amine alkylation reaction utilizing cesium carbonate as a base in THF at 50 degrees Celsius, yielding 60% of 2C. Phenothiazine carbonyl chloride was utilized to introduce the phenothiazine at the linker terminal amine of 2C resulted to 58% yields of 3C.
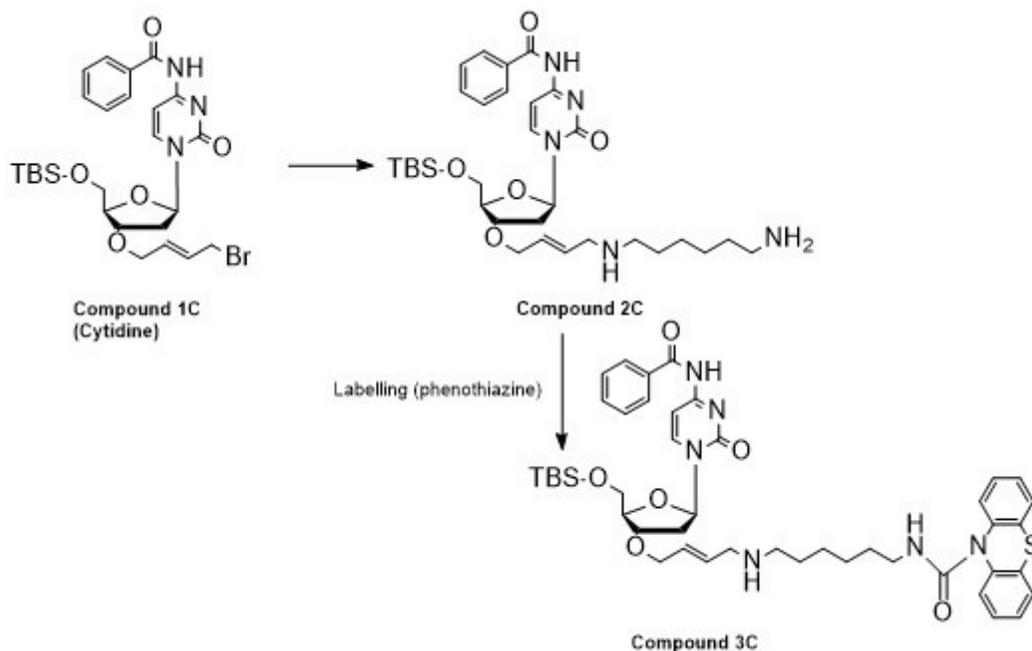

Figure 51 Reaction scheme for the 6 step synthesis of 3'-OH cytodine phenothiazine.
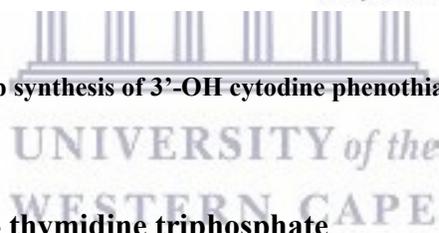
### 5.3.3 Synthesis of 3-O'-ferrocene- thymidine triphosphate

Triphosphorylation reaction was performed utilizing the Ludwig method with modifications. The triphosphorylation of 3-O'-ferrocene- thymidine commenced with the deprotection of tert-butyldimethylsilyl group at "5"-O position to the corresponding primary alcohol compound using tetrabutylammonium fluoride (TBAF) and stirred overnight. The triphosphorylation of the 5'-hydroxyl was then performed under the conditions reported by Ju *et al 2006* [65] and Gillerman *et al 2010* [84] where by the mono-phosphorylation of the nucleoside was performed utilizing phosphoryl chloride in

trimethylphosphate. This was then followed by the triphosphorylation reaction utiling an 5-fold excess of tributylammonium pyrophospate in DMF to afford the 3'-O-ferrocene thymidine triphosphate.

Table 2 Synthetic pathways for labelling thymidine at 3'-OH

	Da-Rae Kim method	Previous method (Chapter 4)	Current method
Linker synthesis	10	10	2
Use of metal hydrides and aluminium hydrides	Yes	No	No
Introduction of linker to 3-OH and triphosphate synthesis (total number of steps required)	17 steps	N/A	5 steps
Cleavage method	Palladium catalysizd chemical cleavage at the double bond	Palladium catalyzed chemical cleavage at the double bond	Palladium catalyzed chemical cleavage at the double bond

Typically, reversibly labeling of nucleotides at the 3'OH is difficult to attain as the label should be far away enough not to introduce steric hindrance on the 5'- position and be cleavable under mild enough conditions not to denature the structure of nucleotide. Although Da-Rae Kim *et al 2014* [79] [78] introduces a label through a hexane linker and the cleavage conditions of the linker are suitable for nucleotides, the achieve this in ~15 step synthetic approach with the use of metal hydrides which are inherently unstable under normal laboratory conditions and making up-scaling. As shown in table 1 in an attempt previously described in "preparation of chemical cleavable linker for reversible termination of nucleotides in 3-OH for DNA sequencing" (previous chapter), we successfully replaced all metal hydrides in modified method for the preparation of a cleavable linker. But the number of steps remained similar to that reported by Da-Rae kim. In this synthetic approach the 3'-OH labeling is achieved in only 3 steps with the first two steps consisting of a simplistic introduction of the linker at the 3'-OH position.
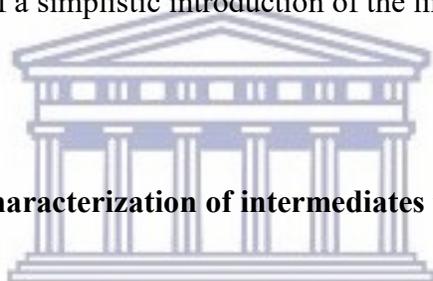
5.3.4 Carbon and Proton NMR characterization of intermediates to 3'-O-thymidine-ferrocene triphosphate

a. **Compound 1T**

The proton and carbon nuclear magnetic resonance (NMR) was utilized to characterize the intermediates for the synthesis of 3'-O-thymidine-ferrocene triphosphate. In addition to the tertbutyldimethylsylil thymidine peaks described in table 1, the proton NMR of the mono-alkylation product compound 1T shown in figure 51, reveal the presence of the two multiplets at 5.96 ppm and 5.81 ppm arising from the two hydrogen's of the double bound thus confirming the successful alkylation of the 3'-OH of tertbutyldimethylsylil thymidine, without the oxidation of the double bond under the reaction condition. Also the two singlets at 0.00 ppm and 0.94 ppm arising from the tertbutyldimethylsylil group show that the 5'OH protected group was retained under the 3'-OH alcohol alkylation reaction.
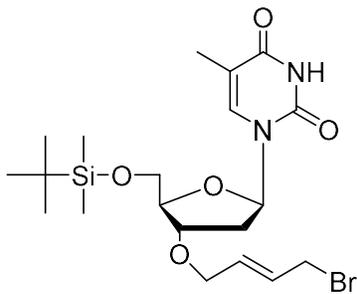
**Table 3 H'NMR assignment for tertbutyldimethylsilyl thymidine backbone structure**
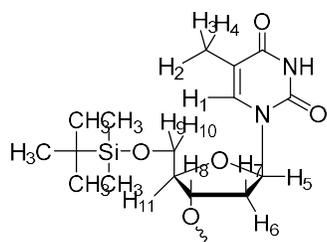
Proton	ppm
H1	7.3 (s, 1H)
H2, H3,H4	1.93 (s, 3H)
H5	6.24 (m, 1H)
H6	2.38 (dd,1H)
H7	2.38 (dd,1H)
H8	3.8 (q,1H),
H9, H10	3.91 (d, 2H)
H11	4.46 (s,1H)
CH3-Si-CH3	0.00 (m,6H)
╬─Si	0.92 (s, 9H
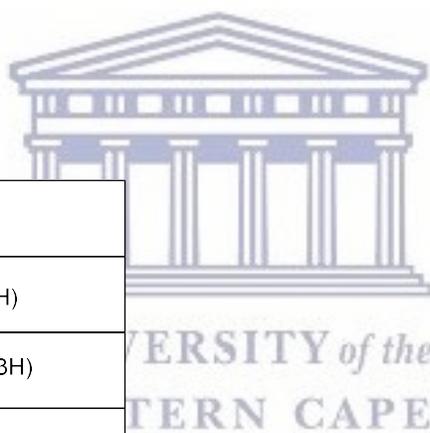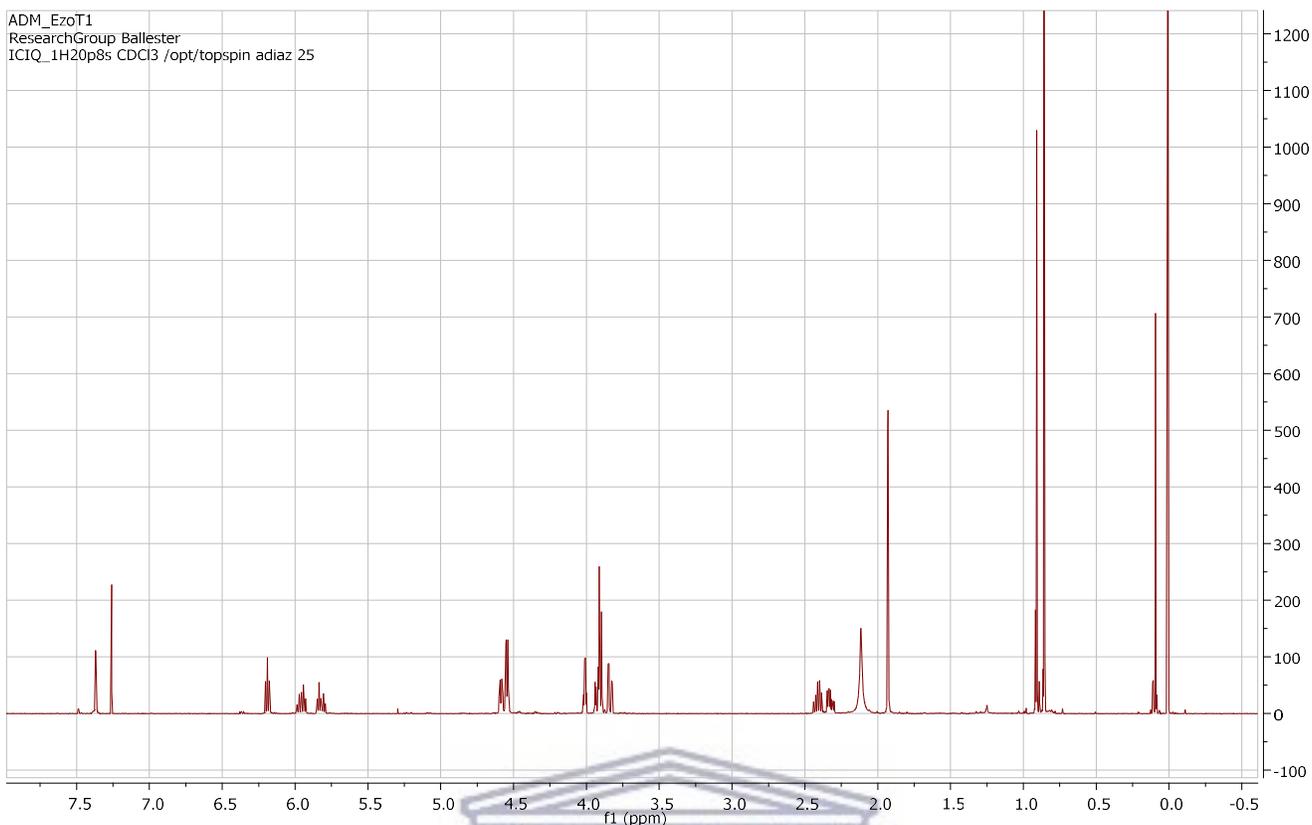
Figure 52 H'NMR of compound 1T (400MHz, CDCl₃) *δ 7.3 (s,1H), 6.24 (m, 1H), 5.96 (dt, 1H), 5.81 (dt, 1H), 4.54 (t,2H), 4.46 (s,1H), 4.06 (d, 1H), 3.91 (d,2H), 3.8 (q,1H), 2.38 (m,1H), 2.10 (m,1H), 1.93 (s, 3H), 0.92 (s, 9H), 0.00 (m,6H).*

Similar observations were also made in the carbon nmr shown in figure 52 whereby the olefin carbon peaks where obtained at 128 ppm and 131 ppm respectively. Mass spectrometry was also utilized to give conclusive information about the success of the mono-alkylation of the 3'-OH to yield compound 1T. The mass of compound 1T was interrogated utilizing positive mode as shown in figure 53 where by the expected mass calculated for $C_{20}H_{33}BrN_2O_5Si$ $[M + Na]^+$: 512.4697 g/mol was obtained as 513.1227 g/mol.
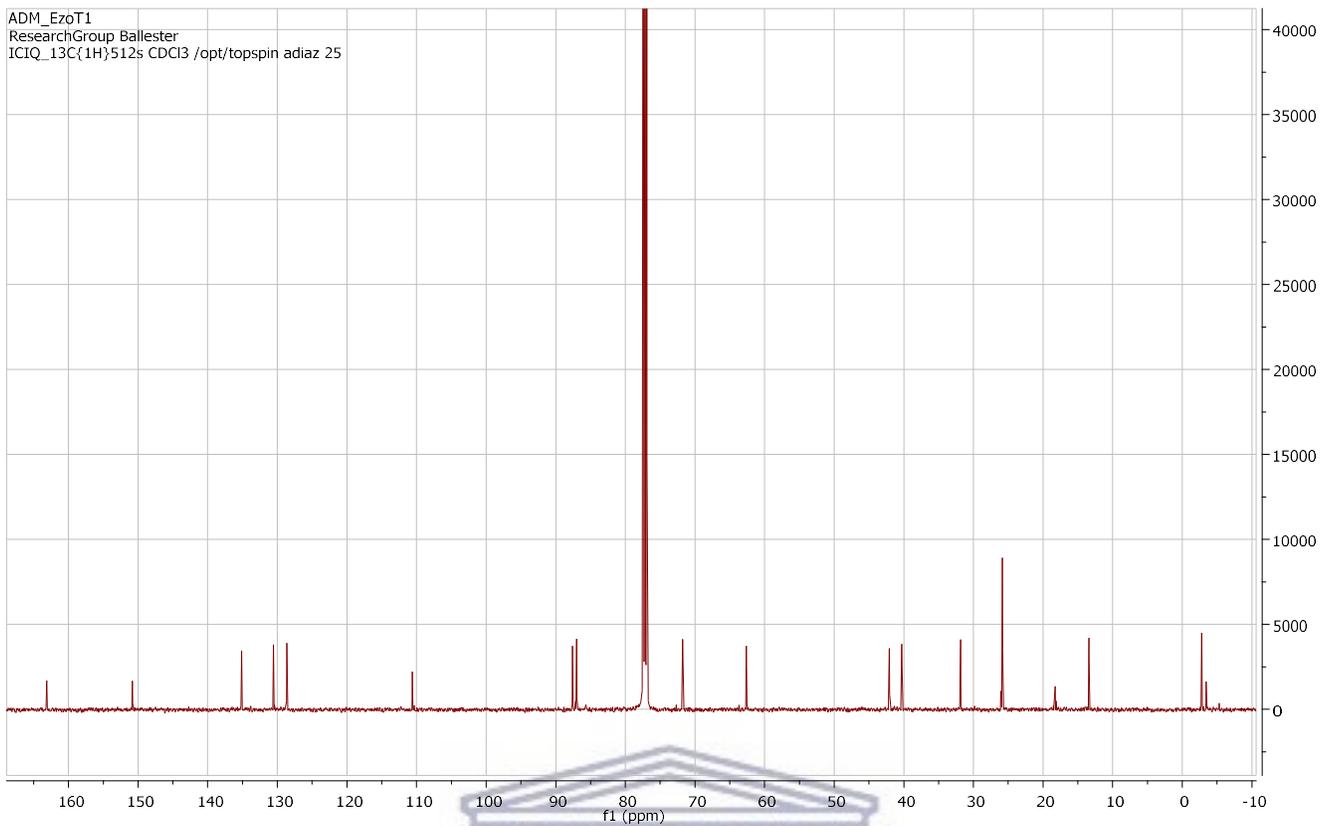
Figure 53 Carbon 13 NMR of compound 1T (500MHz, CDCl3) δ 164, 152, 135,131,128,111, 88, 89, 77, 72, 63, 42,40, 33, 26,17, 14,8, 7, 5
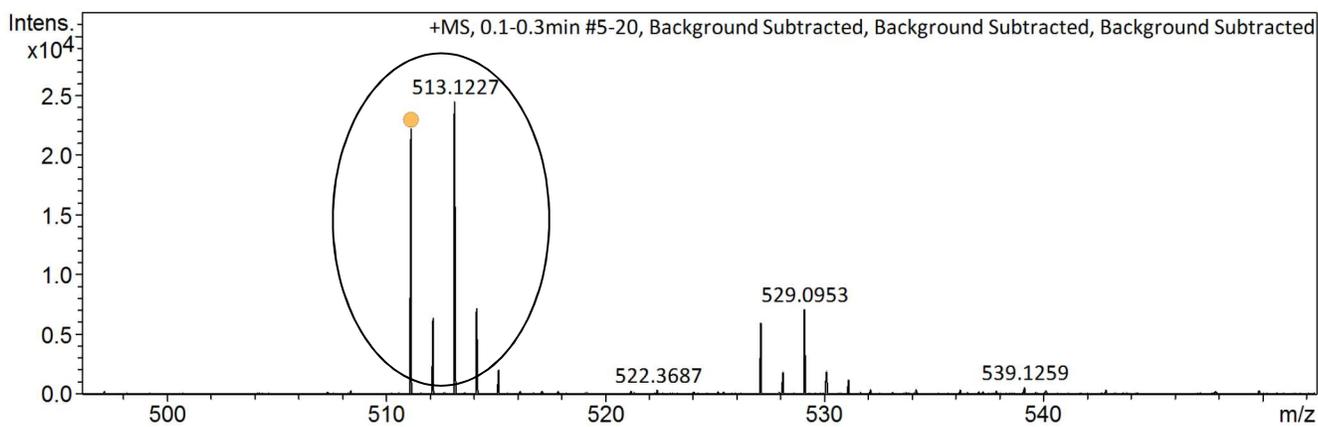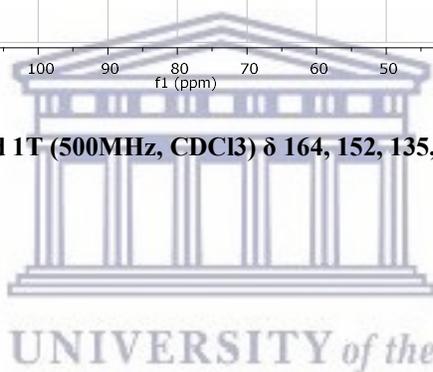

Figure 54 ESI-TOF-MS expected weight calculated for $C_{20}H_{33}BrN_2O_5Si$ [M + Na]+: 512.4697 g/mol was obtained as 513.1227 g/mol.

143

b. Compound 2T

The proton nmr of the amine alkylation product compound 2T is shown in figure 54, whereby the presence the multiplet at 1.35 ppm and the doublet triplet at 1.49 ppm from the CH_2 protons of the aliphatic chain of hexane diamine. The presence of the double bond with its peaks appearing as two multiplets at 5.75 ppm and 5.70 ppm; and the presence of the 5'-OH tertbutyldimethylsylil protecting group with its peak appearing as two 0.93 ppm and 0.13 ppm, confirm that the both the double bond and the 5-OH protecting group were retained under the amine alkylation reaction conditions. Similar observations were also made in the carbon nmr shown in figure 55 whereby the olefin carbon peaks where obtained at 133 ppm and 132 ppm respectively, with a slight shift to higher frequencies due to the presence of the nitrogen group. The mass spectrometry of compound 2T shown in figure 54 was obtained utilizing positive mode as shown in figure 54 where by the expected mass calculated for $C_{26}H_{49}N_4O_5Si$ $[M + H]^+$ is 526.7891 g/mol and obtained as 525.3547 g/mol.
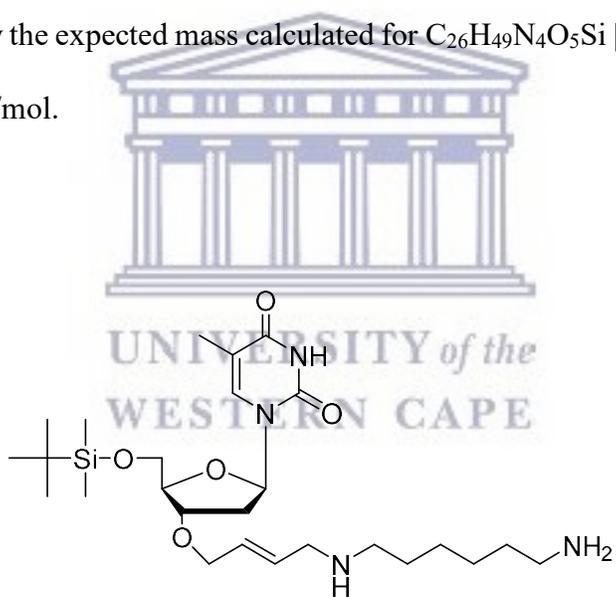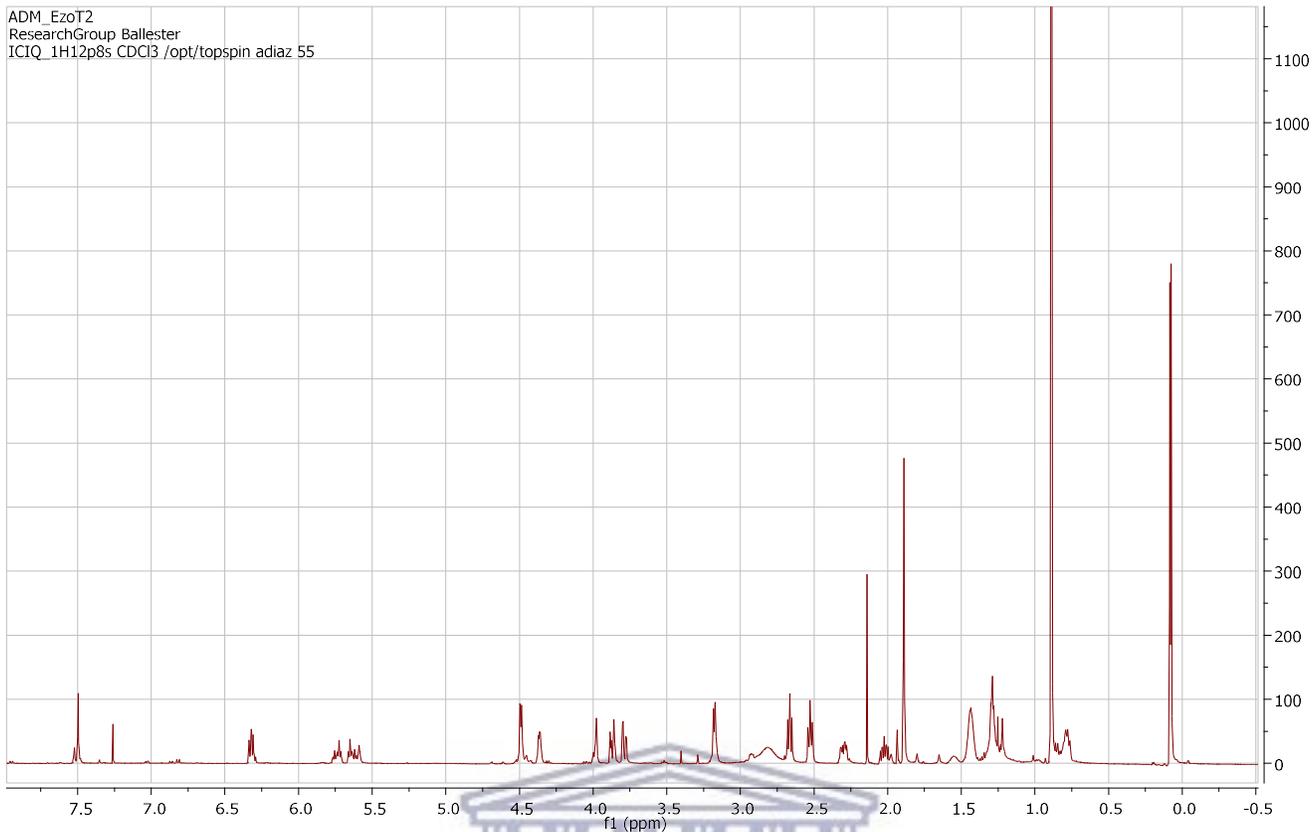
Figure 55 H'NMR of compound 2T (400MHz, CD₃OD) δ 7.66 (d, 1H), 6.29 (m,1H), 5.75 (m,1H), 5.70 (m,1H), 5.50 (m,2H), 4.36 (dt,1H), 3.97(q,1H), 3.87(m,2H), 3.55 (t,1H), 3.30 (dt,1H), 3.17 (m,2H), 2.68 (m,2H), 2.52 (m,2H), 2.29 (ddd,1H), 2.24 (m,1H), 1.90(d,3H), 1.49(dt,4H), 1.35(m,4H), 0.93(s,7H), 0.13
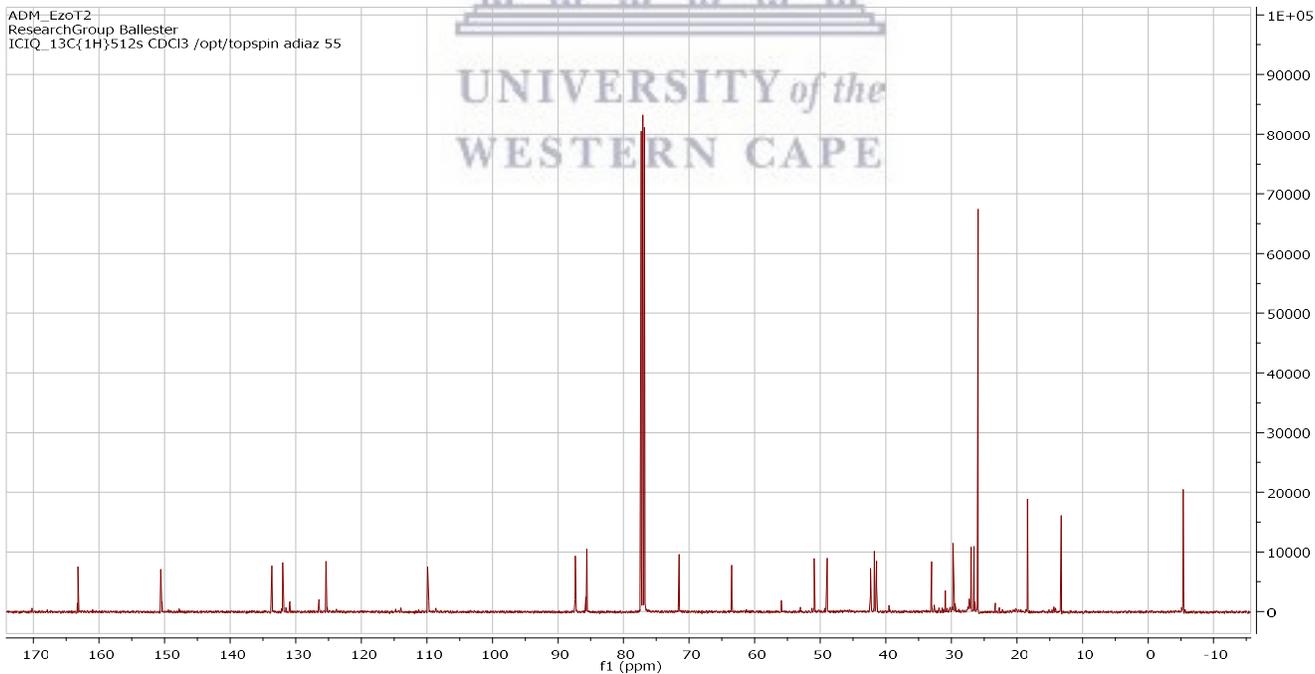

Figure 56 ¹³CNMR of compound 2T (500MHz, CD₃OD) δ 164, 151,133,132,131,125,111, 88, 86, 77, 72, 63, 49,52, 43,42, 33,30,28,27, *26,17, 14,8, 7, 5*
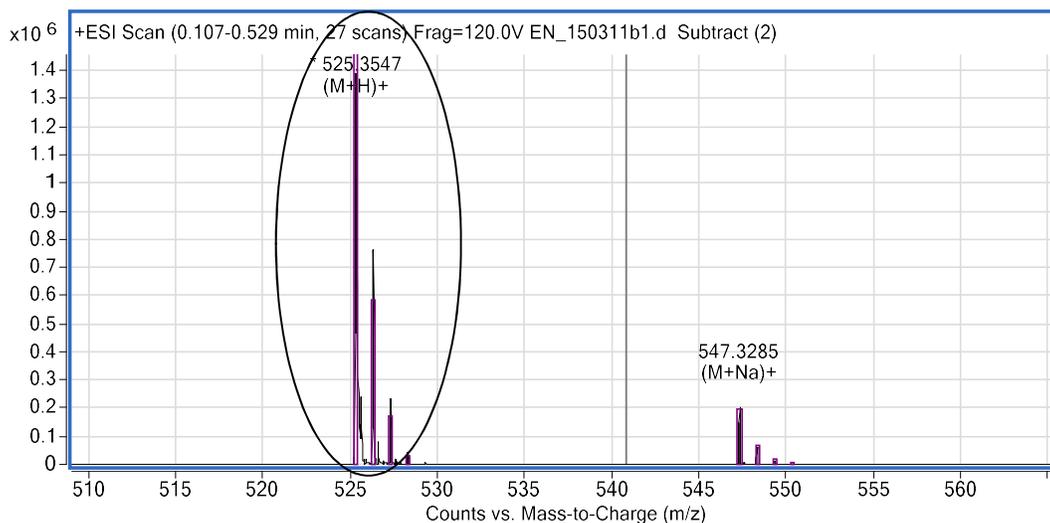
Figure 57 ESI-TOF-MS (FAB+) calculated for C$_{26}$H$_{49}$N$_4$O$_5$Si [M + H]+ is 526.7891 g/mol and was obtained 525.3547 g/mol

c. Compound 4T

Thereafter the ferrocene label was introduced and gave rise to compound 4T, and this was confirmed by the presence of the with the peaks of the cyclopentadiene rings of the ferrocene molecule appearing at *4.94 ppm (multiplet), 4.65 ppm (multiplet), 4.39 ppm (multiplet), 2.87 (singlet) respectively*. Also the presence of the double bond protons at while retaining the tertbutyldimethylsylil protecting group at the 5'-OH position appearing as two singlets at *0.93 ppm* and *0.13 ppm* show that the label was successfully introduced at the 3'OH of the thymidine while retaining the double bond which is crucial for the palladium assisted chemical cleaving of the label. Similar observations were also made in the carbon nmr shown in figure 58 whereby the olefin carbon peaks where obtained at 133 ppm and 132 ppm respectively. Also the peaks arising from the carbons of the cyclopentadiene rings were observed at *71 ppm, 70 ppm, 68 ppm*. The mass spectrometry further concluded the successful synthesis of compound 4T as shown in figure 59, and was obtained utilizing positive mode where by the expected mass calculated for C$_{37}$H$_{57}$FeN$_4$O$_6$Si [M + H]$^+$ 737.8193 g / mol was obtained as 737.3404 g/mol.
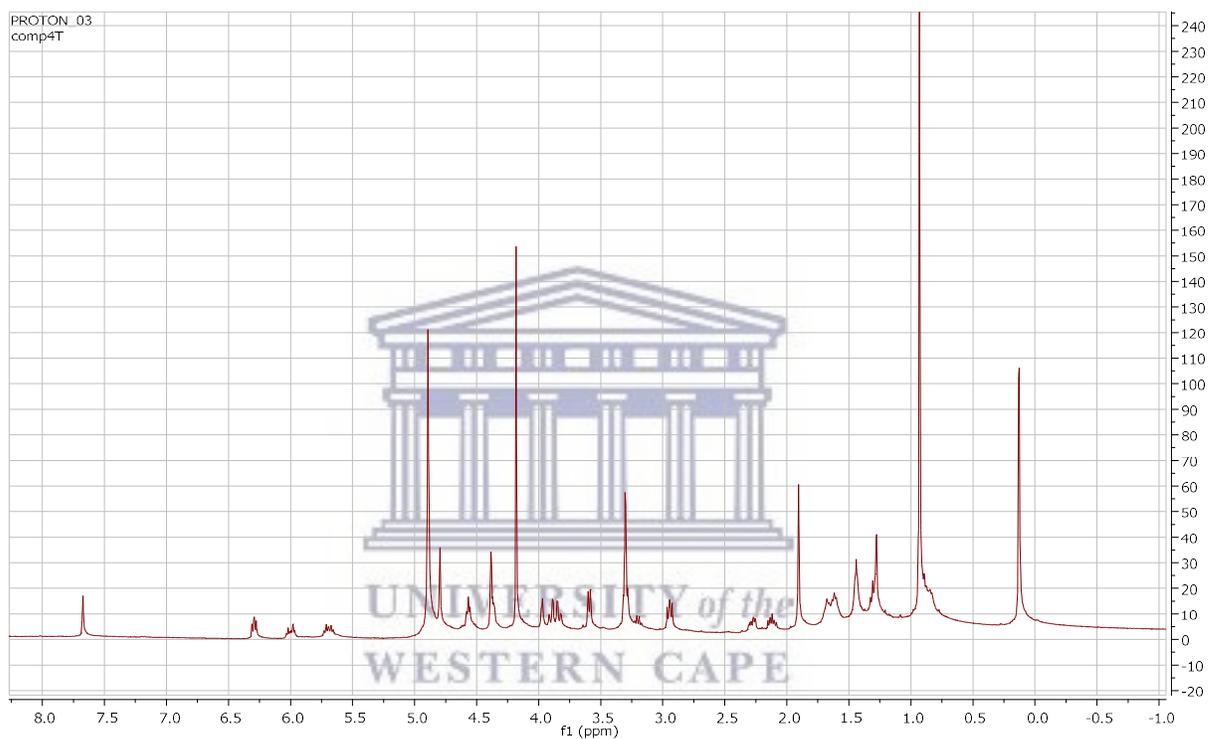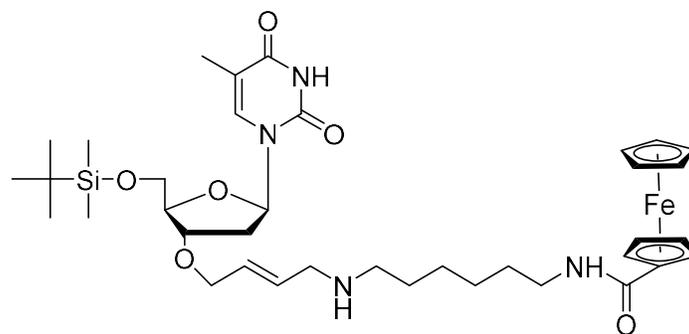
Figure 58 HNMR of compound 4T, 400MHz, (CD₃OD) δ 7.66 (d, 1H), 6.29 (m, 1H), 5.70 (m, 2H), *4.94 (s, 4H), 4.90 (m, 2H), 4.65 (m,2H),* 4.50 (m,2H), *4.37 (s, 5H),* 4.36 (dt,1H), 3.97 (q,1H), 3.87 (m,2H), 3.55 (t,1H), 3.30 (dt,1H), 3.17 (m,2H), 2.68 (m,2H), 2.52 (m,2H), 2.29 (ddd,1H), 2.24 (m,1H), 1.90 (d,3H), 1.49 (dt,4H), 1.35 (m,4H), 0.93 (s,6H), 0.13 (s,9H)

Figure 59 13CNMR of compound 4T (500MHz, CD₃OD) δ 173, 164, 151,134,132,123,109, 88,86, 75, 72,71,70,68, 63,52,49,48, 47, 46, 43,40,39,29,28, 27, *26,17, 14,8,4*

148
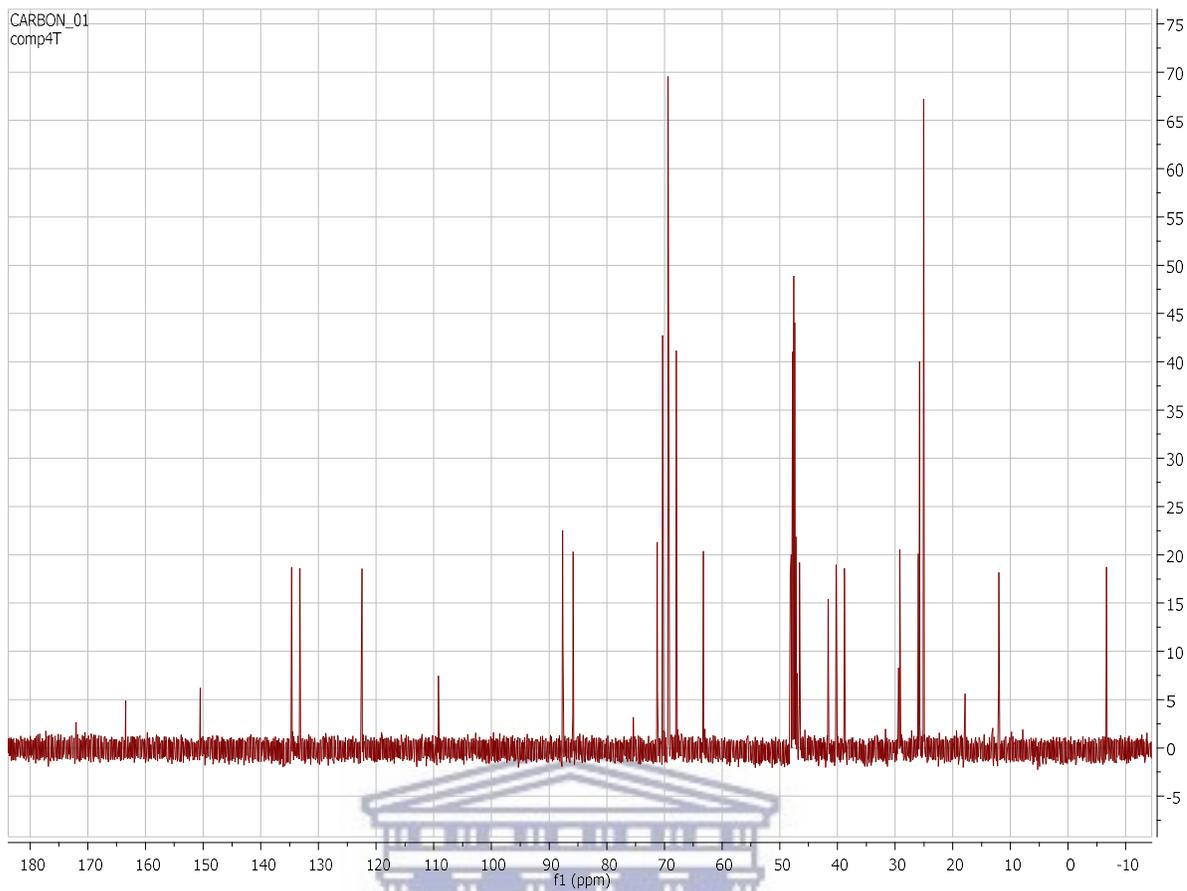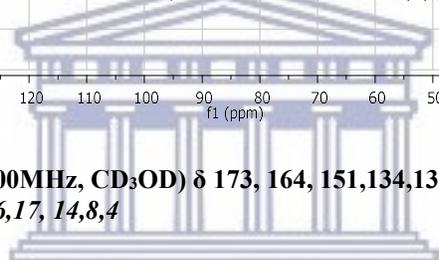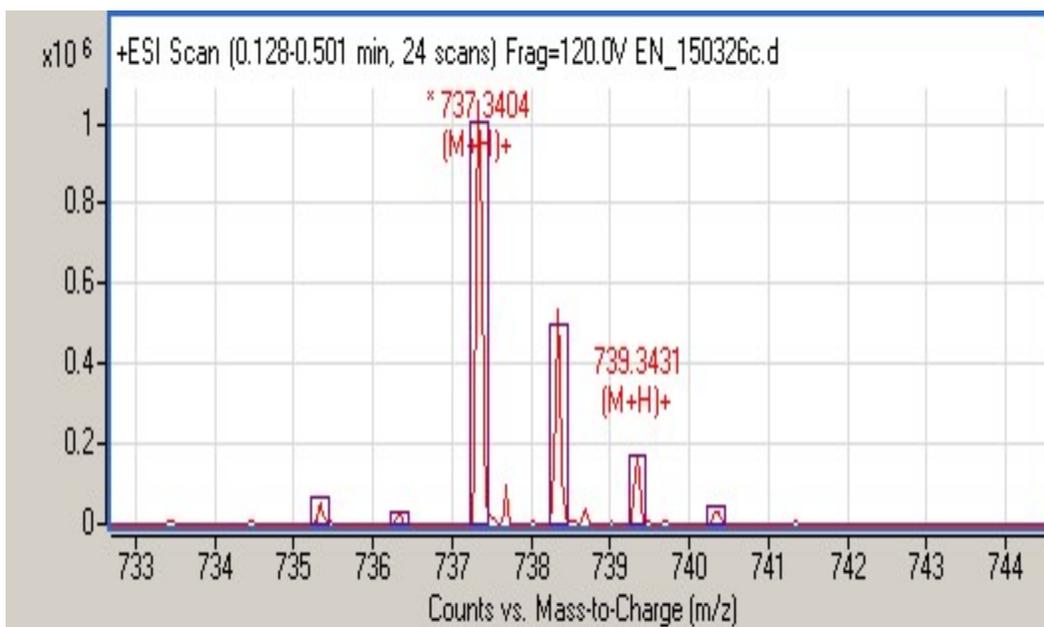
Figure 60 ESI-TOF-MS of compound 4T (FAB$^+$) calculated for C$_{37}$H$_{57}$FeN$_4$O$_6$Si [M + H]$^+$ 738.8272 g/mol g/mol was obtained as 737.3404 g/mol g/mol.
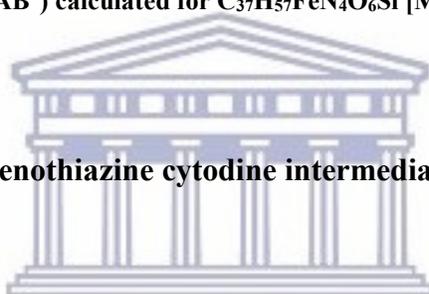
5.3.5 Characterization of 3'-O-phenothiazine cytodine intermediates and product
Mass spectrometry

The alkylation of 5'-OH tertbutyldimethylsylil cytodine at 3'-OH with bromodiene to yield compound 1C was confirmed utilizing mass spectrometry whereby the mass calculated for C$_{26}$H$_{36}$BrN$_3$O$_5$Si [M+H] 579.5843 g/mol was obtained as 600.1473 g/mol shown in figure 60. After the amine alkylation reaction, to extend the linker while introducing an amine group to yield compound 2C, was also confirmed also utilizing mass spectrometry whereby the mass calculated for C$_{32}$H$_{51}$N$_5$O$_5$Si [M+H] 614.8788 g/mol was obtained to be 614.3722 g/mol [M+H] as shown in figure 61. The mass of 3'-O-phenothiazine cytodine was calculated for C$_{45}$H$_{58}$N$_6$O$_6$SSi[M+H] 840.1421 g/mol was obtained to be 839.3979 g/mol [M+H] as shown in figure 62. The masses for all molecules were obtained in positive mode.
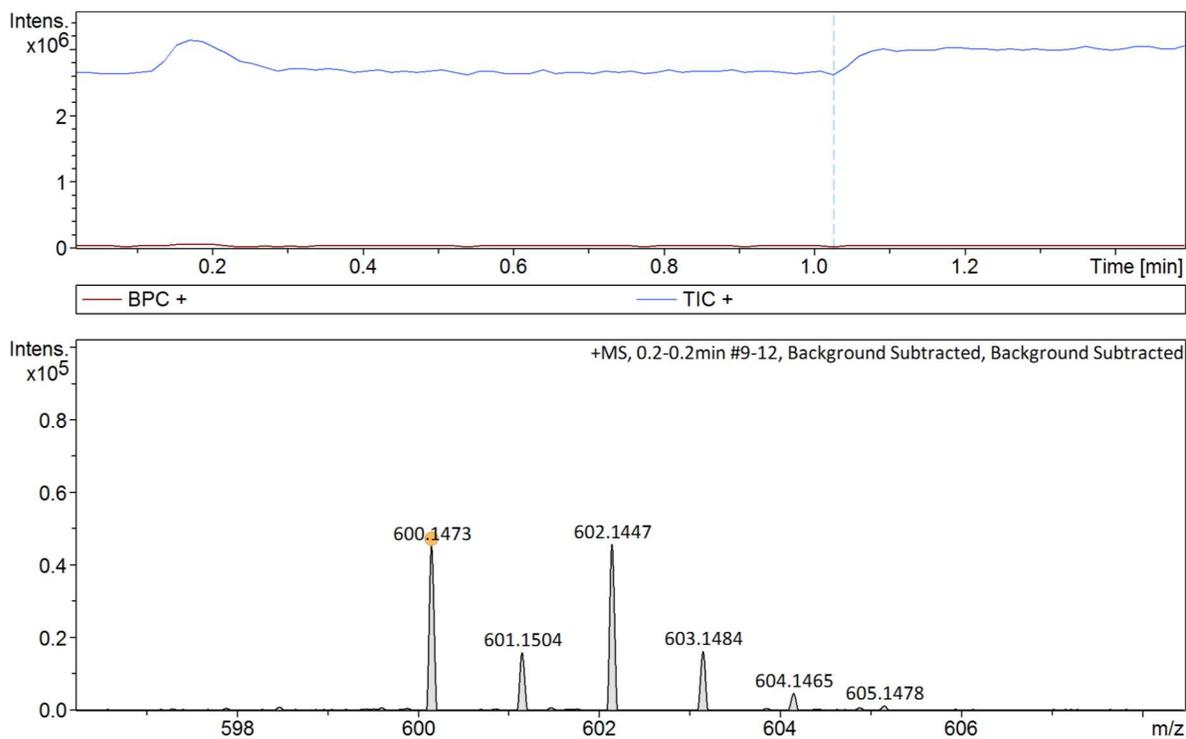
149

Figure 61 ESI-TOF-MS of compound 1C (FAB+) calculated for C$_{26}$H$_{36}$BrN$_3$O$_5$Si [M + H] 579.5843 g/ mol obtained as 600.1473 g/mol.
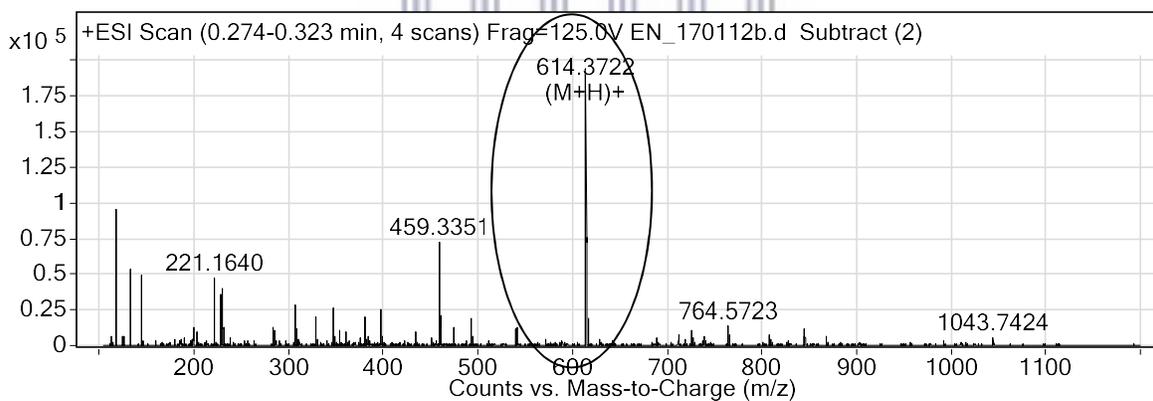
Figure 62 ESI-TOF-MS of compound 2C (FAB+) calculated for C$_{32}$H$_{51}$N$_3$O$_5$Si [M + H] 614.8788 g/mol obtained as 614.3722 g/mol.
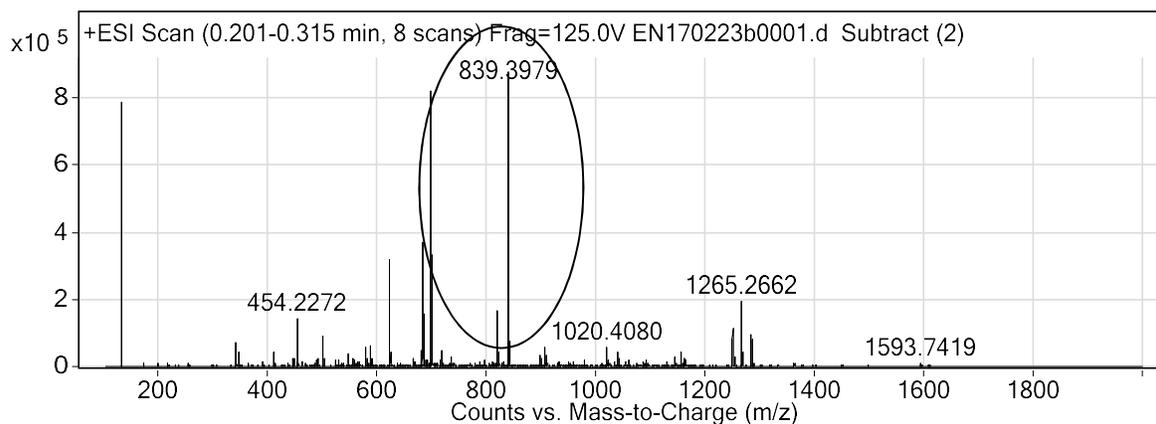
Figure 63 ESI-TOF-MS of compound 3C (FAB+) calculated for $C_{45}H_{58}N_6O_6SSi$ [M+H] 840.1421 g/ mol and was obtained to be 839.3979 g/mol [M+H]

5.3.6 Characterization of 3'-O-ferrocene thymidine triphosphate

a. Phosphorus NMR of the characterization of 3'-O-ferrocene thymidine triphosphate

The Phosphorus Nuclear Magnetic Resonance of the crude product 3'-O-ferrocene thymidine triphosphate mixture was performed and is shown in Figure 64. Phosphorus NMR like other nuclear magnetic resonance techniques is only sensitive to phosphorus nuclei. The spectrum reveals the presence of the 3 distinct triphosphate signals arising from the alpha at -15.42 ppm, the beta phosphate -22.006 ppm and the gamma phosphate -9.02 ppm were observed confirming that the triphosphorylation of the 5'-OH of the thymidine ferrocene was successfully performed.[77]˙[84] The broad peak at -10.90 ppm arises from the pyrophosphate starting material which is used in excess during synthesis.

151
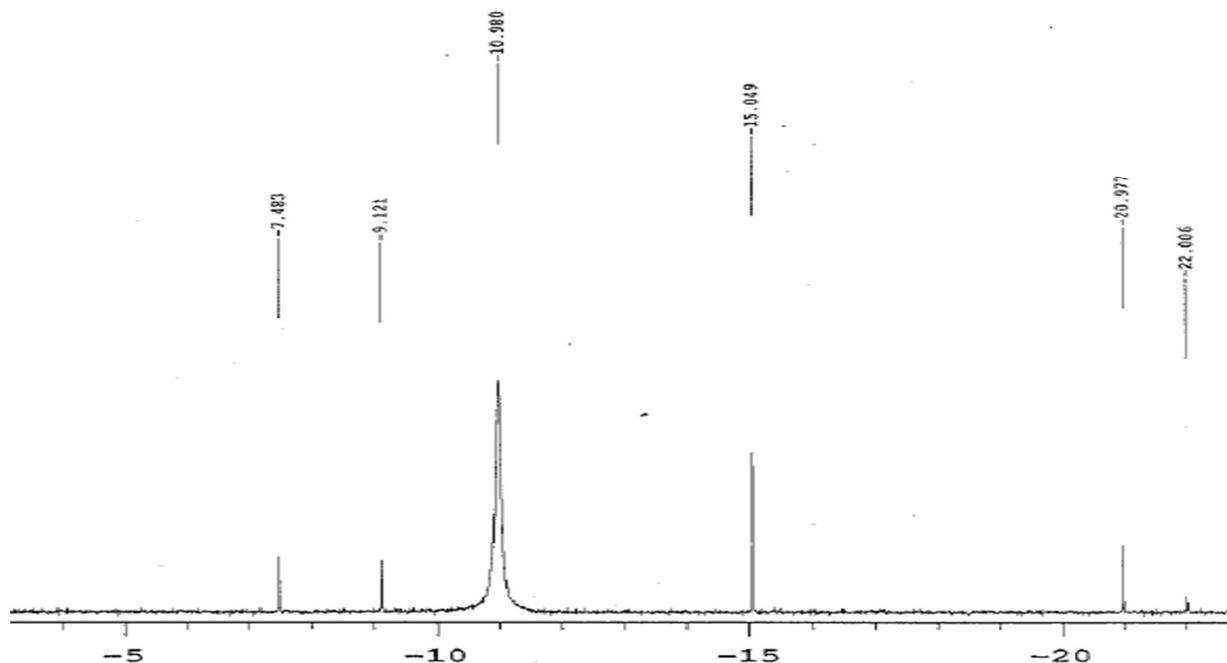
Figure 64 31P-NMR spectrum of crude 3'-O-ferrocene thymidine triphosphate in dueterum oxide utilizing H₃PO₄ as an external standard

b. Mass spectrometry characterization of 3'-O-ferrocene thymidine triphosphate

After the deprotection of the tertbutyldimethylsylil group on the 5'-OH of compound 4T, in preparation for the 5'-O triphosphorylation reaction, the resulting the nucleoside, compound 5T was characterized using liquid chromatography coupled mass spectrometry with acetonitrile and methanol as the mobile phase in negative mode. The mass of compound 5T was obtained as 621.2358 g/mol as shown in figure 65.

Cpd 10: C20 H30 N16 O8: -ESI MFE Spectrum (17.900-18.586 min) Frag=120.0V 150514b_profile.d
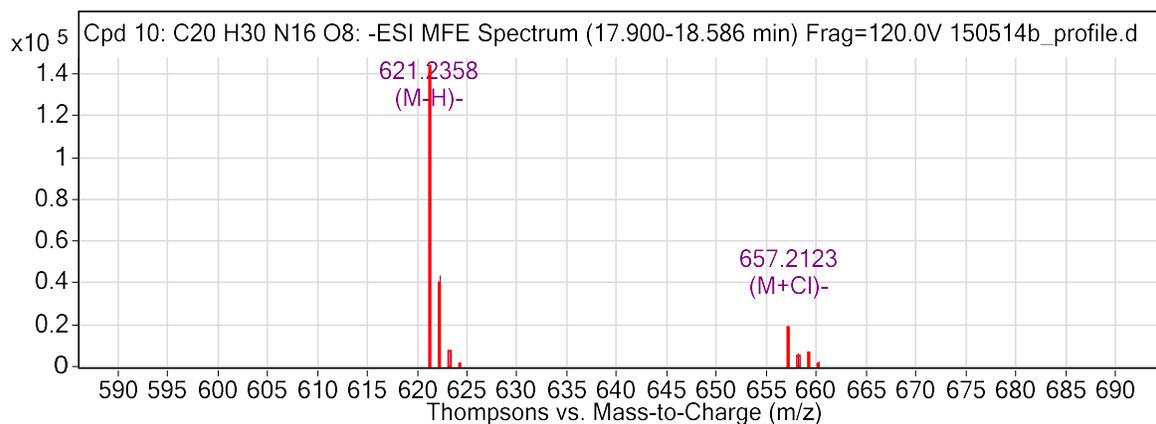
Figure 65 ESI-TOF-LC/MS of compound 5T (FAB-) was obtained as 621.2358 g/mol

Thereafter, the triphosphorylation of 5'-OH of compound 5T was performed and yielded compound 6T, the 3'-O-ferrocene thymidine triphosphate and was characterized utilizing Liquid chromotagraphy coupled mass spectrometry in negative mode. The molecule fragmentated into two major fragments : fragment A and fragment B as shown in figure 66 The expected mass was calculated to be 860.46 g/mol [M-4H] but was obtained as fragments of 494.9665 g/mol [M-H] and 364.2672 g/mol [M-H] to make up 859.2337 g/mol [m-2H].

Cpd 12: C16 H11 N4 O9 P3: -ESI MFE Spectrum (19.422-19.774 min) Frag=120.0V 150514b_profil...

494.9665
(M-H)-

Thompsons vs. Mass-to-Charge (m/z)

Cpd 7: <none>: -ESI MFE Spectrum (17.014-18.352 min) Frag=120.0V 150514b_profile.d

* 364.2672
(M-H)-

367.2752
(M-H)-

Thompsons vs. Mass-to-Charge (m/z)
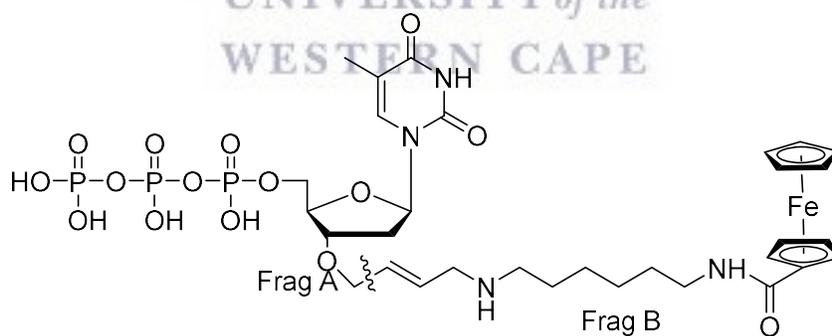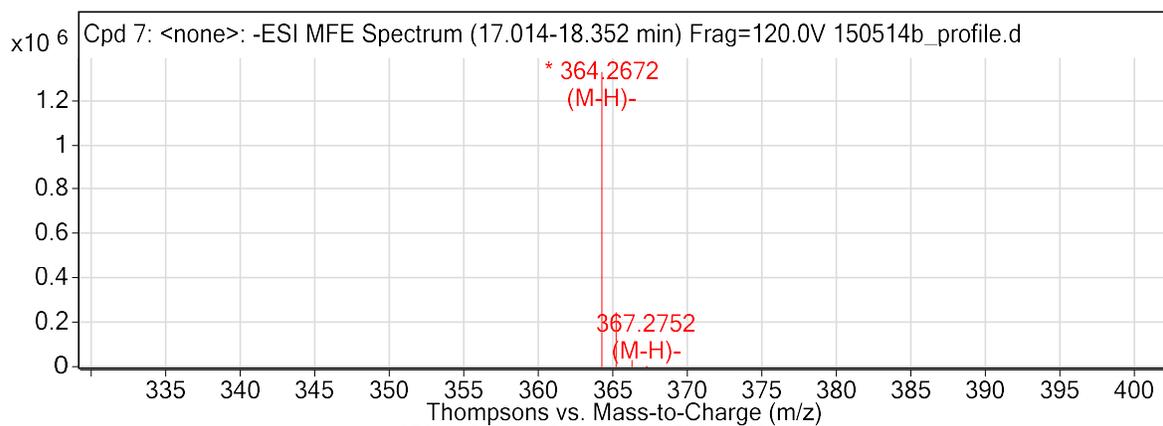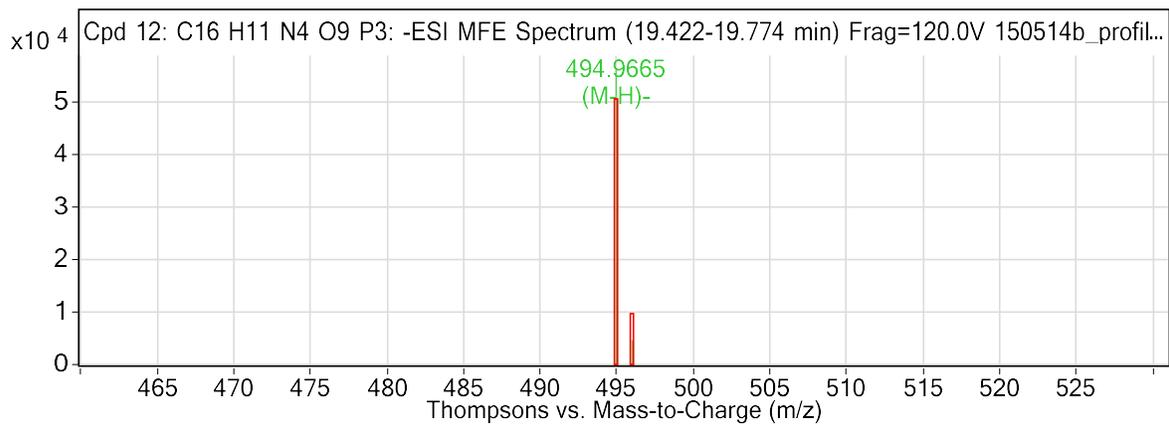
Figure 66 ESI-TOF-LC/MS of compound 6T fragments (FAB-) was obtained as 494.9665 g/mol and 364.2672 g/mol

154
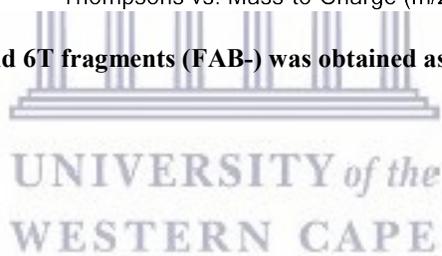
5.3.7 Single base extension of 3'-O-ferrocene thymidine triphosphate by Thermosequanase DNA polymerase on gold electrodes
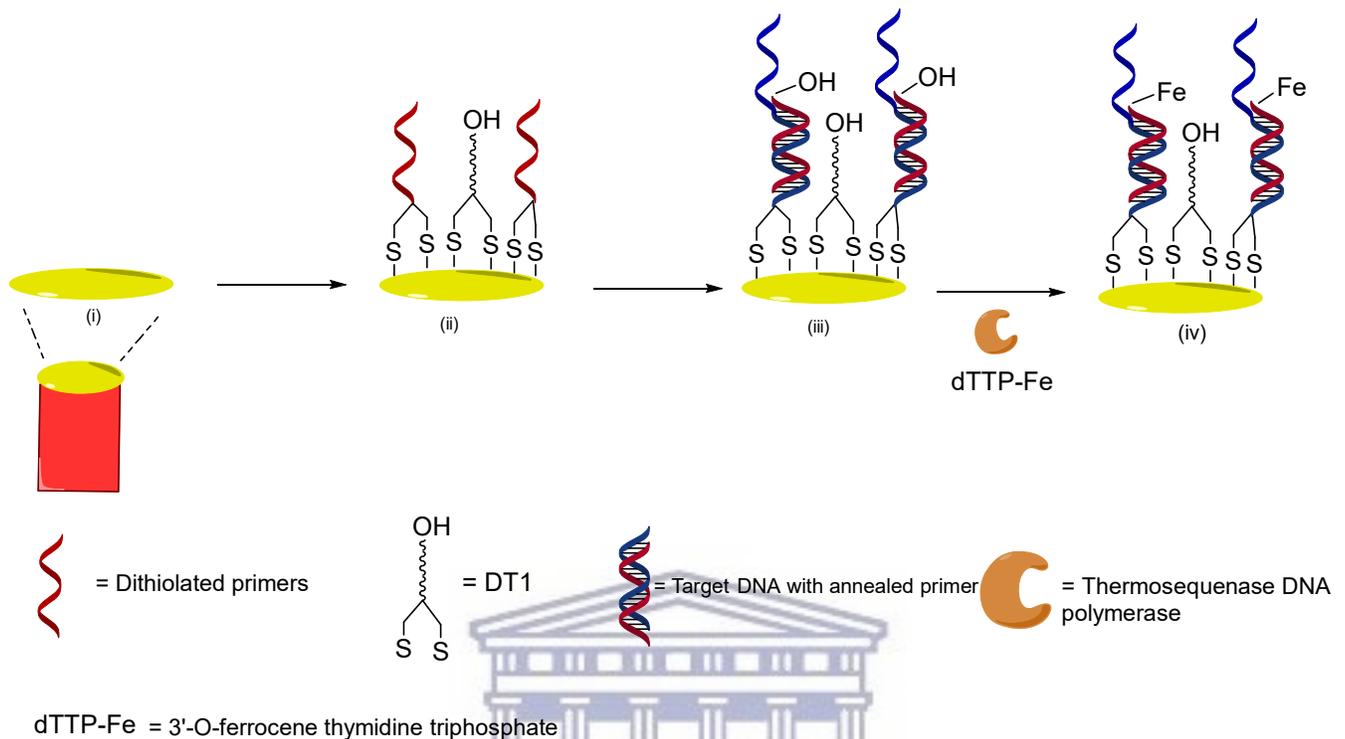
Figure 67 Fabrication of the electrochemical DNA sequencing system whereby (i) immobilization of primer and the spacer dithiol-(16-3,5-bis((6 mercaptohexyl)oxylphenyl)-3,6,9,12,15-pentaoxahexa-decane (DT1), (ii) Target annealing, (iv) Enzyme assisted incorporation of 3'-O-ferrrocene thymidine triphosphate by Thermosequeanase DNA polymerase

To demonstrate the feasibility of utilizing electrochemical techniques as detection methods for DNA SBS technologies, the in-house synthesized 3'-O-ferrocene thymidine triphosphate was then utilized to perform the full DNA sequencing steps namely 1) enzymatic incorporation of the modified nucleotide by Thermosequenase DNA polymerase and detection, 2) label cleaving and 3) re-incorporation and detection. Therefore we designed model primers with dithiol at the 5' end and model target DNA whereby the complimentary base adenine can be detected utilizing 3'-O-ferrocene thymidine triphosphate. As a spacer and blocking agent, dithiol-(16-3,5-bis((6 mercaptohexyl)oxylphenyl)-3,6,9,12,15-pentaoxahexa-decane (DT1) was utilized due to the higher thermal stability of the gold-sulfur bond resulting from the presence

155

of the dithiol. Self-assembled monolayer of the primers and DT1 (1:10 ratio) where allowed to form on gold electrodes at 4 degrees Celsius for 24 hours. Thereafter, primer-target annealing was performed at room temperature for 2 hours, followed by enzymatic incorporation of 3'-O-ferrocene-dTTP by Thermo sequenase DNA polymerase at 62 degrees Celsius for 10 min and after washing with acetonitrile and phosphate buffer yielded the DNA extension product.
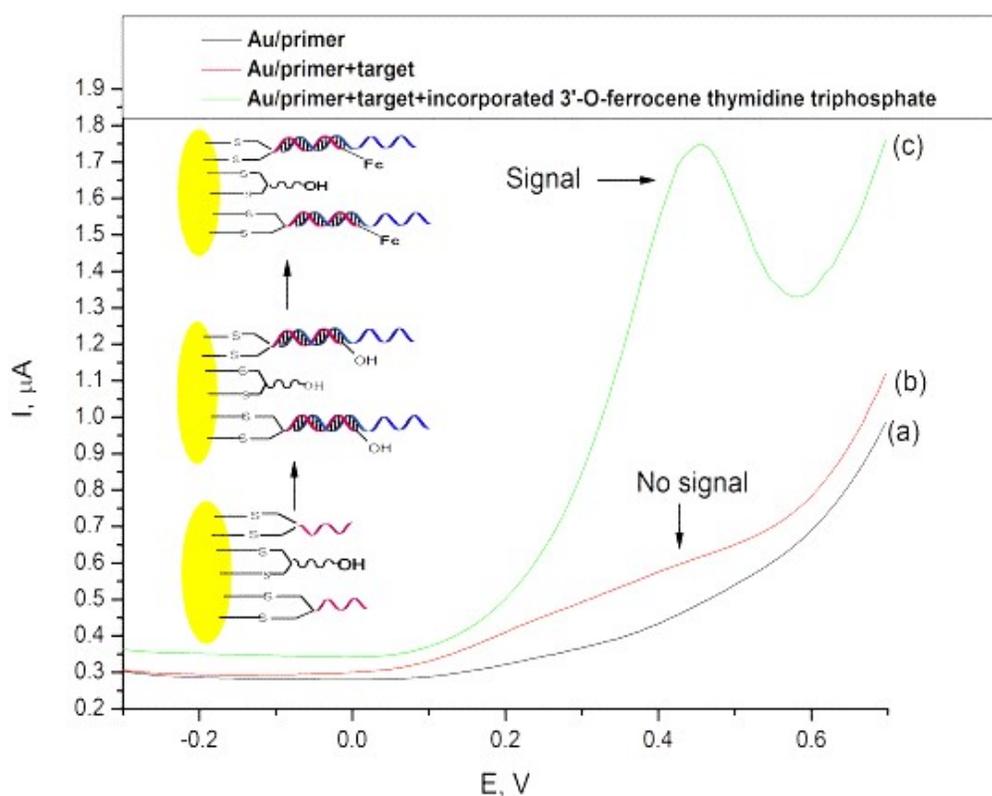
Figure 68 Differential pulse voltammograms of (a) gold electrode modified with primers and DT1, (b) Model target hybridization and (c) detection and characterization of enzymatic incorporation of 3'-O-ferrocene-thymidine triphosphate (compound 5T) in *model target (3'-GGGGGGGGGGGGGGGGGGGAAAAAAAAA-5') DNA by 0.1 u/µL Thermo sequenase after 10 min of incubation at 62 degrees Celsius; with gold electrode as the working electrode versus Ag/AgCl in 0.01M phosphate buffered saline (PBS) at scan rate 20 mV/s.*

Due to its high sensitivity, differential pulse voltammetry (DPV) was utilized to detect and characterize 3'-O-ferrocene-dTTP extension product, complimentary to the base adenine as shown in figure 68. The DPV in 0.01M phosphate buffered saline (PBS) reveal that prior to the enzymatic incorporation reaction of 3'-O-ferrocene thymidine to a) gold electrode modified with primers and DT1 and b) model target hybridization, no signal was obtained as expected. After the enzymatic incorporation of 3'-O-ferrocene-thymidine triphosphate (compound 5T) in model target (3'-GGGGGGGGGGGGGGGGGGGAAAAAAAAA-5') DNA by 0.1 u/µL Thermosequenase DNA polymerase, an oxidation peak was observed at 435 mV which is due to the oxidation of the ferrocene molecule $Fe^{III} = Fe^{II}$.

5.3.8 Characterization of free and incorporated 3'-O-ferrocene thymidine triphosphate utilizing DPV

To further distinguish the incorporated 3'-O-ferrocene thymidine triphosphate from the free (in solution) 3'-O-ferrocene thymidine triphosphate, the DPV of the molecule was performed as shown in figure 69 (above).The single peak at 435 mV was observed. A very significant shift from 355 mV of the free 3'-O-ferrocene thymidine triphosphate) to 435 mV after the incorporation of the 3'-O-ferrocene-thymidine triphosphate towards more positive potentials was observed. The linear relationship between the scan rate and the anodic peak current shown in figure 69 (below), with a linear regression of 99.8% and very low standard deviation of 7.53×10^{-9}, showed that the electrochemical activity arose from surface bound species further confirming the successful incorporation of 3'-O-ferrocene-thymidine triphosphate by Thermosequanse DNA polymerase in target DNA.

157
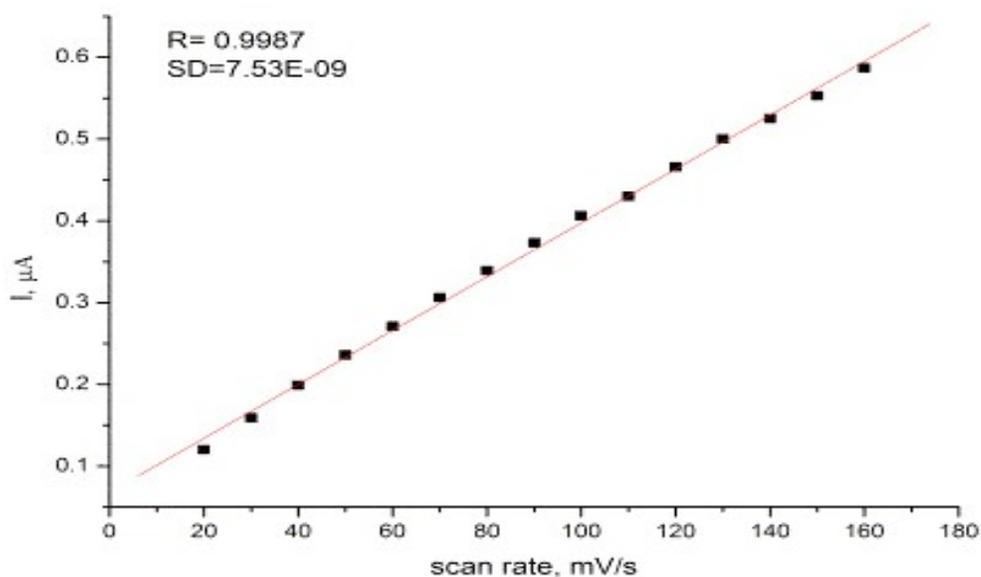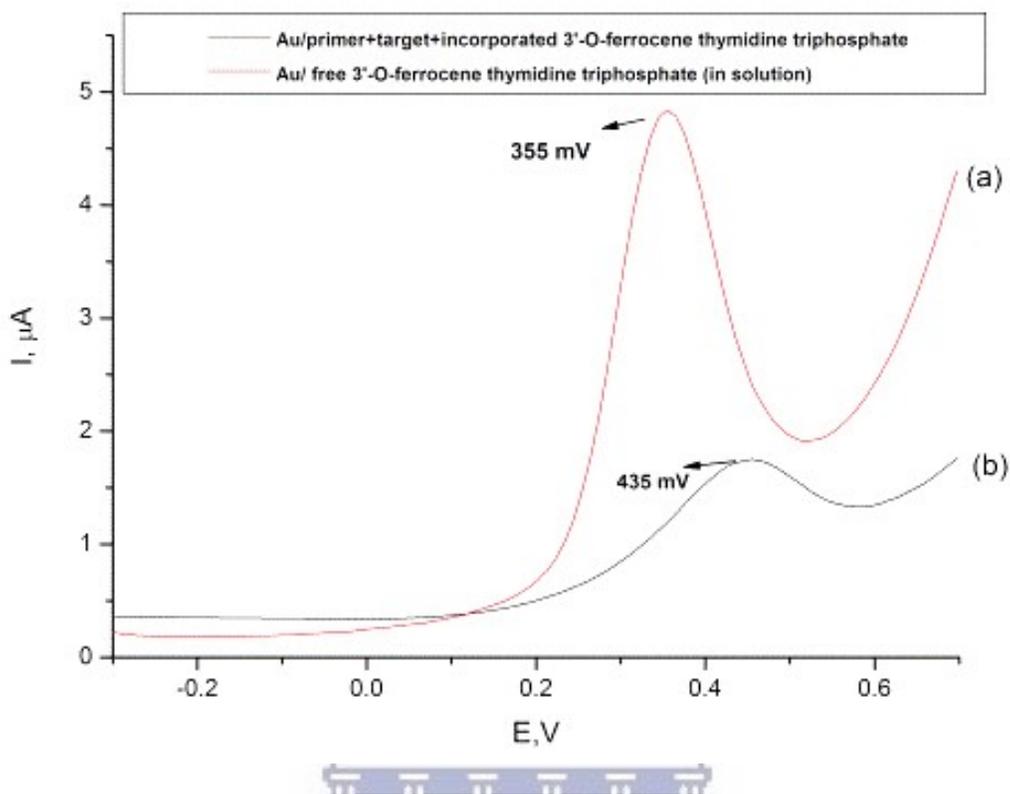
Figure 69 Differential Pulse voltammograms (a) before and (b) after the chemical cleavage of 3'O-ferrocene label and linker by Na₂PdCl₄/ TPPTS)/ Thermo Sequenase reaction buffer for 30 min at 62°C on a gold electrode versus Ag/AgCl at scan rate 20 mV/s in PBS. 78.2% signal loss has been achieved.

5.3.9 Palladium catalyzed selective chemical cleaving of linker and ferrocene label

Palladium catalyzed selective chemical cleavage of the linker and label was performed by treating the electrode bound DNA extension product with triphenylphosphine-3,3',3''-trisulfonic acid trisodium salt (TPPTS) and sodium tetrachloropalladate (II) (7:1) deallylation solution at 62 degrees Celsius for 30 min as described by Dae-Ra Kim *et al 2014* [79] with modifications. The DPV of the cleavage product was then recorded yielding a 78% signal loss indicative that 78% of the extended products have 3'-OH available for the 2nd incorporation reaction as shown in figure 70, signifying that only 30% of labelled DNA remained after the cleavage reaction.
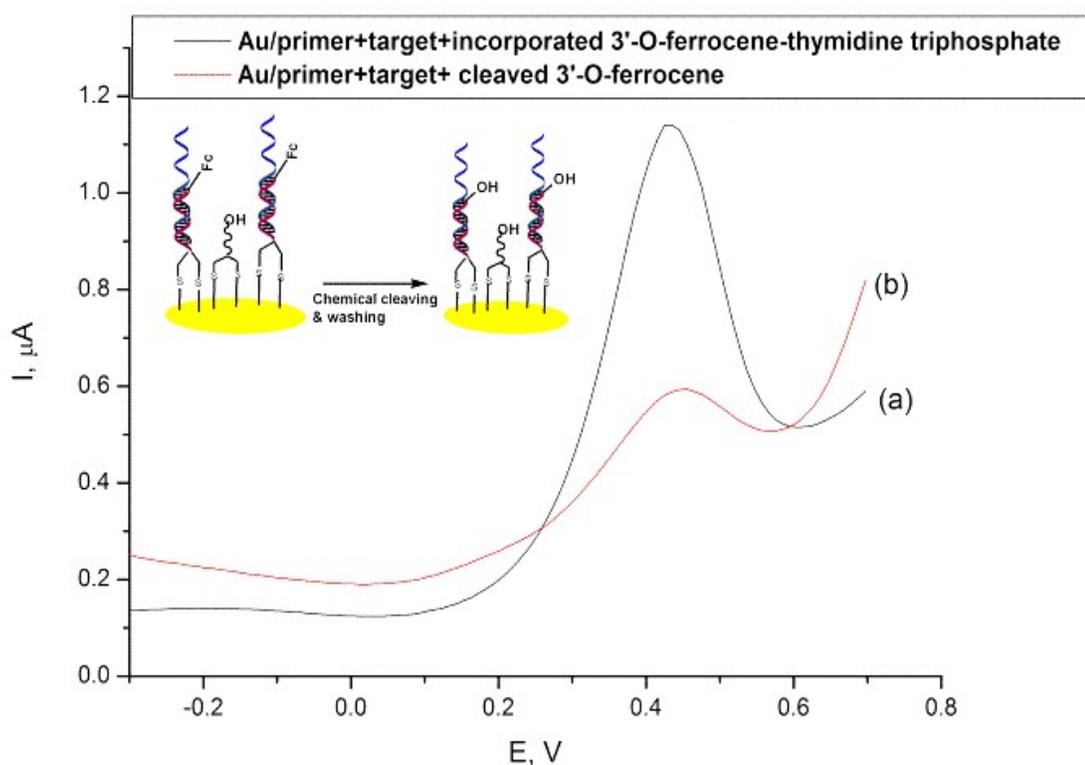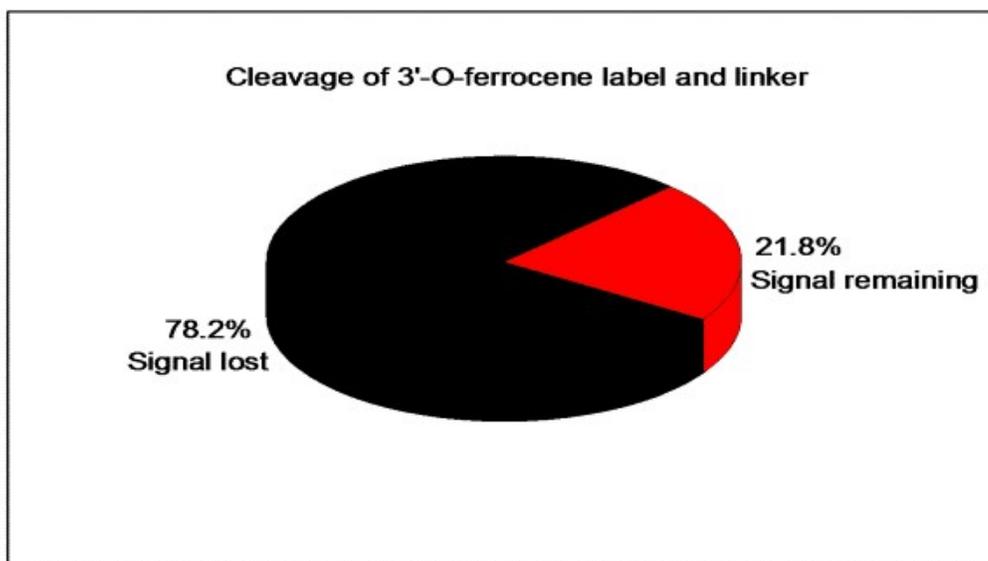
Cleavage of 3'-O-ferrocene label and linker

21.8%
Signal remaining

78.2%
Signal lost

Figure 70 (Above) Differential pulse voltammetry (DPV) of 3'-O-ferrocene-thymidine triphosphate (a) in 0.01M phosphate buffered saline (PBS), (b) incorporated by 0.1 u/µL DNA Thermo sequenase after 10 min of incubation at 62 degrees Celsius; at a gold electrode versus Ag/AgCl at scan rate 20 mV/s, revealing the potential shift caused by incorporation. (Below) Scan rate study of anodic peak of incorporated 3'-O-ferrocene-thymidine triphosphate showing linear relationship between anodic peak current (I) and scan rate, a characteristic behaviour of electrode bound electro-active species.

Furthermore, re-incorporation of 3'-O-ferrocene thymidine triphosphate to the DNA target after the cleavage of the 3'-O ferrocene and linker was then performed as shown in figure 71. A single peak at 435 mV was observed. The DPV results showed the successful re-incorporation of 3'-O-ferrocene thymidine triphosphate, with oxidation potential again at 435 mV thus confirming that the 3'-OH of the thymidine were regenerated and available for the incorporation of the 2nd 3'-O-ferrocene thymidine triphosphate to detect the second complimentary adenine base.
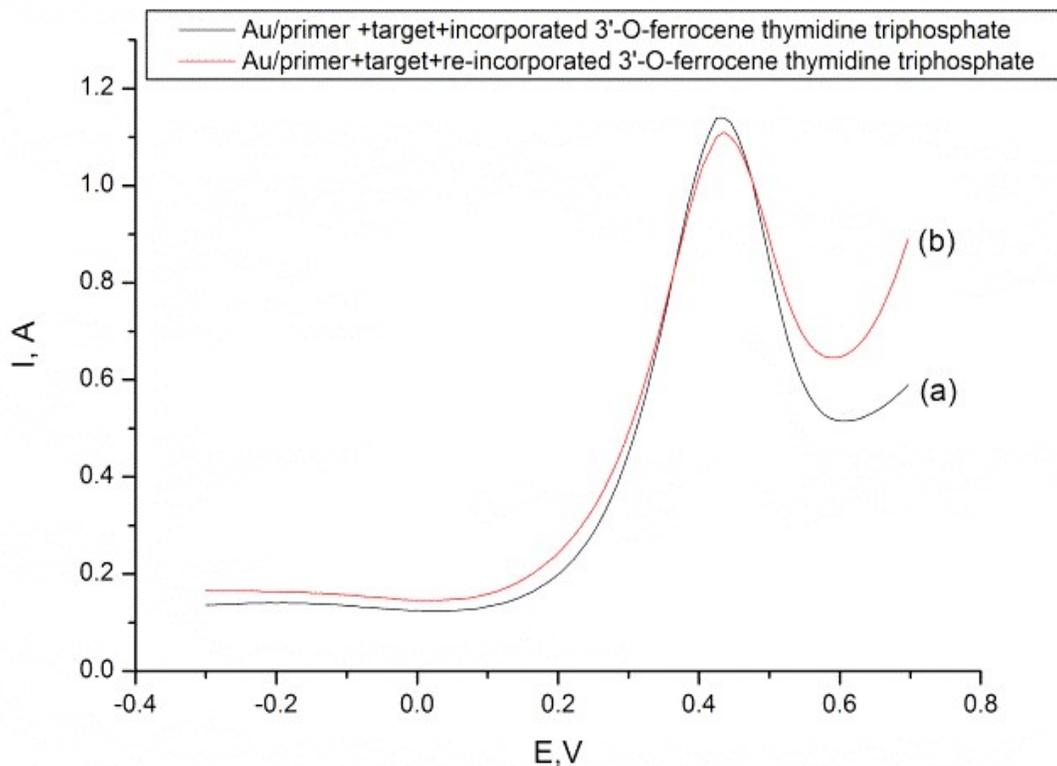
160

Figure 71 Differential pulse voltammetry detection of the (b) 2nd or re-incorporation of 3'-O-ferrocene-thymidine triphosphate on model target DNA by 0.1 u/µL Thermo sequenase after 10 min of incubation at 62 degrees Celsius with gold electrode as the working electrode versus Ag/AgCl in 0.01M phosphate buffered saline (PBS) at scan rate 20 mV/s.
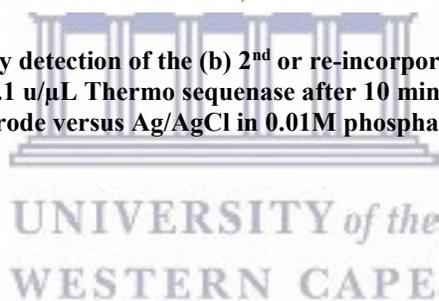
5.6 Conclusion

In this study we have successfully designed and developed a facile 6 step synthetic approach for reversible terminating and labeling nucleotides. Though reversible labels at the 3'-OH offered a promising alternative over base labeling for SBS applications due to the absence of molecular scarring after label removal, the major drawback was the introduction of the olefin for reversibility and spacer chains with stable terminal conjugation groups such as amines and azides, for simplified labeling. Recently, Dongyu Shin *et al 2010* and Da-Rae Kim *et al 2014*.[78].[79]. reported a multi-step synthetic approach involving the use of metal hydrides. Hence our methodology offers a more simplistic, time and cost effective alternative which can also be adapted for fluorescent based DNA sequencing. Furthermore, we

161

successfully developed a novel "next generation" electrochemical DNA sequencing technique and successfully demontrated the 4 main SBS DNA sequencing steps viz 1) enzymatic incorporation and detection of the complimentary adenine base by the ferrocene label at 435 mV, 2) Palladium assisted chemical cleavage with 78% signal loss , 3) re-incorporation and signal regeneration. In general electrochemical techniques carry the intrinsic property of portability and therefore the EcSeq can be further investigated for point of care (POCT) devices on real DNA samples.

References

[63]   E. R. Mardis, "Next-generation sequencing platforms.," *Annu. Rev. Anal. Chem. (Palo Alto. Calif).*, vol. 6, pp. 287–303, 2013.

[64]   M. L. Metzker, "Sequencing technologies - the next generation.," *Nat. Rev. Genet.*, vol. 11, no. 1, pp. 31–46, 2010.

[65]   J. Ju, D. H. Kim, L. Bi, Q. Meng, X. Bai, Z. Li, X. Li, M. S. Marma, S. Shi, J. Wu, J. R. Edwards, A. Romu, and N. J. Turro, "Four-color DNA sequencing by synthesis using cleavable fluorescent nucleotide reversible terminators.," *Proc. Natl. Acad. Sci. U. S. A.*, vol. 103, no. 52, pp. 19635–19640, 2006.

[66]   J. Korlach, A. Bibillo, J. Wegener, P. Peluso, T. T. Pham, I. Park, S. Clark, G. a Otto, and S. W. Turner, "Long, processive enzymatic DNA synthesis using 100% dye-labeled terminal phosphate-linked nucleotides.," *Nucleosides. Nucleotides Nucleic Acids*, vol. 27, no. 9, pp. 1072–1083, 2008.

[67]   E. L. van Dijk, H. Auger, Y. Jaszczyszyn, and C. Thermes, "Ten years of next-generation sequencing technology," *Trends Genet.*, vol. 30, no. 9, pp. 418–426, Aug. 2014.

[68]   J. C. P. Esperança, W. R. R. Miranda, J. B. Netto, F. S. Lima, L. Baumworcel, L. Chimelli, R. Silva, T. P. Ürményi, P. H. Cabello, E. Rondinelli, and D. S. Faffe, "Polymorphisms in IL-10 and INF-γ genes are associated with early atherosclerosis in coronary but not in carotid arteries: A study of 122 autopsy cases of young adults," *BBA Clin.*, vol. 3, pp. 214–220, 2015.

[69]   K. M. Hayden, J. M. McEvoy, C. Linnertz, D. Attix, M. Kuchibhatla, A. M. Saunders, M. W. Lutz, K. a. Welsh-Bohmer, A. D. Roses, and O. Chiba-Falek, "A homopolymer polymorphism in the TOMM40 gene contributes to cognitive performance in aging," *Alzheimer's Dement.*, vol. 8, no. 5, pp. 381–388, 2012.

[70]   B. Li, G. Pan, N. D. Avent, R. B. Lowry, T. E. Madgett, and P. L. Waines, "Graphene electrode modified with electrochemically reduced graphene oxide for label-free DNA detection," *Biosens. Bioelectron.*, vol. 72, pp. 313–319, 2015.

[71]   B. Xu, D. Zheng, W. Qiu, F. Gao, S. Jiang, and Q. Wang, "An ultrasensitive DNA biosensor based on covalent immobilization of probe DNA on fern leaf-like α-Fe2O3 and chitosan Hybrid film using terephthalaldehyde as arm-linker," *Biosens. Bioelectron.*, vol. 72, pp. 175–181, 2015.

[72]   M. Li, Y. Wang, Y. Zhang, J. Yu, S. Ge, and M. Yan, "Graphene functionalized porous Au-paper based electrochemiluminescence device for detection of DNA using luminescent silver nanoparticles coated calcium carbonate/carboxymethyl chitosan hybrid microspheres as labels," *Biosens. Bioelectron.*, vol. 59, pp. 307–313, 2014.

162

[73]   J. Zheng, C. Chen, X. Wang, F. Zhang, and P. He, "A sequence-specific DNA sensor for Hepatitis B virus diagnostics based on the host-guest recognition," *Sensors Actuators, B Chem.*, vol. 199, pp. 168–174, 2014.

[74]   Y. Sun, X. He, J. Ji, M. Jia, Z. Wang, and X. Sun, "A highly selective and sensitive electrochemical CS–MWCNTs/Au-NPs composite DNA biosensor for Staphylococcus aureus gene sequence detection," *Talanta*, vol. 141, pp. 300–306, 2015.

[75]   E. M. Regan, A. J. Hallett, L. C. C. Wong, I. Q. Saeed, E. E. Langdon-Jones, N. J. Buurma, S. J. a Pope, and P. Estrela, "A novel cobalt complex for enhancing amperometric and impedimetric DNA detection," *Electrochim. Acta*, vol. 128, pp. 10–15, 2014.

[76]   P. Ling, J. Lei, L. Zhang, and H. Ju, "Porphyrin-Encapsulated Metal-Organic Frameworks as Mimetic Catalysts for Electrochemical DNA Sensing via Allosteric Switch of Hairpin DNA," *Anal. Chem.*, p. 150305143816005, 2015.

[77]   D. C. Knapp, S. Serva, J. Dapos;Onofrio, A. Keller, A. Lubys, A. Kurg, M. Remm, and J. W. Engels, "Fluoride-cleavable, fluorescently labelled reversible terminators: Synthesis and use in primer extension," *Chem. - A Eur. J.*, vol. 17, no. 10, pp. 2903–2915, 2011.

[78]   T. S. Kim, D. R. Kim, H. C. Ahn, D. Shin, and D. R. Ahn, "Novel 3-O-fluorescently modified nucleotides for reversible termination of DNA synthesis," *ChemBioChem*, vol. 11, no. 1, pp. 75–78, 2010.

[79]   D. R. Kim, T. S. Kim, E. Kim, S. J. Min, D. Shin, and D. R. Ahn, "Synthesis of 3′-O-fluorescently mono-modified reversible terminators and their uses in sequencing-by-synthesis," *Bioorganic Med. Chem. Lett.*, vol. 24, no. 1, pp. 209–213, 2014.

[80]   M. W. Rathke and M. Nowak, "The Horner-Wadsworth-Emmons Modification of the Wittig Reaction Using Triethylamine and Lithium or Magnesium Salts," *J. Org. Chem.*, vol. 50, no. 15, pp. 2624–2626, 1985.

[81]   R. G. Giles, N. J. Lewis, J. K. Quick, M. J. Sasse, and M. W. J. Urquhart, "Regiospecific Reduction of 5-Benzylidene-2 , 4-Thiazolidinediones and 4-Oxo-2-thiazolidinethiones using Lithium Borohydride in Pyridine and Tetrahydrofuran," vol. 56, pp. 4531–4537, 2000.

[82]   C. W. Fuller, L. R. Middendorf, S. a Benner, G. M. Church, T. Harris, X. Huang, S. B. Jovanovich, J. R. Nelson, J. a Schloss, D. C. Schwartz, and D. V Vezenov, "The challenges of sequencing by synthesis.," *Nat. Biotechnol.*, vol. 27, no. 11, pp. 1013–1023, 2009.

[83]   R. N. Salvatore, A. S. Nagle, and W. J. Kyung, "Cesium effect: High chemoselectivity in direct N-alkylation of amines," *J. Org. Chem.*, vol. 67, no. 3, pp. 674–683, 2002.

[84]   I. Gillerman and B. Fischer, "An improved one-pot synthesis of nucleoside 5'-triphosphate analogues.," *Nucleosides. Nucleotides Nucleic Acids*, vol. 29, no. 3, pp. 245–56, 2010.

GENERAL CONCLUSION

Water-soluble IrSe quantum dot have been successfully synthesized at room temperature utilizing H_2ICl_6 and NaHSe as a source of iridium and selenium ion respectively. The spherical 3 nm colloids were studied utilizing HRTEM, EDX, and SAED. Their PL emission was observed at 519 nm while exhibiting a very narrow absorption width thus further indicative of the formation of narrow sized particles. Characteristic reduction potential at 107mV and oxidation at 641 mV in phosphate buffer, pH 7.41 ideal for biological samples, was observed utilizing cyclic voltammetry. Thus the 3-mercaptopropionic acid functionalized IrSe quantum dot exhibited optical and electrochemical properties worthy of further investigation as biological labels and mediators in bio-sensing devices. Furthermore, water-soluble RhSe quantum dot have been successfully synthesized at room temperature The nanoshells were then confirmed utilizing high-resolution transition electron microscope (HRTEM) whereby with sizes ranging from 15 - 20 nm. The HRTEM of the RhSe quantum dot revealed that very narrow sized particles of 3.5 nm have been simultaneously formed The SEM-BSE revealed that RhSe quantum dot, due to their narrow size interwoven themselves into nanotubes of about 251 nm in diameter within the electrode instead of on top of the electrodes, into vein-like networks. The flow behavior of the nanocrystals in water has been investigated using Rheometry and a decrease in viscosity with increasing applied pressure (shear thinning) has been observed, an ideal behavior for biological applications or nanofluids. The electro-activity of the RhSe quantum dot was performed on indium tin oxide electrodes and a characteristic oxidation peak at 450 mV was obtain.

Lastly, also in this study, we have successfully developed a facile 6 step synthetic approach for reversible terminating and labeling nucleotides. Though reversible labels at the 3'-OH offered a promising alternative over base labeling for SBS applications due to the absence of molecular scarring after label removal, the major drawback was the introduction of the olefin for reversibility and spacer chains with

164

stable terminal conjugation groups such as amines and azides, for simplified labeling. Recently, Dongyu Shin and Da-Rae Kim.[78],[79] reported a multi-step synthetic approach involving the use of metal hydrides. Hence our methodology offers a more simplistic, time and cost effective alternative which can also be adapted for fluorescent-based DNA sequencing. Furthermore, we successfully developed a novel "next generation" electrochemical DNA sequencing technique and successfully demonstrated the 4 main SBS DNA sequencing steps viz 1) enzymatic incorporation and detection of the complementary adenine base by the ferrocene label at 435 mV, 2) Palladium assisted chemical cleavage with 78% signal loss, 3) re-incorporation and signal regeneration. The majority of time of the study went into establishing a reliable method towards synthesizing the novel 3'-hydroxyl electro-active nucleoside, consequently the DNA sequencing experiments were demonstrated only on standard DNA. In general electrochemical techniques carry the intrinsic property of portability and therefore the EcSeq can be further investigated for point of care (POCT) devices on real DNA samples.

165